Novel models and methods for the functional characterization of disease-relevant *SDHA* variants

By

Jason D. Kent

A DISSERTATION

Presented to the Department of Cell, Developmental, & Cancer Biology
Oregon Health & Science University
School of Medicine

in partial fulfillment of
the requirements for the degree of

Doctor of Philosophy

December 2023

School of Medicine

Oregon Health & Science University

CERTIFICATE OF APPROVAL

This is to certify that the PhD dissertation of

Jason D. Kent

has been approved

Michael Heinrich, Advisor

Anupriya Agarwal, Chair

Amanda McCullough, Member

Brian O'Roak, Member

Jeffrey Tyner, Member

Contents

List of Tables

List of Figures

Selected Abbreviations

ACMG	American College of Medical Genetics and Genomics
AMP	Association for Molecular Pathology
AUC	Area under the ROC curve
B/LB	Benign/Likely Benign
CI	Confidence interval
ClinGen SVI WG	Clinical Genome Resource Sequence Variant Interpretation Working Group
CSS	Carney Statakis Syndrome
CT	Carney Triad
DMS	Deep mutational scanning
ETC	Electron transport chain
GIST	Gastrointestinal stromal tumors
LOF	Loss of function
LOH	Loss-of-heterozygosity
LOVD	Leiden Open Variation Database
MFI	Median fluorescence intensity
NGS	Next-generation sequence
OXPHOS	Oxidative phosphorylation
P/LP	Pathogenic/Likely Pathogenic
PC/PGL	pheochromocytoma and paraganglioma
PMD	Primary mitochondrial disease
PPV	Positive predictive value
QFR	Quinone:fumarate reductases
RCC	Renal cell carcinoma
ROC	Receiver operating characteristic
ROS	Reactive oxygen species
SDH	Succinate dehydrogenase
SDHA	Succinate dehydrogenase complex flavoprotein subunit A
SDHAF(1-4)	Succinate dehydrogenase complex assembly factor (1-4)
SDHB	Succinate dehydrogenase complex iron sulfur subunit B
SDHC/D	Succinate dehydrogenase complex subunit C/D
SEM	Standard error of the mean
SQR	Succinate:quinone oxidoreductase
TCA	Tricarboxylic acid
TPR	True positive rate
TSG	Tumor suppressor gene
VUS	Variant of uncertain significance
WT	Wild type

i. Acknowledgments

In the introduction of this dissertation, I compare the study of cancer biology to moving through an endless maze. Although daunting, the exploration of new paths and learning where they lead is exciting. Throughout my dissertation work, I have been wandering through this maze making discoveries and sometimes getting lost. I now find myself at the end of a path, about to start anew. As I reflect, this journey has been as challenging as it has been rewarding, and I would not have gotten to this point without the help of many people. First, I would like to thank my mentor and PhD advisor Michael Heinrich for inviting me down this path and being supportive of me the entire time. I also thank Lillian Klug and Amber Bannon who were senior graduate students in the lab when I joined and helped teach me how to navigate, as well as the other members of the Heinrich Lab: Ajia, Arin, Ashley, Diana, Kevin, Limin, Sophie and Tory. A special thanks to each member of my dissertation advisory committee who helped lead me back to the right path the multiple times I took detours. Philip Copenhaver and Lola Bichler also provided support more times than I can count.

This journey would not have been nearly as enjoyable if it were not for my friend and fellow Heinrich Lab graduate student, Homma Khosroyani, who helped me laugh and stay positive even during the most challenging times. This also would not have been possible without the unconditional support of my family throughout my entire life, even when I did not necessarily deserve it, like when I got a red card in soccer when I was four years old. I am still sorry about that.

Finally, thank you to my partner, Kathrina Oñate, who not only joined me on this journey but has been there by my side the entire time, holding my hand.

ii. Abstract

The inheritance of specific germline variants can be associated with a significantly increased lifetime risk of developing cancer. With the advancements in sequencing technology and lowered costs, individuals carrying variants known to cause cancer can now be readily identified. After a recent FDA approval, one can even now get a prescription for a genetic test covering 47 genes associated with heritable cancer to identify risks. Among the genes included in this test is *SDHA*. *SDHA* encodes the largest subunit of the succinate dehydrogenase enzyme complex, which plays a vital role in cellular metabolism. When functional, SDH converts succinate to fumarate and passes electrons to ubiquinone, thereby linking the tricarboxylic acid cycle to the electron transport chain. However, upon SDH dysfunction, the accumulation of succinate can result in metabolic and epigenetic dysregulation, leading to tumor formation. As such, individuals who inherit a loss-of-function mutation in one of the SDH genes, including *SDHA*, are at risk for cancer.

The more individuals that receive genetic testing, the more individuals that carry a known cancer-causing *SDHA* variant will be detected. This provides tremendous opportunities for improved patient outcomes, such as early tumor detection. However, at the same time, the more sequencing is performed, the more we will identify variants for which we cannot properly assess pathogenicity due to insufficient evidence. More than 1,000 missense *SDHA* variants are listed in ClinVar and over 95% have been interpreted as variants of uncertain significance (VUS). As the detection of these VUS cannot be used to guide

clinical decisions, we must improve our ability to interpret the significance of *SDHA* variants before genetic sequencing can be utilized to its fullest potential for assessing cancer risk.

To address the VUS problem in SDHA, we turned to functional data, which can provide strong evidence for variant classification. However, there is not a clear understanding as to what constitutes cancer-like SDHA dysfunction, making it challenging to interpret results. Therefore, we investigated what distinguishes cancer from non-cancer variants using a novel HAP1 *SDHA*-knockout cell line. This analysis revealed that cancer-causing variants are uniquely characterized by complete loss of activity. With this, we were able to establish a threshold for classifying cancer variants which corresponded to a true positive rate and positive predictive value over 95%. Based on the performance of this model, we could obtain strong functional evidence to support the reclassification of SDHA VUS with cancer-like dysfunction as likely pathogenic, following the guidelines and recommendations provided by ACMG and ClinGen.

To supplement this model, we also developed a cell-based assay that interrogates SDHA-variant function. Although it requires further development, it has shown promising potential and has the capacity for high-throughput analysis, which can enable us to characterize a greater number of SDHA VUS. When paired with our exceptional HAP1 $SDHA^{KO}$ functional model to validate results, this represents a framework to determine the functional consequences of SDHA variants, which can be used as evidence to enhance our ability to assess SDHA-variant pathogenicity and greatly benefit those at risk for cancer.

1. Introduction

A. Cancer

To understand human cancer would require one to understand all of human biology. The multitude of genetic and environmental factors underlying tumor formation are outnumbered only by the endless biological pathways that cancers exploit, modify, or seemingly create, to promote aberrant cell proliferation. In 2000, Hanahan and Weinberg attempted to reduce cancer biology's vast complexities and intricacies into six "hallmarks" (1). They further described a mechanism by which pre-malignant cells could obtain these hallmarks and termed it an "enabling characteristic". In 2011, the pair updated their list to include two emerging hallmarks and an additional enabling characteristic (2). After the most recent 2022 update, aptly titled "Hallmarks of Cancer: New Dimensions" the list now stands at eight bona fide hallmarks, two emerging hallmarks, and four enabling characteristics (3). Perhaps it is ironic that the list that attempts to simplify the complexity of cancer biology continues to grow, dare I say, uncontrollably.

The evolution of the hallmarks of cancer is well justified, not because the diseases themselves are changing but because our understanding is constantly advancing. While much progress has been made toward unraveling the complexities of cancer biology, every advancement reveals how far we still must go. Together, we are traversing a maze with no exit. Each discovery we make opens a new door leading to multiple paths. Sometimes, these paths are entirely

unexplored, whereas other times, we find they lead to familiar paths that were previously thought to be unconnected. While the maze has no exit, the more we explore, the less we feel lost. Herein, I describe my journey through this maze, where I investigated the molecular consequences of variants in succinate dehydrogenase (*SDH*) and their associations with cancer. In the introduction, I present the doors that had been previously opened and guided my way. In the subsequent chapters, I unveil the doors opened by my research and the insights that were gained. Lastly, I speculate on the unopened doors that lie ahead.

1. Tumor suppressor genes

In 1969, Harris and colleagues demonstrated that fusing mouse cancer cells with normal cells suppressed malignancy (4). Chromosome segregation analysis revealed this phenomenon was dependent on the presence of specific fragments of DNA. At the time, it was accepted that certain “oncogenes” could initiate tumor formation in a dominant fashion, but the existence of genes that could seemingly keep tumors in check was controversial (5). However, around the same time, Knudson was investigating the curious differences among patients with retinoblastoma, namely the number of tumors present, the age of the patient, and distinct inheritance patterns. Through observation and statistical analysis, Knudson concluded that in contrast to the dominant nature of oncogenes, the genetics of retinoblastoma must act in a recessive manner. Thus, he developed the theory stating two distinct mutational events were necessary for retinoblastoma development, a concept now widely known as Knudson’s “two-hit” hypothesis (**Figure 1**) (6).

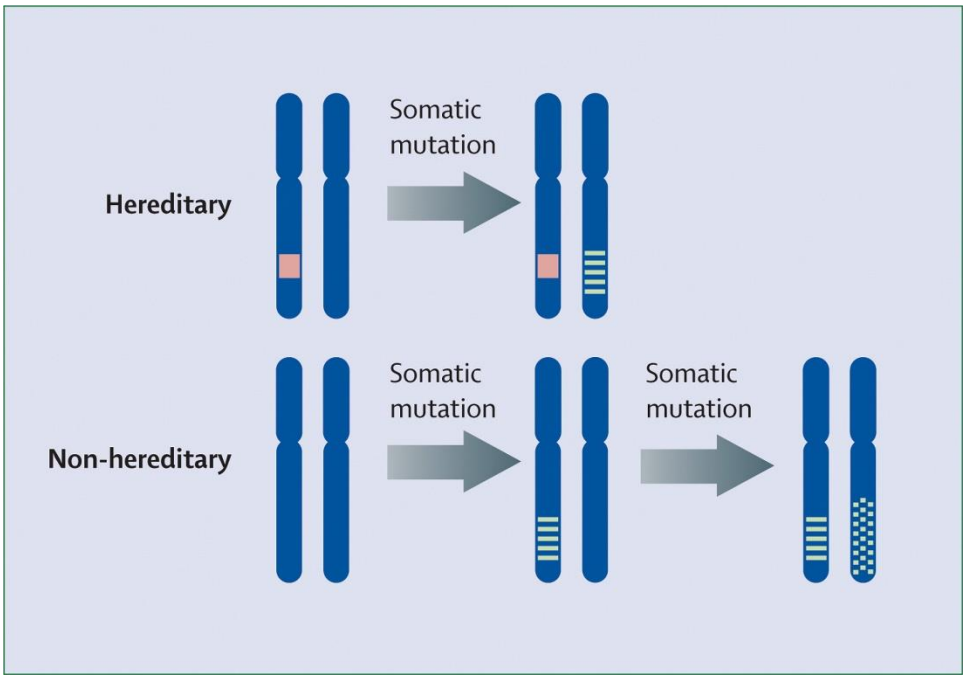

Figure 1. Knudson's "two-hit" hypothesis. For classical TSGs, two hits are required to achieve complete genetic inactivation, leading to tumor development. In hereditary cancers, carriers of pathogenic variants already carry the first hit as a germline mutation and only need a single somatic hit. Non-hereditary cancers require two somatic hits in the same cell. Reprinted from The Lancet Oncology, Possible mechanisms of disease development in tuberous sclerosis, Jozwiak et al., 2014, with permission from Elsevier.

Despite the significance of his work, Knudson's hypothesis alone could not fully explain the finding of Harris and others. One possible explanation for the development of retinoblastoma could be the activation of two independent oncogenes, each individually insufficient for oncogenic transformation. However, over several years, the locus responsible for retinoblastoma was narrowed down, and ultimately, RB transcriptional corepressor 1 (*RB1*) was discovered (7,8). Thus, it was determined that biallelic inactivation of a single gene could lead to cancer. The corollary to this finding was that the presence of just a single functional allele acted to suppress tumor initiation, finally providing the mechanism explaining Harris' observations.

It is now well established that *RB1* and its role in preventing tumor formation is not unique. To date, over 1,000 such genes have been described

and are collectively referred to as tumor suppressor genes (TSGs) (9). The role of TSGs in cancer has been the subject of extensive research, which has revealed a variety of different mechanisms by which their dysfunction leads to cancer, such as regulating cellular division or promoting cell death (5). The most well-studied gene is inarguably *p53*, a TSG mutated in ~50-60% of all human cancers (10,11). The overwhelming majority of cases involve somatic mutations (12). However, what of germline mutations?

2. Inherited cancer susceptibility

In 1969, the hereditary cancer predisposition syndrome Li-Fraumeni Syndrome was described (13). In 1990, it was discovered that the increased susceptibility to this cancer syndrome was due to inherited mutations of *p53*. Just as Knudson described with *RB1* and retinoblastoma, when every cell harbors an inactivating *p53* mutation, only a single somatic event is required for tumor formation. This is far more likely to occur than the same cell developing two somatic alterations and is true of all TSGs. Thus, the inheritance of a loss-of-function (LOF) mutation in a TSG significantly increases one's lifetime risk of developing one or more cancers. The extent of predisposition varies among TSGs but is often substantial. A notable example is carriers of *BRCA1/2* mutations, who have an approximate 60-80% and 20-45% risk for the development of breast or ovarian cancer by the age of 80, respectively (14). In addition to overall increased lifetime risk, needing only a single somatic event often results in an earlier age of tumor onset for carriers of germline LOF mutations in TSGs. This is again exemplified by carriers of *BRCA1* mutations,

who have a greater than 30-fold increased risk of breast cancer before the age of 40 compared to non-carriers (15). Due to these significant risks, the identification of patients harboring such mutations has become a critical focus in clinical practice. This has been enabled by the advancements in genetic sequencing technologies.

3. Genomic sequencing in cancer

Following the invention of Sanger sequencing in 1977, genetic sequencing has led to a countless number of breakthroughs in the field of oncology. The wealth of information that can be gleaned from these analyses and their potential to advance our understanding of cancer and improve patient care has long been known (16). In 2004, a census of cancer genes revealed nearly 300 implicated genes. Since then, several consortiums have been developed in attempts to catalog and characterize various aspects of the genetic landscape of cancer (17,18). However, the extensive knowledge we have today can largely be attributed to the advent of next-generation sequencing (NGS).

In 1990, the Human Genome Project was launched. Fifteen years and 3 billion dollars later, the final sequence was reported (19,20). By 2008, the sequencing of an entire genome took just five months and cost less than 2 million dollars (21). Since then, further advancements in sequencing technology have resulted in even lower costs and higher throughput. To put the accomplishments enabled by NGS in perspective, we can look at seminal work from 2006, which described the diverse genetic landscape underlying malignancy. Sjöblom and colleagues sequenced over 13,000 genes from a total of 22 breast and colorectal

cancers. Even from the small number of samples, this impressive analysis revealed nearly 200 genes that were frequently mutated in just these two cancer types (22). However, with the tools we have now, a single study performed whole-genome sequencing on over 12,000 tumors across 19 types of cancer (23). In less than 20 years, we have gone from sequencing thousands of genes for a few samples to obtaining whole-genome mutational signatures for thousands of samples. While a marvelous feat, one might wonder how we can keep up with the immense quantity of data obtained from such sequencing.

Nonetheless, the more genetic testing becomes utilized, the more we learn, and this knowledge has played a vital role in nearly every aspect of oncology. As described previously, specific mutations have clear associations with cancer, and those who inherit them have a considerable lifetime risk of tumor development. While only 5-10% of cancers are estimated to have a hereditary component, this nonetheless represents a significant number of at-risk patients (24,25). The identification of these at-risk individuals provides significant opportunities to improve clinical outcomes, such as enabling early tumor detection (26,27). Moreover, the development of multi-gene panels (MGPs) has further improved cancer diagnosis, as any gene associated with the disease, even rare ones, could be tested (28).

The underlying genetic heterogeneity of many cancers was also exploited to improve clinical management. For instance, it was identified that prognosis can often differ according to the presence or absence of specific mutations across multiple genes (29-31). Searching for gene-agnostic mutations also led to the

elucidation of several mechanisms of drug resistance (32). The realization that cancers can have distinct molecular pathways also came with the understanding that these different subsets could contain distinct vulnerabilities, which can be leveraged into targeted therapies. These differ from traditional chemotherapy and radiation, as their efficacies are dependent on the presence or absence of specific mutations. Examples include *EGFR* mutations in lung cancer, *IDH1/2* mutations in acute myeloid leukemia, and many others (33-35). This approach, in which clinical decisions are made based on sequencing results from patients' tumors rather than from the general characteristics of a given cancer type, is referred to as precision medicine. Now, many commercial and institutional MGPs specific for solid tumors or hematological malignancies have been developed. Popular examples include FoundationOne CDx and MSK-IMPACT, which are U.S. Food and Drug Administration-approved genetic tests that cover an impressive 324 and 468 genes, respectively. These tests boast that any solid tumor, regardless of site, can be sequenced and provide a comprehensive genomic profile that can be used for diagnosis, prognosis, or identifying therapeutic targets (36,37).

Perhaps the best example of precision medicine enhancing clinical care is the case of gastrointestinal stromal tumors (GISTs). Before 2000, there were no effective medical therapies for advanced-stage GISTs (38). However, a potential therapeutic option emerged from tumor sequencing that identified activating mutations in the receptor tyrosine kinase (RTK) *KIT* (39). The tyrosine kinase inhibitor (TKI) imatinib, a successful cancer therapy for chronic myeloid leukemia

patients carrying a *BCR-ABL* fusion gene, was also found to effectively inhibit KIT *in vitro* (40,41). The effectiveness of imatinib in treating GIST patients was striking, and it obtained accelerated FDA approval (42). However, some GISTs were refractory to imatinib treatment. While unknown at the time, these findings could be explained almost entirely by retroactive molecular testing. Specific mutations in *KIT* or another homologous RTK gene, platelet-derived growth factor receptor alpha (*PDGFRA),* are unaffected by imatinib inhibition (43,44). Additionally, numerous intra-allelic secondary mutations were found to confer imatinib resistance (45). Subsequently, multiple lines of TKIs have been designed to effectively target most primary and secondary mutations that are insensitive to imatinib. However, the optimal treatment strategy is unique to each individual and highly dependent on the specific mutations identified by tumor sequencing (46,47).

Despite its wide success, not all GISTs respond to TKIs. Sequencing these tumors typically revealed the absence of activating mutations in *KIT* and *PDGFRA* (48). This emphasizes the targeted aspect of these therapies and further reinforces the significance of knowing the tumor mutational profile. Instead of containing oncogenic mutations, the majority of RTK-wild-type (WT) tumors contain inactivating mutations in the genes encoding succinate dehydrogenase (SDH) and are now referred to as SDH-deficient GISTs (49).

B. Succinate Dehydrogenase (SDH)

Succinate dehydrogenase (SDH), also called Complex II of the electron transport chain (ETC), is an essential metabolic enzyme complex composed of

the subunits SDHA, SDHB, SDHC, and SDHD. SDH is unique in that it participates in both the tricarboxylic acid (TCA) cycle as well as oxidative phosphorylation (OXPHOS), though it does not directly pump protons across the inner mitochondrial membrane (IMM). Instead, SDH facilitates the stepwise transferring of electrons from succinate to ubiquinone, enabling reduced ubiquinol to pass elections to Complex III (**Figure 2**). Also, unlike the other ETC complexes, SDH is solely encoded by nuclear genes.

SDH is part of the Complex II superfamily of enzymes, which consists of two highly similar yet distinct types of enzymes. Both groups are capable of the oxidoreduction of succinate/fumarate and ubiquinone/ubiquinol but differ in the preferred direction of electron transfer (50). As SDH primarily reduces succinate and oxidizes ubiquinone, it is considered a succinate:quinone oxidoreductase (SQR), whereas enzymes that favor the reverse direction are called quinone:fumarate reductases (QFR) (51). The similarity of SQRs and QFRs across multiple species, including *Escherichia coli, Saccharomyces cerevisiae,* and *Sus scrofa* have made these species valuable models for studying the structure, function, and assembly of the different SDH subunits.

1. SDHA structure, function, and assembly

a) SDHA

The largest subunit of SDH is the flavoprotein SDHA, with a molecular weight of 73 kilodaltons (kDa). Analysis of the crystal structure of the mature porcine SDHA revealed a Rossmann-type fold and four domains: a FAD-binding, capping, helical, and C-terminal domain (**Figure 3**). The complete maturation of SDHA first requires its import into the mitochondria matrix and cleavage of its

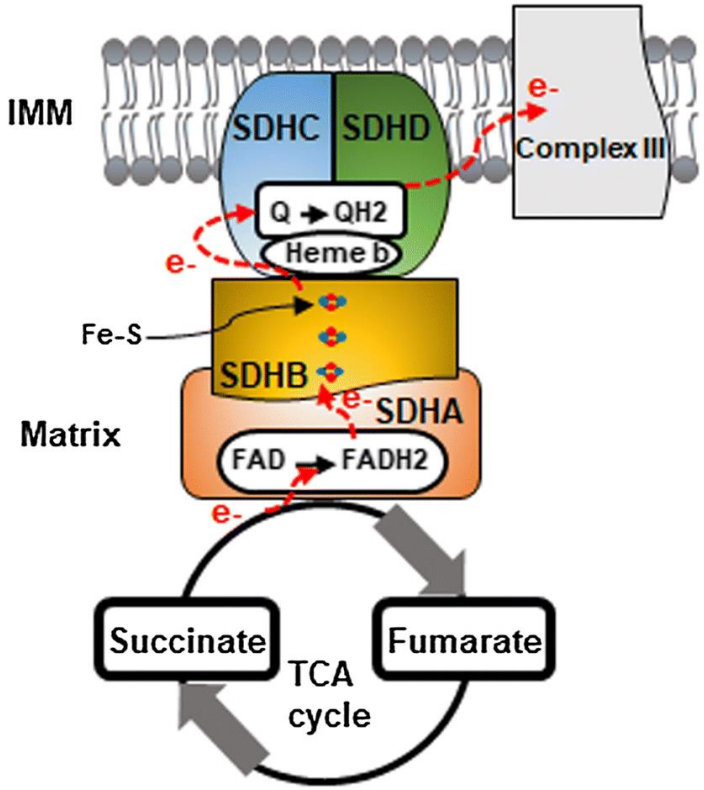

Figure 2. The structure and function of SDH. The catalytic subunits SDHA and SDHB are tethered to the inner mitochondrial membrane (IMM) by SDHC and SDHD. The complex links the TCA cycle to oxidative phosphorylation through the reduction of succinate and oxidation of ubiquinone (Q), producing fumarate and ubiquinol (QH2). Electrons flow from succinate to FAD of SDHA, then through three Fe–S clusters of SDHB, and finally to ubiquinone before being transferred to Complex III. Reproduced from Cell. Mol. Life Sci., The assembly of succinate dehydrogenase: a key enzyme in bioenergetics, Moosavi et al., 2019, with permission from Springer Nature.

mitochondrial targeting sequence at Arg42 (52). SDHA also must be flavinylated at His99 through a covalent 8α-N(3)-histidyl-FAD bond (53). This covalent linkage significantly raises the redox potential of FAD, which is thought to be a key factor in promoting SDH activity over QFR activity (54). Indeed, in 1994, Robinson and others mutated the equivalent residue in yeast (His90) to serine and discovered that although the complex was able to fully assemble and bind FAD non-covalently, SDH activity was fully disrupted, whereas fumarate reductase activity remained intact (55).

In 2009, a Sdh1- (yeast SDHA) binding protein called Sdh5 was found to be required for Sdh1 flavinylation in yeast. Subsequent crystallization studies of this protein complex in *E. coli* (SdhA-SdhE) found that SdhE performs two critical functions. First, the binding of SdhE orients the structure of SdhA into an “open” conformation, which enables covalent FAD attachment. Second, upon flavinylation, SdhE keeps SdhA locked in this inactive confirmation, presumably to prevent electron leakage due to succinate oxidation in the absence of SdhB. Subsequent experiments using purified proteins revealed that SdhE does not directly participate in the catalysis of FAD attachment, but rather, the conformational change induced in SdhA upon its binding enhances SdhA’s autocatalytic flavinylation (54). In fact, flavinylation was observed when SdhA, FAD, and fumarate were the only components present, albeit at a substantially reduced rate.

Recently, the crystallization of the human SDHA-SDHAF2 sub-assembly complex has enabled a more precise understanding of the flavinylation and function of human SDHA (56). When bound to SDHAF2, SDHA exists in an open and non-catalytic conformation, corresponding to a 25˚ rotation of its capping

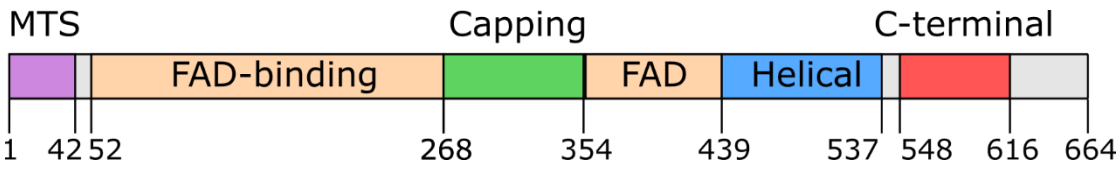

Figure 3. The different domains of the SDHA protein.The mitochondrial targeting signal (purple) ranges from the first amino acid to the 42nd. The FAD-binding domain (beige) extends from residues 52 to 267 and 355 to 439. The capping domain (green) extends from residues 268 to 354. The helical domain (blue) extends from residues 440 to 537. The C-terminal domain (red) extends from residues 548 to 616.

domain relative to the SDHA-SDHB sub-complex. Sharma and colleagues also identified a small dicarboxylate acts as an essential cofactor in SDHA flavinylation, which works in conjunction with SDHAF2 to stabilize this open confirmation. Specifically, oxaloacetate, the dicarboxylate present in the crystal structure obtained, interacted with four SDHA active-site residues, His296, Arg340, His407, and Arg451, as well as a non-active-site residue, Glu309. The role of Arg451 is particularly critical, as its protonation is necessary to stabilize the quinone-methide intermediate formed within the isoalloxazine ring of FAD during covalent attachment (56). The open confirmation enabled by oxaloacetate and SDHAF2 is believed to adjust the pKa of Arg451 to promote its protonation. This likely explains the significantly reduced rate of SDHAF2-independent flavination described above, as Arg451 is buried when SDHA is in a closed state, resulting in significantly lower pKA (56). Mutagenesis of the analogous residues mentioned above in *E. coli*, SdhA, or FrdA (SDHA equivalent in the *E. coli* QFR complex) resulted in a significant reduction of covalent FAD-binding, further demonstrating the importance of the dicarboxylate interaction as well as these individual residues (57,58). While SDHAF2 enhances the flavinylation of SDHA, a second assembly factor dedicated to SDHA, SDHAF4, has been reported to facilitate the binding of SDHA and SDHB. The complete role of SDHAF4 is not fully understood but seems to protect SDHA from auto-oxidation by oxygen and subsequent production of superoxide (59).

The mechanism of succinate oxidation involves hydride transfer from succinate to FAD to generate $FADH_2$. Several of the residues involved in this

process are the same as those that play a key role in flavinylation (56,60). However, at least one residue, Thr308, is only involved in succinate-fumarate interconversion. When the equivalent residue was mutated to alanine in *E. coli*, flavinylation was not impacted, whereas succinate oxidation was defective (61). One of the steps involved in the succinate-fumarate interconversion is the physical twisting of the substrate, which induces a strain and concomitant polarization (62). Thr308 forms a hydrogen bond with the substrate and is thought to stabilize this transition state (61).

In addition to covalent flavinylation, several post-translation modifications (PTM) of SDHA have been described, with varying consequences on function. Phosphorylation of SDHA Tyr604 mediated by FGR kinase has been described to increase SDH activity, whereas dephosphorylation by PTPMT1 suppresses it (63,64). Several other tyrosine and serine residues can be phosphorylated, but the significance of these PTMs is not understood (65).

Several lysine modifications have also been observed within SDHA, including lysine-acetylation. Thirteen acetylated residues have been identified, and their deacetylation mediated by sirtuin 3 (SIRT3) has been shown to increase SDH activity (66,67). Mutagenesis of several candidate lysines to the acetyl-mimetic glutamine or the non-acetylatable arginine revealed that acetylation of Lys335, specifically, may be responsible for the decreased activity observed (68). The mechanism by which acetylation affects function is still unknown.

SDHA Lys547 has also been reported to be a target of succinylation. Desuccinylation mediated by SIRT5 was found to disrupt binding to SDHAF2, thus inhibiting SDH activity (69). Recently, SUMOylation, another lysine PTM, was found to regulate SDH activity under different metabolic conditions. Under glutamine deprivation, SDHA Lys598 is deSUMOylated by SENP2, which affects the assembly of the SDH complex (70). The mechanism for this is not fully known, though it may be similar to that of succinylated Lys547.

b) SDHB

The iron-sulfur protein SDHB is the second catalytic subunit of SDH and has a molecular weight of 32 kDa. SDHB facilitates the sequential transfer of electrons from $FADH_2$ to ubiquinone through three iron-sulfur clusters, 2Fe-2S, 4Fe-4S, and 3Fe-4S (71). Several cochaperones and the SDHB-dedicated assembly factors, SDHAF1 and SDHAF3, are involved in the maturation of SDHB. The iron-sulfur clusters are preassembled in a complex consisting of ISCU, HSC20, and HSPA9. SDHB contains multiple Leucine-Tyrosine-Arginine (LYR) motifs, which directly bind HSC20, thus priming SDHB for insertion of the iron-sulfur clusters (72,73). SDHAF1 further facilitates the interaction between SDHB and the HSC20 complex, as it binds directly to HSC20 through its own LYR motif, as well as to the C-terminal domain of SDHB (**Figure 4**)(73).

The significance of the LYR motifs in SDHB was highlighted by functional analysis following mutagenesis of the LYR-motif residues. These studies showed that the loss of either motif failed to incorporate iron-sulfur clusters or form a

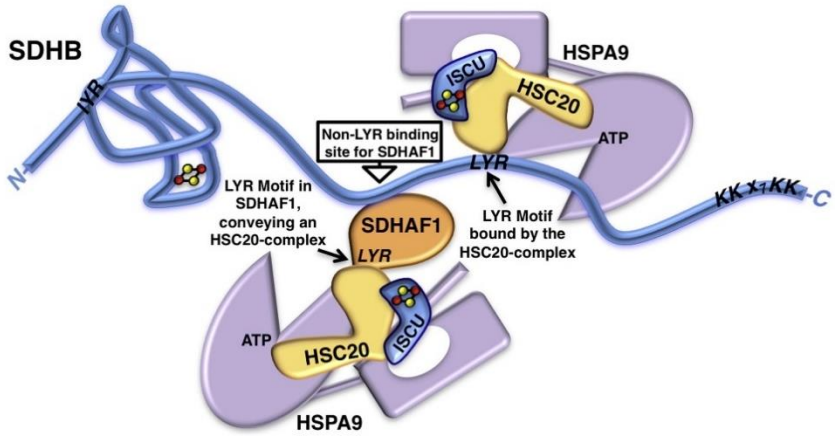

Figure 4. Maturation of SDHB. SDHB binds a complex consisting of ISCU, HSPA9, and HSC20, pre-loaded with iron-sulfur clusters through LYR motif-mediated binding. Assembly of this complex is mediated by SDHAF1. Reprinted from Cell Metab., Cochaperone binding to LYR motifs confers specificity of iron sulfur cluster delivery, Maio et al., 2014.

functional complex with the other SDH subunits (74). Just as important are the eleven cysteine residues that act as ligands for the three iron-sulfur clusters. Mutating an individual cysteine resulted in a complete loss of complex formation or activity. Further, the environment surrounding the iron-sulfur clusters seems to dictate their precise redox potentials, which is crucial in permitting electron flow. Forcefully adjusting the redox potentials by replacing hydrophobic residues surrounding the clusters with charged residues resulted in decreased enzyme activity (75).

Upon the maturation of both SDHA and SDHB, the catalytic dimer can then bind with SDHC and SDHD, forming a fully functional complex (76,77) (**Figure 5**). This process may be mediated by an additional SDHB-dedicated assembly factor, SDHAF3. The exact role of this protein is not fully understood, but it seems to shield the iron-sulfur groups from superoxide-mediated inactivation (78). The protection of SDHB until assembly is akin to that of SDHA

and SDHAF4 and highlights the importance of regulating unassembled activity from both catalytic subunits to protect the cell from reactive oxygen species (ROS).

c) SDHC and SDHD

SDHC and SDHD are small hydrophobic subunits (19 and 17 kDa, respectively) that anchor the SDHA-SDHB dimer to the IMM. The mechanism for their recruitment to the IMM is still unknown. The interface of SDHB, SDHC, and SDHD generates the first of two ubiquinone binding sites (proximal, Q_P), while the second (distal, Q_D) is located solely within SDHD (60,79). A recent analysis of the crystal structure of the human SDH complex confirmed the existence of a heme *b* group and a phosphatidylethanolamine phospholipid situated between SDHC and SDHD, which has been reported in other species (71). Both groups are believed to play a key role in maintaining the structural confirmation and integrity of the two anchor proteins.

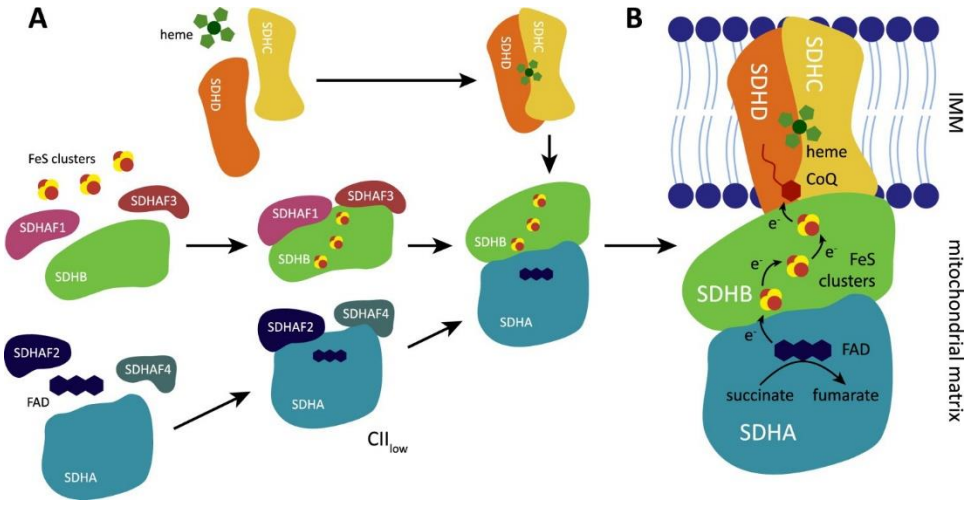

Figure 5. Assembly of the functional SDH complex. The maturation of SDHA and SDHB is dependent on multiple cofactors and occurs before complex assembly. An SDHA-SDHB catalytic dimer can form independently of SDHC and SDHD. Reprinted from Redox Rep., Mitochondrial complex II and reactive oxygen species in disease therapy, Hadrava Vanova et al., 2020. Permission was not required.

Aside from maintaining stability, a possible catalytic function of the heme *b* group has long been questioned. As electrons pass through the iron-sulfur clusters, they can ultimately be delivered to ubiquinone via heme *b* or to ubiquinone directly. However, electrons are most likely transferred directly to ubiquinone at the Q_P site due to closer proximity as well as a higher redox potential (60). In support of this, variants of the *E. coli* and yeast SDH complexes, which cannot bind heme, were found to maintain activity (80,81).

Despite these studies showing heme *b* may not be strictly required for activity, it has been suggested that heme *b* might play a protective role by dispersing electron density. This was proposed after a study investigated the distribution of electrons throughout *E. coli* SDH in the absence of ubiquinone (82). When heme *b* was present, electrons were effectively removed from FAD and moved through iron-sulfur clusters to heme *b.* However, without heme *b*, a significant proportion of electron density was measured within FAD, which could be damaging to the mitochondria via the production of ROS. Additionally, the reduction of ubiquinone occurs in two sequential steps, thus forming an intermediate semiquinone radical, which can also generate ROS. However, heme *b* has been found to stabilize this intermediate through electron equilibration (83).

While electrons can proceed through the iron-sulfur clusters to heme *b* in the absence of ubiquinone, this occurs at a significantly reduced rate (75). This supported the finding that individual mutations of key Q_P-site residues of yeast Sdh3 and Sdh4 impaired ubiquinone binding and complex activity to various

extents (84). Similar to that of the experiments performed above in *E. coli*, this inefficient or complete lack of ubiquinone reduction was associated with the production of ROS.

From converting succinate to fumarate and contributing to oxidative phosphorylation, SDH is critically involved in essential processes in cell biology. Given its importance, it is not surprising that complex mechanisms have evolved to mediate the maturation, assembly, and function of SDH. The fact that these mechanisms are highly conserved between prokaryotes and eukaryotes highlights the importance of regulating SDH function. The consequence of various defects for each subunit has been investigated by structural and functional analyses, which often reveal succinate accumulation, decreased OXPHOS, and ROS production. Given these findings and the importance of these processes in human biology, it is entirely unsurprising that defects in SDH function are associated with human disease.

2. SDH in human disease

Loss of SDH activity is associated with a wide spectrum of human diseases, including primary mitochondrial disease (PMD) and cancer. As mentioned in Chapter 1, disruption of any individual subunit often results in loss of activity for the whole complex. As such, genetic inactivation of each *SDH* gene, as well as several SDH assembly factors, have been identified as causing disease. While there is substantial overlap, each subunit seemingly has its own unique set of disease associations (85) (**Figure 6**). The genetics underlying

these SDH-deficient diseases, as well as their pathobiology, will be discussed in detail below.

3. Primary mitochondrial disease: Complex II deficiency

If there is a single concept that nearly everyone remembers from biology classes, it's that mitochondria are the powerhouse of the cell. The ubiquity of this adage is a testament to the role mitochondria play in providing energy to the cell. Disruption of this energy production can lead to the development of Mitochondrial disease, which consists of a heterogeneous group of disorders (86). A subset of Mitochondrial disease, PMD, is when this dysfunction is specifically caused by inherited mutations of the machinery directly involved in OXPHOS (87). As OXPHOS can contribute to as much as 90% of cellular adenosine triphosphate (ATP) production, tissues with high energy demand, such as brain and heart, muscles are particularly affected (88). As a result, the spectrum of PMD disorders associated with these pathogenic variants often manifests with encephalopathy and cardiomyopathy (87,89).

In 1988, the first genetic alterations in mitochondrial DNA (mtDNA) were discovered as a cause of mitochondrial myopathy (90). In subsequent years, only mtDNA mutations had been discovered in patients with PMD (91). It was not until 1995 that a homozygous mutation in a nuclear-encoded gene was identified in two sisters with the PMD Leigh syndrome (infantile sub-acute necrotizing encephalomyelopathy), a progressive neurodegenerative disorder characterized by focal bilateral lesions in the brain (92). This gene was *SDHA*. Since then, there have been multiple reports of PMD arising due to mutations in *SDHB*,

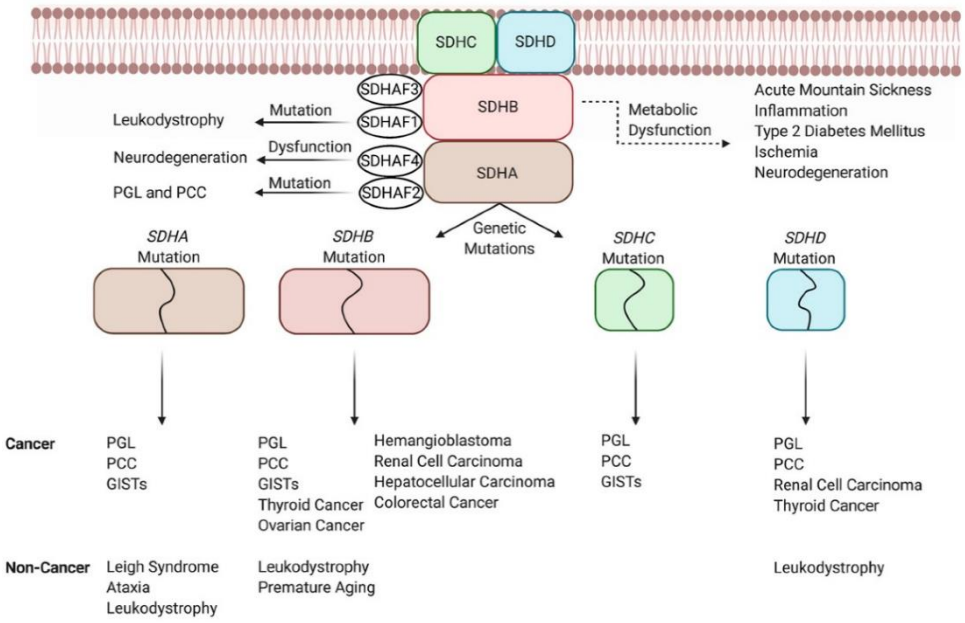

Figure 6. SDH-related human disease. Overview of the various cancer and non-cancer disorders associated with defects of each SDH subunit and assembly factor. Reprinted from Cancers (Basel)., Succinate Dehydrogenase and Ribonucleic Acid Networks in Cancer and Other Diseases, Moreno et al., 2020. Permission not required by copyright.

SDHD, and *SDHAF1;* however, the majority of cases involve *SDHA* (93). While patients display a spectrum of disease and severity, SDH-related PMD is typically associated with Leigh syndrome, leukodystrophy, and/or cardiomyopathy in early childhood (92-94). Complex II deficiency almost exclusively follows an autosomal recessive inheritance pattern, though there have been rare exceptions to this rule reported.

a) Complex II Deficiency: Germline biallelic inactivation

To date, a total of 24 pathogenic *SDHA* recessive variants associated with PMD have been reported in the literature. Twelve of these variants can be considered “null” variants that result in start-loss, early termination, or a frameshift. Typically, these variants exist as compound heterozygous mutations with a missense mutation, though there have been two reported cases of compound heterozygous frameshift mutations in *SDHA* (93).

There have also been 12 reported missense variants in *SDHA*, including c.1660C>T (p.Arg554Trp), the first Mendelian form of PMD reported. Two sisters who were homozygous for this variant presented with Leigh syndrome (92). Another variant observed exclusively as homozygous in patients is c.1664G>A (p.Gly555Glu). Reported in 17 individuals, this variant accounts for the majority of *SDHA*-related PMD, though 15 of these cases stem from two consanguineous families (95). Four additional missense variants, c.454G>A c.409G>C (p.Asp137His), (p.Glu152Lys), c.565T>G (p.Cys189Gly) and c.1571C>T (p.Ala524Val) have been identified with the null variants c.1A>G (p.Met1Val), c.91C>T (p.Arg31Ter) (second two), and c.1A>C (p.Met1Leu), respectively (96-98). In addition, there have been two reported cases which involved compound heterozygous missense mutations. One patient who presented with leukoencephalopathy harbored the mutations c.1523C>T (p.Thr508Ile) and c.1526C>T (p.Ser509Leu) (94). Another patient carrying c.1535G>A (p.Arg512Gln) and c.1753C>T (p.Arg585Trp) was reported without a clinical diagnosis but demonstrated motor disability and epilepsy starting at six months of age (99).

b) Complex II Deficiency: Germline heterozygous variants

Each variant described thus far was associated with an early age of onset, with most presenting symptoms before the age of one (93). Curiously, two sisters presenting with late-onset (mid-40s) bilateral optic atrophy and ataxia were reported to have Complex II deficiency (100). Subsequent sequencing analysis revealed a c.1351C>T (p.Arg451Cys) mutation for both sisters. Unlike all other cases described, these patients were heterozygous carriers (101). Twenty years

after this initial report, another affected family with the same heterozygous mutation was reported. The index patient presented with neurological symptoms and cardiomyopathy and, interestingly, was later diagnosed with bilateral optic atrophy in his mid-40s (102). The index patient's son, who was also heterozygous for p.Arg451Cys, had developed cardiomyopathy early in life as well as progressive bilateral optic atrophy by the age of 30.

More recently, a novel *SDHA* mutation, c.1984 (p.Arg662Cys), was identified in a patient who began to present with bilateral optic atrophy at 10 years of age (103). As with the previous cases of *SDH*-related optic atrophy, this mutation was also heterozygous. Biochemical analysis of patient-derived fibroblasts harboring heterozygous p.Arg451Cys or p.Arg662Cys variants confirmed a significant defect in SDH activity (40-60%), without a corresponding decrease in SDHA protein levels (101-103). As mentioned above, structural analysis and functional studies have shown the importance of the Arg451 residue of SDHA in flavinylation. A similar analysis of Arg662, located in the flavin-binding domain, revealed it may also play a key role in flavinylation, as it bonds with residues in the capping domain, likely aiding the stabilization of the open confirmation (56,103). Indeed, mutating the equivalent residue in yeast to alanine revealed diminished flavinylation, although Sdh1 remained stable (104). Together, these findings strongly suggest a possible, yet rare, dominant negative mechanism for stable SDHA variants with disrupted flavinylation, resulting in autosomal dominant inheritance of PMD with delayed onset, presenting primarily as optic atrophy.

c) SDH-deficient cancer

It is well established that loss of SDH function is associated with the development of multiple types of cancers. In fact, *SDHA, SDHB, SDHC, SDHD, SDHAF2,* and *SDHAF3* are considered classical tumor suppressors, with inactivating mutations in each having been linked to multiple cancer types (105-107). Most commonly, these include pheochromocytomas (PCs) and paragangliomas (PGLs), GIST, and renal cell carcinoma (RCC), but rare instances of others have also been reported (108,109).

(1) Genetics underlying SDH-deficient cancer

Following Knudson's "two-hit" hypothesis, bi-allelic inactivation of an *SDH* gene is required for tumor initiation. The majority of SDH-related cancers are hereditary and are associated with the inheritance of a germline pathogenic mutation (110). The second mutation is often loss-of-heterozygosity (LOH) of the WT allele, though a somatic mutation resulting in compound heterozygosity is not uncommon (108). Interestingly, an alternative mechanism for SDH-genetic inactivation was recently discovered. Killian et al. reported that hypermethylation of the *SDHC* promoter can result in loss of SDHC expression and concomitant loss of SDH activity (111). As this mechanism does not involve the inheritance of a germline mutation, it is not associated with hereditary cancer syndromes. Rather, *SDHC*-promoter hypermethylation is typically associated with Carney triad (CT) and, more rarely, sporadic PGL (112).

(a) Hereditary pheochromocytomas and paragangliomas

PC/PGLs are neuroendocrine tumors arising from neural crest cells. In 1933, the first case of familial carotid body tumors, a form of PGL, was reported

(113). In 1989, it was discovered that similar tumors were inherited almost exclusively via the paternal line, which is consistent with genomic imprinting (114). Over the next decade and several linkage analysis studies, two distinct genetic loci responsible for these tumors, termed *PGL1* and *PGL2*, were narrowed down to multi-megabase (Mb)-spanning regions of chromosome 11q23 and chromosome 11q13 (115-118). Finally, in 2000, the identity of *PGL1* had been determined: *SDHD* (119). Thus, the first link between SDH and cancer had been discovered.

PC/PGL is now recognized as one of the cancer syndromes with the highest rate of heritability (~40%) (120). As with *PGL1* and *PGL2*, several other distinct hereditary PGL syndromes were identified before their molecular driver had been known. These syndromes were given the nomenclature PGL1-5. After *PGL1* was discovered to be *SDHD*, other SDH-related genes were investigated, ultimately revealing mutations in *SDHAF2, SDHC, SDHB,* and *SDHA* were associated with PGL2, PGL3, PGL4, and PGL5, respectively (121). Collectively, *SDH*-mutant PC/PGL accounts for nearly half of all hereditary cases (105). As discussed, PGL1 and PLG2 demonstrate genomic-imprinting patterns, while the others follow classical autosomal dominant inheritance. While mutations in *SDHB* and *SDHD* are the most common, mutations in *SDHA* may contribute to as much as 3% of hereditary PC/PGL (108).

(b) Carney Triad and Carney-Statakis Syndrome (CSS)

First reported in 1977, CT was described as the sporadic co-occurrence of PGL, GIST, and pulmonary chondroma within the same individual, with unknown genetic etiology (122). Over 20 years later, a similar but distinct syndrome, CSS,

was described, of which only PGL and GIST were present. However, a key difference between the two syndromes was that CSS was inherited in an autosomal-dominant pattern, whereas CT was not heritable (123). By the late 2000s, the *SDH* genes and *KIT/PDGFRA* were known drivers of PGL and GIST, respectively. Thus, mutational analysis of these genes was performed to investigate their role in CT and CSS. Curiously, no mutations were found in any CT patients (124). It was later discovered that *SDHC*-promoter silencing is likely the cause of these CT cases. Conversely, molecular investigation of patients with CSS revealed germline mutations in *SDHB, SDHC,* and *SDHD* (125,126). This represented the first discovery of genetic inactivation of SDH associated with a hereditary form of GIST.

(c) Hereditary Gastrointestinal stromal tumors

The history of hereditary *SDH*-mutant GIST not associated with PGL (CSS) is somewhat convoluted. As mentioned above, a small subset of GISTS have no known RTK mutations, termed WT-GIST. Interestingly, when distinguishing patients by age group, the proportion of these WT tumors shifts; 15% of adult GISTs are RTK-WT, whereas it is 85% of pediatric cases (49). In 2010, Gill et al. noted that even though pediatric GISTs did not co-occur with PGL, they resembled the clinical features of CT and CSS-related GISTs more so than sporadic RTK-driven GISTs (127). At the time, germline mutations in *SDH* genes were a known cause of CSS, whereas several studies searched but failed to find *SDH* mutations in CT patients. Pediatric GISTs appeared to be sporadic; thus, the authors speculated that they may be the same types of tumors that

appear in CT. As such, they presumed an *SDH*-WT status and instead turned their focus to a different diagnostic marker: SDHB.

Immunohistochemical (IHC) analysis of SDHB protein was identified as a strong predictor of a mutation in *SDHB*, *SDHC*, or *SDHD* in PGL (128). However, one study identified several PGL tumors displaying loss of SDHB protein in the absence of *SDH* mutations (129). Based on these findings, Gill et al. proposed that these PGL could actually be cases of CT, with only one triad presenting. They further speculated that, like CSS, CT is characterized by loss of SDH function, but unlike CSS, this is caused by factors other than mutations in the *SDH* genes. Therefore, they hypothesized that pediatric GISTs had a dysfunctional SDH complex and that these tumors could be identified using SDHB IHC analysis. Indeed, in their investigation of pediatric GISTs, IHC analysis revealed loss of SDHB, leading to their conclusion that pediatric GISTs are the same tumors that arise in CT (127). While this was the first study to demonstrate a distinct subset of GISTs could be identified via SDHB-IHC, they critically did not perform a genetic sequencing analysis of their cohort.

Less than a year later, a seminal study by Janeway and colleagues supported the findings of Gill et al. but provided additional genomic context. In this work, the authors show WT-GISTs, both pediatric and adult, display markedly decreased levels of SDH activity and SDHB protein (49). Of their cohort consisting of 34 WT cases, four (12%) were found to carry germline mutations in *SDHB* and *SDHC*, representing the first reported cases of *SDH*-mutant GIST not associated with CSS. Nonetheless, no *SDH* mutations were identified in the

remaining SDH-deficient WT-GISTs. Up to this point in time, only a single report of an *SDHA*-mutant PGL had been reported; thus, its involvement in cancer was not well established (130). As such, the authors noted that *SDHA* sequencing was performed for only four samples, and further investigation into *SDHA* was warranted.

This further investigation came quickly, as again, less than one year later, massively parallel, whole-transcriptome sequencing was used to search for mutations in two young adult patients with WT-GIST. This analysis revealed three mutations in *SDHA:* a homozygous nonsense variant c.1151C>G (p.Ser384Ter) in one patient, and heterozygous variants c.91C>T (p.Arg31Ter) and c.1765C>T (p.Arg589Trp) in the other (131). While this was a small sample, the authors speculated that inactivation of *SDHA* could be a common oncogenic event in WT-GIST.

Over 10 years later, this turned out to be very much the truth. It is now recognized that SDH-deficient GISTs account for roughly 9% of all GISTs (38). As Gill and others speculated, 25-50% of these tumors are indeed sporadic and are driven by the same mechanism as CT: *SDHC* promoter epimutation (132,133). However, 30-40% are caused by mutations in *SDHA*, with the rest attributed to mutations in other SDH-related genes or remain unknown (108,133,134). The majority of *SDH*-mutant GISTs occur in the context of a germline mutation, and it has since been appreciated that there is a hereditary component, though with variable penetrance (135). It remains unclear whether stand-alone GISTs represent cases of CT and CSS for only the single triad had

developed at the time of diagnosis. However, a recent analysis indicates mutations in *SDHA* mainly predispose carriers to GIST, and the authors suggest *SDHA*-mutant GIST may be distinct from CSS (136).

(2) Pathobiology of SDH-deficient cancer

The genetic inactivation of SDH-related genes results in tumors characterized by pseudohypoxic signaling (137). Historically, the mechanism by which SDH deficiency promotes this phenotype has been controversial. Early studies identified loss of SDH activity initiates hypoxia-inducible factor-1α (HIF-1α) signaling in tumors (138-140). Two models attempting to explain this aberrant signaling were proposed, both implicating the inhibition of HIF prolyl hydroxylases (PHDs) but by different mechanisms (140). In normoxia, HIF-1α degradation is mediated by PHD and the Von Hippel-Lindau protein (pVHL). As an α-ketoglutarate (α-KG)-dependent dioxygenase, the PHD reaction requires the substrate α-KG as well as the cofactors ascorbate and ferrous iron. As ascorbate and iron can be oxidized by hydrogen peroxide, which had been shown to inhibit PHD, the first model proposed that pseudohypoxia was a result of ROS produced upon SDH deficiency (141,142). The possibility of this was supported by functional studies in *E. coli*, *Caenorhabditis elegans*, and mouse fibroblasts demonstrating defects of SDH results in oxidative stress (82,143). However, despite the findings in these model systems, they had not been supported by several studies of SDH-deficient tumors (138-140,144).

An alternative explanation for HIF-1α stabilization was linked to succinate, which is both the substrate of SDH as well as a product of PHD. Interestingly, it

had been shown that at high concentrations, succinate could inhibit PHDs through competitive product inhibition, and the treatment of SDH-deficient cells with a cell-permeable analog of α-KG could overcome this inhibition and successfully revert pseudohypoxia (145,146). Seminal works by Selak and Pollard demonstrated that succinate accumulates upon SDH dysfunction and that this is sufficient to activate pseudohypoxic signaling in an ROS-independent manner (139). Nonetheless, Guzy et al. opposed this mechanism, stating that the inactivation of all SDH subunits would equally result in succinate accumulation, and at the time, mutations in *SDHA* had only been linked to PMD (147). The authors conducted experiments that showed that a loss of SDHB, but not SDHA, resulted in the accumulation of ROS. As such, they concluded that ROS production was the specific trigger of tumorigenesis. However, less than three years after this study, the first case of *SDHA* mutant cancer was reported, further supporting the succinate model (130). With that said, the contribution to pathogenesis by ROS cannot be discredited and may explain the gene-specific cancer associations described above.

Since then, the contribution of succinate to cancer has been further established, leading to its classification as an oncometabolite, a relatively new term to describe metabolites whose accumulation drives oncogenic pathways (148). In addition to PHD, the accumulation of succinate has been found to inhibit other α-KG-dependent dioxygenases, including ten-eleven translocation (TET)-family methylcytosine dioxygenases and Jumonji-C family of histone lysine demethylases (KDMs). As such, SDH-deficient cancers are also characterized by

epigenetic dysregulation due to global DNA and histone hypermethylation (**Figure 7**) (149,150).

The consequences of aberrant HIF-1α signaling and epigenetic reprogramming that occur in response to loss of SDH activity can explain how SDH-related genes are tumor suppressors. Pseudohypoxic signaling promotes angiogenesis and growth signaling through the upregulation of vascular endothelial growth factor (VEGF) and insulin-like growth factor-1 (IGF1) (151). In

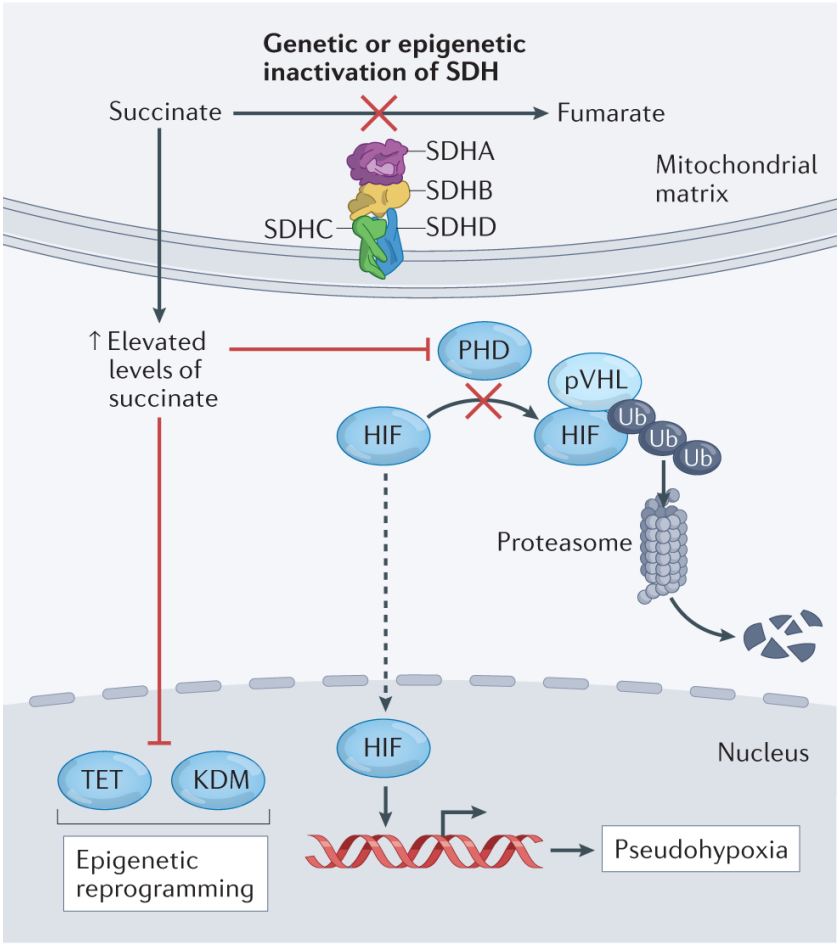

Figure 7. Pathobiology of SDH-deficient cancers. The loss of SDH activity results in the accumulation of succinate, leading to the inhibition of α-KG-dependent dioxygenases, such as TET-, KDM-, and PHD-family enzymes. This inhibition results in epigenetic reprogramming and pseudohypoxia, characteristic features of SDH-deficient tumors. Reprinted from Nat. Rev. Clin. Oncol., New treatment strategies for advanced-stage gastrointestinal stromal tumours, Klug et al., 2022. Copyright jointly held.

SDH-deficient PGL, the altered epigenetic landscape was linked to neuroendocrine dedifferentiation and epithelial-to-mesenchymal transition activation (150). In SDH-deficient GIST, CpG island hypermethylation was found to alter CTCF-insulator topology, leading to upregulation of the *FGF4* oncogene (152). Additionally, TET-family proteins have been described as tumor suppressors; thus, their inhibition activates oncogenic pathways (153,154).

(3) Current management of SDH-deficient cancer

(a) Treatment strategies

Historically, there have been no effective medical therapies for the treatment of unresectable or metastatic SDH-deficient cancer. In SDH-deficient GIST, the objective response rate of imatinib treatment is <5%. The second-line TKI, sunitinib, has had moderately better results, with a partial response rate of ~15% (155). This increased efficacy may relate to the fact that sunitinib also inhibits VEGFR, a tumorigenic pathway activated upon SDH deficiency. Interestingly, regorafenib and pazopanib, which also inhibit VEGFR, had shown moderate success in stabilizing SDH-deficient tumors in phase II trials (156,157). Another phase II trial investigated the use of linsitinib. This TKI targets IGF-1R, which is also upregulated in SDH-deficient GIST, though no objective responses were seen (158).

More recently, the potential use of the alkylating agent temozolomide (TMZ) has become promising and warranted a phase II clinical trial for its treatment of advanced-stage SDH-deficient GIST. Traditional cytotoxic therapeutic agents, including TMZ, have had limited success in GIST patients, which necessitated the development of TKIs (159). However, just as imatinib was

found to be highly effective only for a specific subset of patients, the efficacy of TMZ for SDH-deficient tumors may have been underestimated, as these distinct molecular drivers had not been identified at the time of clinical trials (132). Indeed, a study found the treatment of *SDHB*-mutant PGL with TMZ resulted in a 33% partial response rate and 47% of patients having stable disease (160).

The mechanism of TMZ-sensitivity is believed to be linked to the suppression of the DNA dealkylating enzyme O-6-methylguanine-DNA methyltransferase (MGMT) by promoter hypermethylation (161) (**Figure 8**). Analysis revealed that SDH-deficient GISTs are specifically associated with *MGMT* promoter methylation, suggesting that it may be a non-random and common occurrence resulting from SDH-deficient-global-hypermethylation (162). Patient-derived models of SDH-deficient GISTs supported the sensitivity of these tumors to TMZ (163). Lastly, in a study investigating five SDH-deficient GISTs, two partial responses and three stable diseases were reported, while another study reported a partial response for the sole patient (164).

Despite the promising outlook of TMZ for the treatment of SDH-deficient cancers, surgical resection may offer the best therapeutic outcome. If detected before metastasis, surgical resection of PC/PGL tumors can often be considered curative, with a 1-5% rate of recurrence per year (165). However, it is worth noting that *SDHB*-mutant PC/PGL is strongly associated with an increased risk of metastasis and recurrence (166).

The surgical management of GIST is generally similar, with a reported 15-year recurrence-free survival of 60% (roughly equating to a 3% rate of

recurrence per year), though several studies have indicated surgery is less frequently curative for SDH-deficient GIST compared with RTK-mutant GIST (167). For instance, a retrospective analysis of 76 RTK-WT GISTs reported a 2.5-year median event-free survival, with 71% of patients experiencing tumor recurrence or disease progression (168). Another study by Mason and Hornick reported that 26% of SDH-deficient GISTs developed a gastric recurrence, with a mean of 6.6 years post-resection (169). Another study by Tirumani et al. reported that 35% of patients had a recurrent tumor with a median occurrence of 4 years (170).

In addition to primary recurrence, SDH-deficient GISTs are associated with significantly higher rates of metastasis than non-SDH-deficient GISTs, which frequently develop after surgical resection of the primary tumor (132). In the

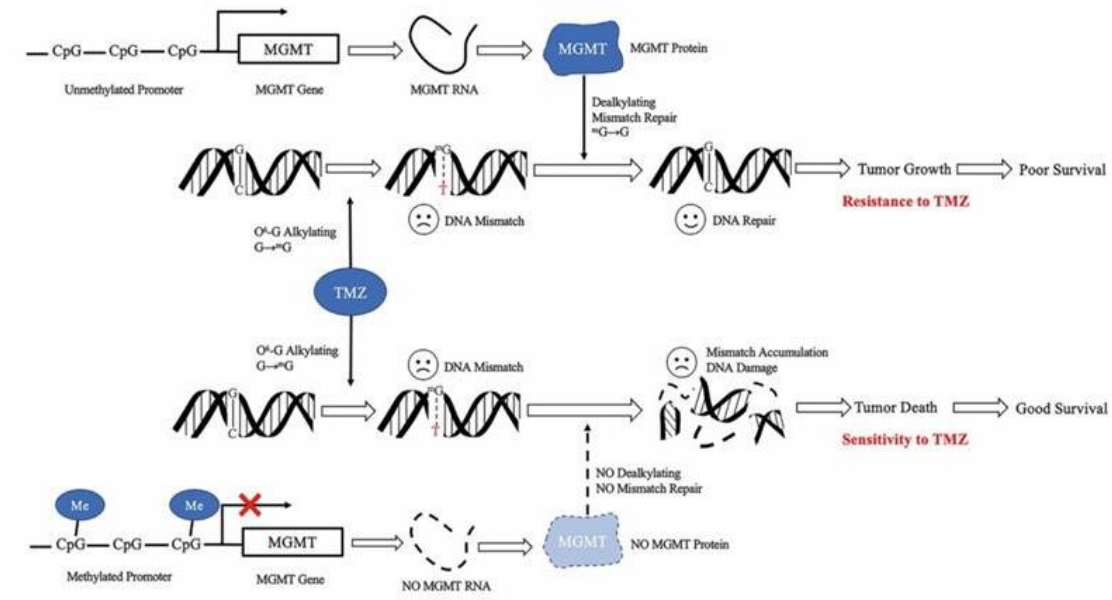

Figure 8. Mechanism of TMZ-sensitivity. The alkylating agent TMZ induces DNA damage. This DNA damage can be repaired by MGMT, providing resistance to cell death. In SDH-deficient tumors, the MGMT promoter is often hypermethylated, resulting in decreased protein expression, thus sensitizing cancer cells to TMZ. Reprinted from J Cancer, Clinical strategies to manage adult glioblastoma patients without MGMT hypermethylation, Liu et al., 2022. Permission not required by copyright.

same study by Mason and Hornick, 40% of patients had developed lymph node metastases, while 74% had developed distant metastases, primarily to the liver. Nonetheless, due to its indolent nature, SDH-deficient GISTs are associated with relatively good overall survival, even in the face of metastatic disease. In the study by Tirumani and colleagues, six metastatic patients died with a median survival of 9.1 years following the diagnosis of metastasis. An additional 22 patients with metastatic disease were still alive, with a median follow-up of 7.3 years.

Due to the high rate of recurrence and metastasis, close follow-up is essential for these positive outcomes (132,171). However, genetic testing is crucial in influencing the quality and rate of follow-up. As SDH-deficient tumors have distinct clinical features and outcomes than non-SDH-deficient tumors, knowing the SDH mutational status can inform clinical decisions. In a multi-center retrospective study of 221 *SDH*-mutant PC/PGL subjects, those who received genetic testing (‘Genetic’ group) within a year of cancer diagnosis had a significantly higher rate of follow-up than those whose mutational status was unknown (‘Historic’ group). Notably, the mean number of complete follow-ups per year for the Genetic group was 0.89 compared to 0.13 for the Historic group. Upon receiving genetic testing, those in the Historic group received more follow-ups, comparable to that of the Genetic group (mean follow-ups per year = 0.9). Due to this enhanced follow-up, new tumors and metastases were detected earlier and were significantly smaller for the Genetic

group (**Figure 9**, top) (172). This also corresponded to a better survival rate following metastasis (**Figure 9**, bottom).

(b) Tumor Surveillance

The early detection of recurrent, secondary, or metastatic tumors enhanced by genetic testing also applies to the initial diagnosis of a primary tumor. As described above, inheriting a germline pathogenic mutation in a *SDH* gene increases the lifetime risk of developing a SDH-deficient tumor. Patients can often harbor asymptomatic tumors; thus, regular tumor screening is recommended once a germline pathogenic *SDH* mutation is identified through genetic testing (173,174). An international consensus on the initial screening and follow-up of asymptomatic *SDH*-mutant carriers with a focus on PC/PGL was recently developed. As patients have been found to develop tumors at very young ages, screening is recommended starting at 5-10 years old, depending on the *SDH* gene mutated (174,175). Patients under 18 years of age are recommended to receive clinical follow-up every year, with biochemical assessments every other year. Additionally, they should be assessed by MRI-imaging every 2-3 years. Similar follow-ups are recommended for adult patients, except with biochemical assessment every year.

(c) Genetic testing

As mentioned, knowing the *SDH* mutation status has significant implications for the clinical care of both affected and asymptomatic carriers. Thus, genetic testing has become an important component of routine care. In patients presenting with PC/PGL, germline testing for all associated genes is recommended, regardless of age or family history (176). As SDH deficiency is

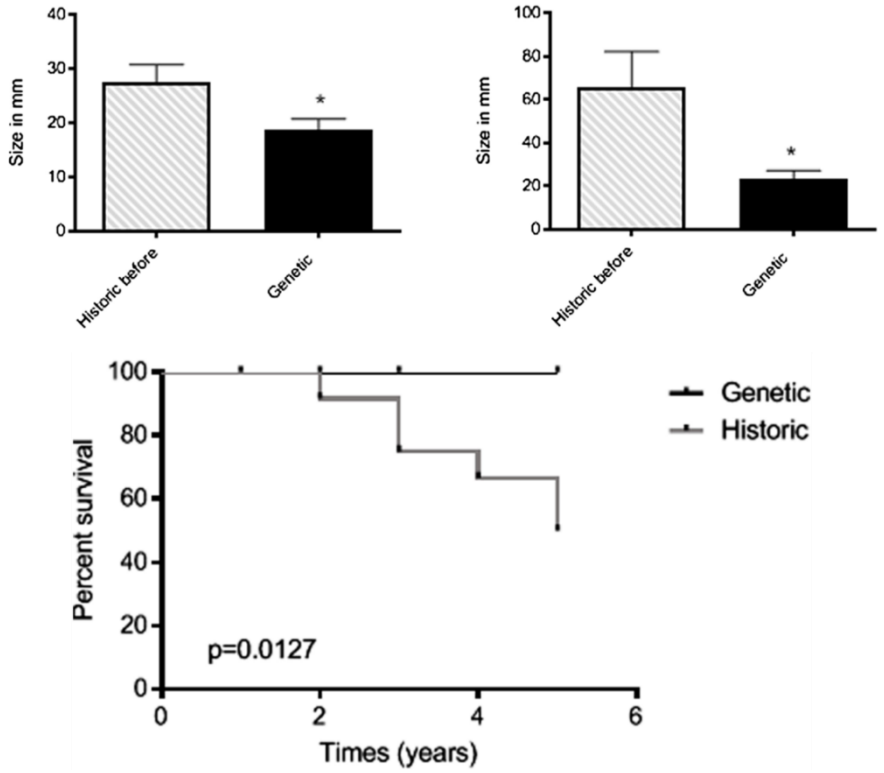

Figure 9. Improved outcomes associated with genetic testing. The size of new tumors (upper left) and metastases (upper right). The survival of patients following the first diagnosis of metastasis (bottom). 'Genetic' describes patients who received genetic testing within one year of initial diagnosis. 'Historic before' and 'Historic' both describe patients before receiving genetic testing. Reproduced from J. Clin. Endocrinol. Metab., Positive Impact of Genetic Test on the Management and Outcome of Patients With Paraganglioma and/or Pheochromocytoma, Buffet et al., 2019, with permission from Oxford University Press.

less common in GIST, it is not immediately investigated. Instead, sequencing for *SDH* genes is performed if there is an absence of mutations in *KIT* and *PDGFRA*¸ and subsequent SDHB IHC analysis is negative (132).

As pathogenic mutations can be inherited, family members of affected patients should also be recommended for genetic counseling and genetic testing (109,177). *SDH* mutations can also be found as a secondary or incidental finding from a genetic test given for another purpose. As described above, the advancements in sequencing technology have enabled the widespread use of MGPs to maximize actionable findings. These MGPs can contain hundreds of

genes and often include SDH-related genes. In fact, each *SDH* gene appears in over 200 different NIH-registered genetic tests, which can lead to the identification of at-risk patients. As I have previously emphasized, the identification of germline *SDH* mutations is critical to the clinical management of patients. While some therapeutic options are promising, surgical resection remains the only chance for a cure. Asymptomatic carriers are at high risk for cancer throughout their lifetime. To improve the likelihood of detecting tumors at early stages, at-risk patients need enhanced tumor surveillance, starting from a young age. However, there is a crucial caveat to the above statements: carriers of germline mutations in *SDH* genes are only clinically considered at-risk if the mutation is *known* to be pathogenic. While genetic sequencing is crucial for the clinical management of SDH-deficient cancer, its utility is limited by our ability to interpret the results.

C. Clinical variant interpretation

The English language is simply complex, often requiring you to read and re-read what you just read. Even with all your might, it might take you a whole minute to see you missed a minute detail in the sea of words, which changes the meaning. It is important to write words the right way, as there are a lot of rules. It is hard to remember what is allowed, but it helps if you say it aloud. Language is an intricate knot that is difficult to unravel, but the effort is not for naught, for knowing how to interpret the meanings of words in the context of their sentences is essential for effective communication.

Having a deep understanding of the language also allows us to identify typographical errors and determine if and how they may affect the meaning of a sentence. “The cat is fit” is a simple sentence that conveys a clear meaning. If an error resulted in a change to “The kat is fit,” we would instantly recognize the mistake, but the original meaning could still be inferred. “The cat is fat” would be harder to identify at first, but if we had a larger context or a reference for comparison, we would know it was incorrect. Even though it is just a single letter, we understand that this error drastically changes the meaning of the sentence, which has significant implications for the health of the animal. However, without fully understanding the language, it is exceedingly difficult to interpret mistakes.

Just as individual letters create words that, when combined, form sentences that convey meaning, nucleotides are the building blocks of genes, which encode proteins that perform functions. In recent decades, the advances in genomic sequencing technology have enabled us to identify the vast number of “typos” in our genomes. However, we do not fully understand the genetic language and struggle to determine how mutations could affect the function of proteins.

We are not entirely uninformed. Genome-wide association studies can be used to identify associations between specific single-nucleotide polymorphisms (SNPs) and phenotypes (178). These have enhanced our ability to find associations between diseases and genes but do not inform us about individually rare variants within those genes. As genetic testing has become increasingly accessible, the rate of novel variant identification has skyrocketed, and we simply

cannot keep up (179). Recommendations for how to utilize available evidence to determine the clinical significance of variants have been issued, and several databases have been developed to encourage the sharing of variant-level evidence and classifications. Despite these efforts, there is often insufficient evidence to make clear determinations, and as a result, genetic testing is often uninformative.

1. Guidelines for clinical variant interpretation

Even before the rapid rise of NGS use in clinical settings, the importance of variant interpretation was recognized. In 2000, the American College of Medical Genetics and Genomics (ACMG) released a set of recommendations for the clinical interpretation of variants. These recommendations have since been updated twice and now exist as joint standards and guidelines issued in conjunction with the Association for Molecular Pathology (AMP). ACMG/AMP provided a framework for combining types of evidence to classify a variant as 'pathogenic', 'likely pathogenic', 'uncertain significance', 'likely benign', or 'benign' (180). The evidence that can be used to make these assertions include population and segregation data, computational predictions, and functional analysis, among others, where each is given a different level of strength ('supporting', 'moderate', 'strong', or 'very strong' (**Figure 10**) (180,181). The final classification is then made according to the combination of all evidence.

More recently, the Clinical Genome Resource (ClinGen) Sequence Variant Interpretation Working Group (ClinGen SVI WG) suggested the ACMG/AMP guidelines were insufficient due to their qualitative nature. Instead, they proposed

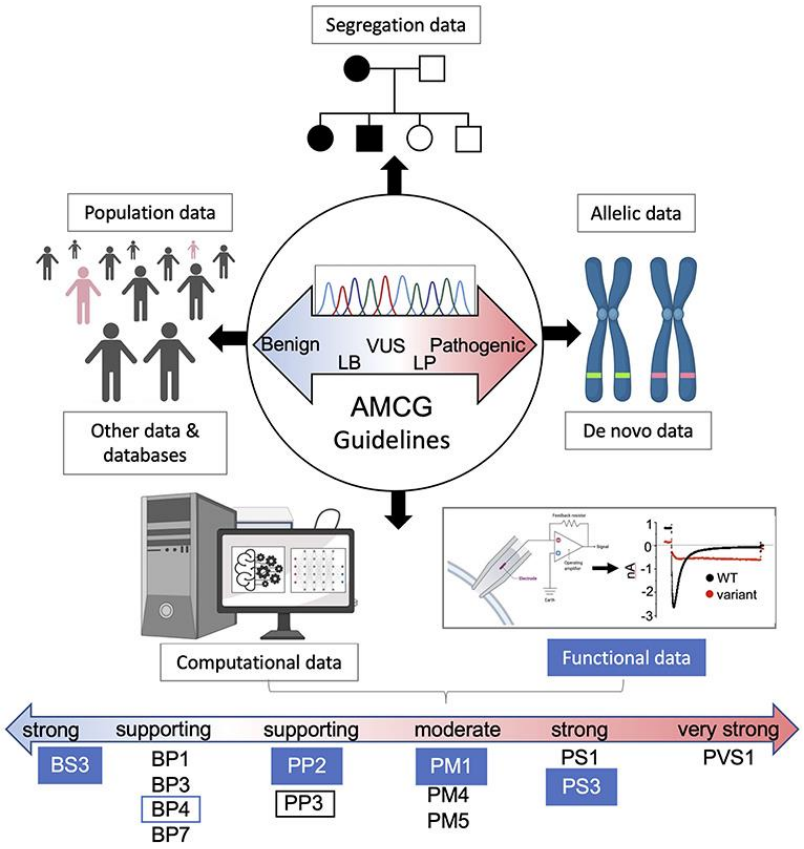

Figure 10. Guidelines for clinical variant interpretation. Multiple types of evidence are combined to reach classifications regarding the pathogenicity of a variant. Each type of evidence can be assigned varying degrees of evidence strength. Reproduced from Front. Cardiovasc. Med., How Functional Genomics Can Keep Pace With VUS Identification, Anderson et al., 2022. Permission not required by copyright.

to transform the guidelines into a Bayesian classifier, which can yield a quantitative estimate of pathogenicity for any combination of evidence (182). Several commercial companies that offer clinical genetic testing services have also developed their own framework for variant interpretation, though they are often based on the ACMG/AMP guidelines (183).

It has also been recently appreciated that many genotype-phenotype relationships have idiosyncrasies, and a general approach to variant interpretation may not be optimal. As such, Variant Curation Expert Panels (VCEPs) are being formed to incorporate gene- and disease-specific expertise

for variant interpretation (184). When variant interpretations are made, they are often deposited to databases such as ClinVar, providing a resource for clinicians and researchers to learn from the evidence obtained by others.

2. Variants of uncertain significance

Regardless of the specific variant interpretation framework used, they all generally incorporate the same types of evidence listed above. However, many of those types of evidence necessarily require more carriers than are typically found for rare variants, and thus, the evidence cannot be applied (179). Population data can also be uninformative with incomplete penetrance. When there is insufficient evidence to reach a ‘likely benign’ or ‘likely pathogenic’ classification, the variant becomes a variant of uncertain significance (VUS).

Our lack of ability to properly assess the clinical significance of rare variants is problematic because the rate of rare variant identification is ever-increasing. To put the scale of this problem into perspective, the Genome Aggregation Database (gnomAD), which currently includes less than 200,000 exomes and genomes, contains nearly five million missense variants (185). To date, over 400,000 single-nucleotide missense variants have been reported in ClinVar, and a staggering 78% have conflicting reports or are considered VUS (186). As these variants cannot be used to guide clinical decisions, we must first improve our ability to interpret VUS before most patients can benefit from genetic testing (180).

3. The utility of functional evidence

Functional evidence perhaps has the highest potential for improving clinical variant interpretation because it does not require the identification of carriers or affected patients. Importantly, it can be considered as ‘strong’ evidence following ACMG/AMP guidelines. Computational predictions can also be made, but these tools also often require choosing between a high false positive rate and a low sensitivity (187-192).

The potential of functional evidence is highlighted by its remarkable capability to reclassify VUS when added to existing data, particularly in the identification of likely pathogenic variants. In the Bayesian classification scheme mentioned above, there are almost 80,000 unique combinations of evidence that would result in a VUS classification in the absence of functional data. If functional evidence were available to demonstrate the variant as a damaging effect, 76% of these combinations would now have sufficient evidence to reach a ‘likely pathogenic threshold (**Figure 11**) (193).

The impact of some genetic alterations can be obvious, such as in the case of large genomic rearrangements or deletions of exons. Similarly, the effect of several types of small nucleotide variants (SNVs) can be easily inferred, such as the “null variants”, which include nonsense, frameshift, and mutations (180). Conversely, the consequences of missense mutations, which alter proteins at a single amino-acid residue, are much more difficult to predict. This is in large part due to the plethora of ways a missense variant could affect a protein, but also in the uncertainty in how any changes relate to disease. In these cases, functional

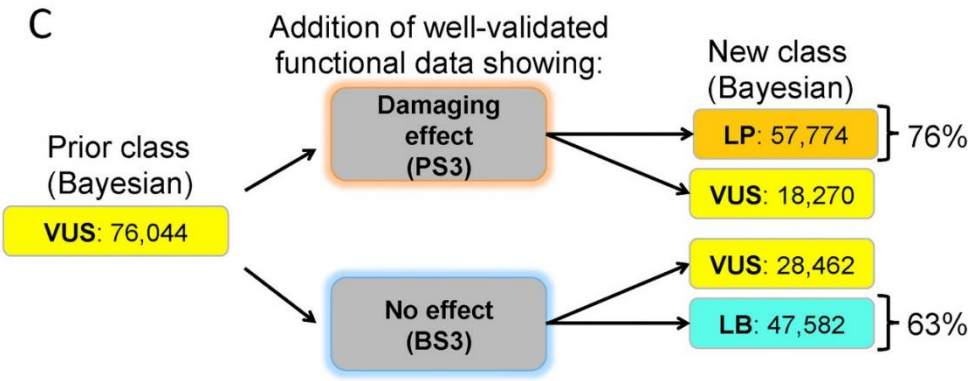

Figure 11. The potential of functional data for VUS reclassification. When functional evidence is added to existing combinations of evidence that reached a VUS classification in the Bayesian framework, the majority of combinations can be reclassified as 'likely pathogenic' (LP) or 'likely benign' (LB). Reproduced from Hum. Mutat., Quantifying the potential of functional evidence to reclassify variants of uncertain significance in the categorical and Bayesian interpretation frameworks, Brnich et al., 2018, with permission from John Wiley and Sons.

assays allow us to directly interrogate the consequence of variants on function and evaluate the corresponding significance in a disease-relevant context.

Several groups have developed recommendations for the design of functional assays to ensure the data is being utilized appropriately (194). An essential component is that the assay readout captures the mechanism associated with disease. For instance, assays that specifically determine protein abundance have been used when protein instability is associated with pathogenicity (195). Alternatively, the assays that probe the consequence of specific catalytic functions may be more informative for informing disease risk, such as for DNA repair by BRCA1/2 (196). Functional assays can also reveal multiple molecular mechanisms underlying dysfunction, which could result in distinct disease associations, as evidenced by studies investigating both PTEN variant stability and phosphatase activity (197,198).

Functional assays can exist in several different formats, from *in vitro* to cell-based, using model organisms or human-based (199). Assays can also be

designed to interrogate individual variants in a piecemeal approach, or more recently, thousands of variants can be assayed simultaneously via deep mutational scanning (DMS) of saturation mutagenesis libraries (179,194).

With the ever-increasing number of variants identified, we fall proportionally behind in our ability to confidently interpret their clinical significance. Developing functional models for genes with clear disease associations will provide meaningful and actionable insights for the direct benefit of patients, including those harboring *SDH* VUS.

D. Succinate dehydrogenase variants of uncertain significance

To date, over 2,300 missense *SDHA, SDHB, SDHC,* and *SDHD* variants have been reported in ClinVar. As many of these variants are rare and the penetrance of *SDH*-associated cancer is incomplete, there is often insufficient evidence to reach a Benign/Likely Benign (B/LB) or Pathogenic/Likely Pathogenic (P/LP) classification. In fact, over 90% of the *SDH* variants reported in ClinVar are classified as VUS (**Figure 12**). Our lack of ability to interpret variants is even more apparent when looking specifically at *SDHA*. The *SDHA* coding sequence is larger than the other three combined, and correspondingly, just over half of the *SDH* variants reported in ClinVar belong to *SDHA.* However, the number of *SDHA* variants classified as B/LB or P/LP is much less than the other genes, with a frightening 97.8% containing VUS classifications.

1. The uncertainty surrounding SDHA clinical variant interpretation

Several factors have likely contributed to the dire state of *SDHA* variant interpretation. The first and most obvious factor is that its association with cancer

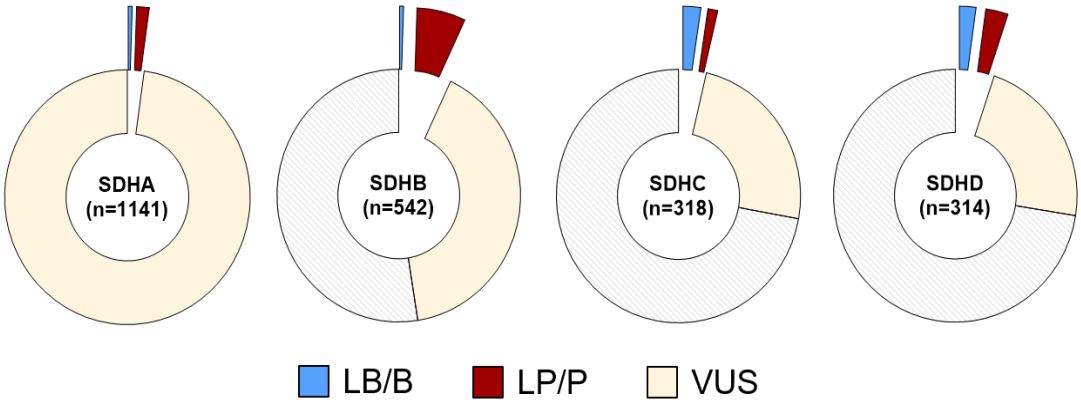

Figure 12. ClinVar classifications of SDH missense variants. The proportion of likely benign/benign (LB/B), likely pathogenic/pathogenic (LP/P), or VUS classifications for the SDHA/B/C/D missense variants reported in ClinVar as of August 1, 2023 (186). Variants with conflicting classifications were considered VUS. All sections were made proportional by adjusting the total count for each gene equal to that of SDHA (n=1141).

was discovered much more recently than that of the other SDH subunits. In the early days of uncovering SDH-deficient tumors, *SDHA* sequencing was not included. As expected, this led to the discovery of several patients harboring SDH-deficient tumors but were declared *SDH*-WT (124,129). We now know a likely cause of these tumors was pathogenic *SDHA* mutations or *SDHC* promoter hypermethylation.

Once genetic inactivation of *SDHA* was identified as a cause of cancer, the reporting of these variants should have increased. Since this discovery, there have been numerous studies investigating various features of *SDHA*-mutant cancer, including further establishing its association with different cancers, characterizing the pseudohypoxic or hypermethylation phenotypes, and investigating the role of SDHA/SDHB IHC analysis for diagnosis. Altogether, there are low-hundreds of tumors that were reported to contain mutations in *SDHA*. Yet, the specific mutations identified across all these studies were seldom

reported. Thus, variants repeatedly appearing in multiple tumors could not be readily identified.

While reporting mutations identified during sequencing analysis should be the minimum standard, it is not informative if the analysis is incomplete. In 2012, soon after it was first associated with GIST, a group performed *SDHA* sequencing analysis on a cohort of RTK-WT GISTs. One of their findings was a somatic SDHA mutation, c.113A>T (p.Asp38Val) (200). Their analysis showed loss of SDHB by IHC, consistent with SDH-deficient tumors. Loss of SDHA protein by immunoblotting was also shown, which the authors speculated could be due to instability caused by the mutation. A major limitation of this study was that only 3 of the 15 *SDHA* exons were sequenced for this sample. To the authors' credit, this limitation was acknowledged; however, the variant should not be interpreted with such limited information. This particular variant is the third-most frequently observed *SDHA* missense mutation in the gnomAD database, with a reported allele frequency of 3.45%, and is highly unlikely to be pathogenic.

The unfortunate existence of four highly homologous pseudogenes has also complicated sequencing analysis, thus interfering with our ability to interpret the clinical significance of *SDHA* variants. These pseudogenes generated from chromosome duplicates have 92-98% sequence identity with *SDHA* exons and flanking intron sequences (201). While they are not expressed and have no impact on SDH function, the pseudogenes have been found to harbor their own mutations, which may have led to misinterpretations. For example, a group of

researchers reported on a novel method for analyzing *SDHA* mutations via long-range NGS. For one of their samples, standard Sanger and capture-based NGS analysis revealed the variant c.1799G>A (p.Arg600Gln); however, the long-range NGS analysis revealed it was actually a SNP in one of the pseudogenes (202). Interestingly, this variant contains one B/LB submission in ClinVar, though no explanations or evidence for the interpretation were provided. Nonetheless, one could envision a scenario in which the lack of pathogenicity determined by the submitters was, in fact, because the variant was actually within a non-functional pseudogene. This would be highly problematic if the variant were actually pathogenic. As it happens, this variant has been identified in several patients with SDH-deficient PGL and GIST (133,136,203-205). It is unclear to what extent the presence of pseudogenes may have confounded previous reports, as they were not all discovered at the same time. For instance, in the seminal paper reporting the very first existence of an SDHA mutation associated with cancer, Sanger sequencing primers were specifically designed to avoid amplifying the pseudogenes, but only two were known at the time (130).

Another example of a possibly misclassified *SDHA* variant due to sequencing issues is c.1367C>T (p.Ser456Leu), which contains two B/LB submissions in ClinVar (186). Again, contradicting the entire point of having databases for the sharing of variant-level evidence, one of these submissions provides no information. The other submission, by Ambry Genetics, cites population frequency as evidence for its benign call. However, in gnomAD, this failed their random-forest quality control filter (185). It is unclear if this is due to

the pseudogenes or the specific context surrounding this nucleotide; nonetheless, one must wonder about the quality of Ambry Genetics' population data for this variant. As with SDHA p.Arg600Qln, p.Ser456Leu has also been reported in SDH-related cancer, calling into question the accuracy of the B/LB calls (133).

2. How deficient is sufficient?

The loss of SDH activity results in the accumulation of succinate, promoting several different oncogenic pathways. But what level of dysfunction is necessary to result in this accumulation? The key to answering this question might be revealed by investigating the distinction between *SDHA*-mutant PMD and cancer. Although both are rare diseases, there is a curious lack of overlap in *SDHA* missense variants between the two. These disease-specific associations may be explained by distinct functional consequences.

Due to its essential role in cell biology, it may not be surprising that studies in rats indicated homozygous knockout of *Sdha* is embryonic lethal (206). As PMD typically involves germline bi-allelic inactivation, one could then surmise that at least one allele must be hypomorphic. Indeed, in all cases in which biochemical analysis of patient fibroblasts was performed, residual activity remained. Interestingly, this also included a case in which cells derived from a patient harboring two early (exon 2 and exon 3) frameshift mutations maintained 46% of the activity of controls (207). These mutations were reported as compound heterozygous, but no evidence showing they existed *in trans* was

provided. Importantly, four additional missense mutations were identified during sequencing, and their possible contributions to PMD should not be discounted.

In contrast, complete genetic inactivation of *SDHA* is a common occurrence in cancer. In 2014, Evenepoel and colleagues sought to improve our understanding of the genetic landscape underlying SDH-deficient cancer. As part of this study, the authors investigated the common mechanisms of the second hit. In the 23 cases of *SDHA*-mutant tumors in which both hits were reported, 40% were the result of bi-allelic null events (i.e., any two combinations of nonsense, frameshift, and LOH) (108). The observations above do not necessarily mean that cancer-associated missense variants must be amorphic, though it does suggest complete-LOF is specifically associated with cancer. Identifying such variants could, therefore, enhance our ability to identify patients with increased risk for cancer.

3. Improving *SDHA* variant interpretation through functional studies

Above, I described the remarkable utility of functional analysis for the reclassification of VUS. Several models that exist could be used, but they each have limitations. For instance, we have previously used a yeast model to characterize 22 ySdh1 variants, but ySdh1 only has 67% sequence identity with SDHA (208). Furthermore, as the maturation and assembly of SDHA is quite complex, requiring the assembly factors SDHAF2 and SDHAF4, as well as binding with SDHB to coordinate the passing of electrons. The sequence identities between species for these proteins are 46%, 34%, and 71%, respectively. Thus, while yeast can be useful for obtaining a better understanding

of SDH structure and function, it can be very difficult to determine which residues can be accurately modeled in yeast. For example, one variant not affecting SDH function in the yeast model, p.Arg171His (human nomenclature), was discovered in a SDH-deficient GIST with LOH (136,208). While the singular finding is not enough to determine pathogenicity, the utilization of a human functional model would eliminate a source of uncertainty.

E. Hypothesis

The identification of pathogenic variants in *SDHA* has significant implications for patients and their family members, allowing for enhanced tumor surveillance and early tumor detection. Unfortunately, few people actually receive these benefits because we do not properly understand the genotype-phenotype relationship, and the majority of *SDHA* variants identified are VUS. As a result, we are failing to properly assess cancer risk in a large number of patients, which may be preventing life-saving interventions.

Hypothesis: Developing functional models for the functional characterization of human SDHA variants can improve our understanding of the genotype-phenotype relationship and enhance our ability to detect patients at risk for cancer.

2. A novel human *SDHA*-knockout cell line model for the functional analysis of clinically-relevant SDHA variants

A. Introduction

Succinate dehydrogenase (SDH) is a critical metabolic enzyme complex comprised of subunits SDHA, SDHB, SDHC, and SDHD. SDH links the tricarboxylic acid cycle to the electron transport chain by coupling the oxidation of succinate to the reduction of ubiquinone (130,209). Genetic inactivation of any subunit results in SDH deficiency and accumulation of the oncometabolite succinate (210-213). This triggers metabolic and epigenetic reprogramming that ultimately results in tumorigenesis (149,212,214). Consequently, individuals that inherit a heterozygous germline loss-of-function (LOF) mutation in a *SDH* gene face a significantly increased lifetime risk of developing one or more cancers, including GIST, PC/PGL, and RCC (215-219). At present, there is no highly effective medical therapy for unresectable or metastatic SDH-deficient cancer. However, if tumors are detected at an early stage, surgical resection can be curative (165).

The emergence of genetic testing has enhanced our ability to identify carriers of pathogenic *SDH* variants, offering opportunities for enhanced tumor surveillance and genetic counseling of at-risk individuals. However, increased sequencing has also led to a drastic increase in the identification of variants with insufficient evidence to determine pathogenicity (179,220). The presence of

these variants of uncertain significance (VUS) cannot be used to guide clinical decisions, including cancer screening procedures (180). Therefore, we fail to identify individuals who could be at risk of developing SDH-deficient cancers and miss opportunities for early intervention.

SDHA missense variants have been particularly challenging to interpret. More than 1,000 such variants are listed in ClinVar, and nearly 98% of these are classified as VUS or have conflicting interpretations (186). The majority of these variants are very rare, and the penetrance of *SDHA*-related cancer is incomplete, rendering population and segregation data insufficient to determine their clinical significance. Nonetheless, even when these forms of clinical evidence are limited, the addition of functional data can often result in the reclassification of VUS (193). Therefore, the functional analysis of *SDHA* variants can enhance our ability to determine pathogenicity and identify patients at risk for SDH-deficient cancer.

For functional data to be applied as strong evidence for clinical variant classification, the criteria underlying pathogenicity must first be well understood (194). However, while it is well established that SDHA deficiency can result in cancer, the precise nature of this dysfunction is confounded by several factors. Tumor development requires the acquisition of an independent inactivating mutation in the remaining WT allele or LOH, even in individuals that inherit a heterozygous null *SDHA* allele (108). This observation raises two possibilities: 50% SDH activity corresponding to the presence of only a single functional allele is still sufficient for tumor suppression, or the normal expression of two functional

alleles has redundancy, such that when one allele is inactivated, the remaining functional allele can still output near-maximal levels of SDH activity. In either case, the risk of cancer for carriers of null *SDHA* variants is clear, as a second somatic hit would lead to a complete loss of function. In contrast, functional data demonstrating varying levels of reduced activity corresponding to missense SDHA variants cannot be properly interpreted until we have a better understanding of what extent of SDH dysfunction contributes to cancer pathogenicity.

Further hindering our ability to utilize functional data to inform cancer risk for *SDHA* variants is the fact that SDHA dysfunction has pleiotropic effects. In addition to cancer, germline LOF *SDHA* variants are known to cause primary mitochondrial disease (PMD) with isolated complex II deficiency, typically presenting as Leigh syndrome, leukodystrophy, and/or cardiomyopathy (93). In contrast to SDHA-related cancer, these forms of PMD are typically congenital, involving bi-allelic germline LOF *SDHA* variants. However, it is unclear if the mode of inheritance is the only distinguishing factor or if distinct SDHA consequences also distinguish each disease. As such, although they are considered pathogenic, it is uncertain if individuals inheriting a heterozygous PMD-associated *SDHA* variant should be recommended for enhanced tumor surveillance and genetic counseling.

Currently, simply demonstrating a *SDHA* variant results in “loss of function” is insufficient to support its role in elevating cancer risk. However, by comprehensively profiling the functional consequences of *SDHA* variants with

previously determined clinical significances, we can reveal the nature of SDHA dysfunction associated with cancer, enhancing our ability to utilize functional data for clinical variant interpretation. Herein, we describe the development of a model for the functional characterization of SDHA variants utilizing a novel human *SDHA*-knockout cell line. We profiled a total of 48 SDHA missense variants previously identified as being benign, cancer-associated, or PMD-associated, to investigate what distinguishes cancer from non-cancer variants. We then demonstrated how these analyses allow for more robust variant interpretation by subsequently profiling 24 SDHA VUS. This novel functional model delivers crucial insights into SDHA-cancer dysfunction, increases the impact of genetic counseling, and paves the way for more effective surveillance and timely interventions in SDH-deficient cancers.

B. Materials and Methods

Cell culture

HAP1 cells (Horizon Discovery) were cultured in IMDM supplemented with 10% fetal bovine serum and 1% Penicillin-Streptomycin and maintained at 37 °C with 5% CO2.

Generation of *SDHA*-knockout cell line

A clonal HAP1 *SDHA*^{KO} cell line was generated by lentiviral transduction of Cas9 and guide RNA (gRNA), followed by selection and single-cell plating. Briefly, the guide RNA sequence TTGGCCTTTCTGAGGCA, which targets SDHA exon 3, was cloned into the lentiCRISPR v2 plasmid (Addgene #52961). Viral particles were made in HEK293TA cells (Genecopia) using the ViraPower

Lentiviral Expression System following manufacturer protocols (ThermoFisher). HAP1 cells were transduced with viral particles in complete media containing 8 mg/mL polybrene. The following day, transduced cells were plated into 96-well plates at <1 cell/well in media containing 1 mg/mL puromycin. After outgrowth, clonal cell lines were screened for SDH deficiency by SDHA and SDHB immunoblotting. Candidate clones were then sequenced to confirm genetic knockout.

Generation *SDHA*-knockout landing pad cell line

A landing-pad cassette was integrated into the genome of a SDHA-knockout-verified clone by lentiviral transduction. The landing pad design was adapted from those reported by Matreyek et al (221). Briefly, a Bxb1 attP recombination sequence was placed downstream of a CMV promoter and upstream of a Bxb1-IRES-neomycin phosphotransferase II (NptII) expression cassette. Additionally, an expression cassette consisting of mCherry driven by the EF-1α core promoter was included. Viral particles were produced as described above. HAP1 *SDHA*^{KO} cells were transduced at a low MOI as determined by fluorescence imaging of mCherry using a BioRad ZOE Fluorescent Cell Imager, followed by selection with G418 at a final concentration of 1.5 mg/mL. Selected cells were single-cell plated to obtain candidate clones for screening.

Screening of *SDHA*-knockout landing pad cell lines

HAP1 *SDHA*^{KO}-landing pad cell lines were screened for recombination capabilities by transfecting a plasmid donor containing a promoterless Blasticidin

S Deaminase (BSD) gene downstream of a Bxb1 attB recombination sequence, followed by a SDHA-IRES-EGFP expression cassette driven by the EF-1α core promoter (attB_BSD+SIG). The coding sequence of SDHA was obtained from pCMV6-AC-SDHA (Origene, SC319054). Prior to cloning into the attB_BSD+SiG vector, silent mutations (c.237 A>C, c.252 G>C) were introduced to disrupt the sgRNA sequence using the Q5 Site-Directed Mutagenesis Kit (NEB), following manufacturer protocols. Although the genomic landing-pad cassette expressed the Bxb1 recombinase, attB_BSD+SIG was co-transfected with pCAG-NLS-Bxb1 (Addgene #51271) plasmid at equal ratios based on molecular weight (222). Transfections were performed using jetOPTIMUS transfection reagent (Polyplus) following manufacturer protocols. Candidate landing-pad cells were screened for highly pure populations of cells with homogenous expression of GFP following transfection and selection. To obtain stable cell lines, cells were cultured in blasticidin 2-4 days post-transfection, at a final concentration of 10 µg/mL. At time points indicated, GFP expression was assessed by flow cytometric analysis using a Guava easyCyte 5 (EMD Millipore). GFP was excited with a 488 nm laser and emission was detected using a 525/30 nm bandpass filter. To assess the landing-pad copy number, a donor plasmid encoding cyOFP1 (attb_cyOFP-IRES-BSD) was co-transfected with attB_BSD+SIG and pCAG-NLS-Bxb1. Detection of GFP was performed as described, while cyOFP1 emission upon excitation by the 488 nm laser was detected through a 583/26 nm bandpass filter. Flow cytometry data were analyzed with Guava InCyte software (EMD Millipore) with figures generated using FlowJo software.

Selection of SDHA variants

We utilized information available from ClinVar and the SDH mutation database, hosted on the Leiden Open Variation Database (LOVD), and the literature to identify variants with previously established clinical interpretations to use as controls (186,223). The data we used and our classification for each variant is listed in **Table 4 (Appendix)**.

We considered any variant with at least one P/LP interpretation as a control cancer variant. Variants identified during literature searches met this criterion only if the authors specifically stated the classifications were made following ACMG/AMP joint guidelines (136,204). However, we excluded a P/LP variant it also received a B/LB submission in ClinVar or LOVD. For instance, $SDHA^{R600Q}$ was classified as Likely Pathogenic by Bausch et. al., while a single submitter to ClinVar considered the variant Likely Benign (204). In total, we selected 21 variants that met our criteria for a known cancer variant, though this does not represent the total number of variants that met our criteria.

Due to some uncertainty in benign classifications, we required a variant to contain at least two independent Benign/Likely Benign (B/LB) classifications to be considered a control benign variant. As with control cancer variants, we excluded a variant as a benign control if there was contradicting evidence available. For instance, although ClinVar contains eight B/LB submissions for $SDHA^{T508I}$, there is also a Pathogenic classification submission, corresponding to a case of PMD. Similarly, $SDHA^{S456L}$ was excluded despite two B/LB submissions in ClinVar as it has been previously reported in a case of SDH-deficient GIST (133). In total, we identified 17 variants meeting our criteria

for a benign SDHA variant. All PMD-associated variants were identified through literature searches. SDHA variants that met the exclusion criteria described above were considered VUS. Further, we included variants identified by the OHSU Knight Diagnostics Laboratory or by other collaborators as VUS. In total, we selected 24 variants we considered SDHA VUS.

Generation of stable SDHA-variant cell lines

For each of the selected SDHA variants, we generated a mutant attB_BSD+SIG (PAM-mutated) plasmid. This was either performed following the protocols of NEB's Q5 Site-Directed Mutagenesis Kit or their NEBuilder HiFi DNA Assembly Cloning Kit. For each plasmid, the entire coding sequence of SDHA was confirmed by in-house Sanger sequencing. Variant plasmids were then co-transfected into HAP1 *SDHA*^{KO}-landing pad cells with pCAG-NLS-Bxb1, as described above, and selected with 10 µg/mL blasticidin 2-4 days post-transfection. Following selection, GFP fluorescence was analyzed by flow cytometry. For a given variant cell line, if the percentage of GFP-negative cells was greater than 3%, the cells were discarded, and transfection was repeated.

WT-normalized expression levels

Expression levels of the integrated landing-pad cassettes were determined by GFP fluorescence intensities. Each cell line was maintained in T25 or T75 culture flasks under blasticidin selection. On days of harvest, cells were rinsed in PBS, detached by trypsin, and neutralized with an equal volume of complete media. Cells were diluted 1/10 in 1X FACS buffer (PBS, pH 7.2 with 0.5% bovine serum albumin (BSA) and 2mM EDTA) and GFP fluorescence intensity was measured by flow cytometric analysis. For

each cell line, the median fluorescence intensity (MFI) was determined in three biological replicates, defined as a population of cells assayed on separate days, after a period of growth between replicates. To convert these measurements to normalized expression scores, the mean MFI corresponding to untransfected HAP1 *SDHA*^{KO}-landing-pad cells (background fluorescence) was subtracted from each variant- and WT-replicate MFI. The resulting values for each variant were then normalized to the average of that for SDHA^{WT} replicates.

SDH activity assays and Activity Score calculations

Cells were harvested by trypsin and counted by a TC20 Automated Cell Counter. Two million cells were spun down, rinsed in PBS, and the resulting cell pellets were frozen at -80 °C until assayed. This process was repeated on different days for three biological replicates for each SDHA variant cell line. All three biological replicates for a variant were assayed together, along with three biological replicates corresponding to SDHA^{WT} and SDHA^{R31X}. On analysis days, cell pellets were thawed on ice and lysed in 75 µL lysis buffer (150 mM NaCl, 20 mM HEPES, pH 7.4, 2 mM EDTA, 15 mM $MgCl_2$, 0.5% NP-40), supplemented with 1X Halt Protease Inhibitor Cocktail (ThermoFisher). After vortexing, lysed cells were left on ice for at least 10 minutes prior to spinning at 13,000 g at 4 °C. After determining protein concentrations using the Pierce 660 nm Protein Assay Kit (ThermoScientific), each sample is normalized to a concentration of 1 µg/uL in lysis buffer. SDH Activity was measured as the transfer of electrons from succinate to decylubiquinone, using reduction of the artificial electron acceptor, 2,6-dichlorophenolindophenol (DCPIP) as a readout (224-226). Briefly, 5 µL (5 µg) protein was added to 15 µL 1X assay buffer (10 mM KH_2PO_4, pH 7.4, 2 mM

EDTA, and 1 mg/mL BSA) containing succinate (100 mM succinate current concentration) to a clear-bottom 96-well plate. The pre-incubation with succinate is necessary to fully activate the SDH complex (227,228). Alternatively, 5 uL of the sample was added to 1X assay buffer without the addition of succinate to serve as an internal background control. Each condition was performed in technical duplication, for a total of four wells per each variant biological replicate. After a 15-minute incubation period at room temperature, the reaction was initiated by adding 80 uL of 1X assay buffer containing decylubiquinone (50 uM final concentration), DCPIP (80 uM), rotenone (4 uM), and antimycin A (2 uM). The final concentration of succinate, when present, was 20 mM. DCPIP absorbance at 600 nm was monitored every 45 seconds with shaking of the plate between each reading using a VersaMax microplate (Molecular Devises). The rates of DCPIP absorbance decrease over a linear range (5-30 minutes) for each technical duplicate were averaged. These data were analyzed by SoftMax Pro software (Molecular Devises). Finally, SDH activity for each biological replicate was calculated as the succinate-containing rate subtracted by the rate without succinate. Finally, to convert these measurements into Activity Scores, we first corrected for relative differences in expression levels according to the WT-normalized expression levels calculated above. Then, each score was normalized to the average of the $SDHA^{WT}$ replicates that were included in the corresponding assay.

SDHA and SDHB Abundance Scores

SDHA and SDHB Abundance Scores were determined by immunoblot analysis. Briefly, 15 μg of the cell lysates (1 ug/uL) obtained during activity assays were separated by SDS-PAGE using AnykD Criterion TGX Precast Protein Gels (Bio-Rad). A sample for each biological replicate corresponding to a variant was on the same gel, along with three replicate lysates corresponding to $SDHA^{WT}$. After electrophoresis, polyacrylamide gels were transferred to nitrocellulose membranes using Bio-Rad's Trans-Blot Turbo Transfer System and consumables. Following protein transfer, membranes were blocked in 5% nonfat dry milk in 20 mM Tris, 150 mM NaCl, and 0.1% Tween 20. SDHB and GFP both have observed band sizes around 28 kilodaltons. In order to detect each protein sequentially by chemiluminescent methods, we took advantage of the ability to inactivate horseradish peroxidase (HRP) by acetic acid (229). First, we probed for SDHB using an anti-SDHB mouse monoclonal antibody (ab14714, Abcam), followed by an appropriate HRP-conjugated secondary antibody. Membranes were incubated in SuperSignal West Pico PLUS Chemiluminescent Substrate (Thermo Scientific) and the signal was detected using the Chemidoc MP system with Image Lab software (Bio-Rad). Membranes were then incubated in 10% acetic acid at 37 °C for 30 minutes to inactivate the HRP. After thorough rinsing, we repeated the standard process for detecting SDHA using a rabbit anti-SDHA antibody (Cell Signaling #5839). Upon addition of chemiluminescent substrate, subsequent imaging served two purposes: first, to detect signal corresponding to SDHA protein levels, and second, to confirm signal

corresponding to SDHB protein levels could no longer be detected. After this was confirmed, rabbit antibodies for GFP (Cell Signaling #2956) and β-tubulin (Cell Signaling #2146) were used for sequential detection of their respective proteins. For each protein, densitometry was performed using ImageLab software. SDHA Abundance Scores were calculated as the ratio of SDHA-to-GFP levels, relative to the mean of that for the three $SDHA^{WT}$ replicates included in the same blot. SDHB Abundance Scores were calculated in the same way, using the ratio of SDHB-to-GFP levels.

In-gel SDHA Flavinylation analysis

The same protein lysates obtained during activity assay preparation were used for the analysis of SDHA flavin levels. To obtain better signal-to-noise than we observed with Bio-Rad TGX Criterion Gels, we separated proteins (15 ug) using 4-12% Bolt Bis-Tris Plus Protein Gels with MES running buffer (Thermo Fisher). Following separation, gels were incubated in 10% acetic acid for 10 minutes, rinsed with water, and subsequently imaged using the Chemidoc MP system with the Blue LED Module Kit (Bio-Rad) to excite flavin in the blue spectrum while fluorescence emission was detected with a 530/28 nm filter (230). Total-protein images corresponding to these gels were acquired using One-Step Blue Protein Gel Stain (Biotium) following manufacturer protocols.

Computational model predictions

CADD, BayesDel (no allele frequency, AF), MetaRNN, MetaSVM, MutationAssessor, and REVEL scores for variants were obtained from dbNSFP v4.4 (231,232).

Statistical analysis

All statistical analyses were performed as indicated using Prism 10 software (GraphPad).

OddsPath calculations

To determine the strength of evidence corresponding to our functional data, we calculated OddsPath scores using the formula: $OddsPath = \frac{P2 \times (1-P1)}{(1-P2) \times P1}$ (194). For classifying cancer-like variants, *P1* represents the proportion of all variants assayed that were known *cancer* variants and *P2* represents the proportion of accurately classified cancer-like variants to the total number of known cancer variants assayed, plus one. For classifying benign-like variants, *P1* represents the proportion of all variants assayed that were known *pathogenic* variants and *P2* represents the proportion of pathogenic variants that received a benign-like classification, plus one, to the total number of variants that received a benign-like classification, plus one.

SDHA VUS reclassification

For each SDHA VUS, the applicable ACMG/AMP criteria that could be applied and at which strength of evidence were obtained from VarSome. Following ClinGen SVI WG's recommendations, VarSome converts each form of evidence into points, depending on the corresponding strength of evidence, and makes classifications according to the final pathogenicity score (233,234). In this system, supporting, moderate, strong, and very strong strengths of evidence are assigned 1, 2, 4, and 8 points, respectively. Further, variants are assigned as Benign, Likely Benign, VUS, Likely Pathogenic, or Pathogenic if the final

pathogenicity scores are less than or equal to -7, between -6 and -1, between 0 and 5, between 6 and 9, or greater than 10, respectively. Thus, we updated the score corresponding to each SDHA VUS as allowed by our functional data and reclassified VUS accordingly.

C. Results

Development of a novel cell-line model for functional characterization of SDHA variants

While several SDHA missense variants are classified as pathogenic, precisely how these variants impact SDHA function remains poorly understood. We previously used a yeast model to characterize orthologs of SDHA variants, but the utility of this model is hampered by the limited evolutionary conservation of SDHA and its interacting proteins (208). Thus, to obtain stronger evidence for variant interpretation, we developed a system for assessing the functional consequences of human SDHA variants using the human HAP1 cell line. We utilized CRISPR-Cas9 and serine-recombinase technologies to enable the generation of isogenic cell lines capable of expressing SDHA variants at comparable levels without the presence of endogenous SDHA. First, we obtained a clonal cell line that harbors a hemizygous 10-basepair frame-shift deletion in exon 3 of *SDHA* (**Figure 13**). We then introduced a landing-pad cassette containing a Bxb1 attP-recognition site, which allows for site-specific integration of donor constructs containing a compatible Bxb1 attB-recognition site (**Figure 14**). Subsequent single-cell plating resulted in the generation of the clonal cell line, HAP1 *SDHA*^{KO}-LP.

We assessed the recombinase-mediated strategy for generating SDHA-variant cell lines by first transfecting a donor construct encoding WT SDHA ($SDHA^{WT}$) co-transcriptionally linked to GFP, along with a plasmid for Bxb1 expression.

Following transfection, a subset of HAP1 *SDHA*^{KO}-LP cells displayed stable fluorescence, indicating integration of the donor plasmid, whereas GFP-positive cells were entirely depleted following transfection into non-landing-pad cells (**Figure 15B and C**). In addition to SDHA and GFP, the donor plasmids contained a promoter-less blasticidin-resistance gene, where drug resistance is dependent on recombination into the genome at the landing-pad site downstream of a promoter (**Figure 14**). Although transfection and recombination efficiencies were low, blasticidin selection resulted in highly

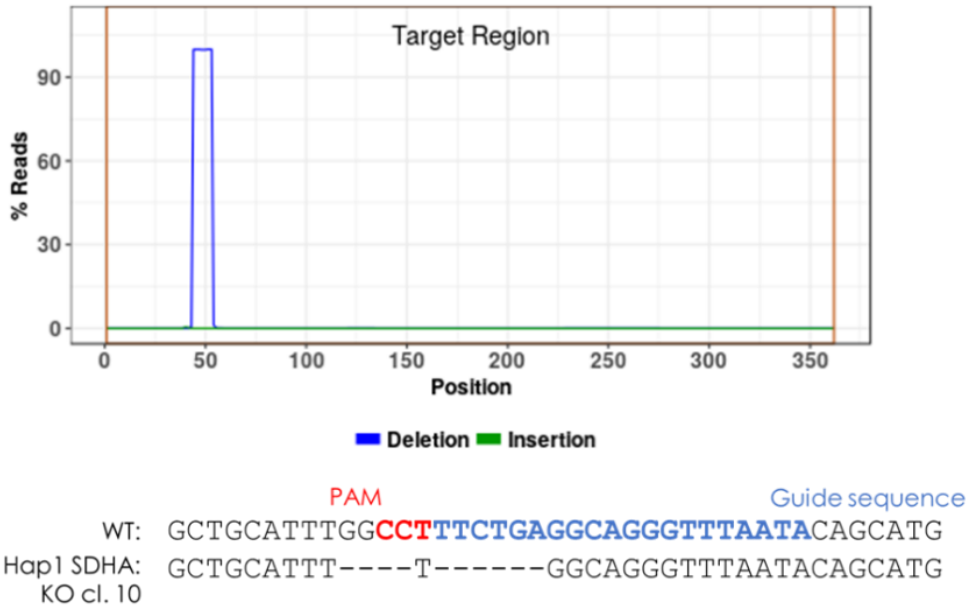

Figure 13. A novel *SDHA*^{KO} cell line.. Top: Plot of insertions/deletions detected upon aligning *SDHA* exon 3 to NGS sequencing results from the clonal HAP1 *SDHA*^{KO} cell line. Bottom: alignment of the frame-shift mutation generated upon CRISPR-editing to the WT sequence, with the guide RNA sequences shown in blue and PAM in red.

pure populations of GFP-expressing cells (**Figure 15A and D**). Lastly, we transfected a mixture of donor constructs expressing GFP or cyOFP1 to ensure the HAP1 *SDHA*^{KO}-LP cell line could only integrate a single copy of the donor construct. Indeed, while many transfected cells expressed both fluorescent proteins, the proportion of such cells was negligible following selection (**Figure 15E**).

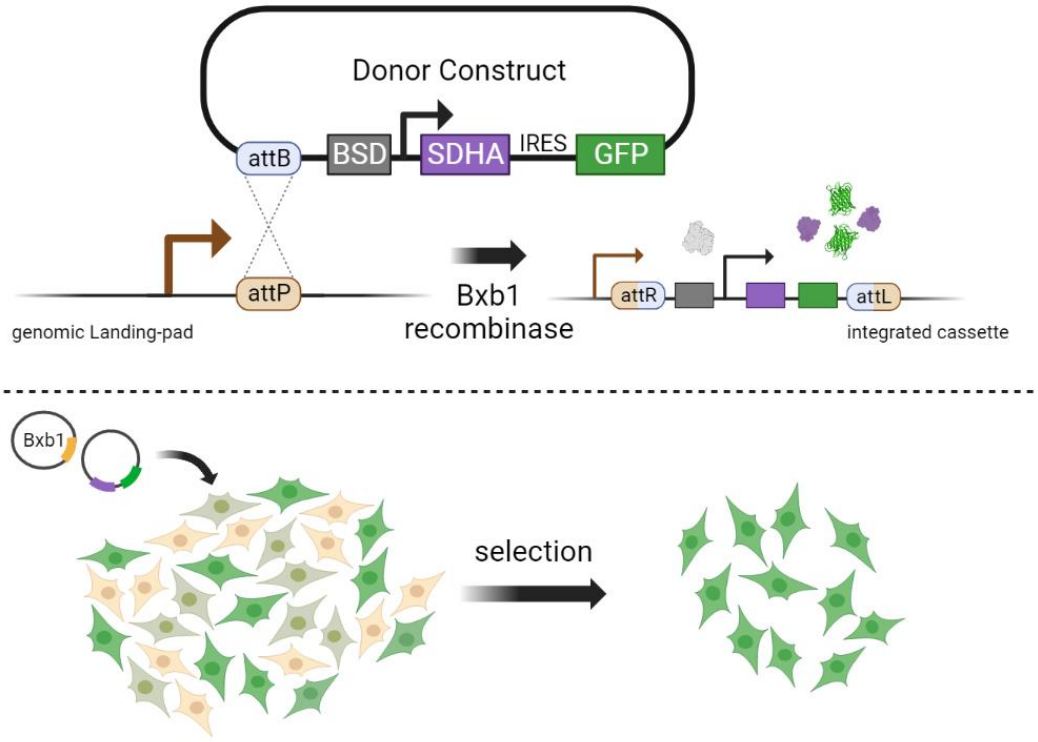

Figure 14. Landing-pad strategy for SDHA variant cell-line generation. Top: simple schematic of recombinase reactants and product. An attP-landing pad site was introduced into the genome by lentiviral transduction. The donor construct contains the attB recombination site upstream of a promoter-less blasticidin deaminase gene (BSD) and a SDHA-GFP expression cassette driven by the Ef1-a promoter (black arrow). Bxb1 mediates the recombination of attB and attP sites, resulting in the integration of the donor construct, allowing for BSD expression driven by the CMV promoter (brown arrow). Bottom: transfection of Bxb1 and donor-construct plasmids into landing-pad cells results in heterogenous expression of GFP. Upon blasticidin selection, only successfully recombined cells survive, resulting in a pure homogenously expressing population. Created with BioRender.com

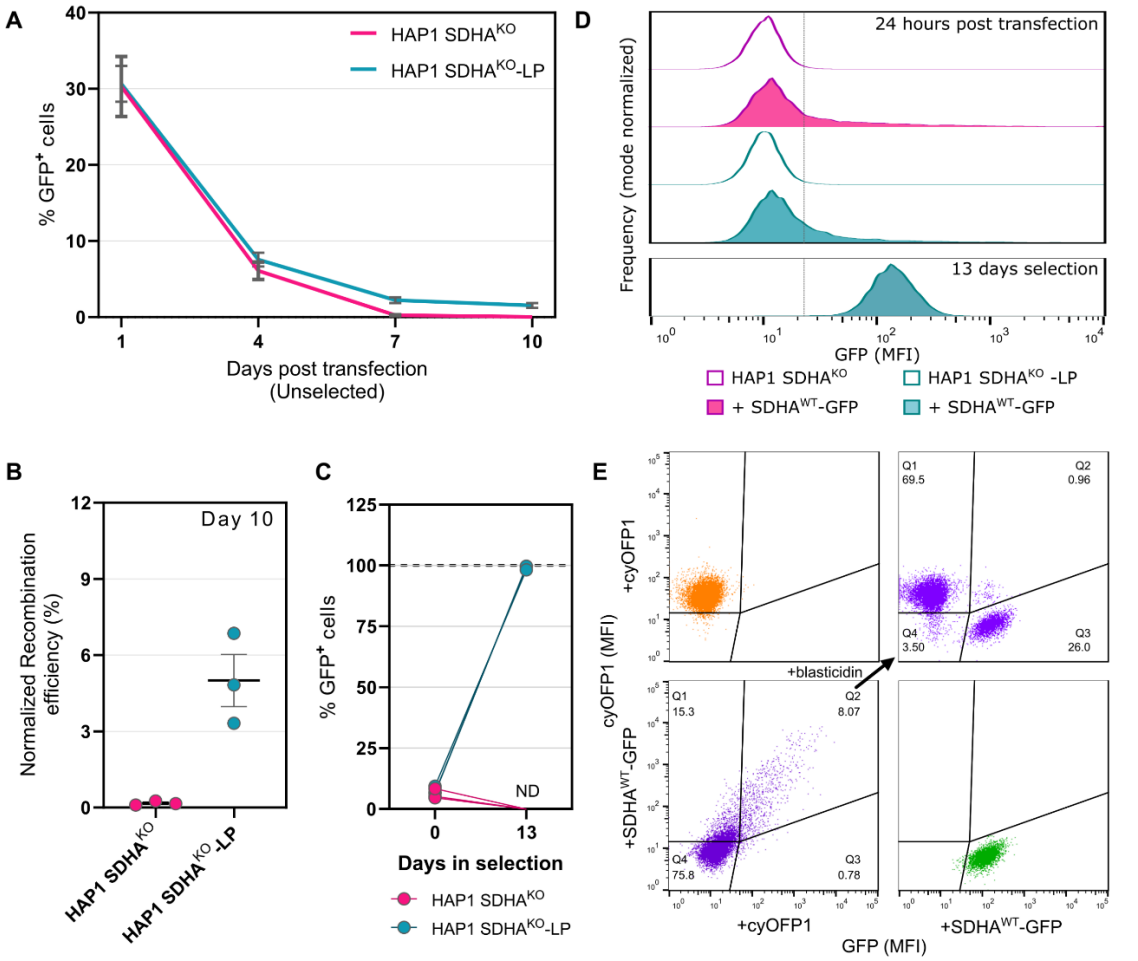

Figure 15. Landing-pad mediated cell-line generation. **A**. The percentage of GFP-positive cells following transfection over multiple days, errors are SEM from three replicates. **B.** Normalized recombination efficiency, calculated as the percentage of GFP⁺-cells at Day 10, relative to that of Day 1, from panel A. **C.** The percentage of GFP-positive cells on the first day of selection (four days post-transfection) and after 13 days of selection. Triplicates are shown except for parental *SDHA*^{KO} cells after selection, as no cells survived for analysis (ND = not detected). **D.** Top: representative mode-normalized GFP MFI distributions for parental or landing-pad *SDHA*^{KO} cells 24 hours after donor constructs were or were not transfected. Bottom: the same population of *SDHA*^{KO}-LP +SDHA^{WT}-GFP following 13 days of selection in blasticidin. **E.** Representative dot plots showing cyOFP1 MFI versus GFP MFI. *SDHA*^{KO}-LP cells were transfected with SDHA^{WT}-GFP (bottom right), cyOFP1 (top left), or both donor vectors (bottom left and top right). The bottom left are cells 24 hours after transfection. The top right is the same population as the bottom left after nine days of blasticidin selection. Both the top left and bottom right are stably selected populations used as controls for cyOFP1- and GFP-only expression, respectively.

Validating the rescue of SDHA function

Upon establishing our method of cell-line generation, we evaluated our capacity to restore WT-SDHA function. First, we confirmed that the landing-pad-based expression of $SDHA^{WT}$ was similar to the endogenous levels of parental HAP1 cells (**Figure 16A**). Rescued $SDHA^{WT}$ was also covalently bound to FAD, demonstrating a proper post-translational modification. Finally, we quantified whole-complex SDH activity by spectrophotometrically tracking the transfer of electrons from succinate to decylubiquinone, an analog of ubiquinone, using DCPIP as an artificial electron acceptor. As expected, the knockout cells displayed a complete loss of succinate-dependent DCPIP-reduction; however, re-expression of $SDHA^{WT}$ successfully restored SDH activity to parental HAP1-like levels (**Figure 16B and C**).

LOF SDHA variants associated with cancer are characterized by severe SDH dysfunction.

After confirming the functional rescue of $SDHA^{WT}$ in our knockout model, we turned our attention to functionally profiling SDHA missense variants. Our ultimate goal is to utilize functional data as evidence for the clinical interpretation of SDHA variants, improving our ability to identify patients with increased cancer risk. However, what constitutes cancer-like dysfunction is not well-defined. Therefore, before functional data obtained from our model can have clinical utility, we must establish guidelines for how to interpret them.

Toward this goal, we generated stable cell lines for 17 variants previously classified as benign and 21 variants classified as cancer-associated and

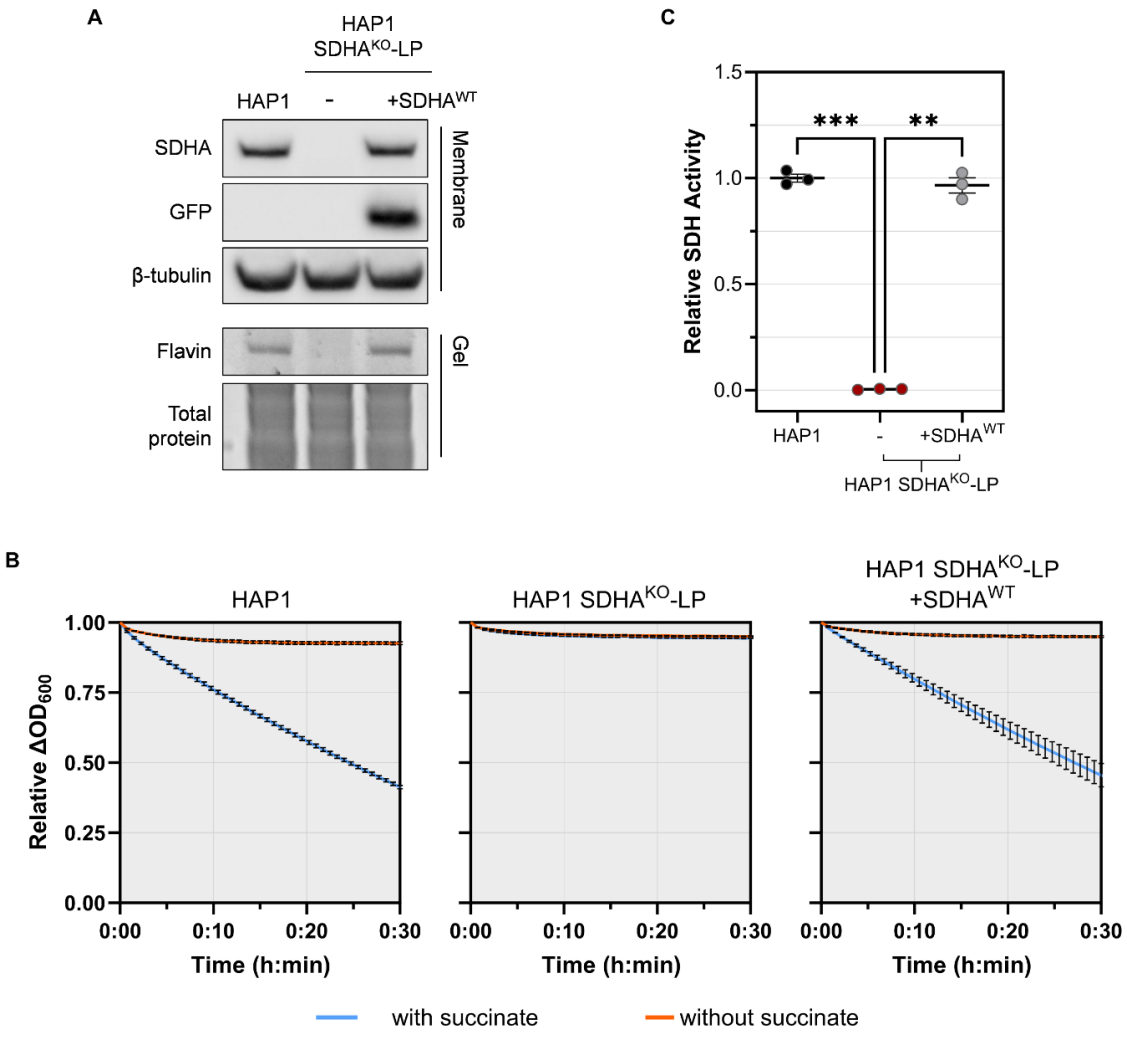

Figure 16. SDH function can be rescued in HAP1 *SDHA*^{KO} cells. **A**. Upper: Representative analysis of SDHA, GFP, and B-tubulin detected by immunoblotting after transfer to nitrocellulose membranes. Lower: Representative analysis of covalently bound FAD by in-gel fluorescence of flavin with corresponding total-protein stain. **B.** SDH Activity measured by the relative change in absorbance at 600 nm over time. Mean and SEM are calculated from three independent biological replicates, each with two technical replicates. **C.** SDH Activity corresponding to time-course data in B, calculated as the rate of succinate-dependent DCPIP reduction from 5 to 30 minutes, relative to the mean of HAP1 replicates. Each symbol represents an independent biological replicate (n=3). Welch's ANOVA with Dunnett's T3 multiple-comparison correction applied, **p < 0.01; ***p < 0.001.

measured their corresponding SDH activities. In addition to these missense-variant cell lines, we generated a cell line expressing SDHA^{R31X}, which was used as a benchmark for amorphic function. We normalized SDH activity measurements using SDHA^{WT} replicates included in each assay to account for

assay-to-assay variability. These normalized activities were further corrected to account for slight differences in observed expression levels, based on their GFP fluorescence intensities, resulting in a final Activity Score, where $SDHA^{WT}$ is equal to 1.

As expected, benign variants were collectively WT-like, with a mean Activity Score of 0.917 (**Figure 17A**). However, there was substantial variability amongst individual variants, with $SDHA^{Y55H}$ having the lowest score at 0.215 (**Figure 17B**). Nonetheless, the extent of SDH dysfunction corresponding to cancer variants was remarkably distinct. Not only was the mean Activity Score of all cancer variants (0.007) significantly lower than that of benign variants, but almost all cancer variants could be described as functionally amorphic, as their Activity Scores were not significantly different from that of a control null variant, $SDHA^{R31X,}$ whose mean Activity Score was 0.004 (**Figure 17A and B**). The lone exception, $SDHA^{G274S}$, had an Activity Score of 0.068, which we consider to be severely dysfunctional.

Importantly, these distinguishable functional outcomes cannot be attributed to differences in expression levels observed. Although cancer variants, on average, did display significantly lower expression than benign variants, the effect size was small (**Figure 17C and D**). Furthermore, the relationship between expression levels and Activity Scores across all variants was weak (Pearson r = 0.27; p = 0.095) (**Figure 17E**). As such, our data indicate that SDHA variants involved in cancer are characterized by complete- or near-complete loss of SDH activity.

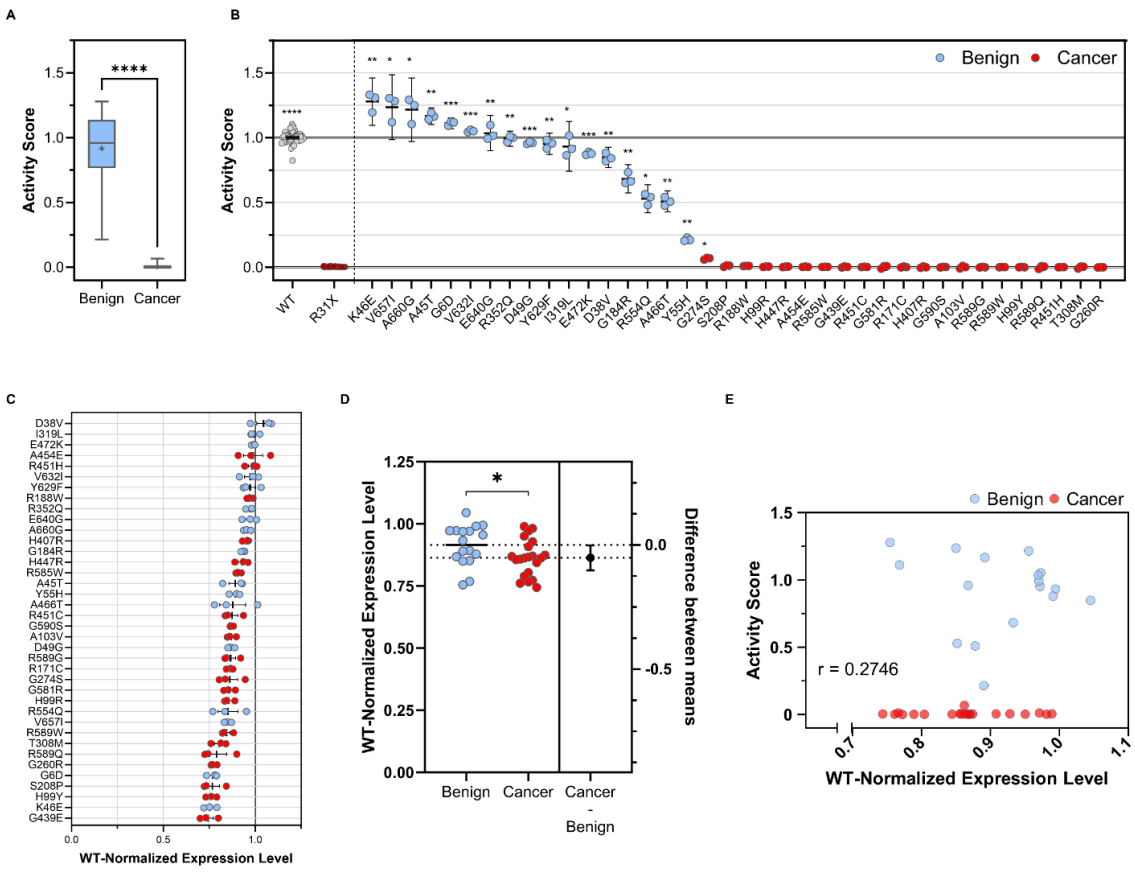

Figure 17. SDH activity analysis of known benign and cancer-associated variants. **A.** Box and whiskers plot of benign (n=17) or cancer (n=21) SDHA variant Activity Scores. Means are represented by a '+' symbol. Group means were compared using Welch's t-test; ****$p < 0.0001$. **B.** Activity Scores corresponding to $SDHA^{WT}$ (n=54), $SDHA^{R31X}$ (n=54), and all clinically classified variants (n=3 replicates each). For benign and cancer control SDHA variants, mean and 95% confidence intervals (CI) are shown. Comparisons were made between $SDHA^{R31X}$ and all other groups using Welch's ANOVA test with Dunnett's T3 multiple-comparison correction applied; *$p < 0.05$, **$p < 0.01$, ***$p < 0.001$, ****$p < 0.0001$, only shown for means significantly higher than $SDHA^{R31X}$. **C.** $SDHA^{WT}$-normalized expression levels for each variant (n=3), calculated from GFP MFI, displaying mean and SEM. **D.** Estimation plot depicting the difference in mean expression levels between benign and cancer variants. Left: Each symbol corresponds to a single variant. Means were compared using an unpaired t-test; *$p < 0.05$. Right: 95% CI of the effect size of the difference between means. **E.** Pearson correlation analysis between normalized expression levels and Activity Scores; r=0.2746, p=0.095 (ns).

Distinguishing cancer- and PMD-related SDHA dysfunction

While our analysis has demonstrated a clear distinction in function between benign and cancer variants, *SDHA* variant pathogenicity is not limited to cancer. Inheriting pathogenic *SDHA* variants is also the most common cause of

PMD cases with isolated complex II deficiency (93). However, it is not known if the degree of dysfunction corresponding to PMD-associated *SDHA* variants is the same as observed amongst cancer variants. PMD typically requires germline bi-allelic alteration of *SDHA*, though animal studies have shown homozygous knockout of *SDHA* or other *SDH* genes results in embryonic lethality. This suggests some minimum level of activity is required for survival until birth (206,235). Accordingly, we hypothesized that at least one allele in patients with PMD must be functionally distinct from the cancer variants with complete or nearly complete loss of activity.

To investigate this hypothesis and shed light on the complex genotype-phenotype relationship, we examined the literature to identify all reported cases of PMD involving at least one SDHA missense variant and generated a stable cell line for each novel variant identified (**Table 1**). As with the benign- and cancer-variant cell lines generated, these PMD-variant cell lines displayed variable expression levels, indicated by GFP fluorescence, though these differences did not result in a significant correlation with subsequent Activity Scores (**Figure 18A and B**). According to our hypothesis, any missense variant that resulted in PMD whose accompanying allele is amorphic must necessarily retain some level of function. In agreement with this, the exclusively homozygous variants ($SDHA^{G555E}$ and $SDHA^{R554W}$) and the variants reported *in trans* with a null variant ($SDHA^{D137H}$, $SDHA^{E152K}$, $SDHA^{C189G}$, and $SDHA^{A524V}$) displayed varying amounts of reduced activity, with Activity Scores ranging between 0.070 and 0.656 (**Figure 18C**). As these variants had reduced activity

yet were significantly different than that of SDHA^{R31X}, we categorize them as hypomorphic PMD variants.

While each of the previous variants was the only missense variant involved in their respective cases, PMD can also occur as the result of germline compound heterozygous missense variants. In one such case, the patient harbored SDHA^{R585W}, a known cancer variant we characterized above, which had an Activity Score of 0.004 (**Figure 17B**). Therefore, we predicted the accompanying variant in this individual, SDHA^{R512Q}, must also retain function. Indeed, the Activity score for this variant was 0.162 and is similarly considered hypomorphic (**Figure 18C**).

The other reported case of missense-compound heterozygosity involved two novel variants. Subsequent analysis revealed a similar pattern, with one hypomorphic variant, SDHA^{T508I}, having significantly more activity than SDHA^{R31X} (Activity Score = 0.270) and the other, SDHA^{S509L}, being marked by severe SDH

Table 1. PMD cases involving SDHA missense variants.

FIRST ALLELE	SECOND ALLELE	REPORTED CASES
HOMOZYGOUS		
G555E	G555E	17 [95,236,237]
R554W	R554W	2 [92]
COMPOUND HETEROZYGOUS W/ NULL		
D137H	M1V	1 [96]
E152K	R31X	2 [238,239]
C189G	R31X	1 [97]
A524V	M1L	1 [98]
COMPOUND HETEROZYGOUS W/ MISSENSE		
T508I	S509L	1 [94]
R512Q	R585W	1 [99]
HETEROZYGOUS		
R451C	WT	5 [100-102]
R662C	WT	1 [103]

dysfunction (Activity Score = 0.010) that could not be distinguished from that of SDHA^{R31X} (**Figure 18C**). We then compared the Activity Scores corresponding to the eight PMD variants identified as hypomorphic to the benign and cancer variants previously analyzed. This analysis revealed the Activity Scores corresponding to the hypomorphic PMD variants were, on average, significantly lower than those of benign variants but higher than those of cancer variants (**Figure 18D**).

Although PMD typically occurs in the context of bi-allelic inheritance, there have also been reports involving two different heterozygous missense variants resulting in late-onset PMD, often presenting with optic atrophy and neurological impairment (93). One of these variants, SDHA^{R451C}, was also a known cancer variant we characterized, which had an Activity Score of 0.003 (**Figure 17B**). Analysis revealed the other heterozygous variant, SDHA^{R662C}, was also non-functional, with an Activity Score (0.013) that was not significantly different than that of SDHA^{R31X} (**Figure 18C**). Although these two variants alone do not contribute activity, *SDHA* is haplosufficient, and a single non-functional allele is not expected to be pathogenic. For instance, roughly one in 5,000 individuals are heterozygous for SDHA^{R31X}, yet PMD has never been reported in any of these individuals (185). Thus, we hypothesized that SDHA^{R451C} and SDHA^{R662C} have dominant negative functions. To test this, we measured SDH activity in a pseudo-heterozygous system by introducing SDHA^{WT} or different variants into parental HAP1 cells that retained endogenous SDHA. Compared to endogenous SDHA expression alone, artificial overexpression of SDHA^{WT} resulted in a slight

increase in activity, whereas activity was not significantly different upon the introduction of the cancer variant SDHA^{H99Y} (**Figure 18C**). In contrast, the presence of either suspected dominant negative variant indeed interfered with endogenous SDHA function, resulting in significantly decreased levels of activity. These data align with the previous analysis indicating SDHA-related PMD is characterized by reduced, but not absent SDH function, unlike SDHA-related cancer.

Exploring the role of SDHA loss in variant dysfunction.

While both diseases are characterized by a reduction in SDH activity, the severity and consistency of the functional impairment observed for cancer variants was striking in comparison to the partial loss of function associated with hypomorphic PMD variants. This prompted us to investigate whether unique mechanisms underlying dysfunction could explain the distinct functional outcomes observed amongst variants from these two classes of pathogenic SDHA missense variants.

Immunohistochemical (IHC) analysis of SDHA has been reported to have clinical utility in the diagnosis of *SDHA*-mutant tumors, which often display markedly reduced or absent SDHA expression. In contrast, retained SDHA is often reported in PMD-patient samples. Whether due to intrinsic protein instability or altered post-translational processing, loss of SDHA protein would necessarily have a drastic effect on overall function. Therefore, we explored the role decreased SDHA abundance may play in underlying severe SDH dysfunction

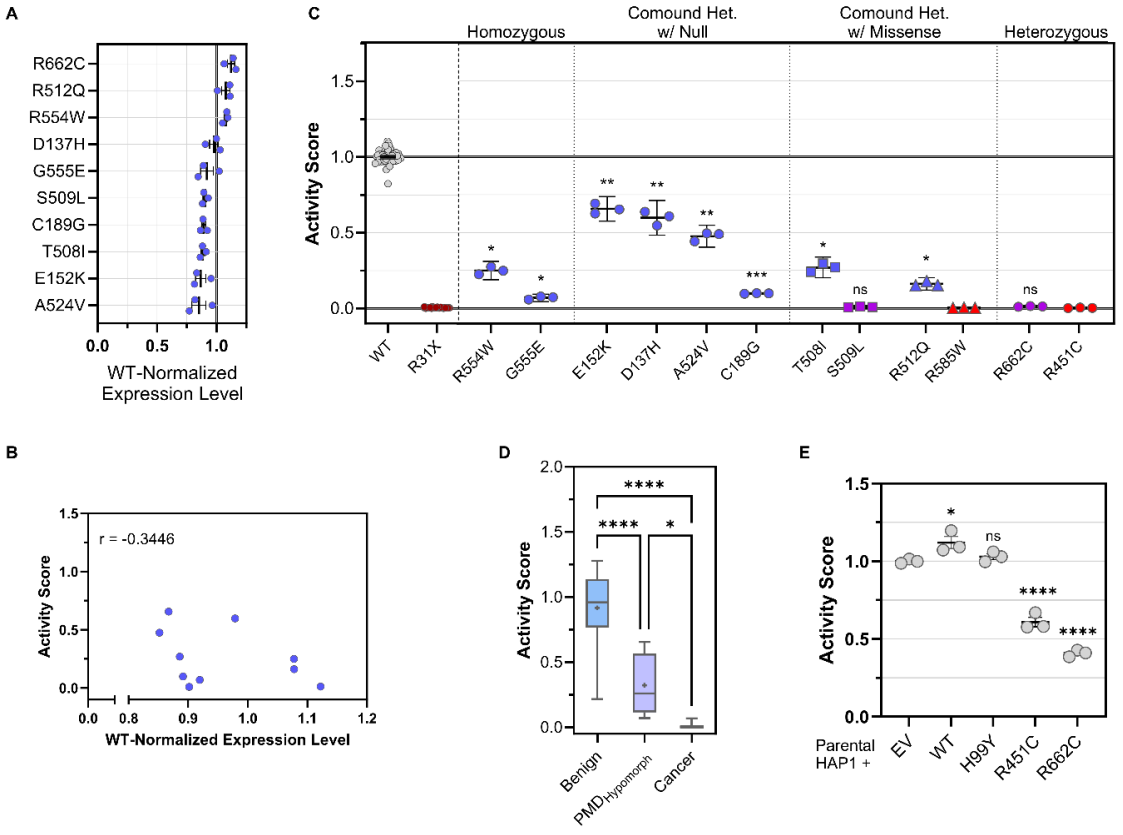

Figure 18. SDHA-related PMD is associated with SDH insufficiency, rather than deficiency. **A**. SDHA^{WT}-normalized expression levels for each variant. Each symbol is an independent replicate (n=3), with mean and SEM shown. **B.** Pearson correlation analysis between normalized expression levels and Activity Scores; r=-0.3446, *p*=0.330 (ns). **C.** Activity Scores corresponding to SDHA^{WT} (n=54), SDHA^{R31X} (n=54), and uncharacterized PMD-associated missense SDHA variants (n=3 replicates each). For PMD variants, mean and 95% CI are depicted. Comparisons were made between SDHA^{R31X} and all other novel groups using Welch's ANOVA test with Dunnett's T3 multiple-comparison correction applied; *p < 0.05, **p < 0.01, ***p < 0.001, ns = p > 0.05. Patient-paired compound heterozygous missense variants are distinguished by color and shape. SDHA^{WT} and SDHA^{R585W} are shown for visual comparisons and were not included in this ANOVA analysis. SDHA variants are color-coded according to their classification: cancer (red), hypomorphic PMD (purple), and severely dysfunctional PMD (magenta). Variants with square or triangle symbols were paired with compound heterozygous variants. **D.** Box and whiskers plot of benign (n=17), hypomorphic-PMD- (n=8), or cancer- (n=21) SDHA variant Activity Scores. Means are depicted by a '+' symbol. Group means were compared using Welch's ANOVA test with Dunnett's T3 multiple-comparison correction applied; *p < 0.05, ****p < 0.0001. **E.** Activity Scores for quasi-heterozygous expression of SDHA^{WT}, SDHA variants, or an empty expression vector (EV) in parental HAP1 cells. Mean and SEM from 3 replicates are shown for each. Means were compared to the EV group using an ordinary one-way ANOVA test with Dunnett's T3 multiple-comparison correction applied; *p < 0.05, ****p < 0.0001.

and the extent to which this characteristic could distinguish cancer variants from hypomorphic PMD and benign variants.For each variant, the ratio of SDHA to GFP protein, relative to that of $SDHA^{WT}$, was converted into a SDHA Abundance Score. As with Activity Scores, the SDHA Abundance Scores did not significantly correlate with the normalized expression levels (Pearson r = 0.14, p = 0.35) (**Figure 19A**). As expected, benign variants collectively exhibited WT-like abundance levels (mean SDHA Abundance Score = 0.87), though with substantial variability amongst the variants. (**Figure 19B**). Although the mean SDHA Abundance Scores of hypomorphic PMD variants (0.65) was lower than that of benign variants, the difference was not significant. In contrast, cancer variants (SDHA Abundance Score = 0.19) collectively displayed significantly lower levels of SDHA protein than non-cancer variants. However, unlike their activities, the SDHA abundance levels of cancer variants were not uniformly low. Most cancer variants indeed displayed a prominent loss of SDHA (median SDHA Abundance Score = 0.07), but a few variants retained remarkably high levels of SDHA, resulting in considerable overlap with both hypomorphic PMD and benign variants (**Figure 19C**). In fact, one cancer variant, $SDHA^{R451C}$, had an SDHA Abundance Score of 1.23, which was higher than nearly all other tested variants. $SDHA^{S509L}$ and $SDHA^{R662C}$, the PMD variants with severe SDH dysfunction, also retained high levels of SDHA (SDHA Abundance Score = 0.83 and 0.78, respectively). Thus, while complete loss of SDH function can be attributed to prominent loss of SDHA protein for many cancer variants, it is clear this is not the only way in which a missense mutation could cause complete loss of activity.

Although the discordance between SDHA abundance and the corresponding functional output for select non-functional variants was exceedingly evident, simple linear regression analyses suggested a similar, yet weaker, discrepancy amongst the hypomorphic PMD variants (**Figure 19D**). The regression coefficient (β) for benign variants was 1.01, indicating their SDH activity levels increased proportionally with SDHA abundance. In contrast, the β coefficient corresponding to hypomorphic PMD variants was significantly lower at 0.47 (**Figure 19D**). Although the effect was not as extreme as seen in some cancer variants ($\beta < 0.001$), these data show hypomorphic PMD variants collectively have lesser functional outputs than would be expected given their SDHA abundance levels, suggesting effects on enzyme catalysis.

Investigating the role of impaired flavinylation in SDHA dysfunction

Our analysis revealed that SDHA abundance levels were insufficient to fully describe the various functional outcomes observed amongst variants. While the impact of prominent SDHA loss on whole-complex activity is clear, how stable SDHA variants affect enzyme activity can be more nuanced. SDHA function requires its import into mitochondria, its maturation into a holoprotein mediated by multiple assembly factors, its assembly into the SDH holocomplex, and the oxidation of succinate to fumarate, all of which involve several significant conformational changes. Different amino-acid substitutions in SDHA could affect one or more of these processes and in unique ways, allowing for the potential of

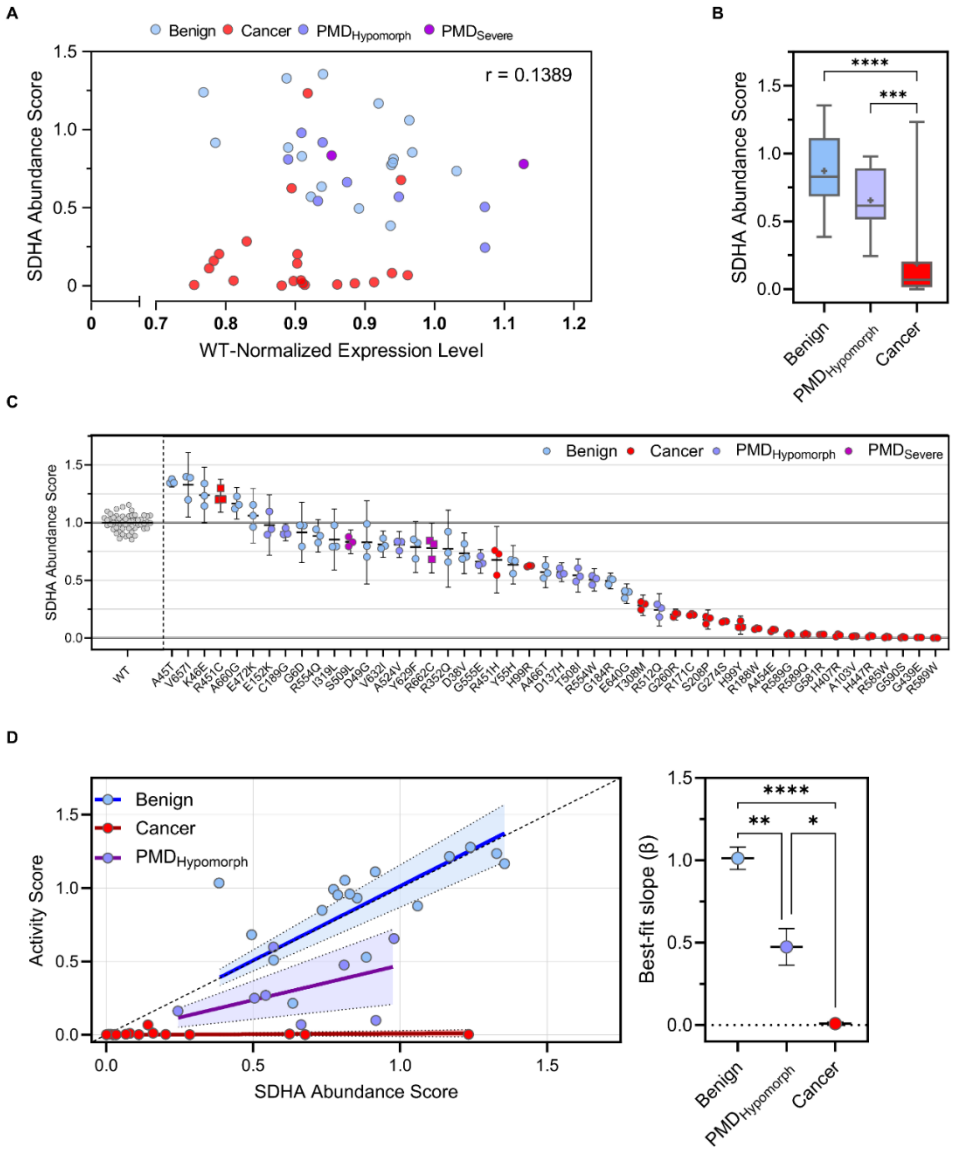

Figure 19. Decreased SDHA steady-state levels correlate with some, but not all, variant functional outcomes. **A**. Pearson correlation analysis between normalized expression levels and Activity Scores; r=0.1389, *p*=0.346 (ns). **B.** Box and whiskers plot of SDHA Abundance Scores for benign (n=17), hypomorphic PMD (n=8), and cancer SDHA variants (n=21). Mean is represented by the '+' symbol. An ordinary one-way ANOVA followed by Tukey's post hoc test was performed to compare all pairs of group means; ***$p < 0.001$, ****$p < 0.0001$. **C.** SDHA Abundance Scores corresponding to $SDHA^{WT}$ (n=54), as well as all benign, PMD, and cancer SDHA variants (n=3 replicates each). For SDHA variants, mean and 95% CI are shown. **D.** Left: Plot of Activity Score versus SDHA Abundance Score for benign, hypomorphic PMD, and cancer SDHA variants. For each group, a simple linear regression was modeled (zero-intercept); the best-fit lines and their corresponding 95% CIs (shaded) are shown. Right: Comparison of regression coefficients using Welch's ANOVA followed by Dunnett's T3 post hoc test for multiple comparisons; *$p < 0.05$, **$p < 0.01$, ****$p < 0.0001$.

a wide range of functional outcomes amongst variants. As such, we hypothesized that the mechanisms by which these amorphic variants with retained SDHA affect catalytic activity must be distinct from those of hypomorphic variants.

Interestingly, the cancer variants retaining the three highest levels of SDHA abundance involve residues known to play key roles in SDHA flavinylation, which is strictly required for its activity. Specifically, the His99 residue of SDHA forms a covalent methyl-histidyl bond with FAD, while Arg451 supports the formation of this bond by stabilizing a quinone-methide intermediate (56,61). As complete loss of this post-translational modification would result in the ablation of activity, we investigated whether loss of this post-translational modification could explain all cases of non-functional variants with severe dysfunction. To determine this, we examined the levels of covalently bound FAD by in-gel fluorescence detection following protein separation by SDS-PAGE. Although there were technical challenges with the quantification of these data, which precluded formal statistical analyses, qualitative observations could still be made. First, we established that representative benign variants ($SDHA^{Y629F}$ and $SDHA^{V657I}$) showed WT-like levels of FAD, whereas FAD could not be detected for the cancer variants affecting the residues involved in flavinylation ($SDHA^{H99R}$, $SDHA^{H99Y}$, $SDHA^{R451C}$, and $SDHA^{R451H}$) (**Figure 20**). In contrast, varying levels of FAD could indeed be detected from all hypomorphic PMD variants, supporting our conclusion that complete loss of flavinylation is a unique consequence of non-functional variants. However, FAD could also be detected in the remaining

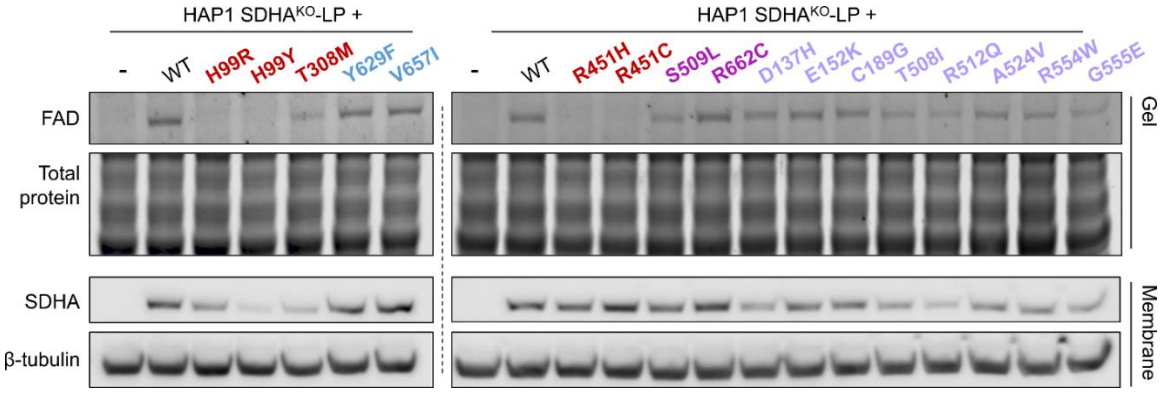

Figure 20. Loss of SDHA flavinylation is a unique, but not required, consequence of non-functional SDHA variants. Upper: Representative analysis of covalently-bound FAD by in-gel fluorescence of flavin with corresponding total-protein stain. Lower: Representative analysis of SDHA and β-tubulin, detected by immunoblotting. The dashed vertical line separates distinct membranes and gels which were processed and imaged independently. SDHA variants are color-coded according to their classification: cancer (red), benign (blue), PMD with severe dysfunction (magenta), or hypomorphic PMD variants (purple).

variants with severe dysfunction, including SDHA^{T308M}, despite low SDHA abundance (**Figure 20**). Thus, while loss of FAD-binding can indeed explain the functional outcome corresponding to some cancer variants, others affect downstream mechanics of SDHA function, in ways our current analyses have not identified.

The dominant negative function of select SDHA variants is associated with retained SDHB levels.

Our previous analyses revealed that amino-acid substitutions can impact SDHA function in multiple ways to result in the complete or nearly complete loss of SDH activity. However, two specific variants involved in heterozygous cases of PMD were not only non-functional, but they were also capable of interfering with SDHA^{WT} function in a pseudo-heterozygous system. In order to display a dominant negative function, we reasoned that a variant must necessarily have abundant SDHA protein levels. Indeed, these two variants, SDHA^{R451C} and

SDHA^{R662C}, had two of the three highest SDHA Abundance Scores among non-functional variants (SDHA Abundance Score = 1.23 and 0.78, respectively). We considered the possibility that these variants could compete with SDHA^{WT} for available FAD, but SDHA^{R451C} was not flavinylated. Although we cannot discount the possibility that this variant could nonetheless sequester available FAD in a non-covalent fashion, we incidentally identified an alternative mechanism to explain the interference with SDHA^{WT} function.

The iron-sulfur complex of SDH, SDHB, is considered a general sensor of SDH function, as it is markedly reduced in response to inactivation of any subunit. This allows SDHB IHC analysis to be used for the diagnosis of any *SDH*-related tumor, even prior to genetic sequencing. As such, we initially investigated the utility of decreased SDHB abundance as a readout for SDH dysfunction in our model. Linear regression analysis indicated Activity Scores were indeed a strong predictor of SDHB Abundance Scores, with a coefficient of 0.79. However, the data corresponding to SDHA^{R451C} and SDHA^{R662C} were highly discordant, as both retained remarkably high levels of SDHB (SDHB Abundance Scores = 0.81 and 1.09, respectively) (**Figure 21**). A possible explanation for these findings is that these variants can each form a stable interaction with SDHB, protecting it from being degraded, despite the complex being non-functional. Thus, in the context of heterozygous expression, these variants may compete with SDHA^{WT} for limited SDHB-binding without themselves contributing to succinate oxidation, resulting in a reduction of overall SDH activity levels.

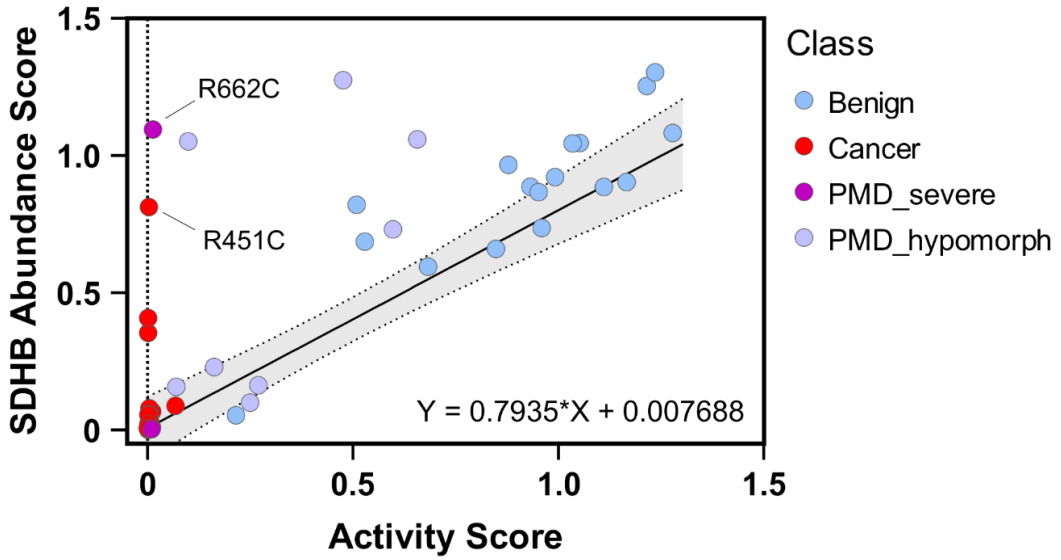

Figure 21. Rare non-functional variants retain high levels of SDHB. Plot of SDHB Abundance Score versus Activity score for SDHA variants. Each symbol represents the mean scores from three independent replicates for each metric (Benign = 17 variants, Cancer = 21 variants, PMD_severe = 2 variants, PMD_hypomorph = 8 variants). A simple linear regression analysis was performed with all variants, and the corresponding best-fit line (with 95% CI, shaded) and equation are shown. Regression analysis demonstrates the Activity Score as a strong predictor of the SDHB Abundance Score. Some variants with extremely low Activity Scores appear to contradict this relationship, in particular the dominant negative variants, SDHAR^{662C} and SDHA^{R451C}, as shown.

Comparison of functional data to computational predictions

In thoroughly profiling SDHA variants with previously established clinical interpretations, we gained several novel insights into SDHA dysfunction and how it relates to disease. Although SDHA amino-acid substitutions implicated in cancer can affect the protein by several distinct mechanisms, each variant results in a complete or near-complete loss of its function. In contrast, SDHA-related PMD is characterized by hypomorphic function. As a result, our functional model has a high capacity to distinguish distinct classes of SDHA according to their Activity Scores. To evaluate precisely how well our functional data could perform in various clinically relevant classification tasks, we performed receiver operating

characteristic (ROC) analyses. We then compared these performances to those of six frequently used computational models that attempt to predict a variant's pathogenicity or effect on function: CADD, BayesDel (no AF), MetaRNN, MetaSVM, MutationAssessor, and REVEL (240-245).

First, we assessed each model's performance in distinguishing cancer from non-cancer variants. For this analysis, only benign and hypomorphic PMD variants were included as 'non-cancer' variants. SDHA^{S509L} was excluded because it existed *in trans* with a hypomorphic variant SDHA^{T508I}, which we considered to be the main contributor to PMD, rather than SDHA^{S509L}. SDHA^{R662C} was excluded because its involvement in PMD is as a dominant negative variant; thus, the functional data for this variant alone is not representative of PMD. For each computational model, we used the raw scores predicted for each variant; however, for the Activity Scores, we accounted for the uncertainty of the means by assigning a 'positive' cancer classification to a variant if the given threshold was within or above its 95% CI. According to the area under the ROC curves (AUCs), the discriminatory power of the computational models in identifying cancer variants was substantial, particularly MutationAssessor and MetaSVM (AUC = 0.983 and 0.947, respectively) (**Figure 22A**). Nevertheless, classification using Activity Scores from our model was even more impressive, with an exceptional AUC of 0.998. However, the AUC metric describes the performance of a classifier across the entire range of thresholds; the practical implementation of a classifier typically requires the selection of a single threshold. This often necessitates prioritizing the positive predictive value (PPV) or true positive rate

(TPR) at the cost of the other. When plotting each variant's score corresponding to the different computational predictions, the trade-off between losing 'true positive' classifications and gaining 'false positive' classifications at different thresholds becomes abundantly clear (**Figure 22B**). When selecting a threshold to correctly identify all cancer variants (100% TPR), the PPVs for the computational models drop between 58 and 84% (**Figure 22C**). However, when considering evidence for cancer-risk assessment, we would prioritize PPV to minimize the probability of recommending life-long screening, resulting in undue expense and stress, for individuals who do not need it. When using a threshold to obtain 100% PPV, the best performing computational model, MutationAssessor, could correctly classify only 76% of the cancer variants, while the next best, MetaSVM, was only able to classify half the variants, and CADD is entirely unable to classify any (TPR = 52% and 0%, respectively) (**Figure 22C**).

In contrast to the outputs of the computational models, there is only a single overlap of 95% CIs corresponding to cancer and non-cancer variant Activity Scores, resulting in virtually no trade-off required when choosing a threshold (**Figure 22B**). Specifically, when using a threshold to classify all cancer variants, our model still achieves an excellent PPV of 95%, while requiring a PPV of 100% still allows our model to classify 95% of all cancer variants (**Figure 22C**). Thus, the Activity Scores obtained from our functional model have a clear advantage over the selected computational models for identifying cancer variants.

For several of the computational models, the high cost of sensitivity when prioritizing PPV could be largely attributed to the cancer variants having similar scores to hypomorphic PMD variants (**Figure 22B**). This is not entirely surprising, as these PMD variants are indeed pathogenic and affect function, which the tools attempt to predict. Therefore, we next assessed how well each model could distinguish all pathogenic variants (cancer and hypomorphic PMD) from benign variants. When using Activity scores for this classification task, only 83% of pathogenic variants could be classified as such when using a threshold that excludes any false positives (**Figure 22D**). However, this performance was highly influenced by the excellent rate of cancer-variant detection, as only three of the eight hypomorphic PMD variants were correctly predicted as pathogenic at this threshold. In contrast, MetaSVM and MetaRNN performed better both in the rate of pathogenic variant detection and the rate of hypomorphic-PMD-variant detection.

Although the capacity to distinguish hypomorphic PMD variants from benign variants according to their Activity Scores was comparatively low, the poor performance can be largely attributed to abnormally low-scoring benign variants, rather than abnormally high-scoring PMD variants (**Figure 22B**). Therefore, we investigated whether the functional data would have higher utility in distinguishing benign variants from pathogenic variants. For this analysis, a variant would obtain a ‘positive’ benign classification if the given threshold was within or below its 95% CI. As expected from the distribution of these CIs, there was a large difference between the optimal thresholds to obtain 100% TPR or

PPV (**Figure 22E**). However, this did not translate to a large effect on the classification performance, as only three benign variants would be affected by choosing between these thresholds. As a result, a TPR of 82% could be achieved at the threshold that excludes the highest-scoring hypomorphic PMD variant (**Figure 22F**). This performance was better than or equal to all computational models, apart from BayesDel, which achieved a TPR of 94% under the same criterion.

Although our model could not clearly distinguish many hypomorphic PMD from benign variants, Activity Scores were the only metric that could identify over 75% of the variants within each of the cancer and benign groups while using thresholds to maintain perfect PPV (**Figure 22F**). When using these thresholds together, an exceptional 89% of all benign and cancer variants could be accurately classified as such, whereas the best-performing computational model could only achieve a 71% detection rate, highlighting the superior performance of our functional model in making clinically relevant classifications.

Establishing guidelines for the interpretation of SDHA VUS functional data

We have demonstrated an impressive capacity to detect cancer and benign variants according to the Activity Scores derived from our functional model. As such, we established guidelines to convert these scores into functional classifications for the interpretation of SDHA VUS, which can subsequently be incorporated as evidence into the clinical variant interpretation framework outlined by ACMG/AMP (**Table 2**) (180). According to our ROC analysis, any threshold between the 95% CIs corresponding to the hypomorphic PMD variant

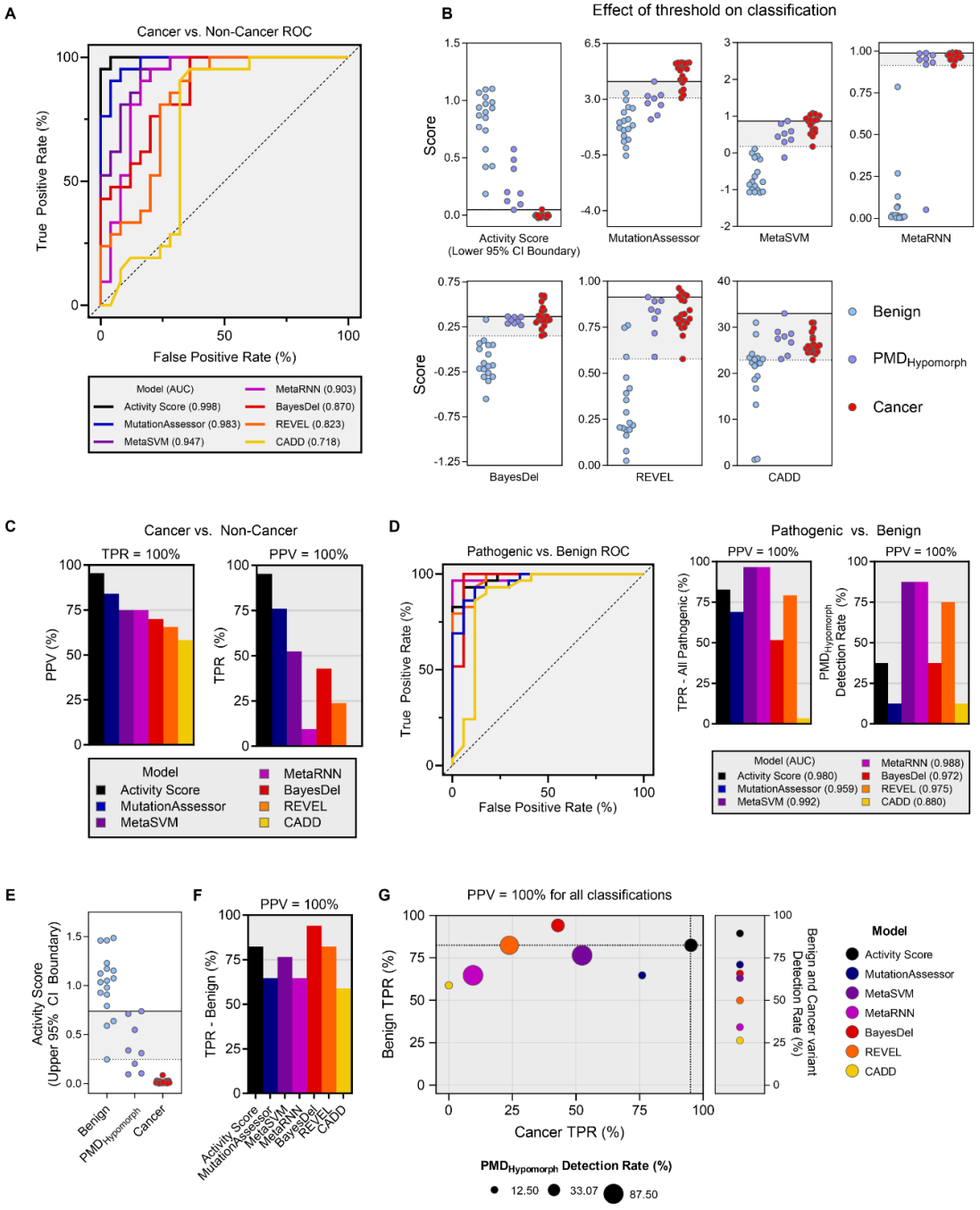

Figure 22. Activity Models derived from HAP1 *SDHA*^{KO} model outperform computational models in predicting clinical classifications of known control variants. **A.** ROC analysis corresponding to cancer (positive) versus non-cancer (negative) classification task. **B.** The scores obtained from each model that was analyzed, for each variant. For Activity Scores, the lower boundaries of the 95% CIs are shown. A solid black line denotes the threshold required to achieve a PPV of 100%. Dashed denotes the threshold required to achieve 100% TPR. Variants falling between these thresholds for each model (grey shading) represent the trade-off required when prioritizing either PPV or TPR. **C.** For each model, the maximal TPR or PPV, when the other is required to be 100%.

D. Left: ROC corresponding to pathogenic (positive) versus benign (negative) classification task. Middle: Rate of pathogenic variant detection (TPR) for each model, at a threshold where PPV is required to be 100%. Right: Same as middle, but for the rate of hypomorphic PMD variant detection. **E.** The upper boundaries of the 95% CIs for Activity Scores for denoted variants. As in B, the thresholds required to obtain 100% PPV (solid black line) or 100% TPR (dashed line), but for the positive identification of benign variants. **F.** The maximal TPR for benign variant detection when PPV is equal to 100%. **G.** Summary of model performances in classifying clinical control variants. Vertical and horizontal dashed lines correspond to Cancer TPR and Benign TPR, respectively, when PPV is equal to 100% for both classification tasks. The size of each symbol corresponds to the rate of hypomorphic PMD variant detection when PPV = 100%.

SDHA^{G555E} (95% CI = 0.045-0.094) and the cancer variant SDHA^{R589Q} (95% CI = -0.026-0.029) would result in the same TPR (95%) and PPV (100%). We opted to take a conservative approach and set the threshold to receive a 'cancer-like' classification at the lower boundary, 0.029. To further increase the confidence associated with these classifications, we would require a variant's 95% CI for the Activity Score to be entirely below the threshold to receive this classification. Following the same guidelines, a threshold of 0.740, corresponding to the benign variant SDHA^{I319L} (95% CI = 0.740-1.12) was chosen as the threshold to receive a 'benign-like' classification. As with the 'cancer-like' classification, a variant would only receive this classification if its Activity Score CI was entirely above the threshold. Due to the poor performance in distinguishing hypomorphic PMD variants, if any part of the Activity Score CI for a variant fell between the two

Table 2. Functional interpretation of Activity Scores and strength of evidence.

Activity Score	Control Cancer Variants	Control Benign Variants	Control Hypomorphic PMD Variants	Functional Classification	ACMG/AMP Criteria (OddsPath)
≥0.740	**0**	**13**	**0**	**Benign-like**	**BS3_strong (0.045)**
0.029-0.740	**1**	**4**	**8**	**(Indeterminate)**	**-**
≤0.029	**20**	**0**	**0**	**Cancer-like**	**PS3_strong (23.8)**

thresholds (0.029-0.740), we would not assign a functional classification and instead consider its consequence indeterminate.Following the recommendation of the ClinGen SVI WG, an OddsPath score can be calculated to determine what level of strength can be applied to the evidence obtained from a functional assay (194). With the threshold for cancer-like dysfunction, 20 of 21 cancer variants could be accurately classified as such. This corresponds to an OddsPath of 23.8, which enables us to utilize these classifications as strong functional evidence (PS3_strong) within the ACMG/AMP framework. With our threshold for benign-like function, 13 of 17 benign variants could be accurately classified, corresponding to an OddsPath of 0.045. As a result, functional data demonstrating benign-like activity for a SDHA VUS could be used as strong functional evidence against the variant's pathogenicity (BS3_strong). For variants not receiving a functional classification (indeterminate), we would not use the data as evidence for variant interpretation.

Functional characterization and reclassification of SDHA VUS for cancer pathogenicity

After establishing guidelines for converting functional data into functional classifications that can be used as strong evidence for variant interpretation, we selected 24 missense SDHA VUS to functionally characterize as a pilot for the reclassification of cancer pathogenicity. For each variant, we generated a stable cell line and measured Activity Scores. As with all previous cell lines we characterized, there was moderate variability in expression levels, but these

levels did not significantly correlate with the corresponding Activity Scores (r = 0.356, p = 0.088) (**Figure 23A**).

The Activity Scores corresponding to the SDHA VUS were similar to those of the clinically classified control variants, allowing for a high rate of functional classification. Four variants, SDHA^{T96I}, SDHA^{P372R}, SDHA^{R232H}, and SDHA^{V425G} had Activity Score CIs above the threshold to receive benign-like classifications (**Figure 23B**). Sixteen variants had CIs below the cancer-like threshold and were classified accordingly. The remaining four SDHA VUS had Activity Score CIs that extended below the benign-like threshold (SDHA^{N118S}), above the cancer-like threshold (SDHA^{C438F} and SDHA^{T143M}) or fell entirely between the two (SDHA^{R465W}). As such, functional classifications for these variants could not be assigned (indeterminate).

In addition to these VUS that were selected before performing experiments, our analyses of clinical control variants revealed two PMD-associated variants, SDHA^{S509L} and SDHA^{R662C}, which resulted in a complete loss of SDH activity. Although they have been described as pathogenic for PMD, their cancer pathogenicity has not been established; thus, we considered them as VUS for cancer. As the Activity-Score CI for both variants is below 0.029, each received a cancer-like functional classification (**Figure 23A**). After obtaining functional classifications, we investigated whether we could identify the mechanisms of dysfunction associated with the cancer-like SDHA VUS. As expected, many of these variants displayed a prominent loss of SDHA protein; however, just as we observed with several control cancer variants,

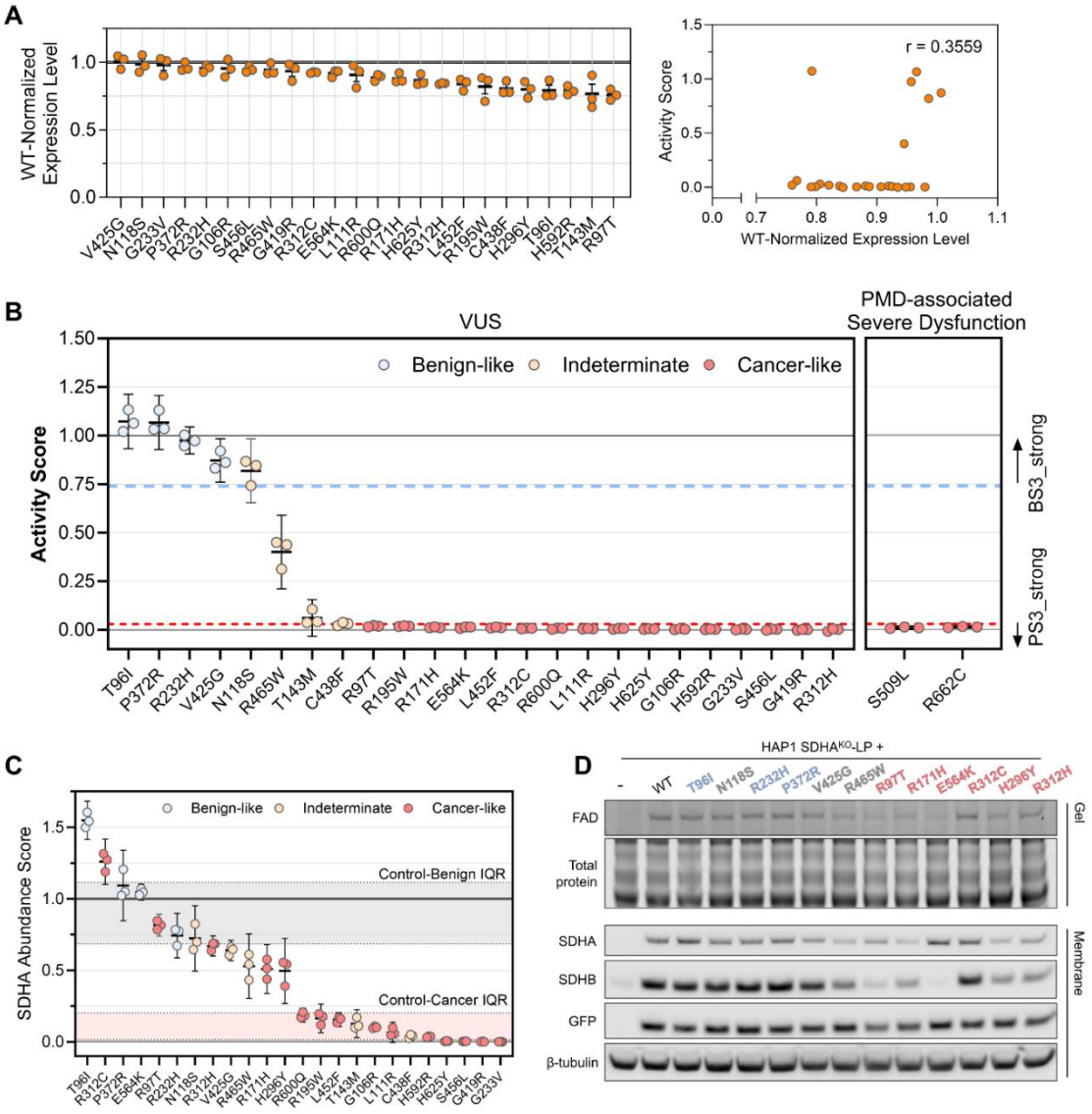

Figure 23. Functional classification of missense SDHA VUS. **A.** Left: SDHA^{WT}-normalized expression levels for each SDHA VUS, with independent replicates (n=3), mean, and SEM shown. Right: Pearson correlation analysis between normalized expression levels and Activity Scores; r=0.3559, *p*=0.088 (ns). **B.** Activity Scores corresponding to selected SDHA VUS (left) and the PMD-associated variants SDHA^{S509L} and SDHA^{R662C} (right) (n= 3 replicates each, mean and SEM shown). Four variants (blue symbols) met the criteria (threshold = 0.740, blue dotted line) for a benign-like classification. Eighteen variants (red symbols) met the criteria (threshold = 0.029, red dotted line) for a cancer-like classification. **C.** SDHA Abundance Scores for selected SDHA VUS, color-coded by their functional classifications (n = 3 replicates each, mean and SEM are shown). For visual comparisons, interquartile ranges of SDHA Abundance Scores correspond to control benign variants (grey shading) and control cancer variants (red shading) are shown.

several of these cancer-like SDHA VUS retained abundant SDHA protein (**Figure 23C**). Furthermore, although we detected a wide range of FAD levels among these variants, none resulted in a complete loss of flavinylation (**Figure 23D**). $SDHA^{R312C}$, and to a lesser extent, $SDHA^{R312H}$, even appeared to have FAD levels comparable to those of $SDHA^{WT}$ and benign-like SDHA VUS. Interestingly, further analysis revealed remarkable levels of SDHB protein corresponding to $SDHA^{R312C}$, suggesting similarly to $SDHA^{R451C}$ and $SDHA^{R662C}$, this variant may have dominant negative capabilities. Thus, just as our analyses could not reveal the mechanism of dysfunction for all control cancer variants, several cancer-like SDHA VUS appear indistinguishable from highly active variants, apart from their SDH activity levels.

Finally, we investigated the effect of incorporating our functional classifications as evidence for the interpretation of these SDHA VUS. We combined our functional evidence with existing evidence obtained from the human genomic variation search engine VarSome. VarSome performs its own germline variant classification and reports the classification that was made, along with the ACMG/AMP criteria that were met and with which strength of evidence. In this implementation, VarSome follows the recommendations of the ClinGen SVI WG by using a points-based system, in which evidence of different strengths is assigned different point values (233). The points corresponding to all available evidence are combined, resulting in a Pathogenicity Score, which has established thresholds required to reach Benign, Likely Benign, Likely Pathogenic, or Pathogenic classifications. This methodology allows us to easily

incorporate our functional evidence, recalculate Pathogenicity Scores, and reclassify variants as allowed.

The evidence available for each of the SDHA VUS and the corresponding strength of evidence, as reported by VarSome, is listed in **Table 3**. Importantly, VarSome was not utilized when initially determining which variants are VUS for cancer pathogenicity. According to VarSome, four of the 26 variants had sufficient evidence for non-VUS classifications prior to the inclusion of our functional evidence. This was in large part due to computational evidence being considered as strong evidence (PP3_strong, BP4_strong) for scores that surpassed a highly calibrated threshold (246). In total, 14 variants met the criteria for strong computational evidence, but the total Pathogenicity Scores for 10 were still insufficient to reach a classification threshold. However, SDHA^{V425G} and SDHA^{S456L} were classified as Likely Benign, while SDHA^{R171H} and SDHA^{H592R} were classified as Likely Pathogenic. Nonetheless, we recalculated the Pathogenicity Scores after incorporating our functional evidence for these four variants, as well as the 22 that VarSome also considered VUS (**Table 3**).

Of the 22 SDHA variants previously classified as VUS by VarSome, three were classified as benign-like by our functional model. The incorporation of BS3_strong evidence was sufficient for each of these variants to reach a Likely Benign classification (**Table 3, Figure 24**). Fifteen of the 22 VarSome-VUS had cancer-like dysfunction in our model. The incorporation of PS3_strong evidence allowed all but SDHA^{R600Q} to reach a Likely Pathogenic classification. The

Table 3. Evidence for the classification of SDHA VUS within the ACMG/AMP framework

	ACMG/AMP Criteria					Classifications (Pathogenicity Score)	
Variant	Population data	Computational predictions	Hotspot	Same Codon as P/LP	Functional data	VarSome Prior	VarSome Revised
T96I	PM2_sup	PP3_mod	-	-	BP3_strong	VUS (3)	LB (-1)
R97T	PM2_sup	PP3_mod	-	-	PS3_strong	VUS (3)	LP (7)
G106R	PM2_sup	PP3_strong	-	-	PS3_strong	VUS (5)	LP (9)
L111R	PM2_sup	PP3_mod	-	-	PS3_strong	VUS (3)	LP (7)
N118S	PM2_sup	BP4_sup	-	-	-	VUS (0)	VUS (0)
T143M	PM2_sup	PP3_mod	-	-	-	VUS (3)	VUS (3)
R171H	PM2_sup	PP3_strong	-	PM5_mod	PS3_strong	LP (7)	P (11)
R195W	PM2_sup	PP3_strong	-	-	PS3_strong	VUS (5)	LP (9)
R232H	PM2_sup	-	-	-	BP3_strong	VUS (1)	LB (-3)
G233V	PM2_sup	PP3_strong	-	-	PS3_strong	VUS (5)	LP (9)
H296Y	PM2_sup	PP3_strong	-	-	PS3_strong	VUS (5)	LP (9)
R312C	PM2_sup	PP3_strong	-	-	PS3_strong	VUS (5)	LP (9)
R312H	PM2_sup	PP3_strong	-	-	PS3_strong	VUS (5)	LP (9)
P372R	PM2_sup	PP3_mod	-	-	BP3_strong	VUS (3)	LB (-1)
G419R	PM2_sup	PP3_strong	-	-	PS3_strong	VUS (5)	LP (9)
V425G	PM2_sup	BP4_strong	-	-	BP3_strong	LB (-2)	LB (-6)
C438F	PM2_sup	PP3_mod	-	-	-	VUS (3)	VUS (3)
L452F	PM2_sup	PP3_strong	-	-	PS3_strong	VUS (5)	LP (9)
S456L	PM2_sup	BP4_strong	-	-	PS3_strong	LB (-3)	VUS (1)
R465W	PM2_sup	PP3_mod	-	-	-	VUS (3)	VUS (3)
S509L	PM2_sup	PP3_mod	-	-	PS3_strong	VUS (3)	LP (7)
E564K	PM2_sup	PP3_mod	-	-	PS3_strong	VUS (3)	LP (7)
H592R	PM2_sup	PP3_strong	PM1_mod	-	PS3_strong	LP (7)	P (11)
R600Q	PM2_sup	-	-	-	PS3_strong	VUS (1)	VUS (5)
H625Y	PM2_sup	PP3_strong	-	-	PS3_strong	VUS (5)	LP (9)
R662C	PM2_sup	PP3_strong	-	-	PS3_strong	VUS (5)	LP (9)

Note: supporting, sup (+/- 1), moderate, mod (+/- 2), strong (+/- 4). Pathogenicity Score thresholds: Likely Benign (LB): between -6 and -1, VUS: between 0 and 5, Likely Pathogenic (LP): between 6 and 9, Pathogenic (P): greater than 10, respectively. Existing data were obtained from VarSome (234).

remaining four VarSome-VUS had indeterminate functional consequences after our analysis, and thus, could not be reclassified. Our cancer-like functional classifications for SDHA^{R171H} and SDHA^{H592R} agreed with the existing Likely Pathogenic classifications made by VarSome, which allowed them to be upgraded to a Pathogenic classification. Only one of the two variants previously classified as Likely Benign by VarSome, SDHA^{V425G}, had a benign-like functional classification from our model, though it could not be upgraded to a Benign classification. In contrast, the other Likely Benign variant, SDHA^{S456L}, received a cancer-like dysfunction classification in our model, with an Activity Score among the lowest measured across all variants, including the known cancer variants. Incorporating PS3_strong evidence for SDHA^{S456L} resulted in its downgrade to a VUS classification.

In total, the functional classifications derived from our functional model provided considerable value for the clinical interpretation of SDHA VUS (**Figure 24**). Of the 26 total missense SDHA variants we considered as VUS for cancer pathogenicity, 22 (85%) received a high-confidence functional classification according to their Activity Scores. Although all of these variants were not originally considered VUS by VarSome, 20 total variants could be reclassified after incorporating our functional evidence into their variant interpretation framework, representing 77% of the VUS assayed and 91% of the VUS for which strong functional evidence was obtained. Importantly, this includes 14 missense SDHA variants that could now be classified as Likely Pathogenic, providing

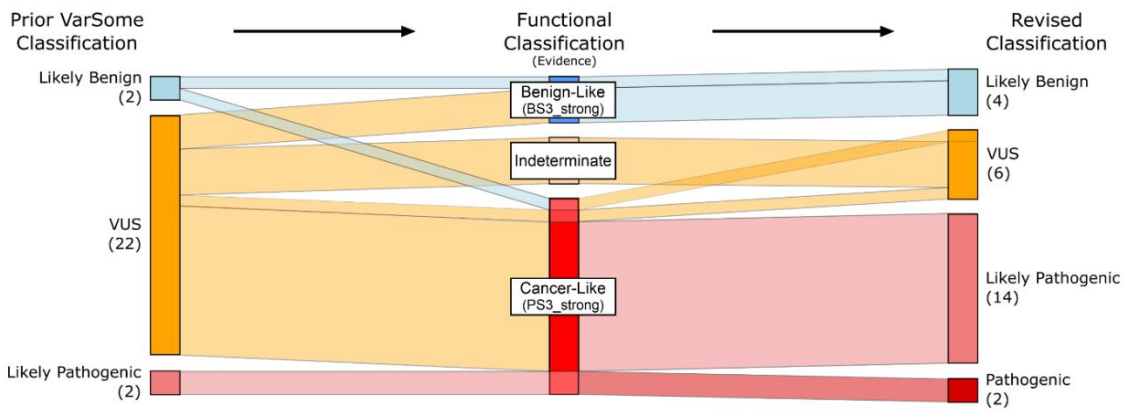

Figure 24. Evidence derived from our functional model enables the reclassification of many missense SDHA VUS. Modified Sankey diagram showing the reclassification fate of SDHA variants upon incorporating functional evidence. Prior classifications were obtained from VarSome (234).

germline carriers of these variants crucial opportunities for early and possibly life-saving interventions.

D. Discussion

SDHA is a key component of the SDH enzyme complex whose compromised function can result in tumor formation (105). Germline LOF variants of *SDHA* confer an increased lifetime risk for the development of cancer, but the identification of such variants through genomic sequence analyses can provide opportunities for early intervention (132,165). Although the rate of SDHA variant detection has increased along with increased sequencing availability, our ability to interpret clinical significance remains severely lacking. Incomplete cancer penetrance often reduces the availability and strength of clinical evidence to firmly establish pathogenicity (179). As such, the overwhelming majority of missense *SDHA* variants identified are VUS, which cannot be acted upon (186). In this study, we aimed to address this problem by providing supplemental functional evidence for or against a variant's pathogenicity.

The VUS problem is not unique to *SDHA* (179). In recent years, many others have focused on developing functional assays to interrogate disease-relevant variants and demonstrated the utility of incorporating functional evidence for clinical variant interpretation (181,199). However, unlike most of these other genes, the relationship between the degree of SDHA dysfunction and cancer is not fully established. Furthermore, mutations affecting SDHA function can also result in PMD, and it is unclear whether a variant's pathogenicity corresponding to each disease is equivalent (93). Therefore, to enable the inclusion of functional evidence for determining a SDHA variant's pathogenicity for cancer, we first elucidated the extent and mechanisms of SDHA dysfunction underlying cancer. We subsequently demonstrated how these insights allow us to interpret the functional consequence of SDHA VUS and use this evidence to help identify variants likely to be associated with cancer.

To achieve this, we developed a novel human *SDHA*-knockout cell line that enables the functional characterization of human SDHA variants. We identified variants with previously established and distinct clinical classifications and interrogated the functional consequences that distinguish them. In this analysis, we utilized an approach to generate stable, isogenic variant cell lines that allows for differences observed to be attributed to the intrinsic properties of the variants with high confidence.

In our analysis, the known benign variants largely had WT-like activity, though some produced surprisingly low Activity Scores. However, nearly all cancer variants resulted in complete loss of SDH activity, and only SDHA^{G274S}

produced an Activity Score (95% CI = 0.050-0.086) that was significantly higher than that of the control null variant, $SDHA^{R31X}$ (95% CI = 0.003-0.004) (**Figure 17B**). In contrast, each case of SDHA-related PMD was associated with varying levels of reduced, but present, levels of SDH activity, and our analysis revealed a novel class of pathogenic SDHA variants that are characterized by hypomorphic function and are specifically associated with PMD (**Figure 18**). The only PMD-associated variants that resulted in a complete loss of SDH activity were either *in trans* with a hypomorphic SDHA variant or were dominant negative heterozygous variants.

To investigate whether the distinct functional outcomes corresponding to cancer and hypomorphic PMD variants can be attributed to unique mechanisms, we investigated SDHA abundance and flavinylation status corresponding to each variant. As expected, the prominent loss of SDHA protein or its covalent flavinylation was strictly associated with a complete loss of SDH activity (**Figure 19 and Figure 20**). However, several cancer variants appeared indistinguishable from benign or hypomorphic PMD variants by these analyses. In addition, these analyses could not reveal distinguishing factors between hypomorphic PMD variants and benign variants with low Activity Scores. Together, these data suggest that some SDHA variants likely result in alternative consequences, such as impaired binding with assembly factors or SDHB. Further investigation may lead to a better understanding of the dysfunction associated with cancer- and PMD-associated SDHA variants.

Although we cannot yet fully explain how each variant affects function, SDH activity data alone nevertheless have a remarkable capacity to distinguish distinct classes of SDHA variants. Several of the computational prediction models also performed well in identifying pathogenic variants from benign variants, but this broad level of discrimination is insufficient. As cancer and PMD are associated with distinct levels of SDH dysfunction, we suggest a variant's pathogenicity for each disease should be interpreted independently. Using a threshold to maintain 100% PPV specifically for classifying cancer-associated variants, the best-performing computational model, MutationAssessor, could only achieve a TPR of 75% (**Figure 22C**). In contrast, our functional model could achieve a TPR of 95% while maintaining a 100% PPV (**Figure 22C**). Furthermore, as the majority of benign variants had distinctive WT-like activity, we could set a threshold for classifying benign variants with an 82% TPR and a 100% PPV (**Figure 22F**). Although our data revealed a novel class of hypomorphic SDHA variants that are associated with PMD, the presence of low-scoring, outlier benign variants hampered our ability to establish criteria for their classification (**Figure 22**). Several factors may contribute to our inability to clearly distinguish between benign and hypomorphic PMD SDHA variants, which are discussed in further detail below.

Nonetheless, the capacity and performance of our functional model for specifically classifying cancer and benign variants translated to high clinical utility for the interpretation of SDHA VUS. Following the recommendation of ClinGen, the OddsPath scores we calculated allow us to incorporate strong evidence in

favor of pathogenicity (PS3_strong) or strong evidence against pathogenicity (BS3_strong) for any SDHA VUS meeting the criteria to receive a cancer-like or benign-like functional classification, respectively (**Table 2**). As such, we determined Activity Scores and derived functional classifications for 26 SDHA variants we identified as having uncertain pathogenicity for cancer (**Figure 23**).

As our initial criteria for selecting SDHA VUS was not based on VarSome's germline variant classifier, four of the SDHA variants we considered to be VUS for cancer pathogenicity were already classified by VarSome as Likely Benign or Likely Pathogenic before the addition of our functional evidence. Nonetheless, after incorporating our functional data with the existing evidence, only six variants had Pathogenicity Scores that met the criteria for a VUS classification. In total, 14 and 3 VUS were reclassified to Likely Pathogenic and Likely Benign, respectively, while $SDHA^{R171H}$ and $SDHA^{H592R}$ were upgraded from Likely Pathogenic to Pathogenic, and $SDHA^{V425G}$ remained Likely Benign.

Four SDHA variants remained VUS as their Activity Scores did not meet the thresholds for strong functional evidence. This is largely a consequence of our highly conservative criteria for functional classification. The Activity Score 95% CI for $SDHA^{N118S}$ partially surpassed the threshold for a benign-like classification, while those of $SDHA^{T143M}$ and $SDHA^{C438F}$ partially fell below the threshold for a cancer-like classification (**Figure 23**). If we were less stringent in assigning strong evidence, none of these variants would remain VUS after recalculating Pathogenicity Scores. Alternatively, we could utilize these functional data as moderate evidence (BS3_moderate and PS3_moderate) to maintain the

confidence associated with strong evidence. In this approach, the total evidence against pathogenicity for SDHA^{N118S} would still be sufficient for a Likely Benign classification. SDHA^{T143M} and SDHA^{C438F} would remain VUS, but with a Pathogenicity Score of 5, even just one additional piece of supporting evidence in favor of cancer pathogenicity would allow for a Likely Pathogenic classification. The last variant we could not derive a functional classification for was SDHA^{R465W}. This was largely due to our inability to properly distinguish between benign and hypomorphic PMD variants, as the variant's Activity Score was 0.400. Although its pathogenicity for PMD remains uncertain, SDHA^{R465W} is unlikely to be pathogenic for cancer.

While the above four variants remained VUS because we could not obtain functional evidence, two variants were classified as VUS even after strong functional evidence was incorporated into their Pathogenicity Scores. The first variant, SDHA^{S456L}, was previously classified as Likely Benign by VarSome but received a cancer-like functional classification from our model (**Table 3**). The initial classification was largely due to the inclusion of strong computational evidence against pathogenicity (BP4_strong) (**Table 3**). However, VarSome utilizes MetaRNN for computational predictions, which heavily weighs allele frequency data from databases such as ExAC and gnomAD (242). In ExAC, the allele corresponding to SDHA^{S456L} has a reported frequency of 0.027, which would strongly support a lack of pathogenicity, but this sequencing data did not pass all quality filters (185,247). In the gnomAD v4.0.0 database, the SDHA^{S456L} variant also failed the allele-specific filter for exomic sequencing but passed the

genomic sequencing filter, and the reported allele frequency is 1.3×10^{-5} (185). As such, the strong computational evidence against pathogenicity may be influenced by low-quality data. This variant also has two independent Likely Benign classifications submitted to ClinVar, which the same evidence may have also influenced. However, in support of our cancer-like functional classification, $SDHA^{S456L}$ was reported as a germline variant a SDHB-IHC negative GIST, which also harbored a somatic compound heterozygous null variant, $SDHA^{R210X}$ (133). Although the reclassification to VUS does not currently impact the course of action for individuals harboring a germline $SDHA^{S456L}$ variant, if additional evidence in favor of pathogenicity becomes available, the Pathogenicity Score may ultimately reach the threshold for a Likely Pathogenic classification.

The last variant, $SDHA^{R600Q}$, received a cancer-like functional classification but remained VUS, as the Pathogenicity Score still did not reach the threshold for Likely Pathogenic (**Table 3**). Interestingly, this variant was reported by Bausch et al. in two independent cases of paraganglioma, each of which demonstrated at least one clinical predictor that suggested heritability (204). $SDHA^{R600Q}$ would have met our criteria for a control cancer variant, as the authors assigned it a Likely Pathogenic classification following ACMG/AMP guidelines, but there was also a single submitter in ClinVar that interpreted the variant as Likely Benign (186). Due to these conflicting reports, we initially considered $SDHA^{R600Q}$ a VUS. As the ClinVar submitter did not specify what condition was associated with the variant or provide any rationale

for their Likely Benign interpretation (Accession: SCV000309994.1), it is difficult to address the discrepancy. However, the mutation encoding SDHA^{R600Q} was recently reported as an example of a variant that was mistakenly attributed to *SDHA* by one method of sequencing, while another method revealed the variant was actually a SNP within one of the four highly conserved pseudogenes of SDHA (202). Thus, it is possible some historical evidence against cancer pathogenicity for SDHA^{R600Q} should not be applied. Lastly, with a Pathogenicity Score of 5, any additional supporting evidence in favor of cancer pathogenicity, such as the patient-level data reported by Bausch et al., would allow SDHA^{R600Q} to be classified as Likely Pathogenic in our framework.

The discrepancies between existing clinical classifications made by independent groups highlight the challenges associated with interpreting variant pathogenicity, especially when evidence is limited. Although we demonstrated how functional evidence can greatly improve variant interpretation, some limitations of our functional analysis pipeline should be considered. We selected the nearly-haploid HAP1 cell line to increase the likelihood of obtaining a *SDHA*-knockout cell line (248). However, as the cell line was derived from a chronic myelogenous leukemia cell line and nearly all genes are hemizygous, our functional data may not fully represent the *exact* consequences of each variant in the context of *SDHA*-related disease.

For example, it has been proposed that the PMD-associated SDHA^{G555E} affects function by disrupting the binding between SDHA and SDHB (56,249). If the relative abundance of SDHB in HAP1 cells is substantially lower than in

normal diploid cells, the dysfunction of SDHA^{G555E} may have been artificially exacerbated, resulting in an underestimated Activity Score. Conversely, the Activity Score of a variant that affects SDHA-intrinsic function, such as succinate-binding, may not have been as susceptible to the idiosyncrasies of the HAP1 cell line. As we could not elucidate the mechanism of dysfunction for many variants, it is difficult to determine how and which variant Activity Scores may have been affected. However, this issue is highly unlikely to concern variants that result in a complete loss of SDH activity, nor our interpretation of cancer and cancer-like variants. Nevertheless, our use of the HAP1 cell line may have contributed to our inability to properly distinguish hypomorphic PMD variants from benign variants.

The difficulty in determining whether variants could be associated with PMD stems from unexpectedly low-scoring benign variants. While the low Activity Scores for these variants could indeed be artifacts of using the HAP1 cell line as a model, there are additional factors to consider. One possible explanation is that several low-scoring variants we used as benign controls are, in fact, not benign. We have already described instances where some interpreted a variant as Likely Benign while others provided evidence for its cancer pathogenicity. We considered such variants as VUS, but if the contradicting evidence had not been reported, these variants may have also been used as benign controls. Variants that are specifically pathogenic for PMD may have been more susceptible to being misclassified as benign. As it had not yet been established that a variant's pathogenicity for PMD and cancer should be interpreted separately, a group may

have had sufficient evidence to demonstrate a lack of cancer pathogenicity and improperly equated that to the variant being benign. This issue can be observed for the PMD-associated variant SDHA^{T508I}, which currently has one Pathogenic and seven Benign/Likely benign interpretations submitted to ClinVar (186).

While other variants we selected as benign controls may also be non-cancer-causing but not truly benign, this is unlikely to apply to all low-scoring benign variants. It is important to emphasize that a benign variant can indeed affect function, so long as the consequence is not sufficient for disease. This raises the possibility that the pathogenicity for PMD is associated with more than just a decrease in SDH activity. We investigated whether hypomorphic PMD variants could be further distinguished from benign variants by SDHA abundance or flavinylation levels, but any differences observed were not significant (**Figure 19 and Figure 20**).

An alternative consequence of SDHA variants that may be required for PMD pathogenicity is the production of ROS. Similar to succinate accumulation, elevated levels of ROS have been proposed to contribute to the pathobiology of SDH-deficient diseases (76,147,250). The greatest source of ROS that SDH can produce involves the interaction between reduced FAD ($FADH_2$) and molecular oxygen (251). Interestingly, the pharmacologic inhibition of SDH at the ubiquinone-binding site, which keeps FAD in the reduced state, increases the rate of ROS production (252,253). In contrast, preventing FAD reduction by inhibiting the succinate-binding site does not affect ROS production (253). Thus, variants with partial dysfunction may have differential effects on ROS production,

depending on whether function is impaired upstream or downstream of FAD reduction. Ultimately, further investigation into the specific consequences of SDHA variants, perhaps in additional cell line models, is required before we can assess the risk of PMD for carriers.

Altogether, we functionally profiled 72 missense SDHA variants revealing novel insights into the SDHA dysfunction that underlies disease (**Table 5, Appendix**). Importantly, we identified SDHA-related cancer and PMD are associated with distinct levels of SDH dysfunction and require separate criteria for evaluating a variant's risk. We identified extreme loss of SDH activity as a unique and extremely common functional outcome of known cancer variants, which provided us the necessary context to interpret 26 SDHA VUS, 22 (84%) of which we could obtain strong evidence in favor of or against their pathogenicity. Importantly, incorporating functional evidence with other forms of existing evidence allowed for most of these VUS to be reclassified, including 14 that can now be considered Likely Pathogenic, highlighting the significance of these analyses. Thus, by obtaining functional data for SDHA variants, we can begin to increase the actionability of clinical sequencing results, leading to improved outcomes for individuals with elevated risk for *SDHA*-related cancers.

3. Development of cell-based models for the functional characterization of SDHA variants

A. Introduction

A recent study reported that for a cohort of over one million cancer patients diagnosed between 2013 and 2019, less than 7% had received germline genetic testing (254). However, as sequencing technologies have improved and costs declined, the proportion of patients receiving genetic sequencing has rapidly increased (255). Additionally, the FDA has approved several multi-gene sequencing panels for clinical use, some covering hundreds of different genes. Most recently, in late 2023, Invitae's Common Hereditary Cancers Panel, which includes *SDHA*, received FDA marketing authorization as a DNA test for the assessment of cancer predisposition. Although the efforts to increase the availability and rate of individuals receiving genetic testing have aided our ability to identify patients at risk for disease, we are currently facing a variant interpretation problem at a massive scale. Despite the establishment of recommendations for the interpretation of variants, such as those from ACMG/AMP and ClinGen, increased genetic sequencing reveals novel VUS at a higher rate than variants that can be interpreted (256-259). In fact, the VUS problem continues to grow exponentially, even amongst the most studied genes, such as *BRCA1* and *PTEN* (220). The same is true for *SDHA*. In 2019, there were under 350 missense *SDHA* VUS reported in ClinVar (186). Today, there are

over one thousand. As the use of sequencing continues to grow, so will the identification of novel *SDHA* VUS.

To begin to address the VUS problem in SDHA, we developed a novel *in vitro* model to investigate the functional consequences of missense variants in *SDHA*, which was introduced in Chapter 2. The comprehensive profiling of variants with previously established clinical interpretations revealed disease-specific levels of SDHA dysfunction, allowing cancer-associated variants to be detected at a high rate according to their activity levels. These findings were instrumental in providing the necessary context for interpreting SDHA VUS, and this functional data could be used as strong functional evidence for clinical variant interpretation. Notably, we could support the reclassification of 21 out of 26 tested SDHA variants. While the clinical value of this model cannot be overstated, the methodology employed poses certain limitations relating to its scalability. As such, it alone cannot fully solve the SDHA VUS problem.

To tackle the scale of the problem, we focused on developing an assay that is amenable to higher throughput analysis. Deep mutational scanning (DMS) is a method that allows for the functional analysis of a large variant library generated by saturation mutagenesis. In such an approach, the functional consequence of every possible amino-acid substitution for SDHA could theoretically be determined simultaneously. This high-throughput approach has previously been used to interrogate the functional consequences of several disease-relevant genes, including other tumor suppressor genes (179,181). Further, recommended guidelines for how multiplexed functional data could be

incorporated into existing clinical variant interpretation frameworks have been proposed (194,260). As such, the development of an assay to interrogate the function consequence of thousands of SDHA variants has great clinical potential.

Herein, I describe two different cell-based assays we investigated as potential models to enable the functional characterization of a greater number of SDHA variants. The first utilizes yeast, a model we previously used to characterize the functional consequences of variants in the SDHA homolog, ySdh1 (208). The second utilizes the HAP1 cell line described in Chapter 2, and thus, is capable of interrogating human SDHA variants. This chapter will provide additional context for each system, the data obtained, and a discussion about the utility and limitations corresponding to each.

B. Methods

Yeast strains and plasmid library generation

The haploid yeast sdh1-deletion strain (sdh1Δ) was purchased from ATCC (catalog #4004998). WT Sdh1 coding sequence was cloned to the pRS416 expression vector as previously described (208). The generation of Sdh1 variants was performed using a method inspired by the parallel single-amino-acid mutagenesis method described by Kitzman et al (261). First, we designed degenerate ‘NNK’ (N=A/G/C/T, K=G/T) primers for the first half of the target residues and anti-sense degenerate ‘MNN’ (M=A/C) primers, each of which corresponds to 32 possible codons and include all possible amino-acids substitutions and a nonsense variant (Eurofins Genomics) (262).

To convert primers into full-length variant plasmid libraries, we first performed individual PCRs containing one mutagenic primer and a universal primer binding to the plasmid. All NNK primers were used in combination with a downstream universal primer and MNN primers were used in combination with an upstream universal primer. Each universal primer was synthesized with six phosphorothioate linkages at the 5’ end to provide resistance to the T7 exonuclease (263). PCRs were performed using Q5 High-Fidelity DNA Polymerase (NEB) and WT-Sdh1 plasmid as a template. Following PCR, all NNK amplicons were combined and all MNN amplicons were combined. Following column purification (Zymo Research DNA Clean & Concentrator) amplicons were converted into single-strand fragments while simultaneously removing plasmid background by combined DpnI and T7 exonuclease digest. The resulting NNK-derived fragments are in the anti-sense direction, spanning from the downstream universal primer site to what corresponded to the 5’ end of the original mutagenic primer. Conversely, the resulting MNN-derived fragments are in the sense direction, spanning from the upstream universal primer site to what corresponded to the 5’ end of the original mutagenic primer. As the NNK primers corresponded to residues in the first half of the targeted region and the MNN residues corresponded to residues in the second half of the targeted region, the 3’ ends of these single-strand fragments now overlap. As such, we column purified each pool and used one another as a template to fill in the remaining portion of the gene by performing repeated cycles of denaturation, annealing, and extension, with Q5 polymerase.

Finally, full-length variant amplicons corresponding to the entire target length were amplified using primers specific to 5' overhangs that were added to each universal plasmid primer. These fragments were then cloned into the pRS416 vector using standard restriction enzyme and ligation cloning procedures. DNA was again column purified and then electroporated into NEB 10-beta Electrocompetent *E. coli* using a BioRad Gene Pulser II. Transformants were grown in LB-media containing ampicillin and DNA was harvested by ZymoPURE II Plasmid Maxiprep. Lastly, the Sdh1 variant plasmid pool was transformed into sdh1Δ yeast using the Frozen EZ Yeast Transformation II kit (Zymo Research). Transformants were grown in solid synthetic-complete media with glucose and lacking uracil (-URA) to maintain plasmid selection.

Yeast variant selection and Effect Score calculations

The yeast library was grown to early-log phase in media containing 2% glucose and then aliquots were seeded into media containing 3% glycerol or taken for genomic DNA extraction. After 48 hours of growth in glycerol, cells were harvested for genomic DNA extraction. Amplicons for Illumina sequencing were prepared by the two-step PCR approach described by Kowalsky et al, using NEBNext Multiplex Oligos for Illumina (NEB) (264). Sequencing was performed using an Illumina MiSeq using 600-cycle v3 reagent kits (2x300 paired-end reads) at the Molecular Technologies Core of the Oregon National Primate Research Center. Demultiplexed paired-end reads were first merged using BBmerge and then trimmed to the targeted region (residues 29-96) using Cutadapt (265,266). Finally, an alignment-free variant counting python script

adapted from one kindly provided by Dr. Taylor Mighell was used to count the abundance of each variant present from the input and 48-hour selected sequencing reads. These variant abundances were converted into Effect Scores by calculating the log_2-fold change between input and selected variant frequencies, relative to that of the WT sequence. For this analysis, we excluded variants that contain less than 50 reads in the input sequencing. For variants absent in the selected sequencing, we added a value of 1 read to enable an Effect Score calculation.

Cell culture

Regular HAP1 media consisted of IMDM supplemented with 10% fetal bovine serum and 1% Penicillin-Streptomycin. The base metabolic depleted media consisted of DMEM (high glucose) with L-glutamine, without sodium pyruvate (ThermoFisher, #11965084) supplemented with dialyzed FBS (Sigma, F0392). As indicated, depleted media was supplemented with 1mM sodium pyruvate (ThermoFisher, # 11360070) or 1X non-essential amino acids (ThermoFisher, #11140050) All cells were maintained at 37 °C with 5% CO_2.

Generation of Cas9-expressing HAP1 clonal cell line

The parental HAP1 cell line was transduced with viral particles derived from the LentiV-Cas9-puro vector (Addgene #108100) and selected with 1 μg/mL puromycin (267). After selection, cells were single-cell plated and clones were screened for high expression of Cas9 by immunoblotting (Cell Signaling #14697).

Generation of SDHA-variant transduced cell lines

Except for the HAP1 *SDHA*^{KO} pilot mutational scanning experiment, all Cas9-resistant SDHA-variant plasmids were generated as described in Chapter 2, with some modifications. Instead of the attB_BSD+SIG landing-pad vector, variants were subcloned into the pLENTI-myc-DDK-IRES Neo (pLiN) vector backbone (Origene). The coding sequences of SDHA variants were cloned in such a way that tags present in this vector were not expressed. Virus production and transduction of HAP1 *SDHA*^{KO} or parental HAP1 cells were performed as previously described for the generation of a landing-pad cell line. Two to three days after transduction, transduced cells were selected and continuously maintained in G418 at a final concentration of 1.5 mg/mL.

For the HAP1 *SDHA*^{KO} pilot mutational scanning experiment, we first generated a lentiviral expression vector containing an eGFP reporter by swapping the neomycin resistance gene in the pLiN-SDHA vector with the coding sequence for eGFP, obtained from pIRES2-eGFP (TaKaRa), generating pLiG-SDHA. This was created by amplifying the two corresponding fragments with overlapping primers and joining them using the NEBuilder HiFi DNA Assembly Cloning Kit (NEB). Then, to generate a library of all possible single-nucleotide variants corresponding to SDHA residues 96-108, we ordered an IDT oPool, which consisted of four oligos for each residue. These corresponded to a single degenerate ‘N’ nucleotide for each position of the codon, as well as an oligo containing a ‘TGA’ codon to ensure there could be a nonsense variant for each residue. Each oligo was designed in the sense direction spanning from the region corresponding to residues 96-108, plus 25

flanking base-pairs on each side. Inverse-PCR primers corresponding to each 25-flanking base-pairs were used to amplify pLiG-SDHA. The pool of oligos was then cloned into the amplified vector using the NEBuilder HiFi DNA Assembly Cloning Kit. After transformation into *E. coli* and subsequent plasmid preparation, virus production, and transduction of HAP1 *SDHA*^{KO} cells were performed as previously described.

Crystal violet staining

To visualize cell growth in different media conditions, cells were seeded into 6-well plates and grown for the indicated time. Cells were then washed twice with 1X PBS, then fixed with ice-cold methanol for 10 minutes. After methanol was aspirated off, cells were incubated in 0.5% crystal violet solution in 20% methanol for 10 minutes. After rinsing in water, plates were dried and imaged using a Chemidoc MP system (Bio-Rad).

Small-scale SDHA mutational scanning analysis

We used the library of single-nucleotide SDHA variants expressed in HAP1 *SDHA*^{KO} cells described above to perform a small-scale mutational scanning analysis based on cell fitness in depleted media. The cells were transduced at a low titer, such that the majority of cells likely integrated only a single variant. From our input population of cells, we harvested a representative cell pellet and extracted genomic DNA. To perform the selection, we plated 1 million cells in a T-75 flask containing metabolic-depleted media. The cells were passaged, and the population of GFP-expressing cells was examined by flow cytometry. After two weeks, corresponding to when the GFP-negative cells were

essentially depleted, a cell pellet was harvested, and genomic DNA was obtained. For both input and selected samples, a 250-basepair region containing mutated residues was amplified with non-Illumina tagged primers. The resulting amplicons were sequenced by Genewiz using the Amplicon-EZ service. The abundances and Effect Scores for each intended variant were obtained as described above.

CRISPR experiments

For all CRISPR-based experiments within this chapter, the LRG2.1 vector backbone was used to introduce sgRNA to cells (267). The sgRNA sequences cloned into the vector are as follows: ROSA: GAAGATGGGCGGGAGTCTTC, SDHA (exon 3): TTGGCCTTTCTGAGGCA, SDHB (exon 3): TTAAAGCATCCAATACCATG, SDHC (exon 5): GCCAAAAAGAGAGACCCCTG, SDHD (exon 2): ATGGAGAGAACATACAATGG. Virus production was performed as previously described. Various Cas9-expressing HAP1 cells were transduced at an MOI to obtain roughly 50% GFP-positive cells. The percentage of GFP-expressing cells was determined at various time points by flow cytometry using a Guava easyCyte 5 and data were analyzed with Guava InCyte software.

C. Results

Massively parallel functional characterization of SDHA variant homologs in a yeast model

Yeast are a powerful model system, especially for investigating the biology underlying mitochondrial dysfunction due to their ability to grow without functional mitochondria. They are easy to culture in vast numbers and genetically

manipulate, making them ideal for DMS analysis. SDHA and its yeast homolog, ySdh1, have moderately high sequence identity (67%), and highly conserved protein structures. As such, many human SDHA variants could be modeled in yeast. In our previous analysis, we characterized 22 SDHA variants identified in tumor sequencing (208). To achieve this, we obtained a strain of yeast with sdh1 deleted (*sdh1*Δ) and created Sdh1-variant complemented strains by introducing mutant expression vectors (268). Transformed yeast strains were grown in synthetic complete medium with either 2% glucose or 3% glycerol as the carbon source. When the non-fermentable glycerol is the sole-carbon source, yeast require ATP generated by the mitochondria. SDH-deficient yeast are unable to grow under these conditions, whereas SDH-proficient yeast can. In our analysis of 22 Sdh1 variants, growth was assessed by dilution plating on agar plates. To confirm this model could be adapted to a multiplexed approach, we grew *sdh1*Δ or WT-rescued yeast in glucose- or glycerol-containing broth and measured their growth by optical density readings over time (**Figure 25**). As expected, only cells with functional SDH could grow in glycerol-containing media. Thus, this model represents an efficient and scalable method to functionally select between SDH-deficient and functionally normal cells.

Next, we developed a strategy to functionally characterize all possible Sdh1 missense variants (**Figure 26**). In this approach, the sdh1 gene is divided into multiple regions and a variant-sub-library is generated for each. After subjecting libraries to glycerol selection, Effect Scores for each variant can be calculated according to their abundances before and after selection, as

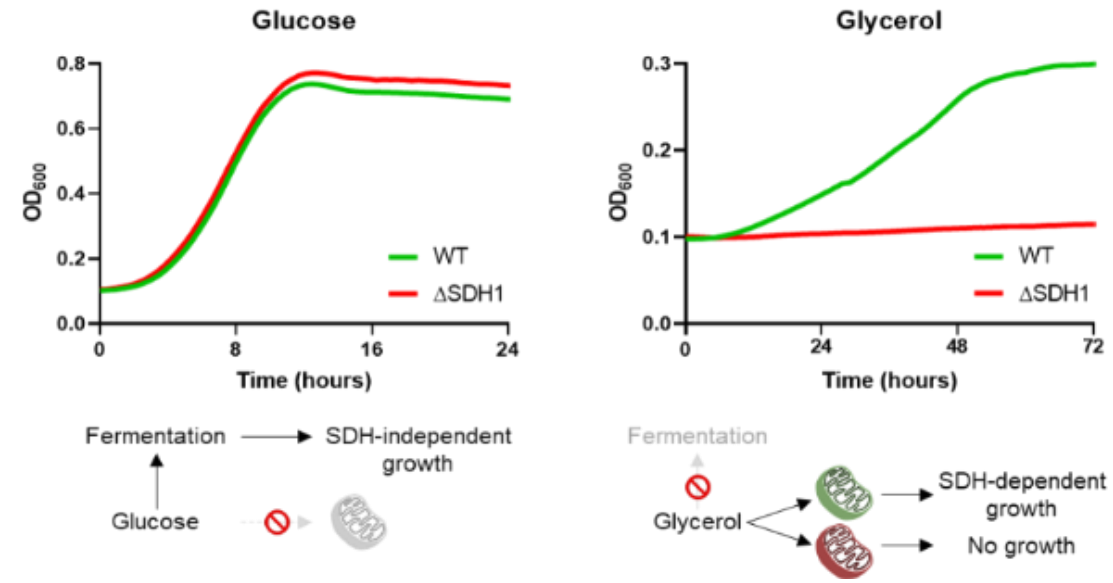

Figure 26. Yeast metabolic pathway usage depends on the available carbon source. Yeast use different metabolic pathways depending on the nutrients available. When fed a fermentable carbon source, such as glucose (left), yeast grow independent of their SDH functional status. When fed a non-fermentable carbon source, such as glycerol (right), yeast must use their mitochondria for energy production, allowing for SDH-dependent growth selection.

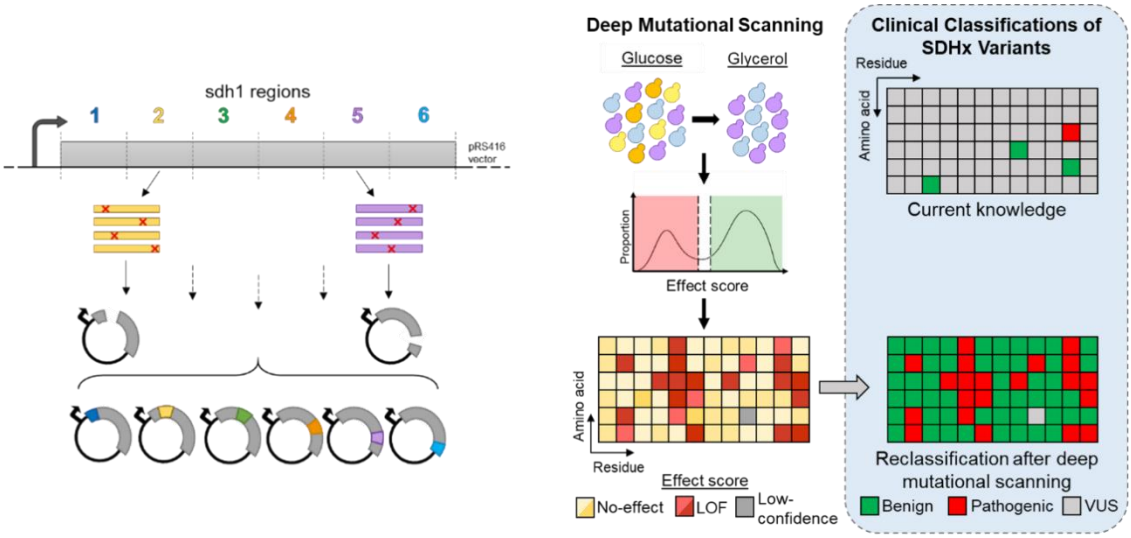

Figure 25. Yeast DMS approach. Left: sdh1 would be divided into 6 regions, with libraries generated for each. Right: Yeast libraries would be subjected to glycerol selection and Effect scores would be calculated. Effect-score distributions for nonsense variants (red) and synonymous variants (green) would be used to create classification thresholds (no-effect, LOF, or none, due to low confidence scores between thresholds. This functional evidence can be used to reclassify SDHA variants following ACMG guidelines.

determined by NGS analysis. From these scores, functional classifications could be made, using the distributions of missense and synonymous variants present within the library. As in Chapter 2, a strength of evidence can be determined for these functional data, which can be subsequently incorporated into the ACMG/AMP variant interpretation framework.

To test this approach, we performed a pilot experiment with a library corresponding to the first 68 residues of the mature Sdh1 protein (cleaved mitochondrial-targeting signal (MTS), residues 29-96). We determined the abundance of each variant before and after glycerol selection by NGS. After filtering out low-read counts and reads containing more than one amino-acid mutation, 87% of the possible 1,292 missense were identified, though there was high variability corresponding to the proportion of each variant (**Figure 27A**). Missense, synonymous, and nonsense variants contributed to 84.0%, 4.8%, and 2.5% percent of the reads, respectively. The remaining 8.7% of reads corresponded to the WT sequence (**Figure 27B**). After selection, WT- and synonymous-reads slightly increased, while missense-reads remained unchanged. As expected, the nonsense variants were largely depleted, falling to just 0.7% of all reads (**Figure 27B**).

In general, each synonymous variant had the same relative change in abundance between input and selection, proportional to its input frequency (**Figure 27A**). Similarly, each nonsense variant generally had a similar decrease in abundance proportional to its input abundance. Surprisingly, the majority of

missense variants seemed to share a fate similar to either synonymous variants or nonsense variants.

To formally evaluate how each variant compared to that of WT, we calculated Effect Scores, as described in the Methods section (**Table 6, Appendix**). As expected, synonymous Sdh1 variants had WT-like growth, with a mean Effect score of -0.10 (**Figure 28A**). Conversely, nonsense Sdh1 variants were strongly depleted and had a mean Effect score of -2.20. Impressively, there was no overlap between the two groups. To classify variants with 'no effect' on function, we used a threshold corresponding to the 5th percentile of synonymous

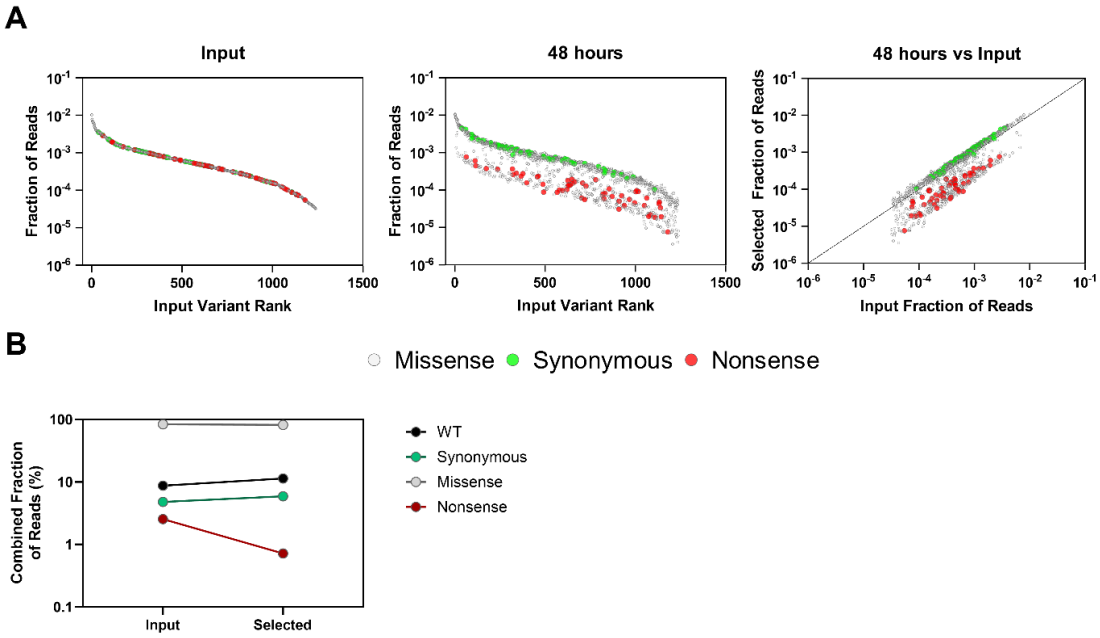

Figure 27. Nonsense and some missense Sdh1 variants deplete after 48 hours of growth in glycerol. **A:** The fraction of sequencing reads before (left) and after (middle) selection in glycerol-containing media. For each plot, the variants are ordered by their input frequency rank. Right: Scatter plot of the fraction of reads from the selected sample versus the fraction of reads from the input sample. The dashed black line of identity indicates no change between input and selected, where samples below are depleted, and samples above are enriched. For each plot, variants are color-coded according to variant type, as indicated. Smaller symbols corresponding to missense variants are for representative purposes only. **B.** Fraction of all reads corresponding to synonymous, missense, or nonsense variants, as well as the WT sequence for input and selected samples.

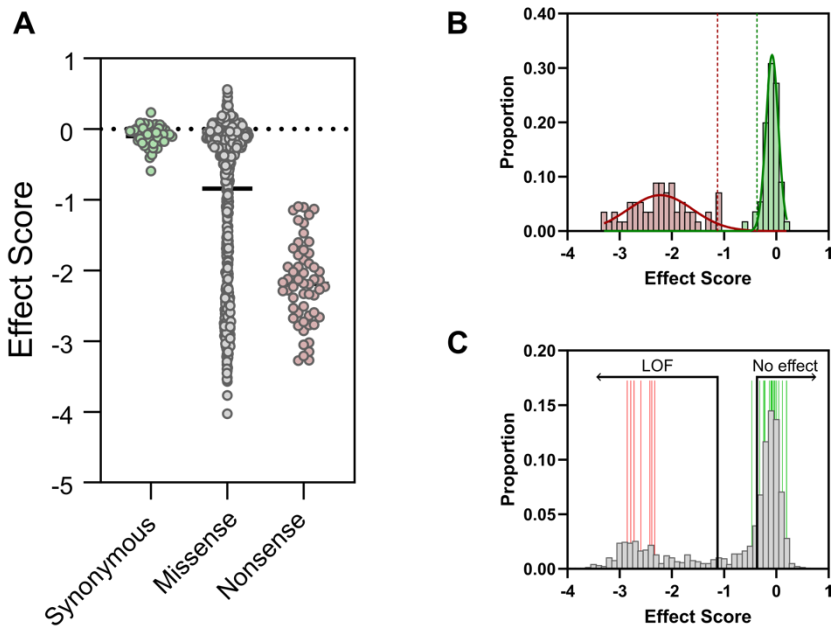

Figure 28. Distribution of mutant Sdh1 Effect scores. **A**. Effect scores of synonymous (n=55), missense (n=1127), and nonsense (n=55) ySdh1 variants, with means represented as horizontal black lines. **B.** The Effect-Score distributions of synonymous (green) and nonsense (red) variants were used to determine thresholds for VUS classification (dashed lines). **B.** The majority of ySDH1 missense variants (grey) can be classified as 'LOF' or 'no effect' using the Effect-Score thresholds (black arrows). Effect scores of individually sampled and confirmed LOF (red) and no-effect (green) variants are indicated by vertical lines.

Effect scores (-0.37) (**Figure 28B**). To consider variants as 'LOF', we used a threshold corresponding to the 95th percentile of nonsense Effect scores (-1.13). Any variant with an intermediate Effect Score between these two thresholds was not classified. The Effect Scores corresponding to missense Sdh1 variants in this library were largely similar to either the synonymous or nonsense controls, allowing for 990 (77%) of the 1,292 possible missense variants to be assigned a functional classification (**Figure 28A and C**). Notably, 327 of these variants were considered LOF. To ensure that the Effect Scores from this assay faithfully represented their actual functional consequences, we selected 30 clones and performed dilution-plating on glycerol agar media. Except for one variant whose

Activity Score was in the intermediate range, the functional classifications from the DMS analysis matched the results from the agar-plating assay (**Figure 28C**).

The region for this pilot experiment was intentionally selected, as many of the residues surround the flavin-binding pocket and are expected to play important roles in activity. To investigate how each amino-acid substitution at every residue affects function, we generated heatmaps of Effect Scores and the corresponding functional classifications (**Figure 29A and B**). Interestingly, this analysis also revealed many of the variants not found in sequencing the input samples were concentrated around specific residues, indicating there may have been primer-specific issues during library construction.

Every variant of the His90 residue, which is the homolog of SDHA His99, which is required for covalent flavinylation and activity, was classified as LOF (**Figure 29B**). Interestingly, His90 appears to be a part of one of two hotspot regions largely intolerable to any change, which are separated by a stretch of residues that affected by only specific variants. This is in stark contrast to the first third of the region for which nearly every variant had no effect on function. When looking at the average Effect Score per residue mapped onto the 3D structure of ySdh1, we see that the stretch of residues for which almost no mutation affects function is largely unstructured; thus, these data are not unsurprising (**Figure 29C**). In contrast, the hotspot of residues intolerable to change are intricately associated with FAD. The region in between the two hotspots faces away from FAD and is partially surface-exposed. Based on these observations, the few

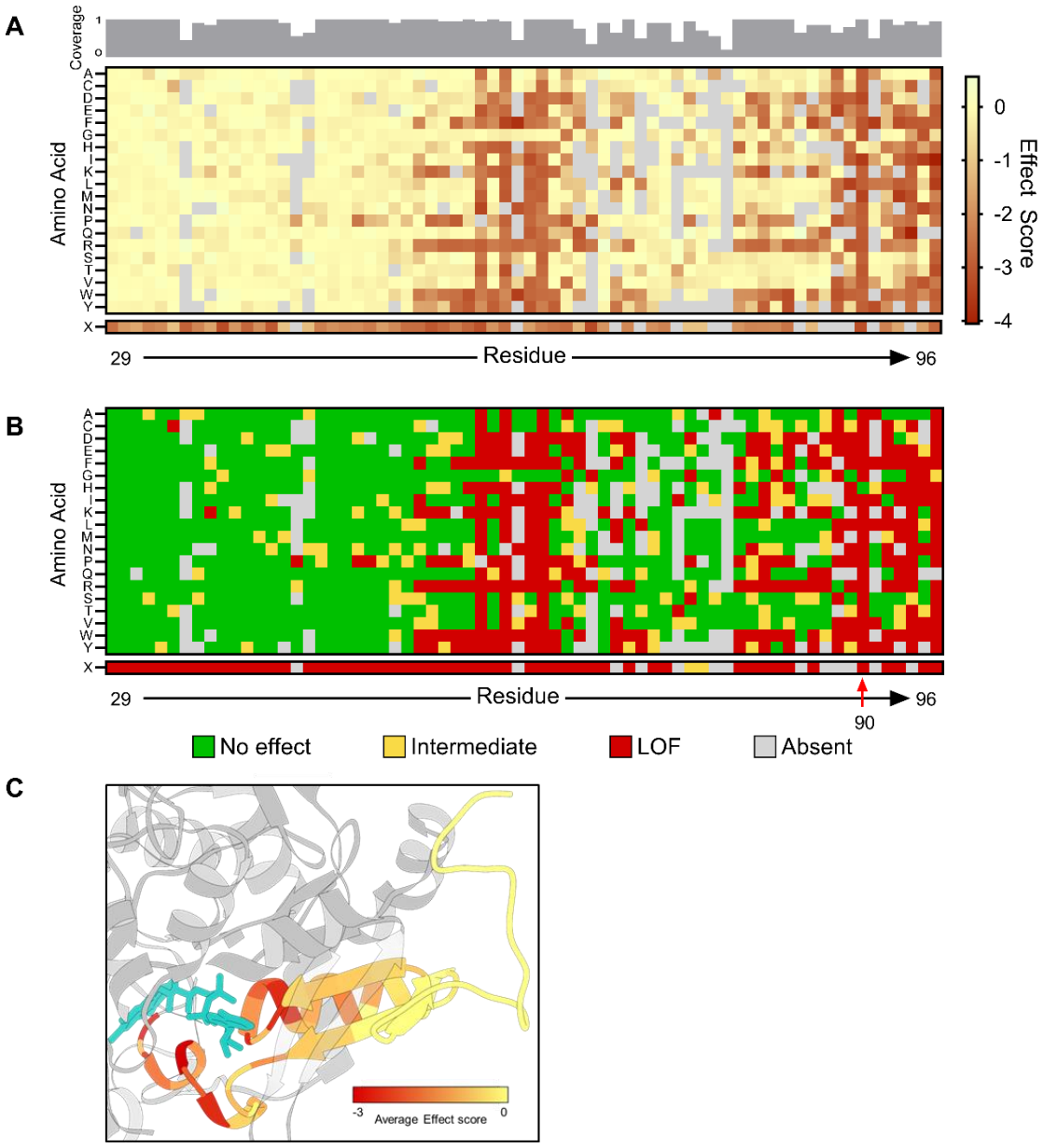

Figure 29. Effect scores and corresponding functional classifications of ySdh1 variants from DMS experiment. **A**. Histogram of variant coverage in the library for each residue (Top). Heatmap of Effect scores for each variant measured. Variants with less than 50 "counts" from input were declared absent (grey boxes). **B**. Heatmap as above, with Effect scores converted into functional classifications according to thresholds, as described. His90 is denoted by a red arrow. **C**. Theoretical model of Sdh1 crystal structure (PDB: 1ZOY) with each residue color-coded by the average effect scores for missense variants suggests intolerant regions are critical for FAD (aqua) co-factor interaction (60). Residues not analyzed in the pilot DMS experiment are colored grey. The image was created using UCSF Chimera software.

variants not directly interacting with FAD possibly affect protein function by disrupting the alpha helix surrounding it.

Although these data were highly encouraging for a pilot, upon its completion, we also began to obtain functional data from human cell-line models. We compared the data reported in Chapter 2 with our previously published interpretations of yeast Sdh1 variants. Although the data were concordant for most variants, there were several exceptions. In particular, two variants that did not affect yeast protein function (human $SDHA^{R171H}$ and $SDHA^{R195W}$) had cancer-like classifications in our analysis using the HAP1 *SDHA*^{KO} model (**Figure 30**). Furthermore, $SDHA^{R465W}$, which fell between our benign-like and cancer-like classification thresholds was found to inactivate yeast protein function. Although the activity corresponding to $SDHA^{R465W}$ in our model was indeed decreased, we consider the yeast dilution agar-plating assay to be substantially more sensitive in detecting growth than would be possible by deep sequencing; thus, we believe DMS analysis of this variant would produce similar results.

Leveraging the metabolic dependencies of SDH-deficient cells into a human cell-based assay

While yeast are remarkable in their ability to grow in certain conditions without functional mitochondria, human cells deserve recognition for their own metabolic rewiring capabilities, as is often seen in cancer. Loss of SDH activity disrupts both OXPHOS and the tricarboxylic acid cycle, yet, somehow, the HAP1 *SDHA*^{KO} cells adapted to survive. Nonetheless, just as yeast require a fermentable carbon source for growth upon mitochondrial dysfunction, we

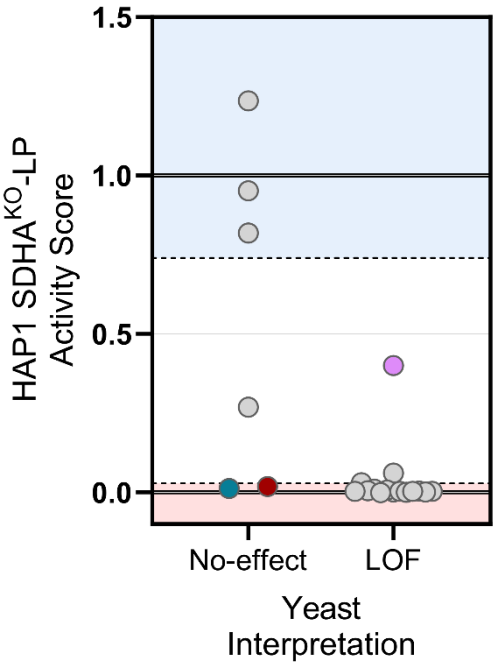

Figure 30. Discordance between yeast and human functional interpretations. Activity scores from the HAP1 *SDHA*^{KO} landing pad model described in Chapter 2 for yeast Sdh1 variants that were previously characterized as No-effect or LOF. The yeast homologs of R171H (teal), R195W (maroon), and R465W (pink) are highlighted. Highlighted regions represent the thresholds for a cancer-like (red) or benign-like classification. Only mean Activity Scores are shown (n=3).

hypothesized our SDH-deficient cell line would have specific metabolic dependencies that could be leveraged into a cell-based assay for the functional characterization of SDHA variants.

Previous work has shown that ethidium bromide treatment of cells results in the depletion of mitochondrial DNA, resulting in mitochondrial dysfunction. These cells were found to be completely dependent upon the supplementation of media with pyruvate and uridine due to the metabolic consequences of the loss of functional TCA cycle and respiration (269). Likewise, more recent studies have shown that sdhb$^{-/-}$ murine cells are dependent upon pyruvate carboxylation to re-supply depleted aspartate pools (211,270). Our complete growth media is

supplemented with pyruvate and non-essential amino acids. Therefore, we tested whether the HAP1 *SDHA*^{KO} cells had similar dependencies. Media supplemented only with dialyzed FBS (depleted media) had little to no effect on the growth of parental HAP1 cells. However, HAP1 *SDHA*^{KO} cells failed to grow completely. Importantly, lentiviral-based expression of SDHA^{WT} rescued the ability to grow in this depleted media (**Figure 31A**).

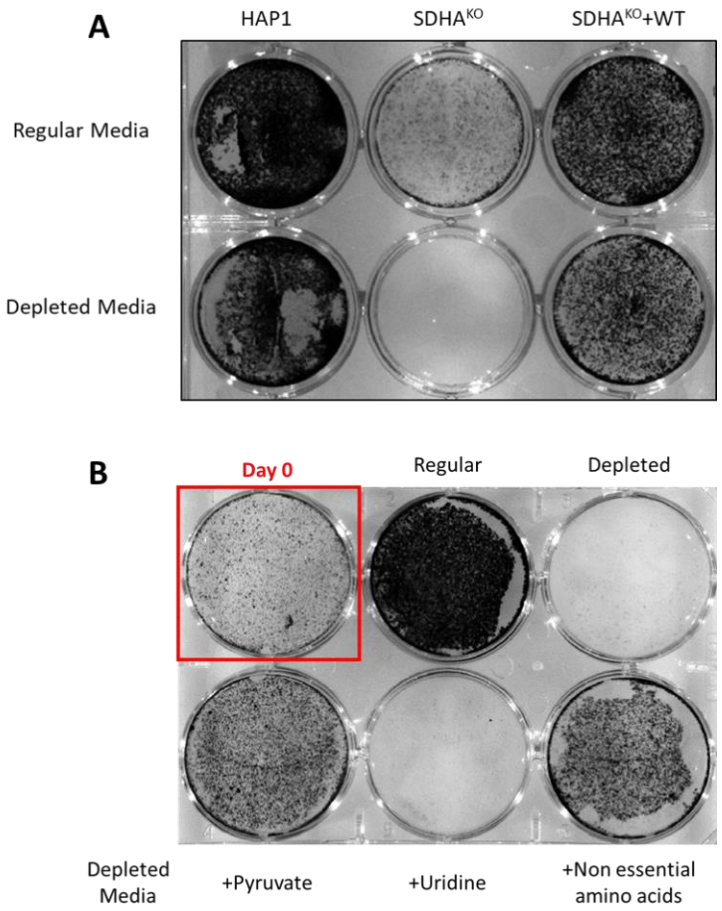

Figure 31. Metabolic dependencies of HAP1 *SDHA*^{KO} cells. **A.** The labeled cell lines were grown in seeded regular media for 24 hours and then replaced with the indicated media. Crystal stain proceeded after 72 hours of additional growth. **B**. Crystal violet staining of HAP1 *SDHA*^{KO} after 5 days of growth in depleted media with or without the indicated supplements. The confluency of cells on the first day of depleted media is shown in the top left. Note, the seeding density of cells between panel A and B were not the same.

To investigate which metabolites are required for SDH-deficient growth, we cultured HAP1 *SDHA*^{KO} cells in depleted media supplemented with pyruvate, uridine, or non-essential amino acids. The addition of pyruvate or non-essential amino acids was able to restore growth, whereas uridine could not (**Figure 31B**).

Next, we investigated whether we could revert these phenotypes by expressing SDHA^{WT} or functional SDHA variants by culturing rescued cells in depleted media. As expected, the functional variant SDHA^{V657I} was fully capable of growing, whereas the LOF controls, SDHA^{R31X} and SDHA^{H99Y} were unable to (**Figure 32A**). Although these variants are known controls, it is important to note that the cell lines tested are not the same as those described in Chapter 2. Although the same *SDHA*^{KO} cell line was used, the methodology of introducing the variants into the cell line was based on a previous system used in the lab, utilizing lentiviral transduction and neomycin resistance to obtain stable over-expressing cell lines. Nonetheless, we confirmed the activity of these cell lines as described previously. In fact, we developed a stable cell line in this system for 53 of the variants characterized in Chapter 2. Although the Activity Scores corresponding to the lentiviral transduction method could not be adjusted to differences in expression levels, the Activity Scores between the two systems were remarkably similar, regardless if the variant was a known control, or VUS that was functionally classified, corresponding to a Pearson's correlation coefficient of 0.948 ($p < 0.0001$) (**Figure 32B**). According to these data, we made two conclusions: first, the lentiviral system for introducing SDHA variants performs similarly to the landing-pad method and can be used reliably, and

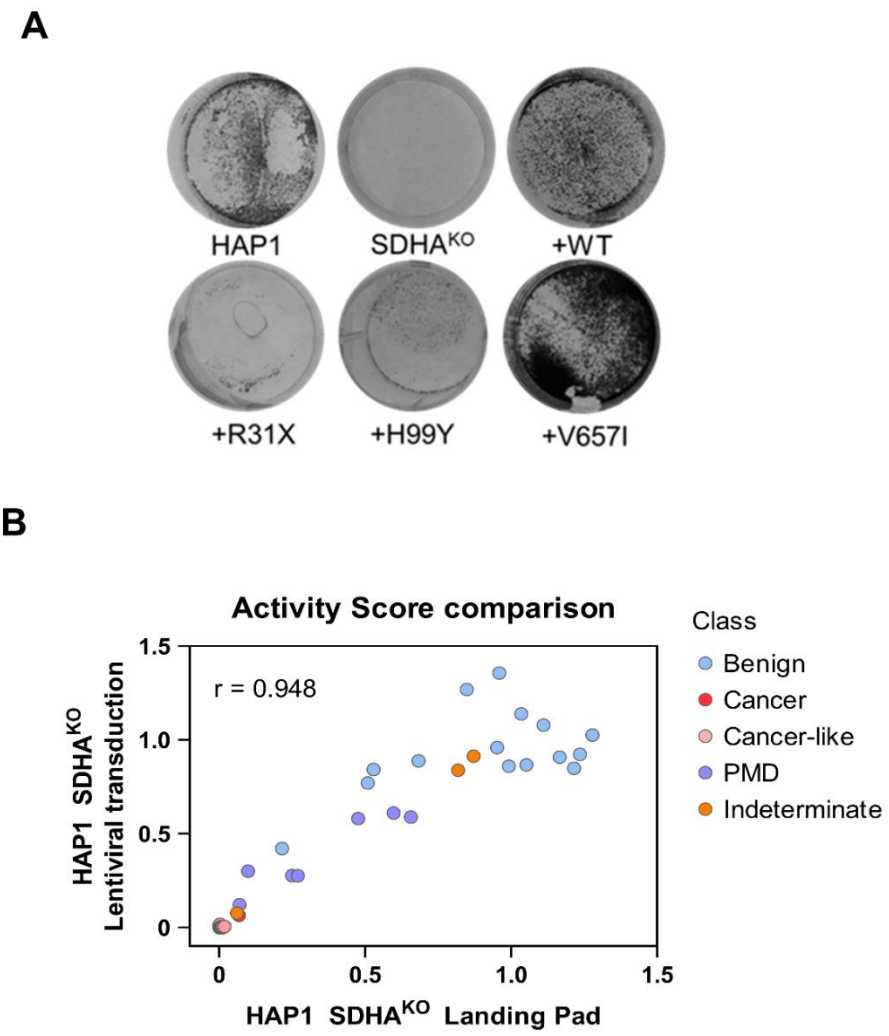

Figure 32. SDHA-variant-cell line growth in depleted media. **A**. Crystal violet staining after 5 days of growth in depleted media. Only cell lines with activity could grow. **B.** Scatter plot of Activity Scores from lentivirally-transduced HAP1 *SDHA*^{KO} cells versus Activity Scores from landing-pad generated HAP1 *SDHA*^{KO} cells. The classes depicted are as described in Chapter 2, before VUS reclassification: Benign (n=15), Cancer (n=16), Cancer-like (n=12) PMD (n=7), and Indeterminate (n=3).

second, SDHA-variant activity can be investigated according to growth in metabolic-depleted media.

In order to work for multiplexed variant analysis, it was crucial that SDH-deficient cells could not grow in depleted media when being co-cultured with SDH-proficient cells. To assess this, we proceeded to perform a small-scale mutational scanning experiment. In order to aid in determining appropriate time

points for harvesting cells, we modified our lentiviral expression vector to include GFP transcriptionally linked to SDHA (**Figure 33A**). With this vector as a template, we generated a library of all possible single-nucleotide mutations spanning a 13-residue region (96-108). To ensure the presence of enough nonsense variants for comparative analysis, we additionally designed primers to generate a nonsense variant for each position, resulting in a total of 130 possible unique nucleotide variants. As we cannot control the integration number as in the landing-pad method, we transduced HAP1 *SDHA*^{KO} cells with the variant virus library at a low MOI to decrease the likelihood that any single cell would receive two different variants. Rather than using a selection marker linked to the lentiviral construct to enrich transduced cells, we performed a bulk selection using the depleted media. As any untransduced, and therefore GFP-negative, cells would be SDH-deficient, their depletion from the population would be representative of the depletion of any non-functional SDHA. Indeed, after two weeks in depleted media, flow cytometric analysis revealed almost all cells remaining were GFP-positive (**Figure 33B**).

After sequencing DNA from cells pre- and post-selection, we calculated Effect Scores (**Table 7, Appendix**). As with the yeast DMS strategy, there was perfect separation between the nonsense and synonymous variants (**Figure 33C**). Further, the Effect Scores for missense variants also tended to group around those of either synonymous or nonsense controls, indicating the variants generally had either no large effect on function or a severe effect on function, as we saw when investigating variant consequences individually. Notably, all

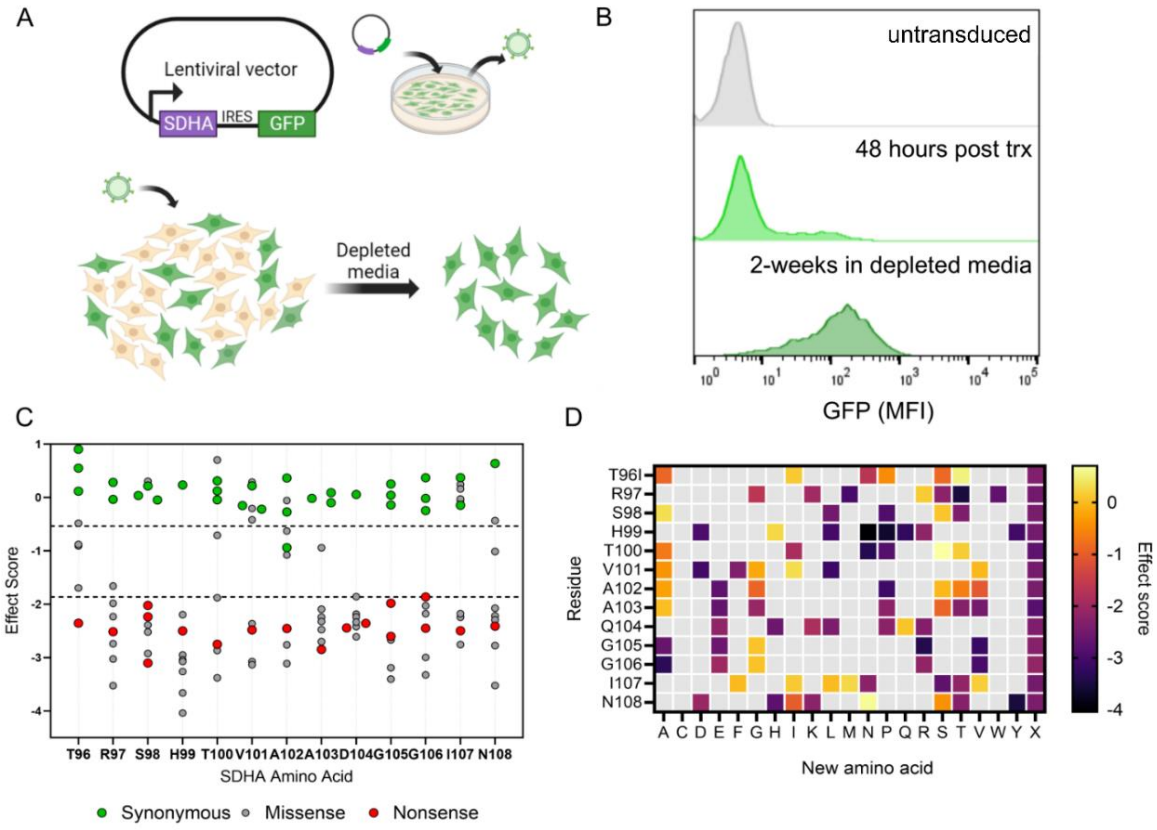

Figure 33. HAP1 *SDHA*^{KO} DMS analysis.A. Schematic of workflow. *SDHA*^{KO} cells are transduced with SDHA- and GFP-encoding virus and then subjected to selection by metabolite restriction. Only cells expressing functional SDHA variants can survive. **B.** Flow cytometry histograms of untransduced cells, cells 48 hours after transduction (trx), and transduced cells after two weeks in depleted media. Non-GFP-expressing cells are out-competed from the population when cultured in depleted media. **C.** Per-residue Effect Scores from depletion experiment. Nonsense mutations have large negative Effect Scores indicating their depletion from the population, while near-zero Effect Scores for synonymous variants demonstrate WT-like fitness. Missense mutations largely have nonsense-like or synonymous-like Effect Scores. Each symbol represents a unique nucleotide variant. **D.** Heatmap of Effect Scores for different amino-acid substitutions observed. A large number of grey cells (variant not present) are expected as the library only contained all-possible single-nucleotide variants. Average Effect Scores are shown for protein variants with more than one contributing nucleotide variant. Panel A created with BioRender.com.

amino-acid substitutions affecting the His99 residue resulted in Effect Scores below the 95th percentile of all nonsense variants, as expected (**Figure 33C**). Further, SDHA^{T96I}, classified as benign-like as described in Chapter 2 (Activity Score = 1.072), demonstrated WT-like growth, with an Effect Score of 0.11. In contrast, SDHA^{R97T}, SDHA^{A103V}, and SDHA^{G106R}, each of which obtained

cancer-like classifications in our previous analysis (Activity Scores = 0.019, 0.002, and 0.003, respectively) corresponded to Effect Scores of -3.52, -2.48, and -2.18, respectively (**Figure 33D**). Thus, this demonstrated the potential of this assay to obtain functional data for many variants simultaneously, which is highly concordant with the individual analysis of variant function.

Due to the promising results described above, we began to move forward with larger libraries of SDHA variants. However, this model had unanticipated limitations which precluded the ability to complete these analyses. Over time, the HAP1 *SDHA*^{KO} cell line lost its capacity to be phenotypically rescued. This was not due to external conditions such as different batches of dialyzed serum, as parental HAP1 cells and SDHA^{WT}-transduced knockout cells that had been used as controls for growth in depleted media could continue to grow. However, newly created SDHA^{WT}-expressing cells as well as those expressing functional SDHA variants which were made by transducing late-passage HAP1 *SDHA*^{KO} cells failed to grow in depleted media, despite high activity levels. Thus, although our data demonstrated that SDH activity was indeed necessary for growth in depleted media, these observations indicated that it was not sufficient. We suspect that the HAP1 *SDHA*^{KO} cell line adapted over time, losing some factor that is required for growth in depleted media, which will require further investigation.

Overcoming challenges for cell-based assessment of human SDHA variants

The dynamic nature of the metabolic dependencies corresponding to the HAP1 *SDHA*^{KO} cell line required us to investigate alternative approaches for the

functional analysis of SDHA variants in a cell-based assay. Initially, we considered whether we could overcome the limitation of the HAP1 *SDHA*^{KO} cell line by creating a less stringent formulation of the depleted media. However, as we were uncertain of what led to the phenotypic drift in the first place, we were wary of the cell line further changing without being able to identify it, nor could we know how it might affect the interpretation of results. We also considered generating additional *SDHA*^{KO} cell lines that we could use at early passages, though there were two significant issues with this. First, we had no way of identifying what passage would be sufficiently early to avoid the metabolic adaptation we observed. Secondly, obtaining a clonal *SDHA*-knockout cell line was profoundly difficult. In fact, the methodology we used to obtain a clone, utilizing an all-in-one vector that expresses both Cas9 protein and a sgRNA linked to puromycin selection, was our second attempt. Initially, we generated a clonal Cas9-expressing HAP1 cell line and then attempted to inactivate *SDHA* by transducing with viral particles encoding a sgRNA that targets *SDHA* as well as GFP reporter (LRG-sgSDHA). However, GFP-expressing cells were rapidly depleted from the population after targeting *SDHA*, but not when using a sgRNA targeting the mouse *ROSA* locus (**Figure 34**). Thus, it was clear that inactivation of *SDHA* resulted in decreased fitness. Accordingly, we concluded that an approach allowing for the selection of edited cells would provide a higher likelihood of obtaining a *SDHA*-knockout clone and switched methodologies, as described. However, upon reevaluating these data, we realized the decreased

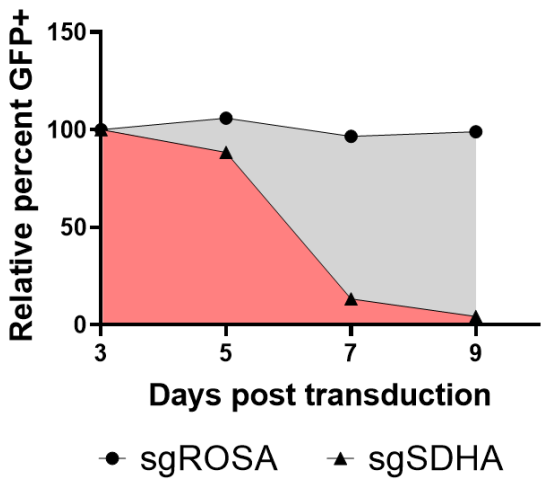

Figure 34. CRISPR-Cas9-mediated inactivation of *SDHA* results in decreased fitness. The percentage of GFP+ cells relative to 3 days after HAP1-Cas9 cells were transduced with guide-RNA targeting SDHA or non-human targeting (ROSA).

fitness upon CRISPR-editing could be leveraged. Rather than overcoming the limitation of the HAP1 *SDHA*^{KO} cell line, we can avoid it completely.

Rather than expressing SDHA variants in the HAP1 *SDHA*^{KO} cell line, we reasoned that variants could be introduced into the parental cell line and then subsequently inactivate the endogenous allele. Just as heterozygous expression of a non-functional SDHA variant is insufficient for tumor progression, due to the presence of a WT allele, we hypothesized that maintaining expression of endogenous SDHA in Cas9-expressing HAP1 cells would prevent phenotypic drift. Mimicking the LOH that results in tumor formation in people, subsequent CRISPR-mediated loss of endogenous SDHA would impose a selection dependent on the activity of the introduced variant (**Figure 35**).

To investigate this approach, we generated stable-variant cell lines derived from a Cas9-expressing HAP1 clone with retained *SDHA*. We selected

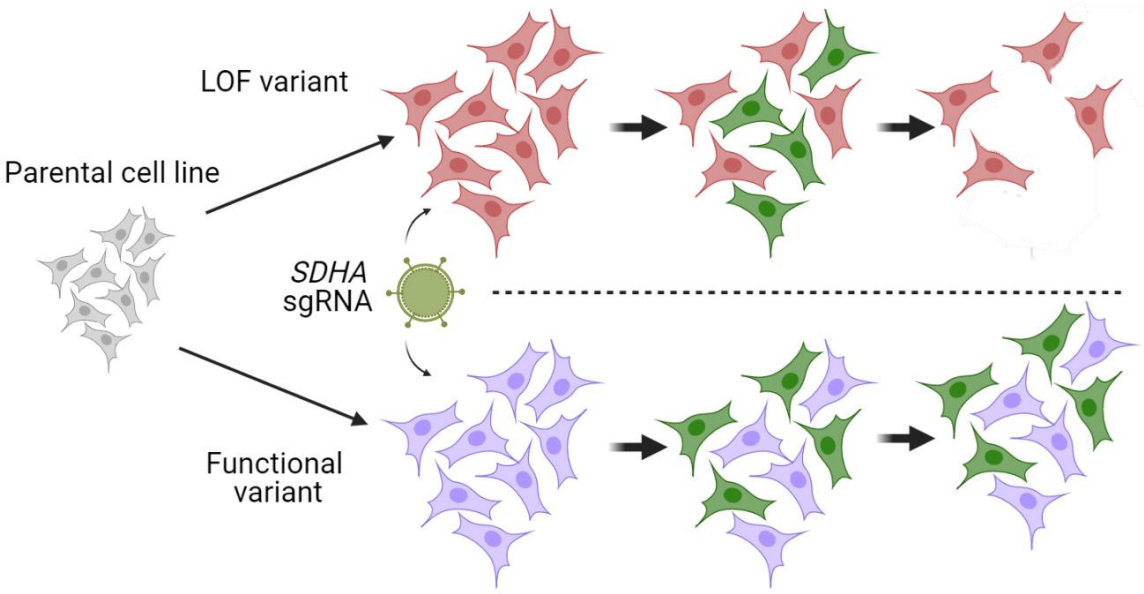

Figure 35. Schematic of novel CRISPR-Cas9 mediated cell-based assay for characterizing SDHA variants. The parental Cas9-expressing cell line is transduced with LOF SDHA variant (top) or a functional SDHA variant (bottom). Upon transduction with SDHA-targeting sgRNA at MOI ~0.5, the endogenous allele is inactivated, and the proportion of GFP cells remaining becomes dependent on the functional status of the variant introduced. Created with BioRender.com

12 variants with various functional capacities as determined in Chapter 2. We also obtained cell lines with $SDHA^{WT}$ or $SDHA^{R31X}$ over-expression, as well as one containing an empty expression vector (EV) to use as controls. These were generated using the lentiviral expression cassette containing a neomycin-resistance gene, previously described (**Figure 32B**). We then transduced each cell line with LRG-sgSDHA virus at a titer to obtain approximately 50% GFP-positive cells and then cultured in depleted media.

Subsequently, we tracked the change in the proportion of GFP-positive cells over time to determine the fitness associated with each variant. For each day and variant, we normalized this proportion to that of $SDHA^{WT}$. Each of the benign and benign-like variants tested ($SDHA^{G6D}$, $SDHA^{G184R}$, $SDHA^{Y629F}$, and

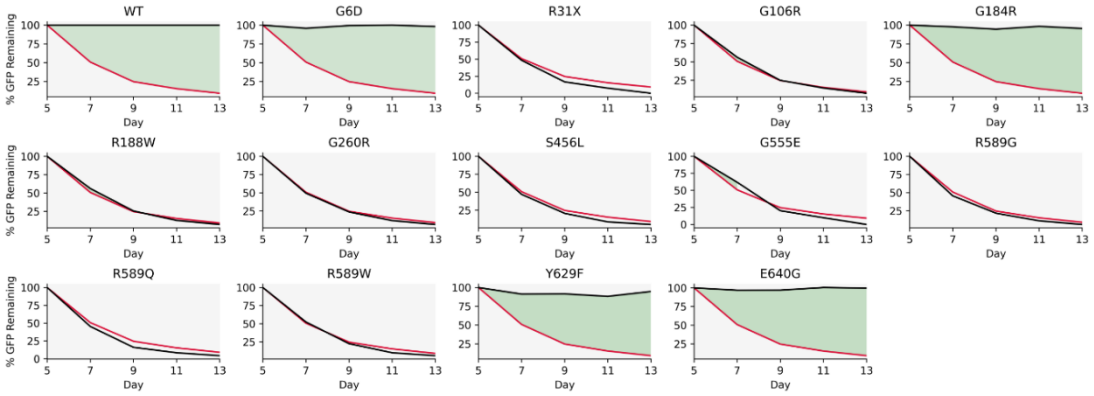

Figure 36. LOF SDHA variants fail to protect from decreased fitness upon CRISPR-Cas9 editing of endogenous SDHA. The percentage of GFP-positive cells for each variant population following transduction with sgRNA + GFP virus targeting SDHA, relative to 5 days after transduction, normalized to that of WT for each time point. For each plot, the variant indicated above is shown in black. The curve for the HAP1-Cas9 – EV control is shown in red. Cells were cultured in depleted media. Each curve represents a single biological replicate.

SDHA^{E640G}) maintained a proportion of GFP-positive similar to that of SDHA^{WT} over a 13-day period following transduction (**Figure 36**). In contrast, the GFP-expressing populations rapidly depleted from cells expressing non-functional variants at the same rate as they did from the EV cell line. Thus, these data indicate that this approach can indeed distinguish between variants with normal function and complete loss of function. However, this set of variants also included the hypomorphic PMD variant SDHA^{G555E}, which in Chapter 2, we reported a low Activity Score of 0.070. Unlike measuring SDH activity directly, in this assay, SDHA^{G555E} appeared indistinguishable from non-functional variants.

As we discussed at length in the previous chapter, the ability to differentiate between variants with low and no functional output is critical in identifying variants likely to be associated with cancer with high PPV. This assay was performed in depleted media as we thought it would lead to stronger and more rapid depletion of non-functional variants. It is possible that depleted media

is too stringent to support variants with very low levels of partial function, such as SDHA^{G555E}. As we saw when initially trying to obtain *SDHA* knockout clones, our regular media still resulted in a strong decrease in fitness after CRISPR editing. This prompted us to repeat this analysis using regular media with select variants. Remarkably, the decrease in fitness displayed by SDHA^{G555E} in regular media was much less than that in depleted media (**Figure 37**). Further, this was the only variant in which media influenced fitness, relative to SDHA^{WT} and a null control, SDHA^{R31X}. Although the performance of SDHA^{G555E} under these conditions does not necessarily represent its true functional capacity as directly

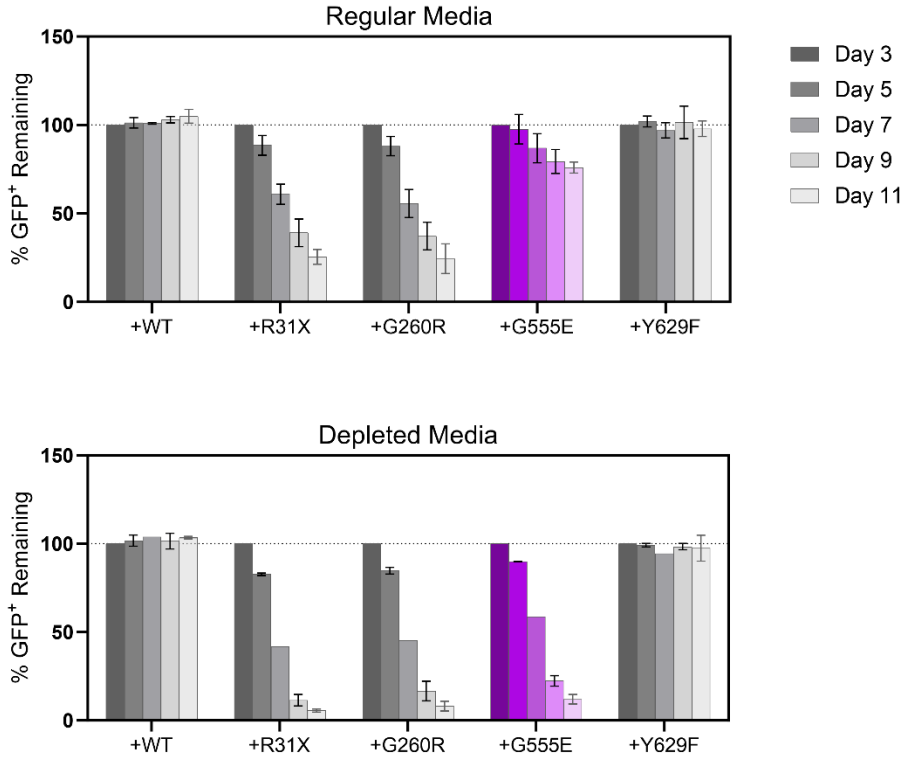

Figure 37. Effect of metabolites in CRISPR-mediated analysis of SDHA variant function. Top: % of GFP-positive cells remaining after growth in regular media relative to Day 3 time-point. Bottom: % of GFP-positive cells remaining after growth in depleted media relative to Day 3 time-point. For both plots, bars indicate the mean from two biological replicates (except for Day 7, Depleted Media (n=1), with each replicate normalized to its corresponding Day-3 timepoint. Error represents SEM.

determined by activity measurements, these data are nonetheless extremely promising for the potential of detecting cancer-like function, as this creates a wide dynamic range in fitness between variants with low and no function. Even though we would likely lose the ability to distinguish benign variants with high confidence, the PPV for cancer-variant detection would likely be high. Furthermore, assays could potentially be performed in parallel using both media conditions to identify variants with intermediate activity. As with the previous iteration of the cell-based assay to interrogate SDHA-variant function, this could be adapted to a high-throughput multiplexed approach, in which the changes in variant abundances are determined by NGS. However, additional analysis to determine how variants with a spectrum of activities perform in this assay is required.

Lastly, while these works have focused on SDHA variants, our lab also has an interest in investigating the functional consequences of variants in other SDH-related genes, which are also tumor suppressor genes. We have been having difficulty in generating knockout cell lines to assess function; however, among the major benefits of this new CRISPR-mediated cell-based assay is that it does not require the creation of a stable knockout cell line to interrogate variant function. To test whether this system could be applied to other SDH variants, we transduced Cas9-expressing HAP1 cells with LRG virus targeting *SDHB*, *SDHC*, or *SDHD* and cultured cells in depleted media. Supporting that general SDH impairment is associated with decreased HAP1 cell fitness, targeting each of these *SDH* genes resulted in the same depletion as observed when targeting

SDHA (**Figure 38**). Although work is still required to demonstrate the loss of fitness can be prevented when functional variants are present, these data are an early indication that this novel assay has the potential to investigate *SDH* variants.

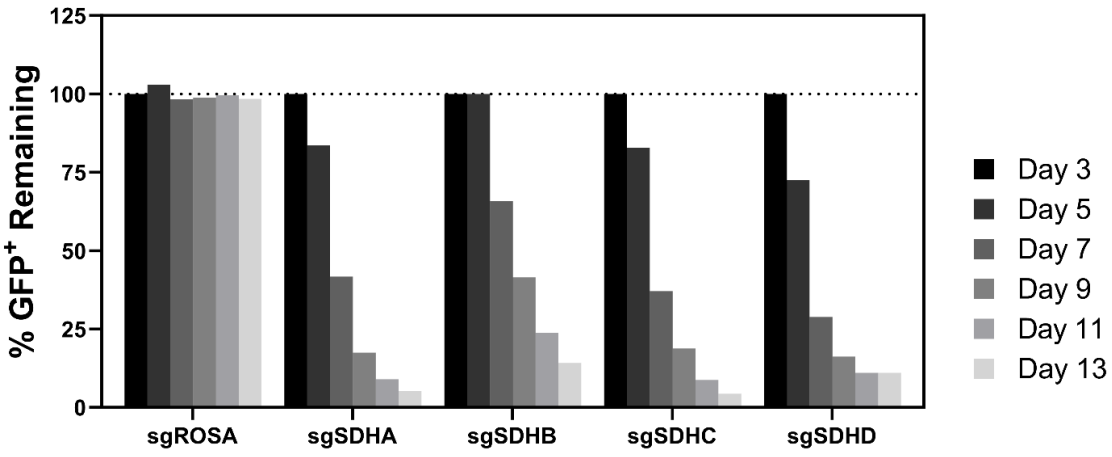

Figure 38. CRISPR-targeting of SDH genes results in universal loss of fitness. Percentage of GFP-positive cells measured over time after sgRNA transduction, targeting mouse ROSA, human SDHA, SDHB, SDHC, or SDHD. Cells were cultured in depleted media.

D. Discussion

Our ability to determine the risk for cancer associated with *SDHA* variants identified from genetic sequencing analyses is severely lacking. To address this issue, we developed a novel *SDHA*-knockout cell line that produces strong functional evidence, which can be incorporated into clinical variant interpretation frameworks. While the functional data obtained from this model enable us to reclassify many *SDHA* VUS, the approach cannot feasibly address the scale of the problem. Over one thousand unique missense *SDHA* VUS have been submitted to ClinVar, and novel variants will continue to be identified as more

sequencing is performed (186,256-259). Thus, we sought to develop cell-based assays that would enable the functional analysis of thousands of SDHA variants simultaneously.

Our first approach utilized yeast, a commonly used model for studying OXPHOS deficiencies (271). When culturing yeast in the non-fermentable glycerol, growth becomes dependent on SDH function (230). As such, expression of a Sdh1 variant in a strain lacking endogenous Sdh1 allows us to attribute growth in glycerol to the variant's function. We previously used an agar-plate format of this approach to assess the function of individual variants (208). Here, we showed that the assay could be adapted to liquid culture, providing a framework for DMS analysis of thousands of Sdh1 variants (**Figure 25 and Figure 26**).

To test this approach, we performed a pilot experiment involving the first 68 residues corresponding to a MTS-cleaved Sdh1. We found that the selection against SDH dysfunction was highly stringent, as the mean Effect Score for nonsense variants was -2.2 (**Figure 27 and Figure 28**). Further, the synonymous variants were largely WT-like, with a mean Effect Score of -0.1. Using the distributions of Effect Scores for these control variants, we established thresholds for classifying the missense Sdh1 variants as having no effect or being LOF (**Figure 28B**). Importantly, these classifications were highly concordant with the traditional analysis of variants by dilution plating on agar (**Figure 28C**).

In total, we obtained a functional classification for 1,127 (77%) of the possible missense variants. While this is already impressive, it is possible that

further optimization of the methodology could move this number closer to all possible variants. For instance, the variants receiving intermediate Effect Scores may be able to be resolved upon a second round of selection, though some may truly have a partial effect on function, akin to the hypomorphic PMD variants. Furthermore, more than half of the variants could not be characterized because they did not appear in our input library at sufficient depth, which may be due to primer issues (**Figure 29**). As such, generating sub-libraries corresponding to the affected residues or re-designing primers can help fill the gaps in functional classifications. Alternatively, it has been shown that the data obtained for the other variants can be used to impute the scores of missing variants with high confidence (272,273).

The preliminary data from this pilot experiment demonstrate the power of yeast as a model for characterizing Sdh1 variants. However, a considerable limitation of yeast is that Sdh1 and SDHA are only partially conserved, with just 67% sequence identity. The use of humanized yeast, which has been used extensively to study human genes in a yeast system, is an attractive alternative; however, in our previous attempt to express $SDHA^{WT}$ in the sdh1Δ strain, growth in glycerol was not restored (data not shown) (274,275). A likely explanation for this is that the maturation and activity of SDHA require complex interactions with assembly factors and SDHB (54,56,77). A similar observation has been made concerning the inability of SDHB-dedicated assembly factor SDHAF1 to rescue the loss of its yeast ortholog (276). Although it may ultimately be possible to fully humanize all SDH-related proteins, it is difficult to determine how translatable the

current yeast data are to human variants. In fact, we have already seen evidence of discordant functional consequences obtained from the HAP1 *SDHA*^{KO} and yeast sdh1Δ models (**Figure 30**). While functional data obtained from this yeast DMS approach can certainly improve our understanding of the structure-function relationship of SDHA, a model characterizing human variants would provide stronger evidence for the clinical interpretation of variants.

Despite its limitations, growth-based analysis of Sdh1-variant function proved robust. Therefore, we investigated whether we could replicate this assay using the HAP1 *SDHA*^{KO} cell line for high-throughput analysis of human SDHA variants. Just as SDH-deficient yeast are dependent on fermentable carbon sources, we found that SDH-deficient HAP1 cell growth is dependent on the presence of specific metabolites, including pyruvate and non-essential amino acids, resulting in SDH-dependent growth when these metabolites are depleted from the media (**Figure 31 and Figure 32**). As with the yeast DMS analysis, a pilot experiment including all possible single-nucleotide variants corresponding to 13 residues was highly promising, with synonymous variants appearing WT-like and nonsense variants strongly depleting from the population (**Figure 33**). Unfortunately, however, it became apparent that the assay would not be suitable for obtaining functional evidence for SDHA VUS.

In subsequent experiments, we found that the expression of active SDHA variants could no longer rescue the growth of HAP1 *SDHA*^{KO} cells in metabolite-depleted media. Ultimately, we were unable to entirely identify the cause for this observation. However, a recent study by Hart et al., investigating

how cells adapt their mitochondrial metabolism upon genetic inactivation of *SDHB,* provides some insight into what may have occurred. Briefly, the authors demonstrated that SDH function plays a significant role in cell proliferation by supporting aspartate production, and for SDH-deficient cells to survive, they must utilize alternative pathways to enable aspartate synthesis (277). Several others have supported this, showing that a loss of SDHB function results in cellular growth dependent on reductive pyruvate carboxylation to support aspartate synthesis (211,270). Hart et al. extended upon these findings by identifying that increased levels of mitochondrial NADH are required to support this reductive anabolism, which SDH-deficient cells achieve by a concomitant loss of Complex I function. Surprisingly, however, the loss of Complex I in SDH-deficient cells was progressive. After several passages, a clonal $SDHB^{KO}$ cell line displayed a loss of Complex I function and corresponding protein levels and increased cellular aspartate levels. We hypothesize that the progressive loss of Complex I is a universal consequence of SDH deficiency, regardless of which subunit is inactivated. We further speculate that growth in metabolite-depleted media is dependent on the activities of both Complex I and SDH. Accordingly, HAP1 $SDHA^{KO}$ cells rescued with functional SDHA protein at late passages may have been unable to grow in metabolite-depleted media due to loss of Complex I.

The involvement of Complex I in modulating the growth dependencies of the HAP1 $SDHA^{KO}$ cell line can be investigated by comparing activity levels among SDH-proficient variant cell lines that can and cannot grow in metabolite-depleted media. If the inability to grow is indeed associated with the

loss of Complex I function, we may be able to modify the HAP1 *SDHA*^{KO} growth-based assay to meet our needs. For instance, supplementing the metabolite-depleted media with aspartate may support the growth of Complex I-deficient cells. Alternatively, the expression of the yeast Complex I analog, NADH-ubiquinone reductase, can rescue Complex I dysfunction (278). However, it remains unclear if these conditions would impose a differential growth rate dependent on the extent of SDH activity.

While further investigation is necessary before determining if the HAP1 *SDHA*^{KO} cell line could still be used for a cell-based assay of SDHA variant functional analysis, we developed an alternative assay that leverages the loss of fitness associated with CRISPR-editing of *SDHA* in the parental HAP1 cell line (**Figure 34**). In this framework, SDHA variants are first expressed, then endogenous *SDHA* is inactivated, resulting in SDH-dependent growth in depleted media (**Figure 35**). Although the data are only preliminary, the results are highly encouraging and generally match the functional consequences determined by Activity Scores from the HAP1 *SDHA*^{KO} cell line (**Figure 36**). The only exception is SDHA^{G555E}, the least-active hypomorphic PMD variant, which had the same consequence as complete-LOF variants in this assay. However, SDHA^{G555E} could be easily distinguished from non-functional variants using complete media instead of metabolite-depleted media (**Figure 37**). As previously shown, a complete LOF is unique to and characteristic of cancer-associated variants; thus, these data provide confidence that the assay will have high PPV and TPR for

cancer-variant detection. Nonetheless, more analysis is required to understand how variants with distinct functional consequences perform in this assay.

As this assay maintains endogenous SDHA expression until the analysis is initiated by CRISPR editing, it does not face the same risk of dynamic metabolic dependencies that affect the HAP1 *SDHA*^{KO} cell line. The ability to study SDHA variants without needing a knockout cell line also presents other advantages of this assay. For instance, this assay is not limited to the HAP1 cell line but would work for any cell line in which loss of SDHA is associated with decreased fitness. Further, we show this approach may be suitable for analyzing variants within *SDHB*, *SDHC*, and *SDHD*, which are also tumor suppressors that contain numerous VUS (**Figure 38**) (105,186).

Although our preliminary experiments with this assay only consisted of characterizing individual variants, it is highly compatible with massively parallel analysis. Fundamentally, the approach is similar to methods of saturation genome editing, which has been used to successfully classify thousands of variants for multiple disease-associated genes (279-284). While such methods allow for variants to be expressed in their native genomic context, achieving this for *SDHA* would be near-impossible due to its four pseudogenes (*SDHAP1-4*), which have over 90% coding-sequence identity (201). Nonetheless, the work presented here provides the crucial first steps for addressing the immense VUS problem surrounding *SDHA* and other SDH-related genes. Continuing to develop and optimize this assay will lead to enhanced clinical variant interpretation, leading to better identification of individuals at high lifetime risk for cancer.

4. Conclusions and Future Directions

Understanding how different SDHA variants affect function is critically important, as SDH-deficiency is associated with cancer and PMD (93,285,286). However, prior to the work presented here, the functional consequences of disease-relevant, missense SDHA variants were largely unknown. Historically, functional studies were focused on elucidating different catalytic mechanisms of SDHA, such as flavinylation and succinate-to-fumarate interconversion (57,58,61,79,104,287). While these analyses enabled a better understanding of general SDHA function, they typically did not investigate variants associated with disease. For those that did, there is some uncertainty in the data due to the inherent limitations associated with using non-human models (92,208).

The limited availability of human SDHA data is related to the challenges associated with generating suitable human models. Even structural analysis had traditionally been performed using *E. coli* or yeast orthologs of SDHA due to persistent technical challenges in obtaining crystal structures of the human complex (58,249,288,289). However, the human structures of the entire SDH complex and the SDHA-SDHAF2 sub-assembly complex, have recently been resolved (56,71). While these structures have enabled more thorough speculation into how known pathogenic variants affect function, it can be difficult to predict if or how a VUS affects function from structural analysis alone. Thus, to aid in SDHA-variant interpretation, the primary goal of my dissertation work was

to develop novel models and methods that enable the functional characterization of human SDHA variants.

I developed a functional analysis pipeline that utilizes a novel HAP1 *SDHA*-knockout cell line. Using this model, I functionally characterized 72 missense SDHA variants, representing the largest study of SDHA variants to date. The data I obtained reveal key insights into SDHA dysfunction associated with disease. Notably, the data support a paradigm shift in how SDHA-variant pathogenicity is defined and assessed. Further, the activity data can be used as strung function evidence for clinical variant interpretation, which has substantial power to reclassify many SDHA VUS.

Functional analysis also demonstrated the complexity surrounding the mechanisms of SDHA dysfunction, as the impact of some variants was readily apparent, whereas others remain to be determined. Unique functional consequences may be linked to specific cancer features, though this requires future analysis. Additionally, the HAP1 *SDHA*^{KO} cell line presents a novel opportunity to study general SDHA-cancer biology.

Despite the wealth of knowledge that was already gained and what can be obtained moving forward, the HAP1 *SDHA*^{KO} cell line does have limitations. In particular, PMD-associated variants could not be readily distinguished from benign variants. Although the functional data reveal new insights into PMD dysfunction, they also highlight the complexity of PMD and the need for further functional analysis.

Another limitation of the model is its inability to address the scale of the VUS problem afflicting SDHA. As such, I investigated cell-based approaches that could be used to characterize thousands of SDHA variants simultaneously. Although assays utilizing yeast and the HAP1 *SDHA*^{KO} cell line each yielded valuable data, both had limitations. To overcome these limitations, I developed another functional pipeline that leverages the loss of cell fitness after CRISPR-mediated inactivation of endogenous *SDHA* in parental HAP1 cells. Although this pipeline is in preliminary stages, the work provides the crucial first steps necessary to tackle the SDHA VUS problem and can ultimately lead to enhanced cancer-risk analysis for carriers of thousands of SDHA variants.

As summarized above, my dissertation work has provided considerable insights into SDHA variant function and pathogenicity. Below, I expand on my findings and their significance in greater detail and address the questions raised that remain to be addressed.

Redefining SDHA-variant pathogenicity

The evaluation of *SDHA* pathogenicity has always been challenging. A little over 15 years ago, a study that has since been cited over 200 times was published, providing support for why genetic inactivation of *SDHA* does *not* result in tumorigenesis (147). No more than two years later, Burnichon et al. published an article in Human Molecular Genetics titled "*SDHA* is a tumor suppressor gene causing paraganglioma" (130). Now, it is well established that LOF mutations in *SDHA* are associated with both PMD and cancer. In 2015, Renkema et al. reported SDHA^{R31X} as the first SDHA variant found to cause both PMD and

cancer (97). As such, the authors proposed that individuals who carry PMD-associated SDHA variants could be recommended for tumor screening. However, it is still unclear whether all pathogenic variants are equally implicated in both diseases. The above patient also carried a compound heterozygous variant, SDHA^{C189G}. Although SDHA^{R31X} is known to confer an increased cancer risk, the same has not been established for SDHA^{C189G}. Understanding what consequences are characteristic of known cancer variants can help us better assess cancer risk for variants that have not yet been linked to cancer.

To improve our understanding of SDHA variant pathogenicity, we functionally characterized SDHA variants with previously established clinical classifications in a novel human HAP1 *SDHA*^{KO} cell line. Nearly all known cancer variants in this study could be described as amorphic. In contrast, almost all known PMD variants could be described as hypomorphic; the only non-functional variants present in cases of PMD were *in trans* with a variant that had at least partial function, such as the case with SDHA^{R31X} and SDHA^{C189G}. Based on these data, we concluded that while PMD and cancer are both characterized by a loss of SDH activity, the two diseases are distinct in the extent of this dysfunction.

These data call for a shift in how we view SDHA variant pathogenicity, as a disease-agnostic approach is insufficient. The risk for each disease should be assessed independently based on the available evidence for a given variant. Accordingly, we agree with Renkema et al. that carriers of PMD-associated *SDHA* variants should be recommended for enhanced tumor surveillance, but only if the variant in question results in complete LOF. Although we cannot

definitively state that hypomorphic variants cannot cause cancer, no data currently supports it. Thus, while SDHA^{C189G} and other hypomorphic variants are pathogenic for PMD, their pathogenicity for cancer remains uncertain, and carriers of these variants do not qualify for tumor screening recommendations. Conversely, complete LOF variants can play a role in both cancer and PMD. Thus, in addition to recommending genetic counseling to carriers of these variants to discuss the risks of malignancy, a discussion of the risks of PMD for family planning should be included.

Providing additional evidence for the interpretation of SDHA VUS

Since the discovery of SDHA^{R31X} in paraganglioma, additional cancer-causing *SDHA* variants have continued to be identified. However, the identification of variants with uncertain clinical significance has increased at a far more rapid rate. Since the beginning of this dissertation work, the number of missense *SDHA* VUS reported in ClinVar has tripled, corresponding to over 95% of all missense *SDHA* variants listed (186). Functional evidence can support the reclassification of many VUS, even when other forms of evidence are sparse (193). However, this requires a robust functional assay, as well as a deep understanding of the degree of dysfunction that contributes to disease, to properly interpret different functional outcomes. As such, our work to identify the distinction between cancer and PMD levels of SDH dysfunction, described above, provided a tremendous opportunity to enhance the cancer-risk assessment of *SDHA* VUS carriers.

Following the recommendations of the ClinGen SVI WG, we evaluated our model's capacity to distinguish cancer-associated variants according to their Activity Scores and found its performance met the criteria for the results obtained to be applied as strong functional evidence in support of a variant's cancer pathogenicity within the ACMG/AMP variant interpretation framework (194). Further, we demonstrate our model can also provide strong evidence against a variant's pathogenicity for cancer or PMD. To demonstrate the clinical utility of this model and the data it provides, we obtained strong functional evidence from 18 of 22 SDHA variants analyzed previously considered as VUS by VarSome. After incorporating our evidence with what was previously available on VarSome, we could support the reclassification for 17 of these variants, including 14 that can now be considered Likely Pathogenic for cancer. With the addition of our functional evidence, we can now support the recommendation for enhanced tumor surveillance for carriers of these variants, which can lead to life-saving interventions. As more variants are characterized within our model, the more evidence we will obtain to properly interpret cancer risk amongst carriers of SDHA variants.

Cancer variants can have unique mechanisms for dysfunction.

In addition to elucidating the dysfunction associated with SDHA-related cancer, leading to an enhanced ability to interpret SDHA VUS, our analysis revealed distinct mechanisms underlying dysfunction. Notably, we identified multiple known cancer and cancer-like variants that maintain relatively high levels of SDHA and even flavinylation. This may seem discordant with the observation

that SDHA IHC analysis has strong utility for the identification of *SDHA*-mutant tumors (134,290,291). However, an important distinction is that our model compares the abundance of SDHA variant protein to that of WT protein in the context of a haploid cell line with hemizygous expression. In the context of tumors, each variant typically corresponds to only half of the maximal possible expression, and it is unclear how a 50% reduction of absolute SDHA protein would be interpreted by IHC analysis. The same holds true for the rare non-functional variants we observed displaying high levels of SDHB. Furthermore, immunoblot and IHC detection are not equivalent; thus, our data should not be interpreted as an indication that IHC analysis of SDHA and SDHB have low clinical utility. Nonetheless, it remains possible that some SDHA-mutant tumors are misdiagnosed as SDH-sufficient based on IHC results. We propose that *SDH* sequencing should be performed if no other driver of a given GIST or PGL could be identified, even if SDHA and SDHB tumor expression are retained.

The identification of stable but functionally null SDHA variants may have great clinical significance. Although the complete LOF corresponds to an increased cancer risk, the retention of a non-functional SDHA protein could have additional consequences, such as the modification of risk or prognosis. A recent study identified that SDHA was maintained in a sub-assembly complex with its dedicated assembly factors in a *SDHB*^{KO} breast cancer cell line (292). Through subsequent siRNA-mediated knockdown of *SDHA,* the authors discovered this alternative assembly complex played a crucial role in cell cycle progression and modulated metabolic pathways. Notably, the *SDHB*^{KO} cell line was able to form

tumors when injected into mice, whereas when cells with a disrupted SDHA sub-assembly complex were injected, tumors were unable to form (292). Interestingly, *SDHB*-mutant tumors are often described as being more malignant than *SDHA*-mutant tumors (150). If this is explained by the presence of the SDHA sub-assembly complex, it may have implications for patients carrying tumors with retained SDHA. Although the precise role this sub-assembly complex played in promoting tumor formation in mice could not be fully elucidated, these data highlight the possibility that cancer variants with retained SDHA expression may have unique consequences. As further investigation provides more insights into the distinct consequences among cancer variants, we may be able to identify associations with specific clinical outcomes which can lead to more tailored patient care.

A novel model to study SDHA cancer

While my dissertation work was focused on enhancing SDHA variant interpretation, the novel HAP1 *SDHA*^{KO} cell line generated has further utility for studying SDHA-deficient cancer biology. As mentioned, 15 years ago evidence was provided to support *SDHA*'s role in PMD while simultaneously supporting its lack of involvement in cancer (147). However, these conclusions were made from experiments utilizing shRNA-mediated knockdown of *SDHA*, in which the two clonal cell lines obtained maintained ~30-60% SDH activity. As such, it cannot be interpreted that *SDHA* inactivation is insufficient for tumorigenesis. Rather, the data only support that partial loss of SDHA function is not tumorigenic, which matches our data. Although it is now well established that *SDHA* is a tumor

suppressor gene, this highlights the need to carefully select the models and methods used to study disease biology.

Much of what we know about SDH-deficient biology is actually based on the inactivation of *SDHB*, and without suitable models, the interpretations were extended to that of *SDHA* loss. Our preliminary observations regarding the metabolic dependencies of the HAP1 *SDHA*^{KO} cell line seem to agree with those of SDHB-deficient cell lines, such as the requirement of pyruvate or aspartate, as well as the progressive rewiring of metabolic pathways (211,270,277). Nonetheless, there are likely distinct cellular consequences associated with the loss of SDHA and SDHB, as described above. Now, with a *SDHA*^{KO} cell model, we can begin to investigate these differences, which may provide insight into long-standing questions, such as why SDHA-deficient tumors tend to have a more indolent nature compared to loss of the other subunits or why *SDHA* variants have a much stronger association with GIST than other types of cancers (105,108,293,294). Furthermore, the knockout cell line now enables us to assess the effectiveness of various therapeutic approaches that have shown promise in SDHB-deficient cells (295-298).

The challenges in interpreting hypomorphic PMD variants

While SDH activity data from the HAP1 *SDHA*^{KO} cell line had an impressive capacity for distinguishing known cancer and benign variants, its ability to distinguish hypomorphic PMD variants was not as strong. At the center of the issue are unexpectedly-low-scoring benign variants that appear PMD-like.

Several factors may have contributed to these observations, some of which are due to limitations of the model, while others are related to external limitations.

The Activity Scores of variants with partial activity may have been influenced by idiosyncrasies of the HAP1 cell line, such as having vastly different abundances of other SDH-related proteins. The extent of these differences likely depends on a variant's specific consequence. For example, the cancer variant $SDHA^{T308M}$ affects the Thr308 residue, which crystal structures of *E. coli* SDHA homologs have shown is necessary to stabilize the succinate-to-fumarate transition intermediate (288,299). Thus, even though our data show this variant is flavinylated, increasing the abundance of SDHAF2 or SDHB will not affect its function. However, a variant that interferes with the process of SDHAF2-mediated flavinylation may have higher functionality if the expression of SDHAF2 is higher. As we were largely unable to identify the mechanisms resulting in partial dysfunction for hypomorphic PMD and low-scoring benign variants, it is difficult to determine how much this influences our data. Experiments modulating the abundance of other SDH-related proteins can be performed to determine precisely how variant activity may be affected. Further, structural analysis using the recently obtained human SDH and SDHA-SDHAF2 structures can help elucidate precisely how each variant may affect function.

In addition to the possibility that the Activity Scores from our model do not fully represent the exact function of SDHA variants in the context of human disease, another possibility is that partial SDH dysfunction alone is not sufficient for PMD. Rather, some benign variants may not be pathogenic despite having

low activity because they do not result in a specific consequence required for disease, such as the production of ROS (76,147,250). Reduced FAD is the largest source of ROS production from SDH; thus, variants may produce differing amounts of ROS, depending on whether function is affected before or after the FAD reduction step (251). It is somewhat difficult to explain the presence of PMD-associated dominant negative SDHA variants in this model, in particular, $SDHA^{R451C}$, which is not flavinylated and cannot be a source of ROS. However, both dominant negative variants that we characterized maintained high levels of SDHB, which likely explains their ability to interfere with $SDHA^{WT}$. The iron-sulfur clusters of SDHB may be a potential source of ROS (300). Future studies should investigate the levels of ROS produced in cells with varying levels of SDH activity. Even if this proposed model is ultimately not supported, it highlights the real possibility that the rate of SDH activity is not the sole determinant of PMD pathogenicity, and other consequences may be involved.

Unfortunately, it may also be the case that we cannot properly distinguish hypomorphic PMD variants because some low-scoring benign variants are not truthfully benign. The uncertainty surrounding the variants we selected as controls is a product of the challenges the field has faced concerning the interpretation of SDHA variant pathogenicity as a whole. For many years, sequencing *SDHA* had difficult due to its multiple, highly homologous pseudogenes, which calls into question the validity of some historical data (201). In some cases, interpretations were made for variants identified in tumor sequencing, even though only three exons were analyzed (200). Alternatively, it

has been shown a variant may be inappropriately attributed to *SDHA* when, in actuality, it is a SNP of one of the pseudogenes (202). As evidence of the effect these issues can produce, we identified variants that have linked to SDH-deficient tumors but have also been classified as Benign/Likely Benign in ClinVar (133,204).

Our incomplete understanding of PMD pathogenicity also adversely affects confidence in the accuracy of some benign classifications. For example, the least-active benign variant in our control set is SDHA^{Y55H}, with an Activity Score of 0.215. This variant has been reported as homozygous 12 times in gnomAD v4.00 (185). As such, the 11 Benign/Likely Benign submissions in ClinVar for SDHA^{Y55H} are indeed appropriate, but this can only be certain for cancer risk (186). As gnomAD excludes individuals with severe childhood-onset disease, SDHA^{Y55H} is also almost certainly not associated with PMD when homozygous (185). However, the same cannot be said if the variant was compound heterozygous with a null allele. This is evidenced by SDHA^{T508I}, which was identified as a compound heterozygous variant (with SDHA^{S509L}) in a boy with PMD, presenting as leukodystrophy and cardiomyopathy (94). In our assay, SDHA^{T508I} was similar to SDHA^{Y55H}, with an Activity Score of 0.270, while SDHA^{S509L} had no activity (Activity Score = 0.010). Also like SDHA^{Y55H}, SDHA^{T508I} has been reported as homozygous eight times in gnomAD v4.00 and has seven Benign/Likely Benign submissions in ClinVar (as well as one Pathogenic and VUS submission) (185,186). This sets a precedent for low-scoring variants to be benign for PMD when homozygous but pathogenic

when compound heterozygous with an amorphic allele. If SDHA^{Y55H} were truly pathogenic for PMD, it may not be entirely surprising that a patient has yet to be identified and reported. The reported allele frequency of SDHA^{Y55H} (7.69×10^{-4}) is only slightly higher than that of SDHA^{T508I} (4.89×10^{-4}), and further, compound inheritance of a rare amorphic allele would be required for disease (185).

Ultimately, it is clear that the interpretation of SDHA-variant pathogenicity for PMD is complicated, even with the addition of functional data. There is a critical need for the creation of a *SDHA* expert panel to develop independent rules for applying evidence to determine PMD and cancer pathogenicity.

Developing high-throughput assays for SDH variant functional characterization

Although the ability to obtain strong functional evidence for cancer pathogenicity is not largely affected by the limitations described above, the HAP1 *SDHA*^{KO} model is nonetheless limited in its capacity. While variants with multiple or conflicting reports can be prioritized for future characterization, the number of *SDHA* VUS is simply too high to address one variant at a time. To address the scale of the problem, we strove to develop a cell-based assay that could be scaled to characterize hundreds or thousands of SDHA variants.

Initially, I adapted a yeast-based model we previously used to characterize individual variants, in which growth in the non-fermentable sugar glycerol is dependent on SDH function (208). Due to the robustness of yeast as a model for studying mitochondrial dysfunction, the strategy was quite successful. All nonsense variants in a pilot library were strongly depleted from the population, as well as all variants affecting the essential histidine residue that binds FAD,

whereas the abundance of synonymous variants remained largely unchanged. However, there was concern regarding the ability to translate this functional data to human variants, as we observed discordance with data obtained from the HAP1 *SDHA*^{KO} cell line. Nonetheless, the yeast functional pipeline still retains considerable value, especially considering the relative ease of performing experiments. For instance, we could use Effect Scores of all possible missense Sdh1 variants to prioritize the order clinically-relevant SDHA VUS are characterized within the HAP1 *SDHA*^{KO} system. Furthermore, the data can help us better understand the structure-function relationship. This may ultimately help elucidate the mechanisms of dysfunction corresponding to variants with partial activity, which currently elude us. As such, these experiments should continue.

Toward developing an assay capable of high-throughput analysis of human SDHA variants, I investigated whether we could leverage the metabolic dependencies of the HAP1 *SDHA*^{KO} cells. As with the yeast model, preliminary data was promising but ultimately had limitations that prevented its further use. In particular, after an unidentified number of passages, cell growth of HAP1 *SDHA*^{KO} in metabolite-depleted media could no longer be rescued by the expression of functional SDHA variants or even SDHA^{WT}. While further investigation is required to determine the cause of this, it may be related to the progressive loss of Complex I associated with SDH-deficiency (277). Although this renders the assay incompatible with high-throughput analysis of SDHA-variant function, we may be able to identify different culturing conditions that permit the growth of Complex I-deficient cells while maintaining dependence

on SDH function. Further, as loss of Complex I is a reported phenotype of SDH-deficient tumors, the HAP1 *SDHA*^{KO} cell line may prove to be a useful model for investigating therapeutic strategies that exploit the metabolic dependencies (270,295-297,301).

As an alternative approach, I developed a new assay utilizing CRISPR-Cas9 technology to mimic *SDHA* LOH that results in tumor formation in people. Using CRISPR to interrogate the function of different variants is not novel. In fact, these methods are often far more sophisticated than what we present in Chapter 3, including various approaches to incorporate variants into endogenous alleles (280,284,302,303). However, with *SDHA*, these approaches would be exceedingly difficult, considering the four pseudogenes (*SDHAP1-4*) that have over 90% coding-sequence identity (201). Nonetheless, our assay provides a simple system for assessing SDHA variant function, and the data largely match the activity data from the HAP1 *SDHA*^{KO} model. Interestingly, a hypomorphic PMD variant with minimal activity, SDHA^{G555E} (Activity Score = 0.07) can either appear similar to cancer variants or benign variants, depending on the metabolic substrates present in the medium. Thus, utilizing both media conditions in tandem may enable us to better distinguish benign-like, hypomorphic, and cancer-like variants. Although the extent of the capacity to distinguish these variants will require the analysis of more variants covering a spectrum of Activity Scores, the observation that a variant with an Activity Score of 0.07 appears largely benign-like when utilizing our normal culture media indicates this assay has a very wide dynamic range corresponding to cancer and

non-cancer function. Thus, this assay is highly promising for obtaining cancer-like functional classifications with high positive predictive value.

In addition to characterizing SDHA variants, we show this assay has strong potential for the characterization of other *SDH* genes, which are also tumor suppressors with high numbers of VUS. Further, the assay is not inherently limited to the HAP1 cell line but to any cell lines in which the *SDH* genes are essential or whose loss results in decreased fitness. However, a clear limitation of this assay is that activity cannot be directly interrogated to validate results. While data from our HAP1 *SDHA*^{KO} cell line and previously established SDHB-deficient cell lines can be used for this purpose, efforts to generate similar models for *SDHC* and *SDHD* are required (74).

Lastly, although the analyses performed with this assay investigated individual variants, this approach can be easily adapted to high-throughput deep-mutational scanning. The implementation of this would optimally include introducing sgRNA linked to antibiotic resistance, as any of the DNA from any untransduced cell in the current version of the assay can still be amplified. Without receiving a sgRNA, these cells would not become depleted even if the variant is amorphic, resulting in a decreased signal-to-noise. Further, the landing-pad approach described in Chapter 2 could be employed to better control variant copy number and expression when introduced into the Cas9-expressing HAP1 cell line. The continuation of this work will have a significant impact on our ability to assess cancer risk for carriers of thousands of *SDH* variants.

5. Appendix: Supplementary data

Table 4. Data used for selecting control variants and VUS

Variant	ClinVar [186]	LOVD [223]	Notes
Benign			
G6D	9 B/LB, 2 VUS	1 B/LB	
D38V	14 B/LB	4 B/LB	
A45T	8 B/LB, 8 VUS	2 B/LB, 3 VUS	
K46E	5 B/LB, 3 VUS	VUS	
D49G	7 B/LB, 1 VUS	1 B/LB	
Y55H	11 B/LB	1 B/LB, 1 VUS	
G184R	10 B/LB	2 B/LB, 1 VUS	
I319L	1 B/LB, 6 VUS	1 B/LB	
R352Q	3 B/LB, 8 VUS	1 VUS	
A466T	5 B/LB, 1 VUS	2 B/LB	
E472K	1 B/LB, 3 VUS	1 B/LB, 1 VUS	
R554Q	4 B/LB, 6 VUS	-	
Y629F	10 B/LB	3 B/LB	
V632I	1 B/LB, 1 VUS	1 B/LB	
E640G	2 B/LB, 5 VUS	1 B/LB	
V657I	11 B/LB	2 B/LB	
A660G	5 B/LB, 8 VUS	1 VUS	VUS in literature[204]
Cancer			
H99R	1 VUS	-	P/LP in literature[204]
H99Y	1 P/LP	1 P/LP	
A103V	1 P/LP, 1 VUS	-	
R171C	3 VUS	1 P/LP, 1 VUS	VUS in literature[136]
R188W	3 P/LP	-	
S208P	1 VUS	-	P/LP in literature[204]
G260R	7 P/LP	1 P/LP	P/LP in literature[204]
G274S	-	-	P/LP in literature[204]
T308M	3 P/LP, 2 VUS	1 VUS	VUS in literature[136]
H407R	1 P/LP, 1 VUS	-	
G439E	2 VUS	-	
H447R	1 P/LP, 1 VUS	1 VUS	P/LP in literature[204]
R451C	5 P/LP, 1 VUS	1 VUS	VUS[136] and PMD[100-102] in literature
R451H	3 P/LP, 1 VUS	1 P/LP	
A454E	2 VUS	VUS	P/LP in literature[204]
G581R	3 P/LP, 1 VUS	-	P/LP in literature[136]
R585W	10 P/LP, 2 VUS	4 P/LP	
R589W	6 P/LP	2 P/LP	P/LP in literature[136]
R589G	1 P/LP	-	
R589Q	3 P/LP	1 P/LP, 1 VUS	P/LP in literature[136,204]
G590S	1 VUS	1 P/LP	

Variant	ClinVar [186]	LOVD [223]	Notes
PMD			
D137H	-	-	PMD in literature[96]
E152K	4 VUS	-	PMD in literature[238,239]
C189G	-	1 P/LP	PMD in literature[97]
T508I	7 B/LB, 1 P/LP, 1 VUS	1 B/LB, 1 VUS	PMD in literature[94]
S509L	1 P/LP, 1 VUS	1 VUS	PMD in literature[94]
R512Q	5 VUS	1 P/LP	PMD in literature[99]
A524V	4 P/LP	1 VUS	PMD in literature[98]
R554W	5 P/LP, 3 VUS	1 P/LP, 2 VUS	PMD in literature[92]
G555E	3 P/LP	1 P/LP, 3 VUS	PMD in literature[95,236,237]
R662C	1 P/LP, 3 VUS	-	PMD in literature[103]
VUS			
T96I	6 VUS	-	
R97T	3 VUS	-	
G106R	1 VUS	-	
L111R	-	-	
N118S	2 VUS	-	
T143M	3 VUS	-	
R171H	7 VUS	-	VUS in literature[136]
R195W	4 VUS	-	
R232H	2 VUS	1 B/LB	
G233V	3 VUS	-	VUS in literature[136]
H296Y	2 VUS	-	
R312C	3 VUS	-	
R312H	2 VUS	1 VUS	
P372R	6 VUS	1 B/LB, 1 VUS	
G419R	3 VUS	1 VUS	
V425G	2 VUS	1 B/LB	
C438F	2 VUS	-	
L452F	3 VUS	-	
S456L	2 B/LB, 2 VUS	1 B/LB	Germline in SDHB-IHC neg. GIST w/ somatic R210X[133]
R465W	2 VUS	-	
E564K	1 VUS	1 VUS	
H592R	2 VUS	-	
R600Q	1 B/LB, 6 VUS	3 VUS	P/LP[204] and VUS[136] in literature
H625Y	1 VUS	1 VUS	

Table 5. Functional data from HAP1 *SDHA*^{KO} model

Variant	Activity Score (SEM)	SDHA Abundance Score (SEM)	SDHB Abundance Score (SEM)	WT-normalized GFP MFI (SEM)
Control				
WT	1.000 (0.006)	1.000 (0.009)	1.000 (0.010)	1.000 (0.011)
R31X	0.004 (0.000)	0.027 (0.007)	0.153 (0.047)	0.230 (0.009)
Benign				
G6D	1.111 (0.010)	0.915 (0.061)	0.885 (0.010)	0.768 (0.017)
D38V	0.848 (0.018)	0.735 (0.041)	0.660 (0.033)	1.045 (0.036)
A45T	1.166 (0.015)	1.355 (0.011)	0.903 (0.023)	0.892 (0.034)
K46E	1.278 (0.042)	1.239 (0.056)	1.082 (0.012)	0.755 (0.021)
D49G	0.959 (0.005)	0.829 (0.084)	0.736 (0.036)	0.868 (0.011)
Y55H	0.215 (0.007)	0.635 (0.039)	0.053 (0.004)	0.890 (0.017)
G184R	0.683 (0.025)	0.495 (0.016)	0.595 (0.024)	0.933 (0.006)
I319L	0.932 (0.045)	0.854 (0.062)	0.886 (0.037)	0.994 (0.015)
R352Q	0.992 (0.014)	0.774 (0.078)	0.921 (0.031)	0.970 (0.011)
A466T	0.509 (0.019)	0.570 (0.031)	0.820 (0.028)	0.878 (0.070)
E472K	0.878 (0.007)	1.060 (0.055)	0.966 (0.036)	0.991 (0.006)
R554Q	0.529 (0.025)	0.885 (0.033)	0.686 (0.029)	0.852 (0.053)
Y629F	0.952 (0.019)	0.788 (0.051)	0.867 (0.048)	0.972 (0.031)
V632I	1.052 (0.005)	0.812 (0.027)	1.045 (0.087)	0.973 (0.031)
E640G	1.035 (0.032)	0.384 (0.020)	1.044 (0.036)	0.969 (0.023)
V657I	1.235 (0.058)	1.328 (0.065)	1.303 (0.053)	0.850 (0.011)
A660G	1.215 (0.057)	1.168 (0.032)	1.253 (0.045)	0.956 (0.011)
Cancer				
H99R	0.002 (0.001)	0.111 (0.018)	0.001 (0.000)	0.761 (0.017)
H99Y	0.006 (0.001)	0.624 (0.003)	0.032 (0.004)	0.856 (0.017)
A103V	0.002 (0.006)	0.015 (0.001)	0.054 (0.009)	0.869 (0.015)
R171C	0.003 (0.002)	0.202 (0.005)	0.006 (0.002)	0.862 (0.011)
R188W	0.011 (0.001)	0.081 (0.004)	0.008 (0.002)	0.971 (0.010)
S208P	0.011 (0.004)	0.160 (0.020)	0.067 (0.011)	0.766 (0.038)
G260R	0.000 (0.000)	0.203 (0.011)	0.006 (0.001)	0.772 (0.010)
G274S	0.068 (0.004)	0.142 (0.003)	0.088 (0.009)	0.862 (0.043)
T308M	0.001 (0.005)	0.284 (0.021)	0.408 (0.049)	0.804 (0.024)
H407R	0.002 (0.003)	0.023 (0.007)	0.013 (0.012)	0.950 (0.010)
G439E	0.004 (0.003)	0.005 (0.000)	0.005 (0.000)	0.744 (0.029)
H447R	0.005 (0.002)	0.015 (0.004)	0.042 (0.012)	0.928 (0.021)
R451C	0.003 (0.001)	1.233 (0.033)	0.812 (0.027)	0.874 (0.031)
R451H	0.001 (0.000)	0.677 (0.067)	0.354 (0.042)	0.981 (0.020)
A454E	0.005 (0.002)	0.067 (0.006)	0.010 (0.002)	0.989 (0.051)
G581R	0.003 (0.006)	0.030 (0.001)	0.057 (0.007)	0.858 (0.018)
R585W	0.004 (0.000)	0.008 (0.003)	0.079 (0.007)	0.908 (0.009)
R589W	0.002 (0.001)	0.001 (0.001)	0.021 (0.008)	0.844 (0.019)
R589G	0.002 (0.001)	0.034 (0.004)	0.000 (0.000)	0.866 (0.027)

Variant	Activity Score (SEM)	SDHA Abundance Score (SEM)	SDHB Abundance Score (SEM)	WT-normalized GFP MFI (SEM)
R589Q	0.001 (0.006)	0.033 (0.003)	0.002 (0.001)	0.789 (0.055)
G590S	0.002 (0.001)	0.005 (0.002)	0.002 (0.001)	0.871 (0.006)
PMD				
D137H	0.597 (0.027)	0.569 (0.019)	0.731 (0.019)	0.979 (0.037)
E152K	0.657 (0.019)	0.979 (0.061)	1.059 (0.044)	0.867 (0.044)
C189G	0.099 (0.001)	0.918 (0.017)	1.051 (0.034)	0.891 (0.017)
T508I	0.270 (0.016)	0.543 (0.034)	0.163 (0.017)	0.886 (0.014)
S509L	0.010 (0.002)	0.834 (0.024)	0.003 (0.000)	0.902 (0.014)
R512Q	0.162 (0.009)	0.244 (0.033)	0.229 (0.011)	1.078 (0.035)
A524V	0.476 (0.017)	0.810 (0.026)	1.274 (0.078)	0.852 (0.059)
R554W	0.249 (0.014)	0.505 (0.023)	0.099 (0.015)	1.078 (0.014)
G555E	0.070 (0.006)	0.663 (0.024)	0.157 (0.005)	0.919 (0.053)
R662C	0.013 (0.001)	0.780 (0.050)	1.095 (0.130)	1.122 (0.030)
VUS				
T96I	0.853 (0.026)	1.549 (0.031)	1.235 (0.054)	0.792 (0.039)
R97T	0.015 (0.001)	0.816 (0.018)	0.140 (0.012)	0.759 (0.024)
G106R	0.003 (0.001)	0.102 (0.004)	0.004 (0.000)	0.956 (0.037)
L111R	0.005 (0.001)	0.068 (0.016)	0.029 (0.004)	0.907 (0.050)
N118S	0.807 (0.038)	0.723 (0.053)	0.677 (0.093)	0.986 (0.037)
T143M	0.049 (0.017)	0.128 (0.023)	0.014 (0.012)	0.767 (0.071)
R171H	0.011 (0.002)	0.509 (0.040)	0.199 (0.017)	0.881 (0.021)
R195W	0.015 (0.001)	0.165 (0.023)	0.089 (0.014)	0.821 (0.055)
R232H	0.932 (0.015)	0.743 (0.036)	0.679 (0.066)	0.957 (0.015)
G233V	0.002 (0.001)	0.001 (0.000)	0.022 (0.004)	0.980 (0.040)
H296Y	0.004 (0.001)	0.496 (0.053)	0.316 (0.028)	0.799 (0.036)
R312C	0.007 (0.001)	1.259 (0.037)	0.927 (0.105)	0.925 (0.003)
R312H	0.002 (0.001)	0.670 (0.016)	0.425 (0.031)	0.844 (0.003)
P372R	1.030 (0.031)	1.093 (0.057)	1.306 (0.103)	0.966 (0.019)
G419R	0.001 (0.000)	0.002 (0.001)	0.006 (0.002)	0.934 (0.038)
V425G	0.877 (0.026)	0.639 (0.016)	0.788 (0.018)	1.006 (0.030)
C438F	0.025 (0.004)	0.040 (0.007)	0.033 (0.005)	0.806 (0.029)
L452F	0.010 (0.001)	0.156 (0.012)	0.102 (0.003)	0.838 (0.026)
S456L	0.002 (0.001)	0.004 (0.000)	0.045 (0.012)	0.948 (0.013)
R465W	0.379 (0.042)	0.529 (0.052)	0.513 (0.084)	0.945 (0.025)
E564K	0.011 (0.002)	1.048 (0.013)	0.003 (0.002)	0.919 (0.016)
H592R	0.002 (0.001)	0.037 (0.003)	0.006 (0.002)	0.791 (0.020)
R600Q	0.006 (0.002)	0.188 (0.011)	0.168 (0.018)	0.887 (0.015)
H625Y	0.003 (0.001)	0.005 (0.001)	0.004 (0.003)	0.866 (0.024)

Data are available via **Figshare**.

Table 6: Effect Scores from yeast Sdh1 DMS pilot

	Amino Acid																				
Residue	A	C	D	E	F	G	H	I	K	L	M	N	P	Q	R	S	T	V	W	Y	X
Q29	-0.05	-0.03	-0.14	0.03	-0.06	0.01	-0.30	0.10	-0.17	0.08	-0.24	-0.08	0.04	-0.24	-0.07	-0.29	-0.06	0.06	0.10	-0.13	-2.60
T30	0.00	-0.04	-0.13	-0.02	-0.01	-0.09	0.12	-0.10	-0.15	-0.13	-0.11	0.07	-0.05	-0.32	-0.01	-0.09	-0.03	-0.05	-0.03	-0.16	-1.85
Q31	-0.09	0.03	0.13	-0.21	0.13	0.01	0.02	-0.11	-0.06	-0.05	0.02	0.03	0.10	-	-0.03	0.12	-0.23	-0.04	0.02	-0.22	-1.60
G32	-0.67	-0.02	0.09	0.33	-0.07	-0.12	0.18	0.05	-0.13	-0.20	-0.10	-0.20	0.01	-0.24	-0.06	-0.55	0.07	-0.10	-0.11	-0.12	-2.28
S33	0.26	-0.11	0.04	-0.29	0.21	-0.31	0.15	0.19	0.07	-0.13	-0.07	-0.08	-0.14	0.06	0.09	0.02	0.00	0.13	-0.06	-0.44	-2.12
V34	0.07	-1.43	-0.28	-0.19	-0.17	-0.12	-0.25	-0.13	0.05	0.10	-0.17	-0.23	-0.03	-0.18	-0.04	-0.11	-0.52	-0.02	-0.03	0.03	-1.15
N35	-0.41	-	-	0.08	-0.21	0.07	-	-	-	0.22	0.18	0.05	-	-	0.40	0.05	-	-	-	-	-2.85
G36	-0.41	-0.11	0.15	-0.15	-0.02	-0.07	-0.04	0.02	-0.35	-0.01	0.09	-	0.24	-0.52	-0.04	-0.40	-0.15	-0.09	0.07	-	-2.23
S37	-0.10	0.13	-0.01	-	-0.52	0.08	-0.49	0.14	-1.14	-0.12	0.22	-	0.15	-0.23	-0.31	0.24	-0.22	-0.35	-	-0.16	-1.69
A38	0.04	0.13	-0.15	-0.09	-0.19	-0.47	0.06	-0.19	-0.04	-0.09	0.00	0.40	-0.10	-0.35	-0.30	-0.08	-0.09	-0.03	0.22	0.08	-3.27
S39	0.07	0.23	-0.14	0.08	0.10	-0.30	-0.22	0.17	-0.65	0.02	-0.36	-0.13	0.16	0.06	0.04	-0.15	-0.19	-0.01	0.12	0.06	-1.90
R40	-0.01	-0.02	-0.48	0.00	0.08	-0.15	0.05	-0.21	0.01	-0.13	-0.32	0.00	-0.03	-0.14	0.01	-0.06	-0.03	-0.06	0.00	-0.45	-2.77
S41	-0.09	0.04	0.12	0.04	0.14	-0.36	-0.19	0.04	-0.01	0.01	-0.43	0.03	-0.05	-0.37	0.03	-0.09	-0.35	-0.08	0.03	-0.16	-2.04
A42	0.03	-0.09	0.16	-0.45	-0.20	-0.04	-0.01	-0.41	-0.09	-0.21	-0.15	-0.41	-0.09	0.08	-0.16	0.07	-0.28	-0.10	0.04	-0.19	-3.02
D43	0.21	0.00	-0.23	-0.42	-0.32	-0.11	0.11	-	-0.09	-0.30	-0.62	-0.01	-0.34	-0.16	0.00	0.09	0.04	-0.21	0.06	-	-1.13
G44	-0.04	-	-	-0.17	0.19	0.07	-0.01	-	-	-	-	-	-1.73	0.09	-0.77	-	-0.14	-0.10	-0.26	-0.15	-
K45	-0.43	-	-	-0.24	-	-0.74	-	-	-	-0.15	-0.09	-0.69	-0.06	-0.15	-0.03	0.52	-0.22	0.18	-	-	-1.21
Y46	0.02	0.00	-0.08	-0.05	-0.13	-0.08	0.16	-0.16	-0.03	-0.08	-0.12	-0.56	-0.76	-0.03	-0.03	-0.10	0.00	-0.13	-0.01	-0.08	-2.33
H47	-0.01	-0.13	0.02	0.06	-0.26	-0.23	-0.09	-0.03	0.05	-0.09	-0.11	-0.12	-0.09	0.12	-0.08	-0.13	-0.18	-0.22	-0.32	-0.07	-2.02
I48	0.05	-0.08	-0.17	-0.10	-0.24	-0.02	-0.23	0.03	-0.22	-0.18	-0.02	-0.07	-0.17	-0.14	-0.08	-0.07	-0.02	-0.07	-0.06	-0.08	-2.17
I49	0.04	-0.09	-0.67	-0.31	-0.13	-0.23	0.06	0.07	-0.91	-0.02	-0.21	-0.50	-2.49	0.04	-0.10	-0.11	-0.11	-0.30	-0.14	-0.01	-2.14
D50	-0.08	0.01	-	-0.24	-0.07	-0.06	-0.11	-0.33	-0.17	-0.16	-0.18	-0.08	-1.29	0.15	-0.10	0.09	-0.02	-0.16	-0.22	-0.20	-2.39
H51	-0.16	-0.30	-0.31	-0.31	-0.05	-0.19	-0.16	-0.76	-0.21	-0.22	-0.26	0.18	-1.09	-0.04	-0.15	-0.23	-0.18	-0.32	-0.06	-0.20	-1.78
E52	-0.23	-0.06	-0.16	-	0.08	-0.12	-0.33	0.02	-0.63	-0.25	0.05	-0.68	-0.16	-0.10	-0.83	-0.70	-	-0.04	-0.72	-	-2.13

Residue	Amino Acid																				
	A	C	D	E	F	G	H	I	K	L	M	N	P	Q	R	S	T	V	W	Y	X
Y53	0.06	0.00	-0.19	0.31	-0.23	-0.13	-0.25	0.06	-0.37	-0.55	-0.34	0.00	-1.13	-0.03	-0.18	-0.44	-0.31	0.05	-0.20	-0.12	-2.64
D54	0.26	-0.76	-0.28	0.00	-2.23	-0.13	-0.19	-1.52	-2.21	-1.00	-0.23	-0.84	0.01	-0.15	-2.31	-1.02	-0.08	-0.47	-2.44	-1.66	-2.66
C55	-0.04	-	-0.08	-0.95	-0.34	-0.05	-0.97	0.06	-2.80	-0.07	0.13	-0.04	-2.70	0.05	-2.31	-0.05	-0.39	-0.60	-2.04	-1.67	-3.05
V56	-0.08	-0.02	-0.54	-0.37	-0.11	-0.20	-0.54	-0.26	-2.51	-0.22	-0.25	-	-2.48	-0.31	-2.76	-0.27	-0.30	0.09	-2.52	-0.85	-2.78
V57	0.00	-0.05	-0.49	-0.11	-2.76	-0.22	-0.04	-0.26	-	-0.27	-0.12	0.08	-2.96	-0.09	-2.80	0.18	-0.33	-0.18	-2.58	-2.70	-2.35
I58	0.07	-0.17	-0.28	-0.21	-1.75	-0.18	-2.00	-0.05	-1.46	-0.13	-0.03	-0.46	-0.66	-0.04	-2.69	0.05	-0.36	-0.09	-3.13	-2.99	-2.77
G59	-2.56	-1.60	-1.29	-3.05	-2.57	-0.03	-2.60	-2.68	-2.41	-2.47	-2.91	-3.38	-	-1.53	-2.89	-2.44	-2.89	-2.45	-2.37	-2.02	-3.15
A60	-0.11	-0.34	-2.54	-2.35	-2.12	-0.27	-2.87	-0.05	-2.82	0.13	-0.03	-0.32	-1.53	-0.39	-2.39	-0.02	-0.33	0.03	-2.75	-2.92	-1.95
G61	-2.53	-2.35	-1.91	-2.71	-3.42	-0.40	-2.98	-2.71	-3.05	-2.97	-3.04	-	-2.86	-2.51	-2.58	-2.15	-3.19	-2.42	-2.15	-2.34	-2.59
G62	0.19	0.02	-	-	-3.77	-0.24	-	-1.84	-	-	-	-3.11	-	-	-2.75	-0.94	-	-0.75	-3.52	-	-
A63	-0.08	-0.36	-2.85	-2.55	-2.58	-0.17	-2.56	-3.22	-2.75	-2.97	-2.81	-2.84	-2.76	-2.96	-2.54	-0.03	-0.56	-2.81	-2.78	-3.05	-1.76
G64	-1.72	-2.69	-2.64	-2.79	-2.43	-0.08	-2.24	-2.70	-2.97	-2.76	-2.89	-2.43	-2.27	-2.62	-2.72	-2.85	-2.71	-2.55	-2.66	-2.33	-2.33
L65	0.05	-0.16	-2.39	-0.10	-1.72	-0.06	-2.10	0.09	-2.71	0.06	-0.09	-0.14	-2.32	-1.07	-2.49	-0.13	-0.05	0.03	-2.61	-2.92	-2.53
R66	-1.58	-1.04	-2.79	-1.22	-0.27	-2.44	-0.14	-2.09	-0.95	-1.07	-0.11	-1.11	-2.96	-1.22	0.03	-0.76	0.06	-2.59	-0.27	-0.22	-2.67
A67	-0.36	-0.04	-1.43	-1.64	-2.51	-0.16	-	-	-	-0.99	-1.11	-	-0.73	-3.07	-2.89	-0.06	-0.55	-0.10	-1.89	-	-1.33
A68	-0.27	-	-	-	-	-1.41	-1.10	-	-	-	-0.08	-0.31	-2.94	-	-2.50	-	-	-	-	-	-3.28
F69	0.45	-0.51	-0.37	-0.13	-	0.04	0.04	-0.02	-1.15	-0.09	-	-	-0.18	-0.59	0.51	-0.20	-0.04	-0.07	0.23	-0.18	-1.95
G70	0.01	-0.37	-1.54	-1.11	-2.56	0.01	-	-	-	-2.77	-1.38	-	-0.01	-	-1.28	0.10	-	-1.76	-1.53	-2.51	-
L71	0.07	-0.30	-1.60	-1.69	0.12	0.12	-0.62	-0.19	-2.03	-0.08	0.04	0.16	-0.25	-0.36	-2.48	0.00	-0.28	0.08	-2.26	-0.64	-2.19
A72	-0.17	0.09	-	-	-	-	-	-	-	-2.27	-	-	-0.11	-0.37	-0.08	0.10	-1.08	-0.01	-2.00	-1.81	-
E73	-0.33	-0.02	-0.16	-	0.18	-0.50	-	-	-0.18	-0.23	-0.38	-0.47	0.01	-0.25	-0.33	-0.22	0.15	-0.27	-0.37	-0.80	-2.02
A74	0.09	-0.19	0.23	-0.05	-	0.02	-0.04	-0.09	0.04	-0.09	-0.05	0.10	-0.19	0.20	-0.28	-0.45	-0.10	-0.17	-0.33	-	-2.27
G75	-0.82	-	-0.07	0.13	-	-0.14	-	-1.58	-	-	-	-	-	-	0.23	0.26	-1.73	-0.81	-	-	-
Y76	0.09	-0.26	-1.92	-0.58	-0.06	-1.51	-0.18	0.03	-	-0.25	-0.25	0.16	-2.50	0.33	-0.73	-1.16	0.05	-0.45	-0.10	-	-1.11
K77	-	-0.08	-	-0.15	-	0.15	-0.76	-	-	0.06	-0.31	-0.02	-	-0.17	-0.07	0.00	-0.24	-0.31	-0.16	-	-1.10
T78	-1.58	-	-	-	-	-0.34	-0.07	-0.40	-	0.13	0.04	-0.14	-0.31	0.19	-	-0.61	-0.17	-0.26	-	-	-

	Amino Acid																				
Residue	A	C	D	E	F	G	H	I	K	L	M	N	P	Q	R	S	T	V	W	Y	X
A79	-	-	-0.34	-	-	-	-	-	-	-	-	-	-	-	-	-0.36	-0.20	-0.01	-	-	-
C80	0.04	-	0.02	-0.29	-1.88	-0.22	-2.72	-0.32	-1.49	-0.17	-0.23	-0.24	-2.35	-0.06	-2.36	-0.29	-0.10	-0.09	-2.03	-1.82	-1.96
I81	-0.09	-0.24	-2.65	-1.78	-0.38	-0.41	-0.14	0.01	-2.54	-0.12	-0.31	-1.38	-1.03	-0.48	-2.74	-0.51	-0.24	-0.07	-2.05	-1.02	-2.23
S82	-0.63	-0.42	-2.12	-2.61	-2.70	0.02	-2.29	-1.16	-3.15	-0.64	-0.16	-0.57	-2.44	-1.67	-2.77	-0.27	-0.39	-0.65	-2.41	-2.91	-2.18
K83	-0.17	-0.44	-0.65	-0.16	-0.41	-1.19	-0.77	-0.40	-	-0.25	-0.29	-0.42	-2.09	-0.33	-1.67	-0.23	-0.20	-0.28	-2.88	-0.23	-2.13
L84	-0.26	0.05	-1.44	-1.22	-2.05	-0.17	-1.26	-0.45	-1.86	-0.07	-0.12	0.09	-2.07	0.02	-2.86	-0.18	-0.20	-0.42	-3.25	-3.20	-2.51
F85	-0.28	-0.42	-2.29	-	-0.14	-	0.20	-0.27	-	-0.05	-0.14	-	-	0.56	-2.57	-0.39	-0.04	-0.01	-0.14	-	-
P86	0.11	0.17	-	-2.02	-3.23	0.08	-	-0.58	-2.81	-0.07	-0.19	-	-0.21	-1.68	-2.72	-0.75	-0.14	0.09	-2.60	-1.19	-1.29
T87	-0.44	-0.70	-1.88	-0.97	-2.39	-0.82	-	-0.99	-1.28	-0.22	-0.58	-0.38	0.12	-2.85	-1.94	-0.23	-0.01	0.15	-0.71	-	-
R88	-2.72	-2.22	-2.97	-3.39	-	-2.31	-	-	-0.04	-2.62	-2.68	-	-3.04	-	-0.07	-2.09	-	-2.96	-3.16	-2.84	-
S89	-0.04	-0.48	-2.89	-2.15	-1.86	-0.19	-2.73	-2.96	-	-3.45	-	-2.36	-2.50	-	-3.10	-0.24	-1.01	-2.08	-2.85	-0.64	-
H90	-2.98	-2.99	-3.33	-2.76	-3.09	-3.12	-0.19	-3.58	-2.90	-2.92	-3.43	-2.98	-2.90	-3.01	-3.04	-2.86	-3.05	-2.96	-2.77	-2.90	-3.21
T91	-1.84	-	-	-	-3.53	-	-0.48	-1.69	-	-2.48	-	-0.25	-0.22	-	-	-0.03	-0.11	-1.68	-	-3.22	-
V92	-0.18	-1.28	-2.41	-1.17	-1.19	-0.13	-2.38	-0.23	-2.02	-2.42	-0.93	-1.71	-1.96	-0.15	-2.39	-0.13	-0.18	-0.17	-2.71	-2.05	-2.29
A93	-0.03	-0.78	-0.30	-2.74	-3.25	-0.04	-2.03	-2.75	-	-2.98	-3.57	-	-2.39	-3.03	-2.08	-0.25	-1.13	-1.12	-2.41	-	-1.59
A94	-0.05	-2.91	-0.71	-2.38	-3.03	-1.63	-2.75	-3.23	-2.92	-2.82	-3.18	-2.82	-2.66	-4.03	-2.25	-0.86	-1.58	-2.70	-2.71	-2.61	-
Q95	-0.04	-	-	-0.54	-2.97	-3.11	-1.58	-3.52	-0.09	-0.75	-0.05	-3.29	-0.14	-	-0.19	0.07	-0.46	-3.07	-2.11	-	-1.71
G96	-2.94	-2.15	-2.26	-2.98	-2.92	-0.59	-2.66	-4.05	-3.22	-3.54	-2.28	-2.80	-2.48	-	-2.66	-2.92	-3.22	-2.45	-2.94	-2.75	-2.73

Data are available via **Figshare**.

Table 7: Effect Scores from *SDHA*^{KO} DMS pilot

	Amino Acid																				
Residue	**A**	**C**	**D**	**E**	**F**	**G**	**H**	**I**	**K**	**L**	**M**	**N**	**P**	**Q**	**R**	**S**	**T**	**V**	**W**	**Y**	**X**
T96	-0.91	-	-	-	-	-	-	0.11	-	-	-	-1.70	-0.48	-	-	-0.88	0.53	-	-	-	-2.36
R97	-	-	-	-	-	-1.66	-	-	-1.98	-	-3.03	-	-	-	0.12	-2.23	-3.53	-	-2.74	-	-2.51
S98	0.31	-	-	-	-	-	-	-	-	-2.52	-	-	-2.92	-	-	0.07	-2.39	-	-	-	-2.45
H99	-	-	-2.95	-	-	-	0.23	-	-	-3.05	-	-4.04	-3.66	-3.26	-2.20	-	-	-	-	-3.07	-2.50
T100	-0.71	-	-	-	-	-	-	-1.88	-	-	-	-3.38	-2.87	-	-	0.70	0.13	-	-	-	-2.75
V101	-0.42	-	-3.07	-	-2.36	-0.21	-	0.29	-	-3.13	-	-	-	-	-	-	-	-0.05	-	-	-2.48
A102	-0.28	-	-	-2.76	-	-0.93	-	-	-	-	-	-	-3.11	-	-	-0.06	-0.63	-1.08	-	-	-2.46
A103	-0.01	-	-	-2.70	-	-2.09	-	-	-	-	-	-	-2.24	-	-	-0.94	-2.33	-2.48	-	-	-2.85
Q104	-	-	-	-2.19	-	-	-2.61	-	-1.86	-2.42	-	-	-2.24	0.06	-2.33	-	-	-	-	-	-2.40
G105	-2.67	-	-	-2.59	-	0.05	-	-	-	-	-	-	-	-	-3.40	-	-	-3.19	-	-	-2.29
G106	-3.33	-	-	-2.03	-	0.04	-	-	-	-	-	-	-	-	-2.18	-	-	-3.00	-	-	-2.16
I107	-	-	-	-	-0.05	-	-	0.11	-	-0.03	0.24	-2.24	-	-	-	-2.76	-2.18	0.16	-	-	-2.50
N108	-	-	-2.08	-	-	-	-2.78	-1.01	-2.22	-	-	0.64	-	-	-	-0.43	-2.29	-	-	-3.53	-2.41

Data are available at **Figshare**.

6. References

1. Hanahan D, Weinberg RA. The hallmarks of cancer. *Cell* 2000;**100**(1):57-70 doi 10.1016/s0092-8674(00)81683-9.
2. Hanahan D, Weinberg RA. Hallmarks of cancer: the next generation. *Cell* 2011;**144**(5):646-74 doi 10.1016/j.cell.2011.02.013.
3. Hanahan D. Hallmarks of Cancer: New Dimensions. *Cancer discovery* 2022;**12**(1):31-46 doi 10.1158/2159-8290.CD-21-1059.
4. Harris H, Miller OJ, Klein G, Worst P, Tachibana T. Suppression of malignancy by cell fusion. *Nature* 1969;**223**(5204):363-8 doi 10.1038/223363a0.
5. Sherr CJ. Principles of tumor suppression. *Cell* 2004;**116**(2):235-46 doi 10.1016/s0092-8674(03)01075-4.
6. Knudson AG, Jr. Mutation and cancer: statistical study of retinoblastoma. *Proc Natl Acad Sci U S A* 1971;**68**(4):820-3 doi 10.1073/pnas.68.4.820.
7. Cavenee WK, Dryja TP, Phillips RA, Benedict WF, Godbout R, Gallie BL*, et al.* Expression of recessive alleles by chromosomal mechanisms in retinoblastoma. *Nature* 1983;**305**(5937):779-84 doi 10.1038/305779a0.
8. Friend SH, Bernards R, Rogelj S, Weinberg RA, Rapaport JM, Albert DM, Dryja TP. A human DNA segment with properties of the gene that predisposes to retinoblastoma and osteosarcoma. *Nature* 1986;**323**(6089):643-6 doi 10.1038/323643a0.
9. Zhao M, Kim P, Mitra R, Zhao J, Zhao Z. TSGene 2.0: an updated literature-based knowledgebase for tumor suppressor genes. *Nucleic Acids Res* 2016;**44**(D1):D1023-31 doi 10.1093/nar/gkv1268.
10. Kastenhuber ER, Lowe SW. Putting p53 in Context. *Cell* 2017;**170**(6):1062-78 doi 10.1016/j.cell.2017.08.028.
11. Baugh EH, Ke H, Levine AJ, Bonneau RA, Chan CS. Why are there hotspot mutations in the TP53 gene in human cancers? *Cell Death Differ* 2018;**25**(1):154-60 doi 10.1038/cdd.2017.180.
12. Kandoth C, McLellan MD, Vandin F, Ye K, Niu B, Lu C*, et al.* Mutational landscape and significance across 12 major cancer types. *Nature* 2013;**502**(7471):333-9 doi 10.1038/nature12634.
13. Li FP, Fraumeni JF, Jr. Soft-tissue sarcomas, breast cancer, and other neoplasms. A familial syndrome? *Ann Intern Med* 1969;**71**(4):747-52 doi 10.7326/0003-4819-71-4-747.
14. Kuchenbaecker KB, Hopper JL, Barnes DR, Phillips KA, Mooij TM, Roos-Blom MJ*, et al.* Risks of Breast, Ovarian, and Contralateral Breast Cancer for BRCA1 and BRCA2 Mutation Carriers. *Jama* 2017;**317**(23):2402-16 doi 10.1001/jama.2017.7112.
15. Antoniou A, Pharoah PD, Narod S, Risch HA, Eyfjord JE, Hopper JL*, et al.* Average risks of breast and ovarian cancer associated with BRCA1 or BRCA2 mutations detected in case Series unselected for family history: a combined analysis of 22 studies. *American journal of human genetics* 2003;**72**(5):1117-30 doi 10.1086/375033.
16. Dulbecco R. A turning point in cancer research: sequencing the human genome. *Science* 1986;**231**(4742):1055-6 doi 10.1126/science.3945817.

17. Tate JG, Bamford S, Jubb HC, Sondka Z, Beare DM, Bindal N*, et al.* COSMIC: the Catalogue Of Somatic Mutations In Cancer. *Nucleic Acids Res* 2019;**47**(D1):D941-D7 doi 10.1093/nar/gky1015.
18. International Cancer Genome C, Hudson TJ, Anderson W, Artez A, Barker AD, Bell C*, et al.* International network of cancer genome projects. *Nature* 2010;**464**(7291):993-8 doi 10.1038/nature08987.
19. International Human Genome Sequencing C. Finishing the euchromatic sequence of the human genome. *Nature* 2004;**431**(7011):931-45 doi 10.1038/nature03001.
20. Hood L, Rowen L. The Human Genome Project: big science transforms biology and medicine. *Genome Med* 2013;**5**(9):79 doi 10.1186/gm483.
21. Majewski J, Schwartzentruber J, Lalonde E, Montpetit A, Jabado N. What can exome sequencing do for you? *J Med Genet* 2011;**48**(9):580-9 doi 10.1136/jmedgenet-2011-100223.
22. Sjoblom T, Jones S, Wood LD, Parsons DW, Lin J, Barber TD*, et al.* The consensus coding sequences of human breast and colorectal cancers. *Science* 2006;**314**(5797):268-74 doi 10.1126/science.1133427.
23. Degasperi A, Zou X, Amarante TD, Martinez-Martinez A, Koh GCC, Dias JML*, et al.* Substitution mutational signatures in whole-genome-sequenced cancers in the UK population. *Science* 2022;**376**(6591) doi 10.1126/science.abl9283.
24. Garber JE, Offit K. Hereditary cancer predisposition syndromes. *J Clin Oncol* 2005;**23**(2):276-92 doi 10.1200/JCO.2005.10.042.
25. Nagy R, Sweet K, Eng C. Highly penetrant hereditary cancer syndromes. *Oncogene* 2004;**23**(38):6445-70 doi 10.1038/sj.onc.1207714.
26. Cragun D, Beckstead J, Farmer M, Hooker G, Dean M, Matloff E*, et al.* IMProving care After inherited Cancer Testing (IMPACT) study: protocol of a randomized trial evaluating the efficacy of two interventions designed to improve cancer risk management and family communication of genetic test results. *BMC Cancer* 2021;**21**(1):1099 doi 10.1186/s12885-021-08822-4.
27. Bansal A, Critchfield GC, Frank TS, Reid JE, Thomas A, Deffenbaugh AM, Neuhausen SL. The predictive value of BRCA1 and BRCA2 mutation testing. *Genet Test* 2000;**4**(1):45-8 doi 10.1089/109065700316462.
28. Kurian AW, Ford JM. Multigene Panel Testing in Oncology Practice: How Should We Respond? *JAMA oncology* 2015;**1**(3):277-8 doi 10.1001/jamaoncol.2015.28.
29. Desmedt C, Haibe-Kains B, Wirapati P, Buyse M, Larsimont D, Bontempi G*, et al.* Biological processes associated with breast cancer clinical outcome depend on the molecular subtypes. *Clin Cancer Res* 2008;**14**(16):5158-65 doi 10.1158/1078-0432.CCR-07-4756.
30. Taieb J, Svrcek M, Cohen R, Basile D, Tougeron D, Phelip JM. Deficient mismatch repair/microsatellite unstable colorectal cancer: Diagnosis, prognosis and treatment. *Eur J Cancer* 2022;**175**:136-57 doi 10.1016/j.ejca.2022.07.020.
31. Belardinilli F, Capalbo C, Malapelle U, Pisapia P, Raimondo D, Milanetti E*, et al.* Clinical Multigene Panel Sequencing Identifies Distinct Mutational Association Patterns in Metastatic Colorectal Cancer. *Frontiers in oncology* 2020;**10**:560 doi 10.3389/fonc.2020.00560.
32. Li X, Li M, Huang M, Lin Q, Fang Q, Liu J*, et al.* The multi-molecular mechanisms of tumor-targeted drug resistance in precision medicine. *Biomedicine & pharmacotherapy = Biomedecine & pharmacotherapie* 2022;**150**:113064 doi 10.1016/j.biopha.2022.113064.

33. Pao W, Miller V, Zakowski M, Doherty J, Politi K, Sarkaria I*, et al.* EGF receptor gene mutations are common in lung cancers from "never smokers" and are associated with sensitivity of tumors to gefitinib and erlotinib. *Proc Natl Acad Sci U S A* 2004;**101**(36):13306-11 doi 10.1073/pnas.0405220101.
34. Buege MJ, DiPippo AJ, DiNardo CD. Evolving Treatment Strategies for Elderly Leukemia Patients with IDH Mutations. *Cancers (Basel)* 2018;**10**(6) doi 10.3390/cancers10060187.
35. Aleksakhina SN, Imyanitov EN. Cancer Therapy Guided by Mutation Tests: Current Status and Perspectives. *International journal of molecular sciences* 2021;**22**(20) doi 10.3390/ijms222010931.
36. Papadopoulos N, Kinzler KW, Vogelstein B. The role of companion diagnostics in the development and use of mutation-targeted cancer therapies. *Nat Biotechnol* 2006;**24**(8):985-95 doi 10.1038/nbt1234.
37. Colomer R, Mondejar R, Romero-Laorden N, Alfranca A, Sanchez-Madrid F, Quintela-Fandino M. When should we order a next generation sequencing test in a patient with cancer? *EClinicalMedicine* 2020;**25**:100487 doi 10.1016/j.eclinm.2020.100487.
38. Klug LR, Khosroyani HM, Kent JD, Heinrich MC. New treatment strategies for advanced-stage gastrointestinal stromal tumours. *Nature reviews Clinical oncology* 2022;**19**(5):328-41 doi 10.1038/s41571-022-00606-4.
39. Hirota S, Isozaki K, Moriyama Y, Hashimoto K, Nishida T, Ishiguro S*, et al.* Gain-of-function mutations of c-kit in human gastrointestinal stromal tumors. *Science* 1998;**279**(5350):577-80 doi 10.1126/science.279.5350.577.
40. Heinrich MC, Griffith DJ, Druker BJ, Wait CL, Ott KA, Zigler AJ. Inhibition of c-kit receptor tyrosine kinase activity by STI 571, a selective tyrosine kinase inhibitor. *Blood* 2000;**96**(3):925-32.
41. Druker BJ. STI571 (Gleevec) as a paradigm for cancer therapy. *Trends Mol Med* 2002;**8**(4 Suppl):S14-8 doi 10.1016/s1471-4914(02)02305-5.
42. Dagher R, Cohen M, Williams G, Rothmann M, Gobburu J, Robbie G*, et al.* Approval summary: imatinib mesylate in the treatment of metastatic and/or unresectable malignant gastrointestinal stromal tumors. *Clin Cancer Res* 2002;**8**(10):3034-8.
43. Heinrich MC, Corless CL, Demetri GD, Blanke CD, von Mehren M, Joensuu H*, et al.* Kinase mutations and imatinib response in patients with metastatic gastrointestinal stromal tumor. *J Clin Oncol* 2003;**21**(23):4342-9 doi 10.1200/JCO.2003.04.190.
44. Corless CL, Schroeder A, Griffith D, Town A, McGreevey L, Harrell P*, et al.* PDGFRA mutations in gastrointestinal stromal tumors: frequency, spectrum and in vitro sensitivity to imatinib. *J Clin Oncol* 2005;**23**(23):5357-64 doi 10.1200/JCO.2005.14.068.
45. Gramza AW, Corless CL, Heinrich MC. Resistance to Tyrosine Kinase Inhibitors in Gastrointestinal Stromal Tumors. *Clin Cancer Res* 2009;**15**(24):7510-8 doi 10.1158/1078-0432.CCR-09-0190.
46. Bode AM, Dong Z. Recent advances in precision oncology research. *NPJ Precis Oncol* 2018;**2**:11 doi 10.1038/s41698-018-0055-0.
47. Khosroyani HM, Klug LR, Heinrich MC. TKI Treatment Sequencing in Advanced Gastrointestinal Stromal Tumors. *Drugs* 2023;**83**(1):55-73 doi 10.1007/s40265-022-01820-1.
48. Heinrich MC, Rankin C, Blanke CD, Demetri GD, Borden EC, Ryan CW*, et al.* Correlation of Long-term Results of Imatinib in Advanced Gastrointestinal Stromal Tumors With Next-Generation Sequencing Results: Analysis of Phase 3 SWOG Intergroup Trial S0033. *JAMA oncology* 2017;**3**(7):944-52 doi 10.1001/jamaoncol.2016.6728.

49. Janeway KA, Kim SY, Lodish M, Nose V, Rustin P, Gaal J*, et al.* Defects in succinate dehydrogenase in gastrointestinal stromal tumors lacking KIT and PDGFRA mutations. *Proc Natl Acad Sci U S A* 2011;**108**(1):314-8 doi 10.1073/pnas.1009199108.
50. Hirsch CA, Rasminsky M, Davis BD, Lin EC. A Fumarate Reductase in Escherichia Coli Distinct from Succinate Dehydrogenase. *J Biol Chem* 1963;**238**:3770-4.
51. Iverson TM. Catalytic mechanisms of complex II enzymes: a structural perspective. *Biochimica et biophysica acta* 2013;**1827**(5):648-57 doi 10.1016/j.bbabio.2012.09.008.
52. Robinson KM, Lemire BD. Covalent attachment of FAD to the yeast succinate dehydrogenase flavoprotein requires import into mitochondria, presequence removal, and folding. *J Biol Chem* 1996;**271**(8):4055-60 doi 10.1074/jbc.271.8.4055.
53. Salach J, Walker WH, Singer TP, Ehrenberg A, Hemmerich P, Ghisla S, Hartmann U. Studies on succinate dehydrogenase. Site of attachment of the covalently-bound flavin to the peptide chain. *Eur J Biochem* 1972;**26**(2):267-78 doi 10.1111/j.1432-1033.1972.tb01765.x.
54. Maklashina E, Iverson TM, Cecchini G. How an assembly factor enhances covalent FAD attachment to the flavoprotein subunit of complex II. *J Biol Chem* 2022;**298**(10):102472 doi 10.1016/j.jbc.2022.102472.
55. Robinson KM, Rothery RA, Weiner JH, Lemire BD. The covalent attachment of FAD to the flavoprotein of Saccharomyces cerevisiae succinate dehydrogenase is not necessary for import and assembly into mitochondria. *Eur J Biochem* 1994;**222**(3):983-90 doi 10.1111/j.1432-1033.1994.tb18949.x.
56. Sharma P, Maklashina E, Cecchini G, Iverson TM. The roles of SDHAF2 and dicarboxylate in covalent flavinylation of SDHA, the human complex II flavoprotein. *Proc Natl Acad Sci U S A* 2020;**117**(38):23548-56 doi 10.1073/pnas.2007391117.
57. Cheng VW, Piragasam RS, Rothery RA, Maklashina E, Cecchini G, Weiner JH. Redox state of flavin adenine dinucleotide drives substrate binding and product release in Escherichia coli succinate dehydrogenase. *Biochemistry* 2015;**54**(4):1043-52 doi 10.1021/bi501350j.
58. Starbird CA, Maklashina E, Sharma P, Qualls-Histed S, Cecchini G, Iverson TM. Structural and biochemical analyses reveal insights into covalent flavinylation of the Escherichia coli Complex II homolog quinol:fumarate reductase. *J Biol Chem* 2017;**292**(31):12921-33 doi 10.1074/jbc.M117.795120.
59. Van Vranken JG, Bricker DK, Dephoure N, Gygi SP, Cox JE, Thummel CS, Rutter J. SDHAF4 promotes mitochondrial succinate dehydrogenase activity and prevents neurodegeneration. *Cell metabolism* 2014;**20**(2):241-52 doi 10.1016/j.cmet.2014.05.012.
60. Sun F, Huo X, Zhai Y, Wang A, Xu J, Su D*, et al.* Crystal structure of mitochondrial respiratory membrane protein complex II. *Cell* 2005;**121**(7):1043-57 doi 10.1016/j.cell.2005.05.025.
61. Tomasiak TM, Maklashina E, Cecchini G, Iverson TM. A threonine on the active site loop controls transition state formation in Escherichia coli respiratory complex II. *J Biol Chem* 2008;**283**(22):15460-8 doi 10.1074/jbc.M801372200.
62. Reid GA, Miles CS, Moysey RK, Pankhurst KL, Chapman SK. Catalysis in fumarate reductase. *Biochimica et biophysica acta* 2000;**1459**(2-3):310-5 doi 10.1016/s0005-2728(00)00166-3.
63. Acin-Perez R, Carrascoso I, Baixauli F, Roche-Molina M, Latorre-Pellicer A, Fernandez-Silva P*, et al.* ROS-triggered phosphorylation of complex II by Fgr kinase regulates cellular

adaptation to fuel use. *Cell metabolism* 2014;**19**(6):1020-33 doi 10.1016/j.cmet.2014.04.015.
64. Nath AK, Ryu JH, Jin YN, Roberts LD, Dejam A, Gerszten RE, Peterson RT. PTPMT1 Inhibition Lowers Glucose through Succinate Dehydrogenase Phosphorylation. *Cell Rep* 2015;**10**(5):694-701 doi 10.1016/j.celrep.2015.01.010.
65. Covian R, Balaban RS. Cardiac mitochondrial matrix and respiratory complex protein phosphorylation. *Am J Physiol Heart Circ Physiol* 2012;**303**(8):H940-66 doi 10.1152/ajpheart.00077.2012.
66. Cimen H, Han MJ, Yang Y, Tong Q, Koc H, Koc EC. Regulation of succinate dehydrogenase activity by SIRT3 in mammalian mitochondria. *Biochemistry* 2010;**49**(2):304-11 doi 10.1021/bi901627u.
67. Finley LW, Haas W, Desquiret-Dumas V, Wallace DC, Procaccio V, Gygi SP, Haigis MC. Succinate dehydrogenase is a direct target of sirtuin 3 deacetylase activity. *PLoS One* 2011;**6**(8):e23295 doi 10.1371/journal.pone.0023295.
68. Li ST, Huang D, Shen S, Cai Y, Xing S, Wu G*, et al.* Myc-mediated SDHA acetylation triggers epigenetic regulation of gene expression and tumorigenesis. *Nat Metab* 2020;**2**(3):256-69 doi 10.1038/s42255-020-0179-8.
69. Ma Y, Qi Y, Wang L, Zheng Z, Zhang Y, Zheng J. SIRT5-mediated SDHA desuccinylation promotes clear cell renal cell carcinoma tumorigenesis. *Free Radic Biol Med* 2019;**134**:458-67 doi 10.1016/j.freeradbiomed.2019.01.030.
70. Liu Y, Liu K, Thorne RF, Shi R, Zhang Q, Wu M, Liu L. Mitochondrial SENP2 regulates the assembly of SDH complex under metabolic stress. *Cell Rep* 2023;**42**(2):112041 doi 10.1016/j.celrep.2023.112041.
71. Du Z, Zhou X, Lai Y, Xu J, Zhang Y, Zhou S*, et al.* Structure of the human respiratory complex II. *Proc Natl Acad Sci U S A* 2023;**120**(18):e2216713120 doi 10.1073/pnas.2216713120.
72. Rouault TA. Biogenesis of iron-sulfur clusters in mammalian cells: new insights and relevance to human disease. *Dis Model Mech* 2012;**5**(2):155-64 doi 10.1242/dmm.009019.
73. Maio N, Singh A, Uhrigshardt H, Saxena N, Tong WH, Rouault TA. Cochaperone binding to LYR motifs confers specificity of iron sulfur cluster delivery. *Cell metabolism* 2014;**19**(3):445-57 doi 10.1016/j.cmet.2014.01.015.
74. Saxena N, Maio N, Crooks DR, Ricketts CJ, Yang Y, Wei MH*, et al.* SDHB-Deficient Cancers: The Role of Mutations That Impair Iron Sulfur Cluster Delivery. *J Natl Cancer Inst* 2016;**108**(1) doi 10.1093/jnci/djv287.
75. Cheng VW, Ma E, Zhao Z, Rothery RA, Weiner JH. The iron-sulfur clusters in Escherichia coli succinate dehydrogenase direct electron flow. *J Biol Chem* 2006;**281**(37):27662-8 doi 10.1074/jbc.M604900200.
76. Hadrava Vanova K, Kraus M, Neuzil J, Rohlena J. Mitochondrial complex II and reactive oxygen species in disease and therapy. *Redox Rep* 2020;**25**(1):26-32 doi 10.1080/13510002.2020.1752002.
77. Van Vranken JG, Na U, Winge DR, Rutter J. Protein-mediated assembly of succinate dehydrogenase and its cofactors. *Crit Rev Biochem Mol Biol* 2015;**50**(2):168-80 doi 10.3109/10409238.2014.990556.
78. Na U, Yu W, Cox J, Bricker DK, Brockmann K, Rutter J*, et al.* The LYR factors SDHAF1 and SDHAF3 mediate maturation of the iron-sulfur subunit of succinate dehydrogenase. *Cell metabolism* 2014;**20**(2):253-66 doi 10.1016/j.cmet.2014.05.014.

79. Iverson TM, Luna-Chavez C, Cecchini G, Rees DC. Structure of the Escherichia coli fumarate reductase respiratory complex. *Science* 1999;**284**(5422):1961-6 doi 10.1126/science.284.5422.1961.
80. Vibat CR, Cecchini G, Nakamura K, Kita K, Gennis RB. Localization of histidine residues responsible for heme axial ligation in cytochrome b556 of complex II (succinate:ubiquinone oxidoreductase) in Escherichia coli. *Biochemistry* 1998;**37**(12):4148-59 doi 10.1021/bi9716635.
81. Oyedotun KS, Sit CS, Lemire BD. The Saccharomyces cerevisiae succinate dehydrogenase does not require heme for ubiquinone reduction. *Biochimica et biophysica acta* 2007;**1767**(12):1436-45 doi 10.1016/j.bbabio.2007.09.008.
82. Yankovskaya V, Horsefield R, Tornroth S, Luna-Chavez C, Miyoshi H, Leger C*, et al.* Architecture of succinate dehydrogenase and reactive oxygen species generation. *Science* 2003;**299**(5607):700-4 doi 10.1126/science.1079605.
83. Anderson RF, Hille R, Shinde SS, Cecchini G. Electron transfer within complex II. Succinate:ubiquinone oxidoreductase of Escherichia coli. *J Biol Chem* 2005;**280**(39):33331-7 doi 10.1074/jbc.M506002200.
84. Szeto SSW, Reinke SN, Sykes BD, Lemire BD. Ubiquinone-binding site mutations in the Saccharomyces cerevisiae succinate dehydrogenase generate superoxide and lead to the accumulation of succinate. *J Biol Chem* 2007;**282**(37):27518-26 doi 10.1074/jbc.M700601200.
85. Moreno C, Santos RM, Burns R, Zhang WC. Succinate Dehydrogenase and Ribonucleic Acid Networks in Cancer and Other Diseases. *Cancers (Basel)* 2020;**12**(11) doi 10.3390/cancers12113237.
86. Niyazov DM, Kahler SG, Frye RE. Primary Mitochondrial Disease and Secondary Mitochondrial Dysfunction: Importance of Distinction for Diagnosis and Treatment. *Mol Syndromol* 2016;**7**(3):122-37 doi 10.1159/000446586.
87. Chinnery PF. Primary Mitochondrial Disorders Overview. In: Adam MP, Feldman J, Mirzaa GM, Pagon RA, Wallace SE, Bean LJH*, et al.*, editors. GeneReviews((R)). Seattle (WA)1993.
88. Zheng J. Energy metabolism of cancer: Glycolysis versus oxidative phosphorylation (Review). *Oncology letters* 2012;**4**(6):1151-7 doi 10.3892/ol.2012.928.
89. El-Hattab AW, Scaglia F. Mitochondrial Cardiomyopathies. *Front Cardiovasc Med* 2016;**3**:25 doi 10.3389/fcvm.2016.00025.
90. Holt IJ, Harding AE, Morgan-Hughes JA. Deletions of muscle mitochondrial DNA in patients with mitochondrial myopathies. *Nature* 1988;**331**(6158):717-9 doi 10.1038/331717a0.
91. Pavlakis SG, Hirano M. Mitochondrial Diseases: A Clinical and Molecular History. *Pediatr Neurol* 2016;**63**:3-5 doi 10.1016/j.pediatrneurol.2016.05.014.
92. Bourgeron T, Rustin P, Chretien D, Birch-Machin M, Bourgeois M, Viegas-Pequignot E*, et al.* Mutation of a nuclear succinate dehydrogenase gene results in mitochondrial respiratory chain deficiency. *Nat Genet* 1995;**11**(2):144-9 doi 10.1038/ng1095-144.
93. Fullerton M, McFarland R, Taylor RW, Alston CL. The genetic basis of isolated mitochondrial complex II deficiency. *Mol Genet Metab* 2020;**131**(1-2):53-65 doi 10.1016/j.ymgme.2020.09.009.
94. Alston CL, Davison JE, Meloni F, van der Westhuizen FH, He L, Hornig-Do HT*, et al.* Recessive germline SDHA and SDHB mutations causing leukodystrophy and isolated

mitochondrial complex II deficiency. *J Med Genet* 2012;**49**(9):569-77 doi 10.1136/jmedgenet-2012-101146.
95. Levitas A, Muhammad E, Harel G, Saada A, Caspi VC, Manor E*, et al.* Familial neonatal isolated cardiomyopathy caused by a mutation in the flavoprotein subunit of succinate dehydrogenase. *European journal of human genetics : EJHG* 2010;**18**(10):1160-5 doi 10.1038/ejhg.2010.83.
96. Yang Z, Cao J, Song Y, Li S, Jiao Z, Ren S*, et al.* Whole-exome sequencing identified novel variants in three Chinese Leigh syndrome pedigrees. *Am J Med Genet A* 2022;**188**(4):1214-25 doi 10.1002/ajmg.a.62641.
97. Renkema GH, Wortmann SB, Smeets RJ, Venselaar H, Antoine M, Visser G*, et al.* SDHA mutations causing a multisystem mitochondrial disease: novel mutations and genetic overlap with hereditary tumors. *European journal of human genetics : EJHG* 2015;**23**(2):202-9 doi 10.1038/ejhg.2014.80.
98. Parfait B, Chretien D, Rotig A, Marsac C, Munnich A, Rustin P. Compound heterozygous mutations in the flavoprotein gene of the respiratory chain complex II in a patient with Leigh syndrome. *Human genetics* 2000;**106**(2):236-43 doi 10.1007/s004390051033.
99. van de Loo KFE, Custers JAE, de Boer L, van Lieshout M, de Vries MC, Janssen MCH, Verhaak CM. Cognitive functioning and mental health in children with a primary mitochondrial disease. *Orphanet J Rare Dis* 2022;**17**(1):368 doi 10.1186/s13023-022-02510-7.
100. Taylor RW, Birch-Machin MA, Schaefer J, Taylor L, Shakir R, Ackrell BA*, et al.* Deficiency of complex II of the mitochondrial respiratory chain in late-onset optic atrophy and ataxia. *Ann Neurol* 1996;**39**(2):224-32 doi 10.1002/ana.410390212.
101. Birch-Machin MA, Taylor RW, Cochran B, Ackrell BA, Turnbull DM. Late-onset optic atrophy, ataxia, and myopathy associated with a mutation of a complex II gene. *Ann Neurol* 2000;**48**(3):330-5.
102. Courage C, Jackson CB, Hahn D, Euro L, Nuoffer JM, Gallati S, Schaller A. SDHA mutation with dominant transmission results in complex II deficiency with ocular, cardiac, and neurologic involvement. *Am J Med Genet A* 2017;**173**(1):225-30 doi 10.1002/ajmg.a.37986.
103. Zehavi Y, Saada A, Jabaly-Habib H, Dessau M, Shaag A, Elpeleg O, Spiegel R. A novel de novo heterozygous pathogenic variant in the SDHA gene results in childhood onset bilateral optic atrophy and cognitive impairment. *Metab Brain Dis* 2021;**36**(4):581-8 doi 10.1007/s11011-021-00671-1.
104. Kim HJ, Jeong MY, Na U, Winge DR. Flavinylation and assembly of succinate dehydrogenase are dependent on the C-terminal tail of the flavoprotein subunit. *J Biol Chem* 2012;**287**(48):40670-9 doi 10.1074/jbc.M112.405704.
105. Gill AJ. Succinate dehydrogenase (SDH)-deficient neoplasia. *Histopathology* 2018;**72**(1):106-16 doi 10.1111/his.13277.
106. Dwight T, Na U, Kim E, Zhu Y, Richardson AL, Robinson BG*, et al.* Analysis of SDHAF3 in familial and sporadic pheochromocytoma and paraganglioma. *BMC Cancer* 2017;**17**(1):497 doi 10.1186/s12885-017-3486-z.
107. Bayley JP, Kunst HP, Cascon A, Sampietro ML, Gaal J, Korpershoek E*, et al.* SDHAF2 mutations in familial and sporadic paraganglioma and phaeochromocytoma. *Lancet Oncol* 2010;**11**(4):366-72 doi 10.1016/S1470-2045(10)70007-3.

108. Evenepoel L, Papathomas TG, Krol N, Korpershoek E, de Krijger RR, Persu A, Dinjens WN. Toward an improved definition of the genetic and tumor spectrum associated with SDH germ-line mutations. *Genet Med* 2015;**17**(8):610-20 doi 10.1038/gim.2014.162.
109. Pitsava G, Settas N, Faucz FR, Stratakis CA. Carney Triad, Carney-Stratakis Syndrome, 3PAS and Other Tumors Due to SDH Deficiency. *Front Endocrinol (Lausanne)* 2021;**12**:680609 doi 10.3389/fendo.2021.680609.
110. Gill AJ, Hes O, Papathomas T, Sedivcova M, Tan PH, Agaimy A*, et al.* Succinate dehydrogenase (SDH)-deficient renal carcinoma: a morphologically distinct entity: a clinicopathologic series of 36 tumors from 27 patients. *Am J Surg Pathol* 2014;**38**(12):1588-602 doi 10.1097/PAS.0000000000000292.
111. Killian JK, Miettinen M, Walker RL, Wang Y, Zhu YJ, Waterfall JJ*, et al.* Recurrent epimutation of SDHC in gastrointestinal stromal tumors. *Science translational medicine* 2014;**6**(268):268ra177 doi 10.1126/scitranslmed.3009961.
112. Bernardo-Castineira C, Valdes N, Sierra MI, Saenz-de-Santa-Maria I, Bayon GF, Perez RF*, et al.* SDHC Promoter Methylation, a Novel Pathogenic Mechanism in Parasympathetic Paragangliomas. *The Journal of clinical endocrinology and metabolism* 2018;**103**(1):295-305 doi 10.1210/jc.2017-01702.
113. Chase WH. Familial and bilateral tumours of the carotid body. *The Journal of Pathology and Bacteriology* 1933;**36**(1):1-12 doi https://doi.org/10.1002/path.1700360102.
114. van der Mey AG, Maaswinkel-Mooy PD, Cornelisse CJ, Schmidt PH, van de Kamp JJ. Genomic imprinting in hereditary glomus tumours: evidence for new genetic theory. *Lancet* 1989;**2**(8675):1291-4 doi 10.1016/s0140-6736(89)91908-9.
115. Baysal BE, van Schothorst EM, Farr JE, Grashof P, Myssiorek D, Rubinstein WS*, et al.* Repositioning the hereditary paraganglioma critical region on chromosome band 11q23. *Human genetics* 1999;**104**(3):219-25 doi 10.1007/s004390050939.
116. Heutink P, van der Mey AG, Sandkuijl LA, van Gils AP, Bardoel A, Breedveld GJ*, et al.* A gene subject to genomic imprinting and responsible for hereditary paragangliomas maps to chromosome 11q23-qter. *Hum Mol Genet* 1992;**1**(1):7-10 doi 10.1093/hmg/1.1.7.
117. Mariman EC, van Beersum SE, Cremers CW, van Baars FM, Ropers HH. Analysis of a second family with hereditary non-chromaffin paragangliomas locates the underlying gene at the proximal region of chromosome 11q. *Human genetics* 1993;**91**(4):357-61 doi 10.1007/BF00217356.
118. Mariman EC, van Beersum SE, Cremers CW, Struycken PM, Ropers HH. Fine mapping of a putatively imprinted gene for familial non-chromaffin paragangliomas to chromosome 11q13.1: evidence for genetic heterogeneity. *Human genetics* 1995;**95**(1):56-62 doi 10.1007/BF00225075.
119. Baysal BE, Ferrell RE, Willett-Brozick JE, Lawrence EC, Myssiorek D, Bosch A*, et al.* Mutations in SDHD, a mitochondrial complex II gene, in hereditary paraganglioma. *Science* 2000;**287**(5454):848-51 doi 10.1126/science.287.5454.848.
120. Dahia PL. Pheochromocytoma and paraganglioma pathogenesis: learning from genetic heterogeneity. *Nat Rev Cancer* 2014;**14**(2):108-19 doi 10.1038/nrc3648.
121. Benn DE, Robinson BG, Clifton-Bligh RJ. 15 YEARS OF PARAGANGLIOMA: Clinical manifestations of paraganglioma syndromes types 1-5. *Endocrine-related cancer* 2015;**22**(4):T91-103 doi 10.1530/ERC-15-0268.
122. Carney JA, Sheps SG, Go VL, Gordon H. The triad of gastric leiomyosarcoma, functioning extra-adrenal paraganglioma and pulmonary chondroma. *N Engl J Med* 1977;**296**(26):1517-8 doi 10.1056/NEJM197706302962609.

123. Carney JA, Stratakis CA. Familial paraganglioma and gastric stromal sarcoma: a new syndrome distinct from the Carney triad. *Am J Med Genet* 2002;**108**(2):132-9 doi 10.1002/ajmg.10235.
124. Matyakhina L, Bei TA, McWhinney SR, Pasini B, Cameron S, Gunawan B*, et al.* Genetics of carney triad: recurrent losses at chromosome 1 but lack of germline mutations in genes associated with paragangliomas and gastrointestinal stromal tumors. *The Journal of clinical endocrinology and metabolism* 2007;**92**(8):2938-43 doi 10.1210/jc.2007-0797.
125. McWhinney SR, Pasini B, Stratakis CA, International Carney T, Carney-Stratakis Syndrome C. Familial gastrointestinal stromal tumors and germ-line mutations. *N Engl J Med* 2007;**357**(10):1054-6 doi 10.1056/NEJMc071191.
126. Pasini B, McWhinney SR, Bei T, Matyakhina L, Stergiopoulos S, Muchow M*, et al.* Clinical and molecular genetics of patients with the Carney-Stratakis syndrome and germline mutations of the genes coding for the succinate dehydrogenase subunits SDHB, SDHC, and SDHD. *European journal of human genetics : EJHG* 2008;**16**(1):79-88 doi 10.1038/sj.ejhg.5201904.
127. Gill AJ, Chou A, Vilain R, Clarkson A, Lui M, Jin R*, et al.* Immunohistochemistry for SDHB divides gastrointestinal stromal tumors (GISTs) into 2 distinct types. *Am J Surg Pathol* 2010;**34**(5):636-44 doi 10.1097/PAS.0b013e3181d6150d.
128. Gill AJ, Benn DE, Chou A, Clarkson A, Muljono A, Meyer-Rochow GY*, et al.* Immunohistochemistry for SDHB triages genetic testing of SDHB, SDHC, and SDHD in paraganglioma-pheochromocytoma syndromes. *Hum Pathol* 2010;**41**(6):805-14 doi 10.1016/j.humpath.2009.12.005.
129. van Nederveen FH, Gaal J, Favier J, Korpershoek E, Oldenburg RA, de Bruyn EM*, et al.* An immunohistochemical procedure to detect patients with paraganglioma and phaeochromocytoma with germline SDHB, SDHC, or SDHD gene mutations: a retrospective and prospective analysis. *Lancet Oncol* 2009;**10**(8):764-71 doi 10.1016/s1470-2045(09)70164-0.
130. Burnichon N, Briere JJ, Libe R, Vescovo L, Riviere J, Tissier F*, et al.* SDHA is a tumor suppressor gene causing paraganglioma. *Hum Mol Genet* 2010;**19**(15):3011-20 doi 10.1093/hmg/ddq206.
131. Pantaleo MA, Astolfi A, Indio V, Moore R, Thiessen N, Heinrich MC*, et al.* SDHA loss-of-function mutations in KIT-PDGFRA wild-type gastrointestinal stromal tumors identified by massively parallel sequencing. *J Natl Cancer Inst* 2011;**103**(12):983-7 doi 10.1093/jnci/djr130.
132. Neppala P, Banerjee S, Fanta PT, Yerba M, Porras KA, Burgoyne AM, Sicklick JK. Current management of succinate dehydrogenase-deficient gastrointestinal stromal tumors. *Cancer metastasis reviews* 2019;**38**(3):525-35 doi 10.1007/s10555-019-09818-0.
133. Boikos SA, Pappo AS, Killian JK, LaQuaglia MP, Weldon CB, George S*, et al.* Molecular Subtypes of KIT/PDGFRA Wild-Type Gastrointestinal Stromal Tumors: A Report From the National Institutes of Health Gastrointestinal Stromal Tumor Clinic. *JAMA oncology* 2016 doi 10.1001/jamaoncol.2016.0256.
134. Miettinen M, Killian JK, Wang ZF, Lasota J, Lau C, Jones L*, et al.* Immunohistochemical loss of succinate dehydrogenase subunit A (SDHA) in gastrointestinal stromal tumors (GISTs) signals SDHA germline mutation. *Am J Surg Pathol* 2013;**37**(2):234-40 doi 10.1097/PAS.0b013e3182671178.

135. Benn DE, Zhu Y, Andrews KA, Wilding M, Duncan EL, Dwight T*, et al.* Bayesian approach to determining penetrance of pathogenic SDH variants. *J Med Genet* 2018;**55**(11):729-34 doi 10.1136/jmedgenet-2018-105427.
136. Pantaleo MA, Urbini M, Schipani A, Nannini M, Indio V, De Leo A*, et al.* SDHA Germline Variants in Adult Patients With SDHA-Mutant Gastrointestinal Stromal Tumor. *Frontiers in oncology* 2021;**11**:778461 doi 10.3389/fonc.2021.778461.
137. Gimenez-Roqueplo AP, Favier J, Rustin P, Mourad JJ, Plouin PF, Corvol P*, et al.* The R22X mutation of the SDHD gene in hereditary paraganglioma abolishes the enzymatic activity of complex II in the mitochondrial respiratory chain and activates the hypoxia pathway. *American journal of human genetics* 2001;**69**(6):1186-97 doi 10.1086/324413.
138. Briere JJ, Favier J, Benit P, El Ghouzzi V, Lorenzato A, Rabier D*, et al.* Mitochondrial succinate is instrumental for HIF1alpha nuclear translocation in SDHA-mutant fibroblasts under normoxic conditions. *Hum Mol Genet* 2005;**14**(21):3263-9 doi 10.1093/hmg/ddi359.
139. Pollard PJ, Briere JJ, Alam NA, Barwell J, Barclay E, Wortham NC*, et al.* Accumulation of Krebs cycle intermediates and over-expression of HIF1alpha in tumours which result from germline FH and SDH mutations. *Hum Mol Genet* 2005;**14**(15):2231-9 doi 10.1093/hmg/ddi227.
140. Selak MA, Armour SM, MacKenzie ED, Boulahbel H, Watson DG, Mansfield KD*, et al.* Succinate links TCA cycle dysfunction to oncogenesis by inhibiting HIF-alpha prolyl hydroxylase. *Cancer Cell* 2005;**7**(1):77-85 doi 10.1016/j.ccr.2004.11.022.
141. Gerald D, Berra E, Frapart YM, Chan DA, Giaccia AJ, Mansuy D*, et al.* JunD reduces tumor angiogenesis by protecting cells from oxidative stress. *Cell* 2004;**118**(6):781-94 doi 10.1016/j.cell.2004.08.025.
142. Bardella C, Pollard PJ, Tomlinson I. SDH mutations in cancer. *Biochimica et biophysica acta* 2011;**1807**(11):1432-43 doi 10.1016/j.bbabio.2011.07.003.
143. Slane BG, Aykin-Burns N, Smith BJ, Kalen AL, Goswami PC, Domann FE, Spitz DR. Mutation of succinate dehydrogenase subunit C results in increased O2.-, oxidative stress, and genomic instability. *Cancer Res* 2006;**66**(15):7615-20 doi 10.1158/0008-5472.CAN-06-0833.
144. Selak MA, Duran RV, Gottlieb E. Redox stress is not essential for the pseudo-hypoxic phenotype of succinate dehydrogenase deficient cells. *Biochimica et biophysica acta* 2006;**1757**(5-6):567-72 doi 10.1016/j.bbabio.2006.05.015.
145. Myllyla R, Tuderman L, Kivirikko KI. Mechanism of the prolyl hydroxylase reaction. 2. Kinetic analysis of the reaction sequence. *Eur J Biochem* 1977;**80**(2):349-57 doi 10.1111/j.1432-1033.1977.tb11889.x.
146. MacKenzie ED, Selak MA, Tennant DA, Payne LJ, Crosby S, Frederiksen CM*, et al.* Cell-permeating alpha-ketoglutarate derivatives alleviate pseudohypoxia in succinate dehydrogenase-deficient cells. *Molecular and cellular biology* 2007;**27**(9):3282-9 doi 10.1128/MCB.01927-06.
147. Guzy RD, Sharma B, Bell E, Chandel NS, Schumacker PT. Loss of the SdhB, but Not the SdhA, subunit of complex II triggers reactive oxygen species-dependent hypoxia-inducible factor activation and tumorigenesis. *Molecular and cellular biology* 2008;**28**(2):718-31 doi 10.1128/MCB.01338-07.
148. Yang M, Pollard PJ. Succinate: a new epigenetic hacker. *Cancer Cell* 2013;**23**(6):709-11 doi 10.1016/j.ccr.2013.05.015.

149. Killian JK, Kim SY, Miettinen M, Smith C, Merino M, Tsokos M*, et al.* Succinate dehydrogenase mutation underlies global epigenomic divergence in gastrointestinal stromal tumor. *Cancer discovery* 2013;**3**(6):648-57 doi 10.1158/2159-8290.cd-13-0092.
150. Letouze E, Martinelli C, Loriot C, Burnichon N, Abermil N, Ottolenghi C*, et al.* SDH mutations establish a hypermethylator phenotype in paraganglioma. *Cancer Cell* 2013;**23**(6):739-52 doi 10.1016/j.ccr.2013.04.018.
151. Wang YM, Gu ML, Ji F. Succinate dehydrogenase-deficient gastrointestinal stromal tumors. *World journal of gastroenterology* 2015;**21**(8):2303-14 doi 10.3748/wjg.v21.i8.2303.
152. Flavahan WA, Drier Y, Johnstone SE, Hemming ML, Tarjan DR, Hegazi E*, et al.* Altered chromosomal topology drives oncogenic programs in SDH-deficient GISTs. *Nature* 2019;**575**(7781):229-33 doi 10.1038/s41586-019-1668-3.
153. Huang Y, Rao A. Connections between TET proteins and aberrant DNA modification in cancer. *Trends Genet* 2014;**30**(10):464-74 doi 10.1016/j.tig.2014.07.005.
154. Tan AY, Manley JL. The TET family of proteins: functions and roles in disease. *J Mol Cell Biol* 2009;**1**(2):82-92 doi 10.1093/jmcb/mjp025.
155. Janeway KA, Albritton KH, Van Den Abbeele AD, D'Amato GZ, Pedrazzoli P, Siena S*, et al.* Sunitinib treatment in pediatric patients with advanced GIST following failure of imatinib. *Pediatr Blood Cancer* 2009;**52**(7):767-71 doi 10.1002/pbc.21909.
156. Ganjoo KN, Villalobos VM, Kamaya A, Fisher GA, Butrynski JE, Morgan JA*, et al.* A multicenter phase II study of pazopanib in patients with advanced gastrointestinal stromal tumors (GIST) following failure of at least imatinib and sunitinib. *Annals of oncology : official journal of the European Society for Medical Oncology / ESMO* 2014;**25**(1):236-40 doi 10.1093/annonc/mdt484.
157. Ben-Ami E, Barysauskas CM, von Mehren M, Heinrich MC, Corless CL, Butrynski JE*, et al.* Long-term follow-up results of the multicenter phase II trial of regorafenib in patients with metastatic and/or unresectable GI stromal tumor after failure of standard tyrosine kinase inhibitor therapy. *Annals of oncology : official journal of the European Society for Medical Oncology / ESMO* 2016;**27**(9):1794-9 doi 10.1093/annonc/mdw228.
158. von Mehren M, George S, Heinrich MC, Schuetze SM, Yap JT, Yu JQ*, et al.* Linsitinib (OSI-906) for the Treatment of Adult and Pediatric Wild-Type Gastrointestinal Stromal Tumors, a SARC Phase II Study. *Clin Cancer Res* 2020;**26**(8):1837-45 doi 10.1158/1078-0432.CCR-19-1069.
159. Trent JC, Beach J, Burgess MA, Papadopolous N, Chen LL, Benjamin RS, Patel SR. A two-arm phase II study of temozolomide in patients with advanced gastrointestinal stromal tumors and other soft tissue sarcomas. *Cancer* 2003;**98**(12):2693-9 doi 10.1002/cncr.11875.
160. Hadoux J, Favier J, Scoazec JY, Leboulleux S, Al Ghuzlan A, Caramella C*, et al.* SDHB mutations are associated with response to temozolomide in patients with metastatic pheochromocytoma or paraganglioma. *Int J Cancer* 2014;**135**(11):2711-20 doi 10.1002/ijc.28913.
161. Liu D, Yang T, Ma W, Wang Y. Clinical strategies to manage adult glioblastoma patients without MGMT hypermethylation. *Journal of Cancer* 2022;**13**(1):354-63 doi 10.7150/jca.63595.
162. Ricci R, Martini M, Ravegnini G, Cenci T, Milione M, Lanza P*, et al.* Preferential MGMT methylation could predispose a subset of KIT/PDGFRA-WT GISTs, including SDH-

deficient ones, to respond to alkylating agents. *Clin Epigenetics* 2019;**11**(1):2 doi 10.1186/s13148-018-0594-9.
163. Yebra M, Bhargava S, Kumar A, Burgoyne AM, Tang CM, Yoon H*, et al.* Establishment of Patient-derived Succinate Dehydrogenase-deficient Gastrointestinal Stromal Tumor Models For Predicting Therapeutic Response. *Clin Cancer Res* 2021 doi 10.1158/1078-0432.CCR-21-2092.
164. De Silva M, Rastogi S, Chan D, Angel C, Prall O, Gill A, Guminski A. Succinate dehydrogenase-deficient gastrointestinal stromal tumor: from diagnostic dilemma to novel personalised therapy in 2 case reports. *Transl Cancer Res* 2021;**10**(7):3588-99 doi 10.21037/tcr-21-131.
165. Amar L, Lussey-Lepoutre C, Lenders JW, Djadi-Prat J, Plouin PF, Steichen O. MANAGEMENT OF ENDOCRINE DISEASE: Recurrence or new tumors after complete resection of pheochromocytomas and paragangliomas: a systematic review and meta-analysis. *Eur J Endocrinol* 2016;**175**(4):R135-45 doi 10.1530/EJE-16-0189.
166. Lenders JWM, Kerstens MN, Amar L, Prejbisz A, Robledo M, Taieb D*, et al.* Genetics, diagnosis, management and future directions of research of phaeochromocytoma and paraganglioma: a position statement and consensus of the Working Group on Endocrine Hypertension of the European Society of Hypertension. *J Hypertens* 2020;**38**(8):1443-56 doi 10.1097/HJH.0000000000002438.
167. Joensuu H, Vehtari A, Riihimaki J, Nishida T, Steigen SE, Brabec P*, et al.* Risk of recurrence of gastrointestinal stromal tumour after surgery: an analysis of pooled population-based cohorts. *Lancet Oncol* 2012;**13**(3):265-74 doi 10.1016/s1470-2045(11)70299-6.
168. Fero KE, Coe TM, Fanta PT, Tang CM, Murphy JD, Sicklick JK. Surgical Management of Adolescents and Young Adults With Gastrointestinal Stromal Tumors: A US Population-Based Analysis. *JAMA Surg* 2017;**152**(5):443-51 doi 10.1001/jamasurg.2016.5047.
169. Mason EF, Hornick JL. Conventional Risk Stratification Fails to Predict Progression of Succinate Dehydrogenase-deficient Gastrointestinal Stromal Tumors: A Clinicopathologic Study of 76 Cases. *Am J Surg Pathol* 2016;**40**(12):1616-21 doi 10.1097/PAS.0000000000000685.
170. Tirumani SH, Tirumani H, Jagannathan JP, Shinagare AB, Hornick JL, George S*, et al.* MDCT features of succinate dehydrogenase (SDH)-deficient gastrointestinal stromal tumours. *Br J Radiol* 2014;**87**(1043):20140476 doi 10.1259/bjr.20140476.
171. Willobee BA, Quiroz HJ, Sussman MS, Thorson CM, Sola JE, Perez EA. Current treatment strategies in pediatric gastrointestinal stromal cell tumor. *Transl Gastroenterol Hepatol* 2018;**3**:53 doi 10.21037/tgh.2018.07.09.
172. Buffet A, Ben Aim L, Leboulleux S, Drui D, Vezzosi D, Libe R*, et al.* Positive Impact of Genetic Test on the Management and Outcome of Patients With Paraganglioma and/or Pheochromocytoma. *The Journal of clinical endocrinology and metabolism* 2019;**104**(4):1109-18 doi 10.1210/jc.2018-02411.
173. Tufton N, Shapiro L, Srirangalingam U, Richards P, Sahdev A, Kumar AV*, et al.* Outcomes of annual surveillance imaging in an adult and paediatric cohort of succinate dehydrogenase B mutation carriers. *Clin Endocrinol (Oxf)* 2017;**86**(2):286-96 doi 10.1111/cen.13246.
174. Tufton N, Shapiro L, Sahdev A, Kumar AV, Martin L, Drake WM*, et al.* An analysis of surveillance screening for SDHB-related disease in childhood and adolescence. *Endocr Connect* 2019;**8**(3):162-72 doi 10.1530/EC-18-0522.

175. Amar L, Pacak K, Steichen O, Akker SA, Aylwin SJB, Baudin E*, et al.* International consensus on initial screening and follow-up of asymptomatic SDHx mutation carriers. *Nature reviews Endocrinology* 2021;**17**(7):435-44 doi 10.1038/s41574-021-00492-3.
176. Muth A, Crona J, Gimm O, Elmgren A, Filipsson K, Stenmark Askmalm M*, et al.* Genetic testing and surveillance guidelines in hereditary pheochromocytoma and paraganglioma. *J Intern Med* 2019;**285**(2):187-204 doi 10.1111/joim.12869.
177. Lenders JW, Duh QY, Eisenhofer G, Gimenez-Roqueplo AP, Grebe SK, Murad MH*, et al.* Pheochromocytoma and paraganglioma: an endocrine society clinical practice guideline. *The Journal of clinical endocrinology and metabolism* 2014;**99**(6):1915-42 doi 10.1210/jc.2014-1498.
178. Marees AT, de Kluiver H, Stringer S, Vorspan F, Curis E, Marie-Claire C, Derks EM. A tutorial on conducting genome-wide association studies: Quality control and statistical analysis. *Int J Methods Psychiatr Res* 2018;**27**(2):e1608 doi 10.1002/mpr.1608.
179. Starita LM, Ahituv N, Dunham MJ, Kitzman JO, Roth FP, Seelig G*, et al.* Variant Interpretation: Functional Assays to the Rescue. *American journal of human genetics* 2017;**101**(3):315-25 doi 10.1016/j.ajhg.2017.07.014.
180. Richards S, Aziz N, Bale S, Bick D, Das S, Gastier-Foster J*, et al.* Standards and guidelines for the interpretation of sequence variants: a joint consensus recommendation of the American College of Medical Genetics and Genomics and the Association for Molecular Pathology. *Genet Med* 2015;**17**(5):405-24 doi 10.1038/gim.2015.30.
181. Anderson CL, Munawar S, Reilly L, Kamp TJ, January CT, Delisle BP, Eckhardt LL. How Functional Genomics Can Keep Pace With VUS Identification. *Front Cardiovasc Med* 2022;**9**:900431 doi 10.3389/fcvm.2022.900431.
182. Tavtigian SV, Greenblatt MS, Harrison SM, Nussbaum RL, Prabhu SA, Boucher KM*, et al.* Modeling the ACMG/AMP variant classification guidelines as a Bayesian classification framework. *Genet Med* 2018;**20**(9):1054-60 doi 10.1038/gim.2017.210.
183. Nykamp K, Anderson M, Powers M, Garcia J, Herrera B, Ho YY*, et al.* Sherloc: a comprehensive refinement of the ACMG-AMP variant classification criteria. *Genet Med* 2017;**19**(10):1105-17 doi 10.1038/gim.2017.37.
184. Rivera-Munoz EA, Milko LV, Harrison SM, Azzariti DR, Kurtz CL, Lee K*, et al.* ClinGen Variant Curation Expert Panel experiences and standardized processes for disease and gene-level specification of the ACMG/AMP guidelines for sequence variant interpretation. *Human mutation* 2018;**39**(11):1614-22 doi 10.1002/humu.23645.
185. Karczewski KJ, Francioli LC, Tiao G, Cummings BB, Alfoldi J, Wang Q*, et al.* The mutational constraint spectrum quantified from variation in 141,456 humans. *Nature* 2020;**581**(7809):434-43 doi 10.1038/s41586-020-2308-7.
186. Landrum MJ, Lee JM, Benson M, Brown GR, Chao C, Chitipiralla S*, et al.* ClinVar: improving access to variant interpretations and supporting evidence. *Nucleic Acids Res* 2018;**46**(D1):D1062-D7 doi 10.1093/nar/gkx1153.
187. Mathe E, Olivier M, Kato S, Ishioka C, Vaisman I, Hainaut P. Predicting the transactivation activity of p53 missense mutants using a four-body potential score derived from Delaunay tessellations. *Hum Mutat* 2006;**27**(2):163-72 doi 10.1002/humu.20284.
188. Castellana S, Mazza T. Congruency in the prediction of pathogenic missense mutations: state-of-the-art web-based tools. *Brief Bioinform* 2013;**14**(4):448-59 doi 10.1093/bib/bbt013.
189. Cline MS, Karchin R. Using bioinformatics to predict the functional impact of SNVs. *Bioinformatics* 2011;**27**(4):441-8 doi 10.1093/bioinformatics/btq695.

190. Frousios K, Iliopoulos CS, Schlitt T, Simpson MA. Predicting the functional consequences of non-synonymous DNA sequence variants--evaluation of bioinformatics tools and development of a consensus strategy. *Genomics* 2013;**102**(4):223-8 doi 10.1016/j.ygeno.2013.06.005.
191. Gnad F, Baucom A, Mukhyala K, Manning G, Zhang Z. Assessment of computational methods for predicting the effects of missense mutations in human cancers. *BMC Genomics* 2013;**14 Suppl 3**:S7 doi 10.1186/1471-2164-14-S3-S7.
192. Thusberg J, Olatubosun A, Vihinen M. Performance of mutation pathogenicity prediction methods on missense variants. *Hum Mutat* 2011;**32**(4):358-68 doi 10.1002/humu.21445.
193. Brnich SE, Rivera-Munoz EA, Berg JS. Quantifying the potential of functional evidence to reclassify variants of uncertain significance in the categorical and Bayesian interpretation frameworks. *Human mutation* 2018;**39**(11):1531-41 doi 10.1002/humu.23609.
194. Brnich SE, Abou Tayoun AN, Couch FJ, Cutting GR, Greenblatt MS, Heinen CD*, et al.* Recommendations for application of the functional evidence PS3/BS3 criterion using the ACMG/AMP sequence variant interpretation framework. *Genome Med* 2019;**12**(1):3 doi 10.1186/s13073-019-0690-2.
195. Matreyek KA, Starita LM, Stephany JJ, Martin B, Chiasson MA, Gray VE*, et al.* Multiplex assessment of protein variant abundance by massively parallel sequencing. *Nat Genet* 2018;**50**(6):874-82 doi 10.1038/s41588-018-0122-z.
196. Toland AE, Andreassen PR. DNA repair-related functional assays for the classification of BRCA1 and BRCA2 variants: a critical review and needs assessment. *J Med Genet* 2017;**54**(11):721-31 doi 10.1136/jmedgenet-2017-104707.
197. Mighell TL, Thacker S, Fombonne E, Eng C, O'Roak BJ. An Integrated Deep-Mutational-Scanning Approach Provides Clinical Insights on PTEN Genotype-Phenotype Relationships. *American journal of human genetics* 2020;**106**(6):818-29 doi 10.1016/j.ajhg.2020.04.014.
198. Matreyek KA, Stephany JJ, Ahler E, Fowler DM. Integrating thousands of PTEN variant activity and abundance measurements reveals variant subgroups and new dominant negatives in cancers. *Genome Med* 2021;**13**(1):165 doi 10.1186/s13073-021-00984-x.
199. Kanavy DM, McNulty SM, Jairath MK, Brnich SE, Bizon C, Powell BC, Berg JS. Comparative analysis of functional assay evidence use by ClinGen Variant Curation Expert Panels. *Genome Med* 2019;**11**(1):77 doi 10.1186/s13073-019-0683-1.
200. Italiano A, Chen CL, Sung YS, Singer S, DeMatteo RP, LaQuaglia MP*, et al.* SDHA loss of function mutations in a subset of young adult wild-type gastrointestinal stromal tumors. *BMC Cancer* 2012;**12**:408 doi 10.1186/1471-2407-12-408.
201. Baysal BE, Lawrence EC, Ferrell RE. Sequence variation in human succinate dehydrogenase genes: evidence for long-term balancing selection on SDHA. *BMC Biol* 2007;**5**:12 doi 10.1186/1741-7007-5-12.
202. Bahrambeigi V, Sinson J, Hu P, Wang Y, Yu H. An Approach for Accurate Molecular Diagnosis of Highly Homologous SDHA Gene. *American journal of clinical pathology* 2016;**146**(suppl_1) doi 10.1093/ajcp/aqw156.005.
203. von Dobschuetz E, Leijon H, Schalin-Jantti C, Schiavi F, Brauckhoff M, Peczkowska M*, et al.* A registry-based study of thyroid paraganglioma: histological and genetic characteristics. *Endocrine-related cancer* 2015;**22**(2):191-204 doi 10.1530/ERC-14-0558.
204. Bausch B, Schiavi F, Ni Y, Welander J, Patocs A, Ngeow J*, et al.* Clinical Characterization of the Pheochromocytoma and Paraganglioma Susceptibility Genes SDHA, TMEM127,

MAX, and SDHAF2 for Gene-Informed Prevention. *JAMA oncology* 2017;**3**(9):1204-12 doi 10.1001/jamaoncol.2017.0223.
205. Ben Aim L, Pigny P, Castro-Vega LJ, Buffet A, Amar L, Bertherat J*, et al.* Targeted next-generation sequencing detects rare genetic events in pheochromocytoma and paraganglioma. *J Med Genet* 2019;**56**(8):513-20 doi 10.1136/jmedgenet-2018-105714.
206. Siebers EM, Choi MJ, Tinklenberg JA, Beatka MJ, Ayres S, Meng H*, et al.* Sdha+/- Rats Display Minimal Muscle Pathology Without Significant Behavioral or Biochemical Abnormalities. *J Neuropathol Exp Neurol* 2018;**77**(8):665-72 doi 10.1093/jnen/nly042.
207. Ma YY, Wu TF, Liu YP, Wang Q, Li XY, Ding Y*, et al.* Two compound frame-shift mutations in succinate dehydrogenase gene of a Chinese boy with encephalopathy. *Brain Dev* 2014;**36**(5):394-8 doi 10.1016/j.braindev.2013.06.003.
208. Bannon AE, Kent JD, Forquer I, Town A, Klug LR, McCann KE*, et al.* Biochemical, Molecular, and Clinical Characterization of Succinate Dehydrogenase Subunit A Variants of Unknown Significance. *Clin Cancer Res* 2017 doi 10.1158/1078-0432.CCR-17-1397.
209. Panizza E, Ercolino T, Mori L, Rapizzi E, Castellano M, Opocher G*, et al.* Yeast model for evaluating the pathogenic significance of SDHB, SDHC and SDHD mutations in PHEO-PGL syndrome. *Hum Mol Genet* 2013;**22**(4):804-15 doi 10.1093/hmg/dds487.
210. Kim E, Wright MJ, Sioson L, Novos T, Gill AJ, Benn DE*, et al.* Utility of the succinate: Fumarate ratio for assessing SDH dysfunction in different tumor types. *Mol Genet Metab Rep* 2017;**10**:45-9 doi 10.1016/j.ymgmr.2016.12.006.
211. Lussey-Lepoutre C, Hollinshead KE, Ludwig C, Menara M, Morin A, Castro-Vega LJ*, et al.* Loss of succinate dehydrogenase activity results in dependency on pyruvate carboxylation for cellular anabolism. *Nature communications* 2015;**6**:8784 doi 10.1038/ncomms9784.
212. Lussey-Lepoutre C, Bellucci A, Morin A, Buffet A, Amar L, Janin M*, et al.* In Vivo Detection of Succinate by Magnetic Resonance Spectroscopy as a Hallmark of SDHx Mutations in Paraganglioma. *Clin Cancer Res* 2016;**22**(5):1120-9 doi 10.1158/1078-0432.CCR-15-1576.
213. Zhang W, Wang C, Zhang X. Mutplot: An easy-to-use online tool for plotting complex mutation data with flexibility. *PLoS One* 2019;**14**(5):e0215838 doi 10.1371/journal.pone.0215838.
214. Eijkelenkamp K, Osinga TE, Links TP, van der Horst-Schrivers ANA. Clinical implications of the oncometabolite succinate in SDHx-mutation carriers. *Clin Genet* 2020;**97**(1):39-53 doi 10.1111/cge.13553.
215. Sen I, Young WF, Jr., Kasperbauer JL, Polonis K, Harmsen WS, Colglazier JJ*, et al.* Tumor-specific prognosis of mutation-positive patients with head and neck paragangliomas. *J Vasc Surg* 2020 doi 10.1016/j.jvs.2019.08.232.
216. Lee H, Jeong S, Yu Y, Kang J, Sun H, Rhee JK, Kim YH. Risk of metastatic pheochromocytoma and paraganglioma in SDHx mutation carriers: a systematic review and updated meta-analysis. *J Med Genet* 2019 doi 10.1136/jmedgenet-2019-106324.
217. Aghamir SMK, Heshmat R, Ebrahimi M, Ketabchi SE, Parichehreh Dizaji S, Khatami F. The Impact Of Succinate Dehydrogenase Gene (SDH) Mutations In Renal Cell Carcinoma (RCC): A Systematic Review. *OncoTargets and therapy* 2019;**12**:7929-40 doi 10.2147/ott.S207460.
218. Li J, Liang N, Long X, Zhao J, Yang J, Du X*, et al.* SDHC-related deficiency of SDH complex activity promotes growth and metastasis of hepatocellular carcinoma via ROS/NFkappaB signaling. *Cancer Lett* 2019;**461**:44-55 doi 10.1016/j.canlet.2019.07.001.

219. Jha A, de Luna K, Balili CA, Millo C, Paraiso CA, Ling A*, et al.* Clinical, Diagnostic, and Treatment Characteristics of SDHA-Related Metastatic Pheochromocytoma and Paraganglioma. *Frontiers in oncology* 2019;**9**(53) doi 10.3389/fonc.2019.00053.
220. Fayer S, Horton C, Dines JN, Rubin AF, Richardson ME, McGoldrick K*, et al.* Closing the gap: Systematic integration of multiplexed functional data resolves variants of uncertain significance in BRCA1, TP53, and PTEN. *American journal of human genetics* 2021;**108**(12):2248-58 doi 10.1016/j.ajhg.2021.11.001.
221. Matreyek KA, Stephany JJ, Chiasson MA, Hasle N, Fowler DM. An improved platform for functional assessment of large protein libraries in mammalian cells. *Nucleic Acids Res* 2020;**48**(1):e1 doi 10.1093/nar/gkz910.
222. Shukla N, Roelle SM, Suzart VG, Bruchez AM, Matreyek KA. Mutants of human ACE2 differentially promote SARS-CoV and SARS-CoV-2 spike mediated infection. *PLoS Pathog* 2021;**17**(7):e1009715 doi 10.1371/journal.ppat.1009715.
223. Bayley JP, Devilee P, Taschner PE. The SDH mutation database: an online resource for succinate dehydrogenase sequence variants involved in pheochromocytoma, paraganglioma and mitochondrial complex II deficiency. *BMC Med Genet* 2005;**6**:39 doi 10.1186/1471-2350-6-39.
224. Kita K, Vibat CR, Meinhardt S, Guest JR, Gennis RB. One-step purification from Escherichia coli of complex II (succinate: ubiquinone oxidoreductase) associated with succinate-reducible cytochrome b556. *J Biol Chem* 1989;**264**(5):2672-7.
225. Miyadera H, Shiomi K, Ui H, Yamaguchi Y, Masuma R, Tomoda H*, et al.* Atpenins, potent and specific inhibitors of mitochondrial complex II (succinate-ubiquinone oxidoreductase). *Proc Natl Acad Sci U S A* 2003;**100**(2):473-7 doi 10.1073/pnas.0237315100.
226. Bajpai R, Sharma A, Achreja A, Edgar CL, Wei C, Siddiqa AA*, et al.* Electron transport chain activity is a predictor and target for venetoclax sensitivity in multiple myeloma. *Nature communications* 2020;**11**(1):1228 doi 10.1038/s41467-020-15051-z.
227. Barrientos A, Fontanesi F, Diaz F. Evaluation of the mitochondrial respiratory chain and oxidative phosphorylation system using polarography and spectrophotometric enzyme assays. *Curr Protoc Hum Genet* 2009;**Chapter 19**:Unit19 3 doi 10.1002/0471142905.hg1903s63.
228. Spinazzi M, Casarin A, Pertegato V, Salviati L, Angelini C. Assessment of mitochondrial respiratory chain enzymatic activities on tissues and cultured cells. *Nature protocols* 2012;**7**(6):1235-46 doi 10.1038/nprot.2012.058.
229. Han S, Cui Y, Helbing DL. Inactivation of Horseradish Peroxidase by Acid for Sequential Chemiluminescent Western Blot. *Biotechnol J* 2020;**15**(3):e1900397 doi 10.1002/biot.201900397.
230. Hao HX, Khalimonchuk O, Schraders M, Dephoure N, Bayley JP, Kunst H*, et al.* SDH5, a gene required for flavination of succinate dehydrogenase, is mutated in paraganglioma. *Science* 2009;**325**(5944):1139-42 doi 10.1126/science.1175689.
231. Liu X, Jian X, Boerwinkle E. dbNSFP: a lightweight database of human nonsynonymous SNPs and their functional predictions. *Human mutation* 2011;**32**(8):894-9 doi 10.1002/humu.21517.
232. Liu X, Li C, Mou C, Dong Y, Tu Y. dbNSFP v4: a comprehensive database of transcript-specific functional predictions and annotations for human nonsynonymous and splice-site SNVs. *Genome Med* 2020;**12**(1):103 doi 10.1186/s13073-020-00803-9.

233. Tavtigian SV, Harrison SM, Boucher KM, Biesecker LG. Fitting a naturally scaled point system to the ACMG/AMP variant classification guidelines. *Human mutation* 2020;**41**(10):1734-7 doi 10.1002/humu.24088.
234. Kopanos C, Tsiolkas V, Kouris A, Chapple CE, Albarca Aguilera M, Meyer R, Massouras A. VarSome: the human genomic variant search engine. *Bioinformatics* 2019;**35**(11):1978-80 doi 10.1093/bioinformatics/bty897.
235. Piruat JI, Millan-Ucles A. Genetically modeled mice with mutations in mitochondrial metabolic enzymes for the study of cancer. *Frontiers in oncology* 2014;**4**:200 doi 10.3389/fonc.2014.00200.
236. Pagnamenta AT, Hargreaves IP, Duncan AJ, Taanman JW, Heales SJ, Land JM*, et al.* Phenotypic variability of mitochondrial disease caused by a nuclear mutation in complex II. *Mol Genet Metab* 2006;**89**(3):214-21 doi 10.1016/j.ymgme.2006.05.003.
237. Van Coster R, Seneca S, Smet J, Van Hecke R, Gerlo E, Devreese B*, et al.* Homozygous Gly555Glu mutation in the nuclear-encoded 70 kDa flavoprotein gene causes instability of the respiratory chain complex II. *Am J Med Genet A* 2003;**120A**(1):13-8 doi 10.1002/ajmg.a.10202.
238. Sturrock BRH, Macnamara EF, McGuire P, Kruk S, Yang I, Murphy J*, et al.* Progressive cerebellar atrophy in a patient with complex II and III deficiency and a novel deleterious variant in SDHA: A Counseling Conundrum. *Mol Genet Genomic Med* 2021;**9**(6):e1692 doi 10.1002/mgg3.1692.
239. Flickinger J, Fan J, Wellik A, Ganetzky R, Goldstein A, Muraresku CC*, et al.* Development of a Mitochondrial Myopathy-Composite Assessment Tool. *JCSM Clin Rep* 2021;**6**(4):109-27.
240. Rentzsch P, Witten D, Cooper GM, Shendure J, Kircher M. CADD: predicting the deleteriousness of variants throughout the human genome. *Nucleic Acids Res* 2019;**47**(D1):D886-D94 doi 10.1093/nar/gky1016.
241. Feng BJ. PERCH: A Unified Framework for Disease Gene Prioritization. *Human mutation* 2017;**38**(3):243-51 doi 10.1002/humu.23158.
242. Li C, Zhi D, Wang K, Liu X. MetaRNN: differentiating rare pathogenic and rare benign missense SNVs and InDels using deep learning. *Genome Med* 2022;**14**(1):115 doi 10.1186/s13073-022-01120-z.
243. Dong C, Wei P, Jian X, Gibbs R, Boerwinkle E, Wang K, Liu X. Comparison and integration of deleteriousness prediction methods for nonsynonymous SNVs in whole exome sequencing studies. *Hum Mol Genet* 2015;**24**(8):2125-37 doi 10.1093/hmg/ddu733.
244. Reva B, Antipin Y, Sander C. Predicting the functional impact of protein mutations: application to cancer genomics. *Nucleic Acids Res* 2011;**39**(17):e118 doi 10.1093/nar/gkr407.
245. Ioannidis NM, Rothstein JH, Pejaver V, Middha S, McDonnell SK, Baheti S*, et al.* REVEL: An Ensemble Method for Predicting the Pathogenicity of Rare Missense Variants. *American journal of human genetics* 2016;**99**(4):877-85 doi 10.1016/j.ajhg.2016.08.016.
246. Pejaver V, Byrne AB, Feng BJ, Pagel KA, Mooney SD, Karchin R*, et al.* Calibration of computational tools for missense variant pathogenicity classification and ClinGen recommendations for PP3/BP4 criteria. *American journal of human genetics* 2022;**109**(12):2163-77 doi 10.1016/j.ajhg.2022.10.013.
247. Lek M, Karczewski KJ, Minikel EV, Samocha KE, Banks E, Fennell T*, et al.* Analysis of protein-coding genetic variation in 60,706 humans. *Nature* 2016;**536**(7616):285-91 doi 10.1038/nature19057.

248. Llargues-Sistac G, Bonjoch L, Castellvi-Bel S. HAP1, a new revolutionary cell model for gene editing using CRISPR-Cas9. *Front Cell Dev Biol* 2023;**11**:1111488 doi 10.3389/fcell.2023.1111488.
249. Iverson TM, Maklashina E, Cecchini G. Structural basis for malfunction in complex II. *J Biol Chem* 2012;**287**(42):35430-8 doi 10.1074/jbc.R112.408419.
250. Mbaya E, Oules B, Caspersen C, Tacine R, Massinet H, Pennuto M*, et al.* Calcium signalling-dependent mitochondrial dysfunction and bioenergetics regulation in respiratory chain Complex II deficiency. *Cell Death Differ* 2010;**17**(12):1855-66 doi 10.1038/cdd.2010.51.
251. Quinlan CL, Orr AL, Perevoshchikova IV, Treberg JR, Ackrell BA, Brand MD. Mitochondrial complex II can generate reactive oxygen species at high rates in both the forward and reverse reactions. *J Biol Chem* 2012;**287**(32):27255-64 doi 10.1074/jbc.M112.374629.
252. Kluckova K, Sticha M, Cerny J, Mracek T, Dong L, Drahota Z*, et al.* Ubiquinone-binding site mutagenesis reveals the role of mitochondrial complex II in cell death initiation. *Cell Death Dis* 2015;**6**(5):e1749 doi 10.1038/cddis.2015.110.
253. Siebels I, Drose S. Q-site inhibitor induced ROS production of mitochondrial complex II is attenuated by TCA cycle dicarboxylates. *Biochimica et biophysica acta* 2013;**1827**(10):1156-64 doi 10.1016/j.bbabio.2013.06.005.
254. Kurian AW, Abrahamse P, Furgal A, Ward KC, Hamilton AS, Hodan R*, et al.* Germline Genetic Testing After Cancer Diagnosis. *Jama* 2023;**330**(1):43-51 doi 10.1001/jama.2023.9526.
255. Goldfeder RL, Wall DP, Khoury MJ, Ioannidis JPA, Ashley EA. Human Genome Sequencing at the Population Scale: A Primer on High-Throughput DNA Sequencing and Analysis. *Am J Epidemiol* 2017;**186**(8):1000-9 doi 10.1093/aje/kww224.
256. Federici G, Soddu S. Variants of uncertain significance in the era of high-throughput genome sequencing: a lesson from breast and ovary cancers. *Journal of experimental & clinical cancer research : CR* 2020;**39**(1):46 doi 10.1186/s13046-020-01554-6.
257. Easton DF, Pharoah PD, Antoniou AC, Tischkowitz M, Tavtigian SV, Nathanson KL*, et al.* Gene-panel sequencing and the prediction of breast-cancer risk. *N Engl J Med* 2015;**372**(23):2243-57 doi 10.1056/NEJMsr1501341.
258. Moghadasi S, Eccles DM, Devilee P, Vreeswijk MP, van Asperen CJ. Classification and Clinical Management of Variants of Uncertain Significance in High Penetrance Cancer Predisposition Genes. *Human mutation* 2016;**37**(4):331-6 doi 10.1002/humu.22956.
259. Lucci-Cordisco E, Amenta S, Panfili A, Del Valle J, Capella G, Pineda M, Genuardi M. Variants of uncertain significance (VUS) in cancer predisposing genes: What are we learning from multigene panels? *Eur J Med Genet* 2022;**65**(1):104400 doi 10.1016/j.ejmg.2021.104400.
260. Gelman H, Dines JN, Berg J, Berger AH, Brnich S, Hisama FM*, et al.* Recommendations for the collection and use of multiplexed functional data for clinical variant interpretation. *Genome Med* 2019;**11**(1):85 doi 10.1186/s13073-019-0698-7.
261. Kitzman JO, Starita LM, Lo RS, Fields S, Shendure J. Massively parallel single-amino-acid mutagenesis. *Nat Methods* 2015;**12**(3):203-6, 4 p following 6 doi 10.1038/nmeth.3223.
262. Acevedo-Rocha CG, Reetz MT, Nov Y. Economical analysis of saturation mutagenesis experiments. *Sci Rep* 2015;**5**:10654 doi 10.1038/srep10654.
263. Nikiforov TT, Rendle RB, Kotewicz ML, Rogers YH. The use of phosphorothioate primers and exonuclease hydrolysis for the preparation of single-stranded PCR products and their

detection by solid-phase hybridization. *PCR Methods Appl* 1994;**3**(5):285-91 doi 10.1101/gr.3.5.285.
264. Kowalsky CA, Klesmith JR, Stapleton JA, Kelly V, Reichkitzer N, Whitehead TA. High-resolution sequence-function mapping of full-length proteins. *PLoS One* 2015;**10**(3):e0118193 doi 10.1371/journal.pone.0118193.
265. Bushnell B, Rood J, Singer E. BBMerge - Accurate paired shotgun read merging via overlap. *PLoS One* 2017;**12**(10):e0185056 doi 10.1371/journal.pone.0185056.
266. Martin M. Cutadapt removes adapter sequences from high-throughput sequencing reads. *EMBnetjournal* 2011;**17**:10-2.
267. Tarumoto Y, Lu B, Somerville TDD, Huang YH, Milazzo JP, Wu XS*, et al.* LKB1, Salt-Inducible Kinases, and MEF2C Are Linked Dependencies in Acute Myeloid Leukemia. *Mol Cell* 2018;**69**(6):1017-27 e6 doi 10.1016/j.molcel.2018.02.011.
268. Winzeler EA, Shoemaker DD, Astromoff A, Liang H, Anderson K, Andre B*, et al.* Functional characterization of the S. cerevisiae genome by gene deletion and parallel analysis. *Science* 1999;**285**(5429):901-6 doi 10.1126/science.285.5429.901.
269. King MP, Attardi G. Human cells lacking mtDNA: repopulation with exogenous mitochondria by complementation. *Science* 1989;**246**(4929):500-3 doi 10.1126/science.2814477.
270. Cardaci S, Zheng L, MacKay G, van den Broek NJ, MacKenzie ED, Nixon C*, et al.* Pyruvate carboxylation enables growth of SDH-deficient cells by supporting aspartate biosynthesis. *Nat Cell Biol* 2015;**17**(10):1317-26 doi 10.1038/ncb3233.
271. Fontanesi F, Diaz F, Barrientos A. Evaluation of the mitochondrial respiratory chain and oxidative phosphorylation system using yeast models of OXPHOS deficiencies. *Curr Protoc Hum Genet* 2009;**Chapter 19**:Unit19 5 doi 10.1002/0471142905.hg1905s63.
272. Mighell TL, Evans-Dutson S, O'Roak BJ. A Saturation Mutagenesis Approach to Understanding PTEN Lipid Phosphatase Activity and Genotype-Phenotype Relationships. *American journal of human genetics* 2018;**102**(5):943-55 doi 10.1016/j.ajhg.2018.03.018.
273. Weile J, Sun S, Cote AG, Knapp J, Verby M, Mellor JC*, et al.* A framework for exhaustively mapping functional missense variants. *Mol Syst Biol* 2017;**13**(12):957 doi 10.15252/msb.20177908.
274. Laurent JM, Young JH, Kachroo AH, Marcotte EM. Efforts to make and apply humanized yeast. *Brief Funct Genomics* 2016;**15**(2):155-63 doi 10.1093/bfgp/elv041.
275. Kachroo AH, Vandeloo M, Greco BM, Abdullah M. Humanized yeast to model human biology, disease and evolution. *Dis Model Mech* 2022;**15**(6) doi 10.1242/dmm.049309.
276. Ghezzi D, Goffrini P, Uziel G, Horvath R, Klopstock T, Lochmuller H*, et al.* SDHAF1, encoding a LYR complex-II specific assembly factor, is mutated in SDH-defective infantile leukoencephalopathy. *Nat Genet* 2009;**41**(6):654-6 doi 10.1038/ng.378.
277. Hart ML, Quon E, Vigil ABG, Engstrom IA, Newsom OJ, Davidsen K*, et al.* Mitochondrial redox adaptations enable alternative aspartate synthesis in SDH-deficient cells. *Elife* 2023;**12** doi 10.7554/eLife.78654.
278. Seo BB, Kitajima-Ihara T, Chan EK, Scheffler IE, Matsuno-Yagi A, Yagi T. Molecular remedy of complex I defects: rotenone-insensitive internal NADH-quinone oxidoreductase of Saccharomyces cerevisiae mitochondria restores the NADH oxidase activity of complex I-deficient mammalian cells. *Proc Natl Acad Sci U S A* 1998;**95**(16):9167-71 doi 10.1073/pnas.95.16.9167.

279. Findlay GM, Daza RM, Martin B, Zhang MD, Leith AP, Gasperini M*, et al.* Accurate classification of BRCA1 variants with saturation genome editing. *Nature* 2018;**562**(7726):217-22 doi 10.1038/s41586-018-0461-z.
280. Findlay GM, Boyle EA, Hause RJ, Klein JC, Shendure J. Saturation editing of genomic regions by multiplex homology-directed repair. *Nature* 2014;**513**(7516):120-3 doi 10.1038/nature13695.
281. Buckley M, Kajba CM, Forrester N, Terwagne C, Sawyer C, Shepherd STC*, et al.* Saturation Genome Editing Resolves the Functional Spectrum of Pathogenic VHL Alleles. *bioRxiv* 2023:2023.06.10.542698 doi 10.1101/2023.06.10.542698.
282. Radford EJ, Tan HK, Andersson MHL, Stephenson JD, Gardner EJ, Ironfield H*, et al.* Saturation genome editing of DDX3X clarifies pathogenicity of germline and somatic variation. *medRxiv* 2022:2022.06.10.22276179 doi 10.1101/2022.06.10.22276179.
283. Hanna RE, Hegde M, Fagre CR, DeWeirdt PC, Sangree AK, Szegletes Z*, et al.* Massively parallel assessment of human variants with base editor screens. *Cell* 2021;**184**(4):1064-80 e20 doi 10.1016/j.cell.2021.01.012.
284. Erwood S, Bily TMI, Lequyer J, Yan J, Gulati N, Brewer RA*, et al.* Saturation variant interpretation using CRISPR prime editing. *Nat Biotechnol* 2022;**40**(6):885-95 doi 10.1038/s41587-021-01201-1.
285. Schipani A, Nannini M, Astolfi A, Pantaleo MA. SDHA Germline Mutations in SDH-Deficient GISTs: A Current Update. *Genes (Basel)* 2023;**14**(3) doi 10.3390/genes14030646.
286. Indio V, Schipani A, Nannini M, Urbini M, Rizzo A, De Leo A*, et al.* Gene Expression Landscape of SDH-Deficient Gastrointestinal Stromal Tumors. *Journal of clinical medicine* 2021;**10**(5) doi 10.3390/jcm10051057.
287. Blaut M, Whittaker K, Valdovinos A, Ackrell BA, Gunsalus RP, Cecchini G. Fumarate reductase mutants of Escherichia coli that lack covalently bound flavin. *J Biol Chem* 1989;**264**(23):13599-604.
288. Sharma P, Maklashina E, Cecchini G, Iverson TM. Crystal structure of an assembly intermediate of respiratory Complex II. *Nature communications* 2018;**9**(1):274 doi 10.1038/s41467-017-02713-8.
289. Maklashina E, Rajagukguk S, Iverson TM, Cecchini G. The unassembled flavoprotein subunits of human and bacterial complex II have impaired catalytic activity and generate only minor amounts of ROS. *J Biol Chem* 2018;**293**(20):7754-65 doi 10.1074/jbc.RA118.001977.
290. Papathomas TG, Oudijk L, Persu A, Gill AJ, van Nederveen F, Tischler AS*, et al.* SDHB/SDHA immunohistochemistry in pheochromocytomas and paragangliomas: a multicenter interobserver variation analysis using virtual microscopy: a Multinational Study of the European Network for the Study of Adrenal Tumors (ENS@T). *Mod Pathol* 2015;**28**(6):807-21 doi 10.1038/modpathol.2015.41.
291. Dwight T, Benn DE, Clarkson A, Vilain R, Lipton L, Robinson BG*, et al.* Loss of SDHA expression identifies SDHA mutations in succinate dehydrogenase-deficient gastrointestinal stromal tumors. *Am J Surg Pathol* 2013;**37**(2):226-33 doi 10.1097/PAS.0b013e3182671155.
292. Bezawork-Geleta A, Wen H, Dong L, Yan B, Vider J, Boukalova S*, et al.* Alternative assembly of respiratory complex II connects energy stress to metabolic checkpoints. *Nature communications* 2018;**9**(1):2221 doi 10.1038/s41467-018-04603-z.

293. Miettinen M, Lasota J. Succinate dehydrogenase deficient gastrointestinal stromal tumors (GISTs) - a review. *The international journal of biochemistry & cell biology* 2014;**53**:514-9 doi 10.1016/j.biocel.2014.05.033.
294. Pantaleo MA, Lolli C, Nannini M, Astolfi A, Indio V, Saponara M*, et al.* Good survival outcome of metastatic SDH-deficient gastrointestinal stromal tumors harboring SDHA mutations. *Genet Med* 2015;**17**(5):391-5 doi 10.1038/gim.2014.115.
295. Sulkowski PL, Sundaram RK, Oeck S, Corso CD, Liu Y, Noorbakhsh S*, et al.* Krebs-cycle-deficient hereditary cancer syndromes are defined by defects in homologous-recombination DNA repair. *Nat Genet* 2018;**50**(8):1086-92 doi 10.1038/s41588-018-0170-4.
296. Pang Y, Lu Y, Caisova V, Liu Y, Bullova P, Huynh TT*, et al.* Targeting NAD(+)/PARP DNA Repair Pathway as a Novel Therapeutic Approach to SDHB-Mutated Cluster I Pheochromocytoma and Paraganglioma. *Clin Cancer Res* 2018;**24**(14):3423-32 doi 10.1158/1078-0432.CCR-17-3406.
297. Sarkadi B, Meszaros K, Krencz I, Canu L, Krokker L, Zakarias S*, et al.* Glutaminases as a Novel Target for SDHB-Associated Pheochromocytomas/Paragangliomas. *Cancers (Basel)* 2020;**12**(3) doi 10.3390/cancers12030599.
298. Liu Y, Pang Y, Zhu B, Uher O, Caisova V, Huynh TT*, et al.* Therapeutic Targeting of SDHB-Mutated Pheochromocytoma/Paraganglioma with Pharmacologic Ascorbic Acid. *Clin Cancer Res* 2020;**26**(14):3868-80 doi 10.1158/1078-0432.CCR-19-2335.
299. Maher MJ, Herath AS, Udagedara SR, Dougan DA, Truscott KN. Crystal structure of bacterial succinate:quinone oxidoreductase flavoprotein SdhA in complex with its assembly factor SdhE. *Proc Natl Acad Sci U S A* 2018;**115**(12):2982-7 doi 10.1073/pnas.1800195115.
300. Grivennikova VG, Kozlovsky VS, Vinogradov AD. Respiratory complex II: ROS production and the kinetics of ubiquinone reduction. *Biochim Biophys Acta Bioenerg* 2017;**1858**(2):109-17 doi 10.1016/j.bbabio.2016.10.008.
301. Lorendeau D, Rinaldi G, Boon R, Spincemaille P, Metzger K, Jager C*, et al.* Dual loss of succinate dehydrogenase (SDH) and complex I activity is necessary to recapitulate the metabolic phenotype of SDH mutant tumors. *Metab Eng* 2017;**43**(Pt B):187-97 doi 10.1016/j.ymben.2016.11.005.
302. Niu Y, Ferreira Azevedo CA, Li X, Kamali E, Haagen Nielsen O, Storgaard Sorensen C, Frodin M. Multiparametric and accurate functional analysis of genetic sequence variants using CRISPR-Select. *Nat Genet* 2022;**54**(12):1983-93 doi 10.1038/s41588-022-01224-7.
303. Wang B, Wang Z, Wang D, Zhang B, Ong SG, Li M*, et al.* krCRISPR: an easy and efficient strategy for generating conditional knockout of essential genes in cells. *J Biol Eng* 2019;**13**:35 doi 10.1186/s13036-019-0150-y.